TARGETED NANOSYSTEMS FOR TUBERCULOSIS PERICARDITIS INTERVENTIONS

SIMISOLA AYOBAMI AYODELE

A dissertation submitted to the Faculty of Health Sciences, University of the Witwatersrand, in fulfilment of the requirements for the degree of Master of Pharmacy

Supervisor:

Professor Yahya Essop Choonara,

Department of Pharmacy and Pharmacology, Faculty of Health Sciences, University of the Witwatersrand, Johannesburg, South Africa

Co-Supervisors:

Professor Pradeep Kumar,

Department of Pharmacy and Pharmacology, Faculty of Health Sciences, University of the Witwatersrand, Johannesburg, South Africa

Doctor Armorel Van Eyk,

Department of Pharmacy and Pharmacology, Faculty of Health Sciences, University of the Witwatersrand, Johannesburg, South Africa

Johannesburg

2024

DECLARATION

I, Simisola Ayobami Ayodele, declare that this dissertation is my own work. It is being submitted for the degree of Master of Pharmacy in the Faculty of Health Sciences at the University of the Witwatersrand, Johannesburg, South Africa. It has not been submitted before for any degree or examination at this or any other University.

Signature

This …28st... day of …February…2024...

ANIMAL ETHICS DECLARATION

I, Simisola Ayobami Ayodele, hereby confirm the study entitled "'Targeted nanosystems for TB pericarditis intervention'." was approved by the Animal Research Ethics Committee (AREC) of the University of the Witwatersrand with Ethics waiver number: AREC-101210-002.

APPENDIX A

HUMAN ETHICS DECLARATION

I, Simisola Ayobami Ayodele, hereby confirm the study entitled “Targeted nanosystems for TB pericarditis intervention”. was approved by the Human Research Ethics Committee (HREC) (Medical) of the University of the Witwatersrand with Approval number: M230545.

APPENDIX B

RESEARCH OUTPUTS

1. Review Paper

S Ayodele, P Kumar, A van Eyk, Y Choonara. Advances in Immunomodulatory Strategies for Host-directed Therapies for Combating Tuberculosis. Biomedicine and Pharmacotherapy 162, 114588. DOI: 10.1016/j.biopha.2023.114588 (2023).

APPENDIX C

2. Book Chapter

S Ayodele, P Kumar, A van Eyk, Y Choonara. Surface-modified Drug Delivery Systems for Tuberculosis Intervention. In Book: Tubercular Drug Delivery Systems, 261-287. DOI: 10.1007/978-3-031-14100-3_13 (2023).

APPENDIX D

3. Research Papers

S Ayodele, P Kumar, A van Eyk, Y Choonara. Synthesis of Novel Mannan-Chitosan Oligosaccharide Lactate Nanoparticles for the Enhanced *Ex vivo* Permeation of Bedaquiline across the Pericardium in Tuberculosis Pericarditis. (For submission in 2024).

APPENDIX E

S Ayodele, P Kumar, A van Eyk, Y Choonara. RP-HPLC method development and Validation for the Determination of Bedaquiline at Physiological pH 7.4. (For submission in 2024).

APPENDIX F

4. Research presentation

Simisola Ayobami Ayodele, Pradeep Kumar, Armorel van Eyk, Yahya Essop Choonara, Targeted Nanosystems for TB pericarditis Interventions. 2023 RSG Science Communication (Second Place), 06th September 2023.

APPENDIX G

ABSTRACT

Tuberculosis (TB) maintains its infamous status regarding its detrimental effect on global health, causing the highest mortality by a single infectious agent. It presents as the second most lethal infectious disease after HIV/AIDS. The presence of resistance and immune-compromising disease favors the disease in maintaining its footing in the health care burden despite various anti-TB drugs. The main factors contributing to resistance and difficulty in treating disease include prolonged treatment duration (at least 6 months) and severe toxicity, which further leads to patient non-compliance, and thus a ripple effect leading to therapeutic non-efficacy. The efficacy of new regimens demonstrates that targeting host factors concomitantly with the *Mycobacterium tuberculosis* (*M.tb*) strain is urgently required. Due to the huge expenses and time required of up to 20 years for new drug research and development, drug repurposing may be the most economical, circumspective, and conveniently faster journey to embark on. Host-directed therapy (HDT) will dampen the burden of the disease by acting as an immunomodulator, allowing it to defend the body against antibiotic-resistant pathogens whilst minimizing the possibility of developing new resistance to susceptible drugs. Repurposed drugs in TB act as host-directed therapies, acclimatizing the host immune cell to the presence of TB, improving its antimicrobial activity and time taken to get rid of the disease, whilst minimizing inflammation and tissue damage. Anti-TB drugs incorporated in nanosystems may reduce side effects by delivering the drug selectively into infection reservoirs such as macrophages, which may assist in clearing the TB bacilli faster and reducing the duration of therapy. Tuberculosis pericarditis (TBP) is a type of extrapulmonary tuberculosis caused by the retrograde lymphatic spread of the bacilli from lymph nodes. TBP is known to have a high burden in southern Africa due to the high prevalence of HIV and its contribution to TBP. Traditional anti-TB drugs have poor permeation across the pericardium, making TBP a difficult disease to treat with high mortality. Rapid HPLC methods were initially established for the detection and quantification of isoniazid and pyrazinamide at a physiological pH (pH 7.4). These methods were subsequently used for the detection and quantification of both compounds in the *ex vivo* pericardium studies. Although both drugs diffused across the pericardium, only isoniazid has anti-tubercular effects at physiological pH. Both drugs permeated across the pericardium at pH 7.4, but only isoniazid has anti-tubercular effects at this pH. Bedaquiline is known to shorten the duration of therapy but has limitations e.g., poor solubility and adverse effects such as prolongation of QT interval, causing careful use and close monitoring of its adverse effects and possible drug interactions. In this study, bedaquiline was incorporated into an inherently targeted nanosystem made of mannan (host-directed therapy) for improved permeation of the drug across the pericardium. The bedaquiline-loaded mannan-chitosan oligosaccharide lactate nanoparticles were prepared by a one-step ionic gelation probe sonication method. A PermeGear 7-in-line flow-through system was used for the *ex vivo* diffusion studies across porcine and human pericardium. The nano gel was loaded into the donor compartment. Phosphate buffer saline (pH 7.4 with 0.2% sodium lauryl sulphate) was pumped through the receptor compartments at 1.5 $ml.h^{-1}$ (37 °C). Samples were collected every 2 h for 24 h and analyzed via HPLC. Bedaquiline loaded nanoparticles with particle size and potential of 192.4 nm and 40.5 mV, respectively, were synthesised. The chitosan-mannan bedaquiline loaded nanoparticles had an encapsulation efficacy of 98.7% and drug loading of 0.6%. Diffusion data of bedaquiline in the nanosystem indicated a flux of 2.889 and 2.346 $\mu g.cm^{-2}.min^{-1}$ for porcine and human pericardium, respectively, as compared to 0.991 $\mu g.cm^{-2}.min^{-1}$ and 1.1578 $\mu g.cm^{-2}.min^{-1}$ for isoniazid and pyrazinamide, respectively. The permeation of the nanosystem indicated a consistent and linear diffusion pattern across both porcine and human pericardium, additionally approving the porcine pericardium as a great comparable tissue to human tissue for pericardial studies. The nanosystem, therefore, presents an exceptional direction for the treatment of tuberculosis pericarditis with prospectively minimized systemic side effects and host-directed therapy.

ACKNOWLEDGEMENTS

I return all glory to the Lord God, Almighty, for the strength and guidance he bestowed to bring me this far. I sing praises to the name of the Lord, the most high. I give thanks for he is good, and his mercies endure forever.

I would like to express my gratitude to my absolute Gem of a mother, a friend, and an outstanding example of a parent. Mrs. Toyin Ayodele, for her financial and spiritual support throughout this research. A special thanks to my uncle, Adegbuyi Fasanya for his fatherly guidance and support. Busolami Ayodele and Fikunolami Ayodele, you guys are as rare as rhodium, thank you for your steadfast motherly and sisterly support to ease the challenges I face daily.

A humongous thanks to my supervisors, Prof. Yahya Choonara; Prof. Pradeep Kumar and Dr Armorel van Eyk, for their relentless efforts and drive to ensure a success in the outcome of my research. Your guidance, mentoring and advice have made me confident in highlighting my master's as a huge milestone in my development as a scientist and as a critical thinker as a person.

I would like to thank Dr. Pieter van der Bijl for his contribution in my project in acquiring human pericardial tissue that further enhance the quality of my research.

I would like to appreciate and acknowledge my friends and loved ones. Special mention to Christian Nwaka, you have treated me more than a brother would treat one. Timileyin Martins, Comfort Okobama, Ugochi Umah, Uchechi Umah, Bianca Nwagbara, Timilehin Owolabi, Claudia Mpofu, Mulanga Mathoho, Logan Spinickum, Kundai Mazarura, Mosibudi Rampya, Natachi Chukwuezi, Simbarashe Chiparawi, Mark Gama, Sithadekile Ncube, Mpho Maake, Unathi Chiliza, and Khomotso Matemotsa. You have in one way or the other directly contributed to this degree, so thank you for being there to listen to me through my struggles and success. You have either eased my mind, amplified my joy, or taken my mind away from my troubles when needed.

To all members of the Wits Advanced Drug Delivery Platform (WADDP) and the members of the Department of Pharmacy and Pharmacology, I have found family in you all., Mashudu Mphapula, Sarjan Patel, Leon Khoza, Nombeko Sikhosana, Lindokuhle Ngema, Atang Motaung, Ahmed Abdelgader, Johnathan Chayandura, Clarence Dhege, Theresa Varughese, Kimaya Moodley, Divesha Essa, Kate De Silva, Ranya Mukhtar, Magdi Abobaker. To the staff, Dr Hillary Ndlovu, Dr Mduduzi Sithole, Mr Siya Maphumulo, Mrs Tshidi Mosete, Mr Bafana Temba, Mr Kleinbooi

Mohlabi, Dr Gillian Mahumane, Dr Samson Adeyemi, Dr Pavan Walvekar thank you all, for your welcoming presence, assistance, and contribution in one way or the other.

To the family of the Adams that have availed themselves as a second home, thank you all. You have always welcomed me with open arms and taken me as a family. Special thanks to Mummy Uhloma Adams, Ijeoma Adams and CC Adams, for your prayers and belief in me that gave me the strength to push through with this degree.

Special thanks to all my funders, Departmental Community Transformation Grant (CTG), and Postgraduate Merit Award (PMA), for their financial support during this program.

To those of you who are reading this who have always had well wishes for me, whether mentioned above or not, thank you so much. My soul rejoices with yours.

And quickly to my haters and all those who thought I would not make it, thank you because, without you, I wouldn't have anyone to prove me wrong. Stay tuned for more.

God bless every single one of you with the best of your heart desires.

DEDICATION

I dedicate this thesis to my mother and sisters, Mrs. Toyin Ayodele, Busolami Ayodele, and Fikunolami Ayodele. You all gave me the strength to keep going.

TABLE OF CONTENTS

CHAPTER ONE

INTRODUCTION AND BACKGROUND

CHAPTER TWO

IMMUNOMODULATORY STRATEGIES EMPLOYED BY HOST-DIRECTED THERAPIES FOR COMBATING TUBERCULOSIS

CHAPTER THREE

SURFACE-MODIFIED DRUG DELIVERY SYSTEM FOR TUBERCULOSIS INTERVENTION

CHAPTER FOUR

PRELIMINARY STUDIES: VALIDATED METHOD AND PERMEATION STUDIES OF ISONIAZID AND PYRAZINAMIDE ACROSS THE PERICARDIUM

CHAPTER FIVE

PREFORMULATION STUDIES: DESIGN, PREPARATION, AND CHARACTERIZATION OF POTENTIAL NANOSYSTEMS FOR THE TREATMENT OF TUBERCULOSIS PERICARDITIS

CHAPTER SIX

SYNTHESIS AND EVALUATION OF NOVEL MANNAN-CHITOSAN OLIGOSACCHARIDE LACTATE NANOPARTICLES FOR THE ENHANCED DELIVERY OF BEDAQUILINE IN TUBERCULOSIS PERICARDITIS

APPENDICES

LIST OF ABBREVIATIONS

AMP	Adenosine monophosphate
AMPK	Adenosine monophosphate-activated protein kinase
AMs	Alveolar macrophages
APCs	Antigen-presenting cells
APTES	Aminopropyl triethoxysilane
AREC	Animal Research Ethics Committee
ART	Antiretroviral therapy
ASA	Acetylsalicylic acid
ATT	Anti-tuberculosis therapy
BBB	Blood brain barrier
BCG	Bacillus Calmette-Guérin
BDQ	Bedaquiline
BGs	Bacterial ghosts
CARD	Caspase activation and recruitment domain
CD206	Mannose receptor
Cdonor	Concentration in the donor compartment
CHMP	Committee for Medicinal Products
Chol	Cholesterol
CLR	C-type lectin receptors
CNS	Central nervous system
COS	Chitosan oligosaccharide lactate
COS-MN-BQ	Chitosan oligosaccharide lactate and mannan copolymeric nanoparticles
Creceiver	Concentration in the receptor compartment
CTG	Community Transformation Grant
D-1	Dectin-1
DCM	Dichloromethane
DCs	Dendritic cells
DC-SIGN	DC-specific intercellular adhesion molecule-3-grabbing non-integrin
DEE	Drug entrapment efficiency
DLC	Drug loading capacity
DNA	Deoxyribonucleic acid
DS	Drug sensitive

EDA	Ethylene diamine
EDA-PPI	Ethylene diamine polypropylene imine
EDC	Ethyl carbodiimide
EMB	Ethambutol
EPTB	Extrapulmonary tuberculosis
FcRγ	Fc receptor common y-chain
FeCl2·4H2O	Ferrous chloride tetrahydrate
FeCl3·6H2O	Ferric chloride hexahydrate
FITC	Fluorescein Isothiocyanate
FR	Flow rate
FRET	Förster resonance energy transfer
FRβ	Folate receptor β
FTIR	Fourier transform infrared
G′	Elastic modulus
G″	Viscous modulus
Ga	Gallium
GalM-h	Hydrolysed galactomannan
GAT	Gatifloxacin
GMS	Glyceryl monostearate
H_2SO_4	Sulfuric acid
HA	Hyaluronic acid
HDT	Host-directed therapy
HIV	Human immunodeficiency virus
HPLC	High-performance liquid chromatography
HREC	Human Research Ethics Committee
IBU	Ibuprofen
IFN-γ	Interferon-y
IL-10	Interleukin-10
IL-12	interleukin-12
IL-17	Interleukin-17
INH	Isoniazid
IP3	Inositol triphosphate
ITAM	Immunoreceptor tyrosine-based activation motif
JNK	Jun N-terminal kinase

KH2PO4	Potassium dihydrogen orthophosphate
KLF	Kruppel-like factor
LC	Lecithin
Lf	Lactoferrin
LPS	Liposomes
LTBI	Latent tuberculosis infection
M.tb	*Mycobacterium tuberculosis*
M2	N-Monodesmethyl
M3	N-Didesmethyl-bedaquiline
MAN	Mannitol
ManLAM	Mannose-capped lipoarabinomannan
MAPK	Mitogen-activated protein kinase
MBL	Mannose-binding lectins
MBSA	Methylated bovine serum albumin
MDR	Multi-drug resistant
MHC	Major histocompatibility complex
MIC	Minimum inhibitory concentration
MINCLE	Macrophage-inducible C-type lectin receptors
MMDA	Mass median aerodynamic diameter
MMPs	Matrix metalloproteinase
MN	Mannan oligosaccharide
MOX	Moxifloxacin
MPEG-PDLA	Monomethoxy PEG poly(ethylene glycol)-poly(D-lactide)
MPEG-PLLA	Monomethoxy PEG poly(ethylene glycol)-poly(L-lactide)
MSCs	Mesenchymal stromal cells
NAG	N-acetyl glucosamine
NaOH	Sodium hydroxide
NF-κB	Nuclear factor κB
NHS	N-hydroxysuccinimide
NKs	Natural killer cells
NLC	Nanostructured lipid carrier
NLRs	Nucleotide-binding and oligomerization domain-like receptors
NO	Nitric oxide
NPs	Nanoparticles

Nrp1	Neuropilin-1
NSAIDs	Non-steroidal anti-inflammatory drugs
NSCLC	Non-small cell lung cancer
O-SAP	O-stearoyl amylopectin
PA	Palmitic acid
PAMPs	Pathogen-associated molecular patterns
PBA	Phenylbutyrate
PBCA	Polybutylcyanoacrylate
PBS	Phosphate buffer saline
PC	Phosphatidylcholine
PDE-I	Phosphodiesterase inhibitors
PDI	Polydispersity index
PEG	Poly(ethylene glycol)
PEG-PASP	Poly(ethylene glycol)-poly(aspartic acid
PEHAM	Poly-ether hydroxyl-amine
PEO–PPO	Poly(ethylene oxide)-poly(propylene)
PK	Pharmacokinetics
PLA	Polylactic acid
PLBMGA	Poly(lactic-co-benzyloxy methyl glycolic acid)
PLGA	Poly(lactic-co-glycolic acid)
PLHMGA	Poy(lactic-co-hydroxymethyl glycolic acid)
PMA	Postgraduate Merit Award
PNPs	Polymeric nanoparticles
PRR	Pattern recognition receptor
pTUF-OA	Oleic acid tuftsin-modified peptide
PZA	Pyrazinamide
QC	Quality control
R2	Correlation coefficient
RBC	Red blood cells
RES	Reticuloendothelial system
RIF	Rifampicin
RP-HPLC	Reverse phase high-performance liquid chromatography
RSD	Relative standard deviation
SA	Stearic acid

SAEs	Serious adverse events
SAPK	Stress-activated protein kinases
SARM	Sterile α- and armadillo-motif-containing protein
SD	Standard deviation
SDGs	Sustainable development goals
SEM	Scanning electron microscopy
SLNPs	Solid lipid nanoparticles
SLS	Sodium lauryl sulphate
SOCS1	Suppressor of cytokine signaling-1
StAT-TB	Statins as Adjunctive Therapy for Tuberculosis
SUSARs	Suspected unexpected serious adverse reactions
TAG	TRAM adaptor with golgi dynamics
TB	Tuberculosis
TB-IRIS	Tuberculosis-immune reconstitution inflammatory syndrome
TBP	Tuberculosis pericarditis
TCM	T central memory
TEA	Triethylamine
TEM	T effector memory
TEOS	Tetraethyl orthosilicate
TGA	Thermogravimetric analysis
TGF	Transforming growth factor
TH1	T helper 1
Thunb.	Tinospora cordifolia
TIR	Toll-IL-1 receptors
TLRs	Toll-like receptors
TNF	Tumor necrosis factor
TP set	Tripalmitin
TS	Tocopherol/succinate
WGA	Wheat germ agglutinin
WHO	World Health Organization
XDR	Extensively drug-resistant
XRD	X-ray diffraction

LIST OF FIGURES

LIST OF TABLES

LIST OF EQUATIONS

CHAPTER ONE

INTRODUCTION AND BACKGROUND

1.1. BACKGROUND OF THIS STUDY

Tuberculosis (TB), an infection caused by *Mycobacterium tuberculosis (M.tb)* is the principal cause of mortality by disease from a single infectious agent, ranking in the top 10 global causes of death (World Health Organization Global Tuberculosis Report 2020). As of 2019, extrapulmonary tuberculosis contributed to 16% of worldwide tuberculosis cases (WHO) and has proven to be a difficult manifestation of tuberculosis, demonstrating both diagnostic and therapeutic challenges (Howlett et al., 2020). In comparison to other extrapulmonary TB manifestations, TB of the pericardium precedes TB of the central nervous system (CNS) into its devastating morbidity and mortality (Mutyaba and Ntsekhe, 2017). Tuberculosis pericarditis (TBP) is the most common cause of pericardial disease in Africa (Noubiap et al., 2019). The infection develops through retrograde lymph spread from the mediastinal, paratracheal, and peribronchial lymph nodes. It may also reach the pericardium through hematogenous spread in immunocompromised hosts (Ntsekhe et al., 2013). Additionally, other rare forms of entry such as direct spread into the pericardium due to its close adjacent proximity to the lungs have been reported (Spodick et al., 1956; Mutyaba and Ntsekhe, 2017).

Lymph is generated when interstitial fluid enters the lymphatic network. Lymphatic capillary networks act as a drainage system, removing surplus fluid (lymph) from the surrounding interstitial tissue spaces. Lymph nodes are numerous in the mediastinum and various other sites. Individual lymph nodes are divided into sinuses by the trabeculae that extend from the capsule of the lymph nodes, with structural components circulating in the fluid. These components consist of large numbers of T-lymphocytes, B-lymphocytes, macrophages, and dendritic cells (DCs) as depicted in Figure 1.1.

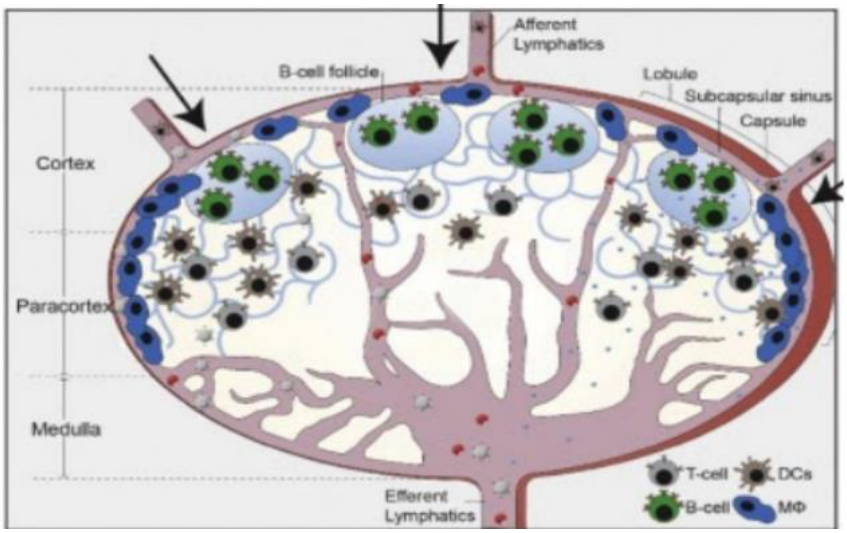

Figure 1.1: A diagram illustrating a lymph node and its various components (Ke et al., 2019).

Macrophages adhere to the trabecular meshwork and trap bacteria, cell debris, and other particles present in the lymph as they flow through the lymph node (Willard-Mack et al., 2006). In the lung and surrounding lymph nodes, macrophages and DCs harbour *M.tb* and present antigens to $CD4^+$ T cells. Although macrophages and DCs activate $CD4^+$ T cells, they have been found to do so poorly, implying either ineffective, infrequent, T-cell recognition of infected DCs, or ineffective expression of *M.tb* activity to $CD4^+$ T cells (Srivastava et al., 2014). Infected cells have a mechanism of transferring antigens to uninfected cells for them to prime $CD4^+$ T cells (Srivastava et al., 2014). An intervention that increases uninfected DC cells may provide a mechanism for host cells to avoid the inhibitory effects of *M.tb* on macrophages and DCs, allowing for productive priming of $CD4^+$ T cells without causing a harmful inflammatory cascade.

Macrophages are sub-classified into M1 and M2 macrophages. M1 macrophages (pro-inflammatory) are responsible for the enhancement of inflammation, whilst M2 macrophages (anti-inflammatory) are responsible for the settling of the inflammatory process. M2 macrophages' functions include producing anti-inflammatory cytokines which promote tissue healing as detailed in Figure 1.2 (Saqib et al., 2018). Many macrophages and DCs have various receptors expressed on their surfaces that can be used for drug targeting, these receptors include mannose (CD206) and CD44 receptors. These receptors on the surface of lymph node components show prospects as targeting sites to affect TBP prognosis. The pericardium is a double-layered fibrous sac that rings the heart and great vessels, segregating it from the mediastinum and acting as a border to the pleural space of both lungs. Assisted by the pericardial fluid of 20-25 ml found in between the two layers, the pericardium lubricates the surface of the heart, ensuring the dilation of the heart is controlled. The pericardial fluid

prevents excessive dilation of the heart that may cause a reduction in the cardiac stroke volume, due to a pressure-volume imbalance in the ventricles (Rehman et al., 2020). In addition to its functional properties, it protects the heart from infection. In the case of TBP, the infected pericardium hinders its functions and ultimately renders the pericardium fibrotic.

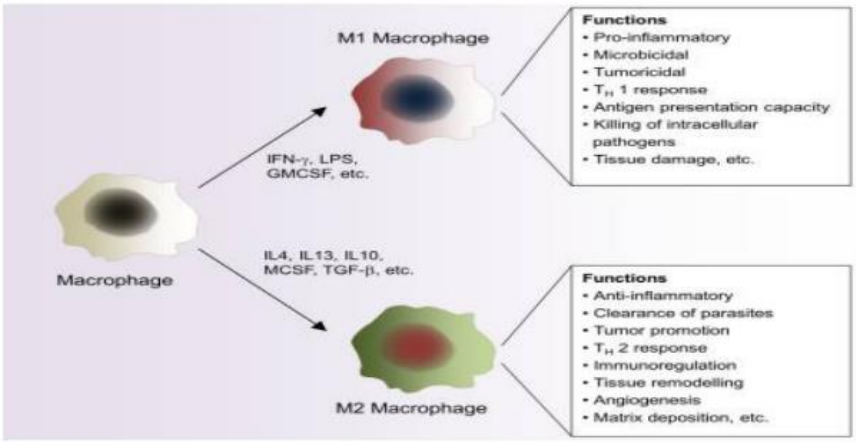

Figure 1.2: Macrophages sub-classification and specific functions of M1 and M2 macrophages (Saqib et al., 2018).

Over the years, clinical presentations of TBP have been nonspecific from TB of the lungs, which presents as nocturnal diaphoresis, fatigue, and weight loss (Sanduzzi et al., 2016). Various case studies have shown the need for a thorough examination to assist in the diagnosis. Patients with pericarditis usually also present with other underlying infections, with human immunodeficiency virus (HIV) being the predominant precipitation factor. In general examinations, auscultation of the heart may present as muffled with an associated pericardial rub. Other patients may present with enlarged mediastinal and hiatal lymph nodes (Jakimów-Kostrzewa et al., 2017). These patients in clinical cases present with tachycardia, hypotension, inflammatory markers, and a drop of SBP >10 mmHg during inspiration, known as pulsus paradoxus. The patient may present with pericardial effusion that could result in constrictive pericarditis that prevents the natural expansion of the heart, impairing cardiac function (Lima et al., 2019; Isiguzo et al., 2020).

1.2. RATIONALE AND MOTIVATION OF THIS STUDY

Tuberculosis pericarditis is therapeutically challenging due to the limited ability of antibiotics to penetrate the pericardium at adequate non-protein bound concentrations and then into the bacteria to inhibit its intracellular biochemical processes (Shenje et al., 2015). In the treatment of TBP, the standard anti-tuberculosis drugs are used and have been applied for decades, mainly due to a lack of newer agents with comparative effectiveness studies (Isiguzo et al., 2020).

An *in vitro* study measured drug binding to the caseum (necrotic centre of TB lesions) and the ability of the drug molecules to passively diffuse through the caseum, to study drug distribution in TB lesions or abscesses (Sarathy et al., 2017). The results showed, of 36 TB drugs, isoniazid presented with >99.9% fraction unbound drug in plasma and caseum, whilst plasma protein binding of drugs including rifampicin, resulted in poor caseum binding. In an *in vivo* experiment by Shenje and co-workers, fixed-dose combination drugs were given to subjects. Pericardial fluid samples were collected for 24 h, and at no sample time point was the concentration of free rifampicin, pyrazinamide, or ethambutol in the pericardium above the minimum inhibitory concentration (MIC) of the drugs. The very low unbound concentration of rifampicin could be due to pericardial fluid having specific gravity and it being highly protein-bound, (often >6 g/dL) in TBP (Phelan et al., 2015). In the same study, isoniazid reached MIC in the pericardial fluid, with concentrations approximate to the concentration in the blood, due to the hydrophilic and low protein binding nature of isoniazid (10%), with a median peak concentration 64-fold higher than the median MIC (Shenje et al., 2015). Pericardial permeation, therefore, favours drugs with a low protein binding nature, therefore incorporation of drugs with a higher protein binding nature in the nanosystem may allow improved permeation of the drug. Drugs like bedaquiline (BDQ) have a very high protein binding nature (99%) but have advantages such as a very low MIC and long half-life. Incorporation of such a drug with nano-particle drug delivery systems may show some prospects to improve drug bioavailability in the pericardial fluid to effectively treat pericarditis and prevent constrictive pericarditis with a lower frequency and duration of drug administration.

Accompanied by the influx of *M.tb* into the pericardial fluid are pro-inflammatory mediators and profibrotic mediators. Matthews et al., (2015) reported transcriptomic gene expression signatures of 17 genes that were connected to profibrotic mediators or actual fibrosis. Most of the protein markers in the pericardial fluid corresponded in amount with the mRNA transcripts in the blood. The investigators found growth factors, transforming growth factor-beta (TGF-β) and interleukin 10 (IL-10) as distinct markers in the disease and main contributors to the formation of fibrosis (Ntsekhe and Mayosi, 2013). Based on the results of the study, it is evident that with further study of the proteins and other markers, the mechanism of inflammation at the molecular level may be understood and used as a pathway to improve host-directed therapy. The use of host-mediated response includes enchantment of the autophagosome process or modification of lung and macrophage to clear pathogens in the case of TB (Hawn et al., 2013). Modification of macrophages' pro-inflammatory responses could enhance the treatment of conditions caused by inflammation-induced tissue damage, such as TBP. An example of this is a clinical trial that showed the safety of the therapy and potential use of mesenchymal stromal cells (MSCs) from the patient's bone marrow and uses its anti-scarring

and angiogenesis properties to combat drug-resistant TB and prevent the progression of TB (Skrahin et al., 2014). Nanoparticles are an ideal approach for chronic inflammatory disease, as demonstrated in an experiment by Jain et al., (2015), using alginate nanoparticles loaded with IL-10 plasmid deoxyribonucleic acid (DNA) administered intraperitoneally. The nanoparticles polarised macrophages from M1 to M2 state, improving the M2 state from untreated arthritic rats from ~9% to ~66%. This model of drug delivery may be incorporated with TB drugs and delivered subcutaneously and intrapericardially, for lymph node and pericardial targeting to stimulate an anti-inflammatory response in the treatment of TBP.

The effects of systemic corticosteroids in treating pericarditis have been experimented with by Mayosi and colleagues (2014). Resulting in a significantly lower incidence of constrictive pericarditis, suggesting that patients with large effusion, accompanied by high levels of inflammatory cells in pericardial fluid and patients with early stages of constriction may benefit from immunomodulatory therapy (Chaisson et al., 2014). It is to be noted though that prednisolone therapy unfavourably increased the incidence of HIV-related cancer in HIV-positive patients (Chaisson et al., 2014).

In vivo or *ex vivo* studies are crucial for an in-depth understanding of biological processes and the response to the nanoparticle-based formulation. This study will perform *ex vivo* studies on porcine tissue as swine has similarities with human tissues; this includes hemodynamic values and their size (Lelovas et al., 2014). Preliminary studies on porcine tissue will also assist in gaining a concise understanding of porcine tissue and the possibility of the system working for human tissue. Based on the aforementioned rationales, the loading of anti-TB hydrophobic drugs such as bedaquiline into hydrophilic-surfaced targeted nanosystems may improve pericardial penetration of the drug, whilst simultaneously targeting *M.tb* reservoirs thus controlling the proliferation of TB.

The hydrophobic core and hydrophilic surface of chitosan lends to a suitable polymer for the encapsulation of highly hydrophobic drugs such as bedaquiline to enhance its permeation across the pericardium (Chebl et al., 2016 and Lee et al., 2020). Furthermore, its antimicrobial, immunostimulant and anti-inflammatory properties, provide additional specifications to make it the appropriate polymer for the study (Gulati et al., 2021). Chitosan oligosaccharide lactate is a derivative of chitosan that is readily soluble in water and has additional properties making it biocompatible, non-toxic, mucoadhesive and non-allergenic with higher cellular transduction (Naveed et al., 2019). Mannan has over the years shown its targeting abilities in nanoparticles by acting as a ligand for the target delivery of a nanosystem to macrophages (Yu et al., 2010). Mannan oligosaccharide has been studied to have potent immunomodulatory effects in alveolar macrophages due to its ability to alter the cytokine responses of bacterial endotoxin-

induced alveolar macrophages by secreting TNF-α (Che et al., 2012). The combinatory use of chitosan oligosaccharide lactate and mannan oligosaccharide is expected to provide an enhanced host-directed immunomodulatory response to avoid harmful overstimulation of the immune system as evident in tuberculosis pericarditis (Che et al., 2012).

1.3. AIMS AND OBJECTIVES

This research aimed to develop a chitosan-mannan conjugated nanosystem for improving drug delivery of bedaquiline across the pericardium for the treatment of TBP. The system's mechanism of delivery may be attained through intraperitoneal and/or intra-pericardial injection to target the lymph node and pericardial membrane. The following objectives needed to be met to attain this:

1. To develop and validate a reverse-phase high-performance liquid chromatography (RP-HPLC) method for the detection and quantification of isoniazid, pyrazinamide and bedaquiline permeants across pericardial tissue.

2. To synthesise and optimise a bedaquiline-loaded chitosan-mannan nanosystem to a size of 100~200 nm, whilst ensuring adequate drug loading of bedaquiline. To perform physicomechanical and physiochemical characterisation of the bedaquiline loaded nanosystem.

3. To investigate the *ex vivo* diffusion behaviour of hydrophilic anti-TB drugs isoniazid, pyrazinamide across porcine pericardial tissue as compared to the *ex vivo* diffusion behaviour of bedaquiline-loaded nanosystem across porcine pericardium and human pericardial tissue.

4. To undertake compatibility analysis of the bedaquiline-loaded nanosystem on tissue samples using FTIR and transepithelial electrical resistance.

1.4. NOVELTY OF STUDY

1. The design of a novel easily reproducible copolymeric nanosystem made of chitosan-oligosaccharide lactate and mannan oligosaccharide for selective delivery of bedaquiline.

2. The nanosystem design was first to allow the penetration of lipophilic drugs across the pericardium. This was attained due to its hydrophilic and mucoadhesive surface made of mannan and chitosan. This enlightens a possible alternatively more effective treatment of TBP as compared to the conventional anti-TB regimen.

3. The study has shown that the ionic gelation of the polymer results in the surface modification of the nanosystem with mannan for prospective targeted delivery through mannan-binding lectin-induced phagocytosis.

1.5. OVERVIEW OF DISSERTATION

Chapter 1: This chapter provides a general overview of tuberculosis, extrapulmonary tuberculosis and the pericarditis category of the disease is introduced, and its pathophysiology was discussed. The challenges faced with standard anti-tubercular medicines permeating across the pericardium were also highlighted. This chapter further addressed the rationale and motivation of the study, the aims and objectives were detailed, and the novelty was outlined.

Chapter 2: This chapter reviews various types of immunomodulatory recognition receptors and their corresponding ligands. It collated recent conventional and complementary medicine with immunomodulatory effects used and/or in clinical trials for the treatment of tuberculosis through host-directed therapy.

Chapter 3: This chapter discusses the state-of-art in the recent development of surface-modified drug-delivery systems employed for targeted delivery. Several approaches used in the synthesis of modified polymeric nanosystems, and their outcomes were discussed. Furthermore, future perspectives regarding the formulation of nanosystems for active targeting using ligand-receptor pattern recognition were discussed.

Chapter 4: This chapter presents the development and validation of a RP-HPLC method for the quantification of isoniazid and pyrazinamide. *Ex vivo* diffusion studies of isoniazid and pyrazinamide across the pericardium were conducted and quantified on the HPLC to determine the steady state and permeation coefficient of the drugs across the pericardium.

Chapter 5: This chapter covers the pre-formulation design studies conducted to determine the appropriate nanosystem and parameters required to synthesise a nanosystem with good permeability properties. Various ratios and parameters of bedaquiline-loaded chitosan oligosaccharide lactate- mannan copolymeric (COS-MN-BQ) were synthesised and validated for their physicochemical properties using dynamic light scattering to determine their particle size and surface potential. The desired particle size and zeta potential were selected for further analysis. This chapter discusses the validation of a method for the quantification of mannan in the formulation using a nanophotometer UV-Vis. Lastly, this chapter describes the development and validation an RP-HPLC method for the quantification of bedaquiline.

Chapter 6: In this chapter, the selected COS-MN-BDQ nanoparticles were prepared and validated for fourier transform infrared (FTIR), thermal behaviour (TGA), x-ray powder diffraction (XRD), and scanning electron microscopy (SEM). The drug loading capacity (DLC), drug entrapment efficiency (DEE), and drug release were also validated. *Ex vivo* permeation studies of the formulation across the pericardium were then conducted and quantified on the HPLC to determine the amount of bedaquiline that passes through the porcine and human pericardium and determine the steady state and permeation coefficient of the drug across the pericardium.

Chapter 7: This chapter concluded the dissertation and provided an insight into future perspectives and recommendations in which the study can be enhanced.

1.6. REFERENCES

Baykal A., Amir M., Günerb S., and Sözeri H., (2015). Preparation and characterization of SPION functionalized via caffeic acid. Journal of Magnetism and Magnetic Materials, 395, 199-204.

Brodin B., Steffansen B., and Nielsen C.U., (2010). Passive diffusion of drug substances: the concepts of flux and permeability. Molecular Biopharmaceutics, 135-152.

Chaisson R.E., and Post, W.S., (2014). Immunotherapy for tuberculous pericarditis. New England Journal of Medicine, 371(1155), 7.

Fischer A.H., Jacobson K.A., Rose J., and Zeller R., (2008). Hematoxylin and eosin staining of tissue and cell sections. Cold Spring Harbor Protocols, 2008(5), pdb-prot4986.

Hawn T.R., Matheson A.I., Maley S.N., and Vandal O., (2013). Host-directed therapeutics for tuberculosis: can we harness the host?. Microbiology and Molecular Biology Reviews, 77(4), 608-627.

Howlett P., Du Bruyn E., Morrison H., Godsent I.C., Wilkinson K.A., Ntsekhe M., and Wilkinson R.J., (2020). The immunopathogenesis of tuberculous pericarditis. Microbes and Infection, 22(4-5), 172-181.

Isiguzo G., Du Bruyn E., Howlett P., and Ntsekhe M., (2020). Diagnosis and management of tuberculous pericarditis: What is new?. Current Cardiology Reports, 22(1), 1-8.

Jain S., Tran T.H., and Amiji M., (2015). Macrophage repolarization with targeted alginate nanoparticles containing IL-10 plasmid DNA for the treatment of experimental arthritis. Biomaterials, 61, 162-177.

Jakimów-Kostrzewa A., Małek Ł.A., Grabowski K., Werner B., and Brzewski M., (2017). A case of tuberculous pericarditis on cardiac magnetic resonance. Kardiologia Polska, 75(12), 1354.

Ke X., Howard G.P., Tang H., Cheng B., Saung M.T., Santos J.L., and Mao H.Q., (2019). Physical and chemical profiles of nanoparticles for lymphatic targeting. Advanced Drug Delivery Reviews, 151, 72-93.

Kulkarni P., Rawtani D., Kumar M., and Lahoti S.R., (2020). Cardiovascular drug delivery: a review on the recent advancements in nanocarrier based drug delivery with a brief emphasis on the novel use of magnetoliposomes and extracellular vesicles and ongoing clinical trial research. Journal of Drug Delivery Science and Technology, 60, 102029.

Lelovas P.P., Kostomitsopoulos N.G., and Xanthos T.T., (2014). A comparative anatomic and physiologic overview of the porcine heart. Journal of the American Association for Laboratory Animal Science, 53(5), 432-438.

Li L., Okada H., Takemura G., Kosai K.I., Kanamori H., Esaki M., Takahashi T., Goto K., Tsujimoto A., Maruyama R. and Kawamura I., (2009). Postinfarction gene therapy with adenoviral vector expressing decorin mitigates cardiac remodeling and dysfunction. American Journal of Physiology-Heart and Circulatory Physiology, 297(4), H1504-H1513.

Lima N.A., Lino D.O.D.C., Coelho N.M., and Melgar T., (2019). Tuberculous constrictive pericarditis. British Medical Journal Case Reports, 12(7).

Liu S., Chen X., Bao L., Liu T., Yuan P., Yang X., Qiu X., Gooding J.J., Bai Y., Xiao J. and Pu F., (2020). Treatment of infarcted heart tissue via the capture and local delivery of circulating exosomes through antibody-conjugated magnetic nanoparticles. Nature Biomedical Engineering, 4(11), 1063-1075.

Luque-Michel E., Lemaire L., and Blanco-Prieto M.J., (2021). SPION and doxorubicin-loaded polymeric nanocarriers for glioblastoma theranostics. Drug Delivery and Translational Research, 11(2), 515-523.

Matthews K., Deffur A., Ntsekhe M., Syed F., Russell J.B., Tibazarwa K., Wolske J., Brink J., Mayosi B.M., Wilkinson R.J. and Wilkinson K.A., (2015). A compartmentalized profibrotic immune response characterizes pericardial tuberculosis, irrespective of HIV-1 infection. American Journal of Respiratory and Critical Care Medicine, 192(12), 1518-1521.

Mayosi B.M., Ntsekhe M., Bosch J., Pandie S., Jung H., Gumedze F., Pogue J., Thabane L., Smieja M., Francis V. and Joldersma L., (2014). Prednisolone and *Mycobacterium indicus* pranii in tuberculous pericarditis. New England Journal of Medicine, 371(12), 1121-1130.

Mutyaba A.K., and Ntsekhe M. (2017). Tuberculosis and the heart. Cardiology Clinics, 35(1), 135-144.

Noubiap J.J., Agbor V.N., Ndoadoumgue A.L., Nkeck J.R., Kamguia A., Nyaga U.F., and Ntsekhe M., (2019). Epidemiology of pericardial diseases in Africa: a systematic scoping review. Heart, 105(3), 180-188.

Ntsekhe M., and Mayosi B.M., (2013). Tuberculous pericarditis with and without HIV. Heart Failure Reviews, 18(3), 367-373.

Peng N., Wu B., Wang L., He W., Ai Z., Zhang X., Wang Y., Fan L., and Ye Q., (2016). High drug loading and pH-responsive targeted nanocarriers from alginate-modified SPIONs for anti-tumor chemotherapy. Biomaterials Science, 4(12), 1802-1813.

Phelan D., Collier P., Grimm R.A., Cleveland Clinic, Disease Management Published: July 2015. https://www.clevelandclinicmeded.com/medicalpubs/diseasemanagement/cardiology/pericardial-disease/) Accessed on the 03/22/2021.

Quy D.V., Hieu N.M., Tra P.T., Nam N.H., Hai N.H., Thai Son N., Nghia P.T., Anh N.T.V., Hong T.T. and Luong N.H., (2013). Synthesis of silica-coated magnetic nanoparticles and application in the detection of pathogenic viruses. Journal of Nanomaterials, 2013.

Rehman I., Nassereddin A., and Rehman A., (2020). Anatomy, Thorax, Pericardium. StatPearls [Internet] [Accessed on the 24 December 2023].

Sanduzzi A., Ponticiello A., Bocchino M., Perna F., and Vatrella A., (2016). Latent tuberculosis infection (LTBI): a real host defence or a permanent threat. Le Infezioni in Medicina, (3), 179-182.

Saqib U., Sarkar S., Suk K., Mohammad O., Baig M.S., and Savai R., (2018). Phytochemicals as modulators of M1-M2 macrophages in inflammation. Oncotarget, 9(25), 17937.

Sarathy J.P., Liang H.P.H., Weiner D., Gonzales J., Via, L.E., and Dartois, V., (2017). An *in vitro* caseum binding assay that predicts drug penetration in tuberculosis lesions. Journal of Visualized Experiments, (123), e55559.

Shao L., Zhang Y., Pan X., Liu B., Liang C., Zhang Y., Wang Y., Yan B., Xie W., Sun Y. and Shen Z., (2020). Knockout of beta-2 microglobulin enhances cardiac repair by modulating exosome imprinting and inhibiting stem cell-induced immune rejection. Cellular and Molecular Life Sciences, 77(5), 937-952.

Shenje J., Adimora-Nweke F.I., Ross I.L., Ntsekhe M., Wiesner L., Deffur A., McIlleron H.M., Pasipanodya J., Gumbo T. and Mayosi B.M., (2015). Poor penetration of antibiotics into pericardium in pericardial tuberculosis. EBioMedicine, 2(11), 1640-1649.

Skrahin A., Ahmed R.K., Ferrara G., Rane L., Poiret T., Isaikina Y., Skrahina A., Zumla A. and Maeurer M.J., (2014). Autologous mesenchymal stromal cell infusion as adjunct treatment in patients with multidrug and extensively drug-resistant tuberculosis: an open-label phase 1 safety trial. The Lancet Respiratory Medicine, 2(2), 108-122.

Spodick D.H., (1956).Tuberculous pericarditis. American Medical Association Archives of Internal Medicine, 98(6), 737-749.

Srivastava S., Ernst J.D., and Desvignes L., (2014). Beyond macrophages: the diversity of mononuclear cells in tuberculosis. Immunological Reviews, 262(1), 179-192.

Vu T.T., Marquez J., Le L.T., Nguyen A.T.T., Kim H.K., and Han J., (2018). The role of decorin in cardiovascular diseases: more than just a decoration. Free Radical Research, 52(11-12), 1210-1219.

Willard-Mack C.L., (2006). Normal structure, function, and histology of lymph nodes. Toxicologic Pathology, 34(5), 409-424.

World Health Organization Global tuberculosis report (2020). Licences: CC BY-NC SA 3.0 IGO.

CHAPTER TWO

IMMUNOMODULATORY STRATEGIES EMPLOYED BY HOST-DIRECTED THERAPIES FOR COMBATING TUBERCULOSIS

Biomedicine & Pharmacotherapy 162 (2023) 114588

Contents lists available at ScienceDirect

Biomedicine & Pharmacotherapy

journal homepage: www.elsevier.com/locate/biopha

Review

Advances in immunomodulatory strategies for host-directed therapies in combating tuberculosis

Simisola Ayodele [a], Pradeep Kumar [a], Armorel van Eyk [b], Yahya E. Choonara [a,*]

[a] Wits Advanced Drug Delivery Platform Research Unit, Department of Pharmacy and Pharmacology, School of Therapeutic Sciences, Faculty of Health Sciences, University of the Witwatersrand, Johannesburg, 7 York Road, Parktown, 2193, South Africa
[b] Department of Pharmacy and Pharmacology, University of the Witwatersrand, Johannesburg, 7 York Road, Parktown, 2193, South Africa

Tuberculosis (TB) maintains its infamous status regarding its detrimental effect on global health, causing the highest mortality by a single infectious agent. The presence of resistance and immune-compromising disease favours the disease in maintaining its footing in the health care burden despite various anti-TB drugs used to fight it. The main factors contributing to resistance and difficulty in treating disease include prolonged treatment duration (at least 6 months) and severe toxicity, which further leads to patient non-compliance, and thus a ripple effect leading to therapeutic non-efficacy. New drugs and other means of treatment are urgently required to curtail and minimize the global presence of the disease. The efficacy of new regimens demonstrates that targeting host factors concomitantly with the *Mycobacterium tuberculosis* (*M.tb*) strain is urgently required. The urgent need for a solution makes new drug research and development an unattractive idea, due to the huge expense and time required of up to 20 years, to put this into effect. For this reason, drug repurposing may be the most economical, circumspective, and conveniently faster journey to embark on. Host-directed therapy (HDT) will dampen the burden of the disease by acting as an immunomodulator, allowing it to defend the body against antibiotic-resistant pathogens whilst minimizing the possibility of developing new resistance to susceptible drugs. Repurposed drugs in TB act as host-directed therapies, acclimatizing the host immune cell to the presence of TB, improving its antimicrobial activity and time taken to get rid of the disease, whilst minimizing inflammation and tissue damage. In this review, we, therefore, explore possible immunomodulatory targets, HDT immunomodulatory agents, and their ability to improve clinical outcomes whilst minimizing the risk of drug resistance, through various pathway targeting and treatment duration reduction.

2.1. INTRODUCTION

Tuberculosis has over the years, proven to be of extreme clinical importance, affecting a large proportion of the world's population and persisting as the leading cause of death by a single infectious agent (Cohen et al., 2019). South Africa is one of the eight countries that account for two-thirds of the global TB cases, contributing approximately 3% of the total (Organization, 2020). The reduction in the burden of the disease had shown great proportionality with the clinical and scientific efforts employed in combating the disease when anti-TB drugs were introduced but since the emergence and progression of resistant Mycobacteria tuberculosis (*M.tb*) strains, the cycle of the burden continues. Although TB is predominantly a pulmonary disease, it also affects other sites (extrapulmonary TB) presenting as other serious manifestations of the disease, contributing to 16% of worldwide tuberculosis cases (WHO, 2020). Even with its lesser percentage, extrapulmonary TB has also caught the attention of researchers due to diagnostic and therapeutic challenges (Howlett et al., 2020).

Presently, the standard first-line anti-TB treatment used is the 4-drug combination of Rifampicin (RIF), Isoniazid (INH), Pyrazinamide (PZA), and Ethambutol (EMB) for 6 months. Although 85% of the patients are successfully treated, the side effect profile and lengthy duration of treatment affect patient compliance (Tousif et al., 2014). For this reason, various other treatments with a mechanism of action that may shorten the treatment regimen and improve tolerance and adherence to therapy have been and are being studied to obtain a better overall outcome (Fatima et al., 2021). Multi-drug resistant TB (MDR-TB) treatment regimens, have an even lesser success rate as compared to susceptible first-line treatment, successfully treating only 57% of MDR-TB cases (WHO, 2020). Paramount limitations of these MDR-TB treatments include atypical and immoderate host inflammatory response to the bacteria causing tissue destruction, which further compromises the body's response and ability to eradicate the bacteria. These limitations have also been presented in extrapulmonary TB such as TBP. Since HIV is the main co-morbidity of TB, it is worthwhile to know that early restoration of immune cells in HIV-TB patients following antiretroviral therapy (ART) can result in the development of immune reconstitution inflammatory syndrome (TB-IRIS). TB-IRIS is an exaggerated inflammatory reaction in response to antiretroviral therapy for immune recovery in HIV patients due to a short interval between starting an anti-TB regimen and ARTs (Gopal et al., 2017). This IRIS may also cause tissue damage and promote a high mortality rate, therefore needs to be taken cognisance of and avoided.

Immunomodulation is the alteration of immune response productively or detrimentally using a drug or compound (Saroj et al., 2012). Drug repurposing HDTs is mainly being employed in TB immunomodulatory therapy, to treat harmful inflammatory responses in MDR/ extensively drug-resistant TB (XDR-TB) patients to avoid tissue damage. Although these strategies have proven to be mainly advantageous, exigent studies are required to improve and assure the prospect of this adjunct therapy in the treatment of inflammatory-related TB conditions. Drug repurposing/repositioning is the identification of new therapeutic usage of an already existing drug, paying attention to its pharmacodynamics and interaction with other receptors that may enhance the treatment of a disease it was not originally approved to treat. Drug repositioning was discovered in drugs like sildenafil by serendipity, whereby it was initially used as an anti-hypertensive and then discovered to be used for erectile dysfunction (Fatima et al., 2021; Moreland et al., 1999). A typical repurposed drug for TB is avermectin which was initially indicated for river blindness and elephantiasis as in Figure 2.1. Due to the drugs already being approved for an indication, the safety of the drug is already established, and only the quality and efficacy in the new indication will be needed for the approval. The duration of 12 years on average for new drug discovery and development is then cut to ~3-4 years for a drug to enter the clinic (Chan et al., 2019; Fatima et al., 2021).

Host-directed Immunomodulators are expected to decrease treatment duration and decrease host-response inflammatory toxicity that further hinders the efficacy of treatment (Fatima et al., 2021). Furthermore, HDT is prospective as it may allow the treatment of drug-resistant TB, with minimal exposure to TB drugs in order to prevent/ slow down the development and/or spread of superbugs. Combinatory use of HDTs with conventional therapy uses a dual/multi-mechanism treatment allowing synergism and thus permitting a possible dose lowering of the drugs, to minimize toxicity without affecting the treatment efficacy. Immunomodulation in TB is not restricted to the use of traditional anti-inflammatory drugs like non-steroidal anti-inflammatory drugs (NSAIDs) and corticosteroids. Drugs like vitamin D, phenylbutyrate (PBA), metformin, and even thalidomide have also been studied as adjunct therapy for their immunomodulatory functions in TB infections (Bekele et al., 2018; Schoeman et al., 2004).

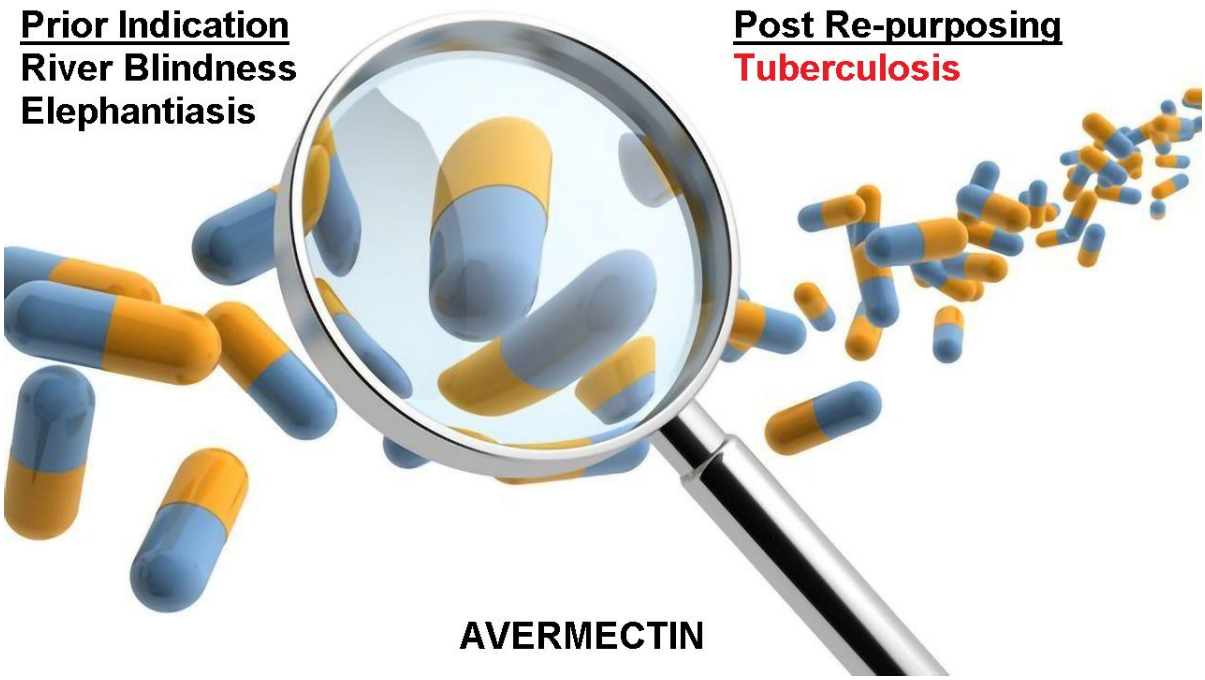

Figure 2.1: Repurposed indications of avermectin.

2.2. INNATE AND ACQUIRED IMMUNITY IN CURTAILING THE PROLIFERATION OF TB.

The immune system includes cells that act as a guard that is initially activated upon contact with antigens. These cells are innate immune cells that are activated when pathogens like TB enter the body namely dendritic cells (DCs), macrophages, monocytes, natural killer cells (NKs), and neutrophils. They are vital in preventing 90-95% of TB from being active and laying only latent TB (Pahari et al., 2017). These sentinels are active in the complement pathway, assisting in phagocytosis by opsonization, inflammation, and membrane attack for cell lysis (Pahari et al., 2017).

The infection primarily gains access to the body from the lungs through the respiratory tract. As in other inflammatory responses, neutrophils are initially activated and confront the bacterium, phagocytose it and alert the other cells of the immune system. Macrophages and DCs are activated and together with alveolar epithelial cells and connective tissue contribute to curtailing and entrapping the bacterium. Epithelial cells produce chemokines like interleukin-8 and interferon-γ (IFN-γ) against *M.tb* (Sharma et al., 2007). Interleukin-8 activates neutrophils attracting them towards the alveolar cells, which releases granzymes, and other cellular changes which include degradation of connective tissue constituents (Bickel, 1993). IFN-γ assists in the priming of cells to produce nitric oxide (NO) at concentrations that are mycobactericidal, representing the first line of innate immunity (Sharma et al., 2007). The infected macrophages are attacked by NK cells which subsequently further release IFN-γ and

major cytokines such as type 1 IFN. This further activates more macrophages and DCs (Pahari et al., 2017). Gamma delta T cells (γδ T cells) are other cells also involved in presenting antigens that activate CD4 and CD8 T cells.

A simultaneously effective innate and acquired immunity (circulating regulatory T cell levels) is expected to decrease susceptibility to *M.tb*. In a study population of infants, a well-defined difference in the immune responses and circulating regulatory T cell levels contributed to their susceptibility to the *M.tb* (Whittaker et al., 2018). The Bacillus Calmette-Guérin (BCG) as well as other vaccines such as typhoid, cholera, rotavirus, and smallpox vaccines have effectively enhanced the nasopharynx immunity and enhanced the first-line immunity of the respiratory tract in eliminating the infection before reaching the alveolar cells.

BCG is the only TB vaccine available for use, and even though it demonstrates enhancement in nasopharynx immunity and neonatal disseminated and meningeal TB, it fails to protect against adult pulmonary TB (Singh et al., 2016, 2020). The cells important in acquiring immunity include T effector memory (T_{EM}) cells and T central memory (T_{CM}) cells. T_{EM} cells with little to no proliferative abilities are responsible for protecting against acute TB infections through Th1 IFN-y-producing cells and T_{CM} cells generate T_{EM} cells providing vaccine efficacy. Therefore, an ample amount of T_{CM} cells is ideal for an effective and long-term protective vaccine. T_{CM} cells will allow the continuous production of T_{EM} cells, IFN-y release and M1 macrophage-mediated bacterial elimination. T_{EM} cells and T_{CM} cells are expressed with Kv1.3 and KCa3.1 ion channels, respectively. The inhibition of Kv1.3 induces the reversal of T_{EM}: T_{CM} cell ratios, favouring a higher T_{CM}: T_{EM} cell ratio which is necessary for enhanced host immunity (Gocke et al., 2012; Singh et al., 2016, 2020).

The innate system maintains specificity during the pro-inflammatory cascade by pathogen-associated molecular patterns (PAMPs), using pattern recognition receptors (PRRs) expressed on cells serving to perform both innate and acquired immunity as in Figure 2.2 (Turvey and Broide, 2010). The PRRs recognize molecular patterns/structures that are expressed by a diverse number of microbes (Janeway, 1989). The receptors include toll-like receptors (TLRs), C-type lectin receptors (CLRs), NOD-like receptors (NLRs), and DC-specific intercellular adhesion molecule-3-grabbing non-integrin (DC-SIGN). Studies have shown that these receptors play a crucial role in ensuring cell internalization, entrapment, and elimination of microbes. These receptors can therefore be used for drug selective and specific delivery against TB.

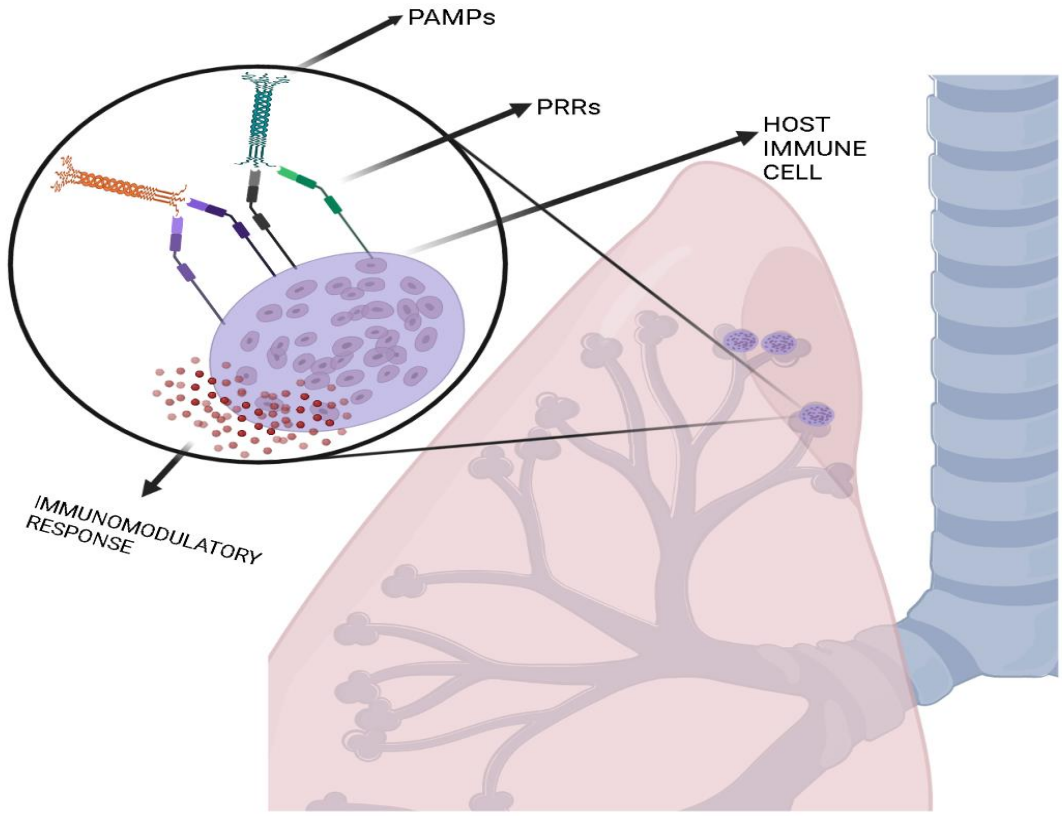

Figure 2.2: Diagram showing the interaction of pathogen-associated molecular patterns with pattern recognition receptors to elicit an immune response. Created in Biorender.com.

The interaction of macrophages and DCs engulfed *M.tb* antigens and the PRRs further triggers the production of cytokines like tumor necrosis factor-α (TNF-α) and interleukin-12 (IL-12), which together with the chemokines trigger various immune cells to surround the phagocytes and cause the formation of granulomas which bolster a microenvironment for the interaction of the *M.tb* antigen with immune cells. The same granulomas have conflictingly been found to be a 'niche' for the pathogen to grow continuously by preventing the fusion and acidification of phagolysosomal compartments which promotes the killing of the pathogen (Deretic et al., 2006; Kolloli and Subbian, 2017; Orme and Basaraba, 2014).

Macrophages remain vital in their contribution against tuberculosis due to their ability to polarize in favour of or against cell proliferation and tissue repair. M1-type macrophages release cytokines responsible for inhibiting cell proliferation and maintaining inflammation whilst the M2-type macrophages release cytokines responsible for enhancing cell proliferation, resolving inflammation and tissue repair. In the early stages of TB, macrophages are polarised towards the M1 type to fight the infection and in the later stage of the disease towards the M2 type for tissue repair. The imbalance in the M1-M2 polarization tends to result in complications, such as excessive inflammation and tissue damage in M2 deficiency and disease progression

in M1 deficiency. Activation of recognition receptors can drive macrophages towards either M1 or M2 polarization. M1 macrophages can be polarised to M2 macrophages in the presence of Th2 cytokines such as IL-4, IL-10 and IL-13 whilst M2 can be repolarised to M1 in the presence of TLRs and Th1 cells cytokines such as IFN-y (Abdelaziz et al., 2020; Lee, 2019; Martinez and Gordon, 2014; Wang et al., 2014).

Additionally, infected phagocytes together with other cells like γδ T cells (Meraviglia et al., 2011), can migrate to regional draining lymph nodes and prime $CD4^+$ and $CD8^+$ cells to produce pro-inflammatory IFN-γ and interleukin-17 (IL-17) in acquired immunity. IFN-γ for *M.tb* infected cells causes apoptosis and attracts $CD4^+$ and cytotoxic T lymphocytes to the granuloma site for further antigen presentation and *M.tb* killing (Russell et al., 2009). IL-17 cytokine enhances the Th1 immune response by triggering an enhanced release of IFN-γ and IL-12 from antigen-presenting cells (APCs) (Lin et al., 2009). Furthermore, NK cells, NK T cells, and $CD8^+$ T cells secrete an array of cytotoxic molecules, such as perforin, and enzymes such as granzymes that kill intracellular bacteria and in addition to all aforementioned pro-inflammatory cascade, causes excess inflammation. This inflammation necrotises the infected cells leading to lung tissue damage, as well as other tissue damage in extrapulmonary TB, such as constrictive pericarditis (Ramasamy et al., 2018).

Consequently, treatment strategies to alleviate the disease such as minimizing or preventing host cell damage by modulation and suppression of host inflammatory response, runs a risk of elevating the possibility of latent infections to reactivate, or accelerate the progression of already established TB disease. For example, countering TNF-α led to the reactivation of TB in latent infections and disease progression (Keane et al., 2001; Lin et al., 2010), and even though this study shows great prospects, more ground-breaking research is needed to be established.

2.3. RECOGNITION RECEPTOR AND CORRESPONDING LIGANDS FOR INNATE IMMUNITY MODULATION.

2.3.1. Toll-Like Receptors (TLRs)

TLRs are the first class of the PRRs to be identified, immensely studied, and characterised (Kawasaki and Kawai, 2014). They are part of the first-line components to attack a pathogen in the innate immune response (Pahari et al., 2017). They are expressed on both macrophages and dendritic cells as well as non-immune fibroblast and epithelial cells. TLRs are subclassified into cell surface TLRs and intracellular TLRs ranging from TLR 1-13, with cell surface TLRs including TLR-1, 2, 4, 5, 6, and 10. TLR-1, 2, and 6 recognizes a wider

variety of diverse PAMPs from pathogens than the other receptors, including lipoproteins, peptidoglycans, lipoteichoic acids, zymosan, mannan, and tGPI-mucin (Kawai and Akira, 2010). TLR-4 recognizes bacterial lipopolysaccharide (LPS), and TLR-5 recognizes bacterial flagellin (Akira et al., 2006). TLR-10 can also sense influenza A virus infection and together with TLR-2 recognize ligands from listeria (Lee et al., 2014; Regan et al., 2013). Intracellular TLRs generally recognize bacterial or viral nucleic acids. When TLRs recognise a PAMP and recruit a specific set of adaptor molecules, which bind to structural domain Toll-IL-1 receptors (TIR), such as MyD88 (myeloid differentiation primary response gene 88) and TRIF (TIR-domain-containing adapter-inducing IFN-β), it results in downstream signalling events which include cytokines, chemokines, type I IFNs, and antimicrobial peptides (Kawai and Akira, 2010). *M.tb* mediated cellular activation is mainly through TLR-2 and 4 (Pahari et al., 2017), and intracellular TLR-9, which recognizes bacterial and viral DNA that is ample in unmethylated CpG-DNA whilst also recognizing the byproduct of haemoglobin degradation by plasmodium falciparum's hemozoin (Coban et al., 2010).

TLR-2 signalling elicited response is through mycobacterial lipoproteins, protease-resistant, soluble heat stable, and heat resistant membrane-associated factors which trigger induction of cytokines like IL-12 (Thoma-Uszynski et al., 2000). TLR-4 signalling is also elicited for heat-resistant membrane-associated factors (Underhill et al., 1999) and is pivotal because studies have shown that the absence of intact TLR-4 minimizes macrophages recruitment and pro-inflammatory cytokine responses thus increasing susceptibility to tuberculosis infection (Abel et al., 2002). The signalling through the ligand Pam2Cys on TLR-2 has been shown to rescue Th1 cells from wearing out during chronic *M.tb* infection (Chodisetti et al., 2015). Furthermore, the TLR-9 found in APCs triggers a potent Th1 response whilst cooperating with TLR-2 in mediating an optimal antimycobacterial effect against *M.tb* (Bafica et al., 2005).

To prevent inflammatory tissue damage and fibrosis, mitigation of the TLR signalling using negative regulators is employed to target adaptor molecules that are key in TLR signalling. MyD88 or TRIF are hindered from binding to TLRs. The MyD88-dependent pathway is suppressed by ST2825, suppressor of cytokine signaling-1 (SOCS1), and Cbl-b, whilst the TRIF-dependent pathway is suppressed by sterile α- and armadillo-motif-containing protein (SARM) and TRAM adaptor with Golgi dynamics [GOLD] domain (TAG) (Kawai and Akira, 2010). The ST2825 molecule significantly hinders the production of pro-inflammatory and anti-inflammatory cytokines mediated by the activation of the LPS-TLR-4 pathway (Ramírez-Pérez et al., 2020). SOCS1 negatively regulates the LPS signalling of TLR-4 (Kinjyo et al., 2002). SARM represses both TRIF- and MyD88-mediated AP-1 activation (Peng et al., 2010). TAG is a splice variant of the adaptor (Toll/IL-1R domain-containing adaptor-inducing IFN-β-related

adaptor molecule) TRAM, which has GOLD domain-containing proteins localized to late endosomes which can down-regulate TRIF-dependent signalling by displacing TRIF from TRAM during signalling (Palsson-McDermott et al., 2009).

Decorin is an extracellular matrix protein that modulates the process of inflammation and fibrillogenesis responsible for fibrosis and tissue damage (Robinson et al., 2005). Decorin has been found to bind to TLR -2 and -4 in the tumor microenvironment to suppress inflammation (Zhang et al., 2018). Most recently its use was employed in COVID-19 studies, and it showed positive outcomes in preclinical studies by improving lung functions during COVID-19 related complications such as lung fibrosis (Allawadhi et al., 2021). Although no studies have been performed on the use of decorin for *M.tb*, it may be suggestive of adjunct immunomodulatory therapy in preventing tissue damage and fibrosis caused by *M.tb*.

2.3.2. C-Type Lectin Receptors (CLR)

CLRs are found on the surfaces of large groups of proteins, unlike TLRs which have multiple possible domains for signalling pathogens including *M.tb* and are expressed on macrophages DCs, and additionally NK cells (Kerrigan and Brown, 2011). Their interaction enhances antigen presentation to modulation and differentiation of T helper cells inducing both innate and acquired immunity. CLRs present as either soluble proteins found in serum or as transmembrane proteins such as mannose-binding lectins (MBL) or Dectin-1 (D-1). MBL acts by activating the complement system and attaches to a broad range of carbohydrate structures on its target pathogen (Yamasaki et al., 2008). D-1 collaborates with TLR-2 to stimulate cytokine response in macrophages as well as stimulate DC maturation (Gantner et al., 2003; Romero et al., 2016).

DC-SIGN (DC-specific intercellular adhesion molecule (ICAM)-3-grabbing non-integrin; also known as CD209) expressed on CD1c+, subepithelial, inflammatory DC cells, as well as some macrophages, is the most vastly researched CLR (Geijtenbeek and Gringhuis, 2009). Although the activation of DC-SIGN by carbohydrates does not induce cytokine expression, it modulates signalling pathways induced by other PRRs (Geijtenbeek and Gringhuis, 2016). DC-SIGN recognizes intracellular pathogens such as mycobacteria, viruses, and fungi through mannose-containing PAMPs (Geijtenbeek and Gringhuis, 2009), and together with other PRRs like TLR-4, they enhance the protective response of TH-1 and -17 as in Figure 2.3. *M.tb* expresses mannose-capped lipoarabinomannan (ManLAM) PAMP, which simultaneously triggers TLR-4 and activates p65–p50 transcriptional complexes. A downstream signalling expression event results in the production of pro-inflammatory cytokines such as IL-12p35, IL-12p40, and IL-6 (Gringhuis et al., 2009). In DC-SIGN, binding to RAF-1 results in the

phosphorylation and acetylation of NF-κB subunit p65 at Ser276 and together with TLR-4 increases transcription of IL-12A, IL-12B, and IL-6 by TLR (Gringhuis et al., 2007), as well as active IL-12p70 which promotes the protective response of TH-1 cell. A DC-SIGN homologue, SIGNR3 (CD209D) triggered in a study of *M.tb* infected mice, showed similar activation of RAF-1 and cooperation with TLR-2 to induce pro-inflammatory cytokine expression and protective immunity (Tanne et al., 2009).

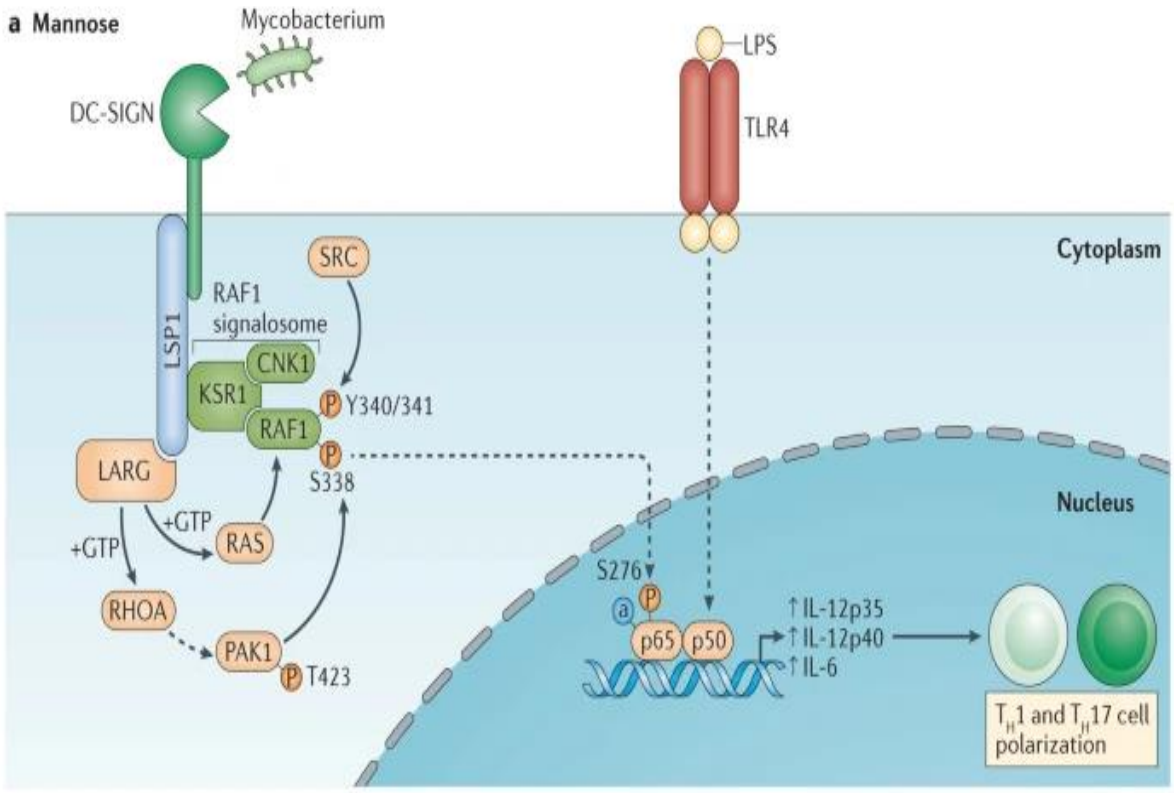

Figure 2.3: Recognition of mycobacteria, a mannose containing DC-specific intercellular adhesion molecule-3-grabbing non-integrin, and toll-like receptor -4 simultaneous ligation, to activate p65–p50 complexes, which enhances expression of genes, which promotes T helper 1 (TH1) and TH17 cell differentiation. Figure obtained with permission.

Dectin-2 unlike DC-SIGN, which signals itself, collaborates with the signalling adaptor Fc receptor common γ-chain (FcRγ) which stimulates signalling through its immunoreceptor tyrosine-based activation motif (ITAM). They have been seen to interact with mycobacterial ManLAM on subsets of various macrophages and DCs. These interactions stimulate a pro- and anti-inflammatory cascade which is composed of the release of pro-inflammatory TNF, IL-6, IL-12p40, and IL-23 cytokines which ultimately promote TH-17 cell differentiation and anti-inflammatory IL-10 and IL-2 cytokines (Yonekawa et al., 2014).

Macrophage-inducible C-type lectin receptors (MINCLE) are responsible for sensing necroptosis, a form of inflammatory induced cell death (Yamasaki et al., 2008). Found on the

surfaces of DCs, macrophages, and neutrophils, they also contribute to immunity against *M.tb* (Schoenen et al., 2010). *M.tb* contains a glycolipid structure, mycobacterial cord factor, which is composed of trehalose dimycolate on its outer membrane and is a ligand for MINCLE (Jégouzo et al., 2014). MINCLE function is partially modulated by macrophage C-type lectin coexpression which consequently increases the expression of MINCLE. MINCLE together with MCL recognises trehalose dimycolate and induces innate immune signalling, via FcRγ, resulting in NF-κB activation and T cell polarizing cytokines release of IL-6, IL-1β, IL-23, and IL-12 that promotes protective TH1 and TH17 differentiation (Werninghaus et al., 2009).

Table 2.1: C-type lectin receptors target *Mycobacterium tuberulosis* and its cytokines responsible for TH cells polarization.

PAMP/Ligand	Cytokines released	Polarised cells	References
Mannose-capped lipoarabinomannan (ManLAM)	TLR-4, IL-12p35, IL-12p40 and IL-6	TH1 and TH17 cell	(Geijtenbeek and Gringhuis, 2016)
RAF	NF-κB subunit p65 at Ser276, TLR-4, IL12A, IL12B and IL6, IL-12p70	TH-1 cell	(Gringhuis et al., 2007)
Immunoreceptor tyrosine-based activation motif (ITAM)	(TNF), IL-6, IL-12p40 and IL-23, and anti-inflammatory IL-10 and IL-2 cytokines	TH17 cell	(Yonekawa et al., 2014)
Macrophage-inducible C-type lectin receptors (MINCLE)	NF-κB, IL-6, IL-1β, IL-23, IL-12 activation	TH1 and TH17 cells	(Werninghaus et al., 2009)

2.3.3. Nucleotide-Binding and Oligomerization Domain- Like Receptors (NLRs)

Nucleotide-binding and oligomerization domain, NLRs, is the most recent PRRs. NOD-1 and NOD-2 are subclasses that both have an amino-terminal caspase activation and recruitment

domain (CARD), which contribute by stimulating NF-κB signalling, subsequently causing the enhanced release of pro-inflammatory cytokines which include, IL-1β, IL-6, TNF, and IL-8. Additionally, chemokines, nitric oxide, and antimicrobial peptides (β-defensin 2) are also released (Pahari et al., 2017). Mitogen-activated protein kinases (MAPK), Jun N-terminal kinase (JNK), and p38 signalling pathways are intensified by NOD-2 and adaptor protein CARD9 (Hsu et al., 2007). It is seemingly that NLRs have a pivotal role in innate and protective immunity and are very important in TB. Although its specific role is still undefined, a mutation in the gene gives an opening for opportunistic infection. A study of NOD-2−/− *M.tb* infected mice showed impaired macrophages and DCs cytokine production for T cell differentiation, thereby causing higher *M.tb* morbidity and mortality (Divangahi et al., 2008; Saiga et al., 2011). With more studies performed on the effect of NLRs on T cell differentiation, more light might be shed on a more specific pathway at which NOD-1 and -2 perform.

NOD-2 is thought to collaborate with TLR-2/TLR-4 in pro-inflammatory cytokines stimulation as evident in the synergistic activation of DCs for antigen presentation to T cells, $CD4^+$ and $CD8^+$ cells and reduction in the dose required of TB drugs through NOD-2 and TLR-4 to combat intracellular *M.tb* (Khan et al., 2016). The antigen-antibody interactions resulting in enhanced IFN-γ and TNF-α cytokines release, important in promoting sustained protective immunity (Kaufmann, 2001; Pahari et al., 2017).

2.4. DRUGS AS IMMUNOMODULATORS FOR TREATMENT TB THROUGH HOST-DIRECTED THERAPIES

Although most host-directed therapies are from repurposed drugs as in Figure 2.4 with different currently approved indications, one of the first-line anti-TB drugs, RIF, has shown immunomodulatory properties. A study on lipopolysaccharide-stimulated human monocytes showed a significant up-regulatory effect on IL-6 and IL-10 and a down regulatory effect on IL-1β and TNF-a (Ziglam et al., 2004). Apart from its antibacterial properties, its uses have also been employed in auto-immune disease and dermatological inflammatory diseases such as the suppression of inflammation in psoriasis through suppression of humoral and cellular immunological response as well as T cell function (Păunescu, 1970; Pradhan et al., 2016). Other skin diseases treated include hair follicles and granulomatous. It suppressively alters immunomodulatory gene expression on inflammatory cells like neutrophils, basophils, and eosinophils (Mebazaa et al., 2009). RIF has been interestingly suggested as a drug that can be repurposed as a TLR- inhibitor for use in neuropathic pain, due to its inhibitory effect on TLR-4 signalling by targeting myeloid differentiation protein 2. RIF suppresses LPS-induced TNF-α and IL-1β production in RAW 264.7 macrophage cells (Wang et al., 2013). LPS was employed for TLR-4 blocking. By inhibiting NF-kB which is involved in MyD88-dependent and

independent TLR-4 pathways. Although no studies on its immunomodulatory effects on TB have been reported. Based on its targets, it may be suggestive to have added properties other than its anti-mycobacterial effects. Like RIF, INH's apparent effect of use in other immune conditions, such as auto-immune psoriasis, causes psoriasis lesions to almost disappear in 6 weeks (Chiriac et al., 2014). More studies need to be performed to understand the mechanism of action of this observed effect.

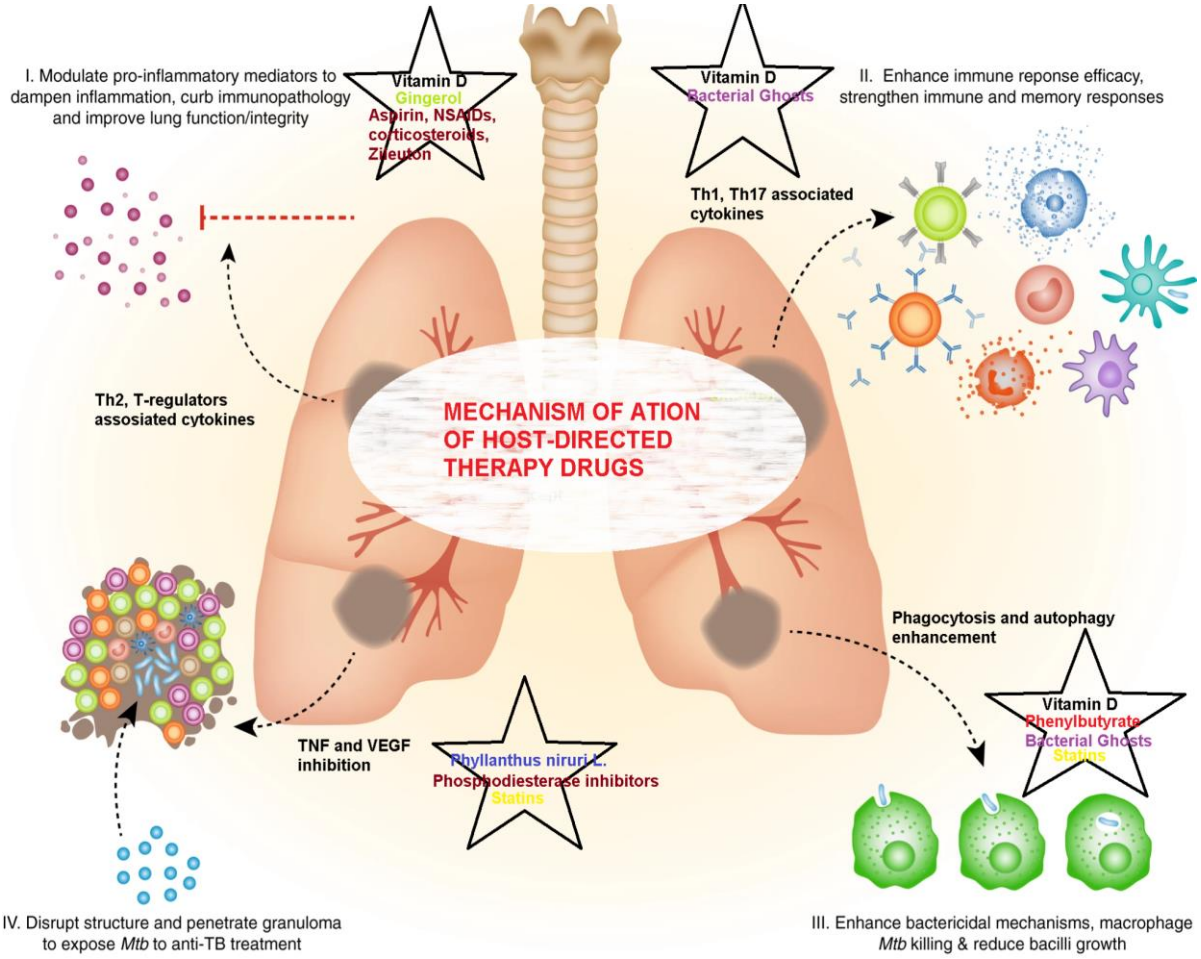

Figure 2.4: Diagram showing the mechanism of action of various repurposed immunomodulatory drugs for the treatment of *Mycobacterium tuberulosis*. Figure adapted with open access permission from [71], http://creativecommons. org/licenses/by/4.0.

Macrolides are another class of antibiotics that act by interfering with bacterial protein synthesis, binding to the 50S ribosomal subunit. In a study checking the effects of RIF and erythromycin on immunomodulatory gene expression in human polymorphonuclear lymphocytes, it was found that apart from the TLR-2, TLR-4, CD-14, and IL-8R expression inhibition by RIF, erythromycin also inhibited the expression of TLR2 and TNF-α suggesting an anti-inflammatory role of macrolide in the treatment of TB (Mu et al., 2013). Clarithromycin is a group example 5 anti-TB drug according to the World Health Organisation (WHO) and although the macrolides present with a lower anti-tubercular activity against *M.tb*, their

potential benefits present from their immunomodulatory effects and synergism with other anti-TB drugs. They accumulate in the relevant compartments and cells in the lungs, by disorganizing the cell envelope for improved permeation of the bactericidal anti-TB drugs (van der Paardt et al., 2015). To gain more insight into the immunomodulatory effect of macrolides, a clinical trial on azithromycin is being conducted.

2.5. REPURPOSED HDT INTERVENTIONS

2.5.1. Vitamin D3

Vitamin D deficiency has been found in active TB patients, with studies stating that it is associated with increased susceptibility to TB, activation of latent TB, seriousness, and worsening of the infection (Mehta et al., 2013). The dietary supplement, vitamin D has for a long time been considered in the treatment of TB, even back to the pre-antibiotic era (Martineau et al., 2007). Vitamin D acts via the vitamin D receptor in activated immune cells which are upregulated following ligation of TLR. Studies indicate that 1,25-dihydroxyvitamin D3 (1,25(OH)2D3) bolsters innate immunity through TLR which induces expression of antimicrobial peptides (cathelicidin and beta-defensin-4), production of reactive oxygen, and nitrogen intermediates through CAMP and DEFB4 (Liu et al., 2007). Furthermore, 1,25(OH)2D3 enhances macrophages autophagy by up-regulating the expression of Atg5 and Beclin-1 (Campbell and Spector, 2012) which further minimizes intracellular growth and proliferation of *M.tb* whilst consequently improving T cell responses. It exhibits a pro-inflammatory response by collaborating with IL-15, IL-32, and IFN-γ, to control TB (Montoya et al., 2014). It also exhibits immunosuppressive effects by suppressing the NF-κB signalling pathways and expression of matrix metalloproteinase (MMPs) proinflammatory cytokines and chemokines (Coussens et al., 2009). Its inhibition of MMPs may present a prospective treatment for TB meningitis since MMP-9 levels increases resulting in inflammatory destruction during the disease progression, a mechanism of action applied by also doxycycline and SB-3CT for the treatment of TB (Majeed et al., 2016; Walker et al., 2012). Lastly, it downregulates Major histocompatibility complex (MHC) class II molecules and impairs the CD4 T cell activation, whilst enhancing differentiation of regulatory T cells to prevent harmful inflammatory cascade and resolve inflammation to prevent tissue damage during treatment (Harishankar et al., 2016).

2.5.2. Phenylbutyrate

Enhanced recovery of patients in pulmonary TB through the innate system macrophages has also been found to be improved in coordination with the inhibition of the enzymes histone

deacetylases by 4-PBA. PBA is a drug approved for use in urea cycle disorders, cancer, muscular dystrophy, and Parkinson's disease (Young et al., 2020; Zumla et al., 2016). It is responsible for removing acetyl groups from histones (Mily et al., 2013) and promotion of the CAMP/LL-37, atg5, and beclin-1 gene expression which is suggested to have a significant role in the expression of antimicrobial peptides in *M.tb* infection to restrict bacterial growth in macrophage cells (Rekha et al., 2015; Steinmann et al., 2009). Dendritic cell development is also found to be encouraged and together with 1,25(OH)2D3 display enhanced antimicrobial properties in some studies (van der Does et al., 2014). It was seen in other studies that 1,25(OH)2D3 may pace recovery in pulmonary TB, as an adjunct therapy with phenylbutyrate. They are synergistic, enhancing cathelicidin production, efficacy, and patients' response to pulmonary TB treatment (Mily et al., 2015; Salahuddin et al., 2013; Tukvadze et al., 2015). Most recently, the synergism of Vit D3 and phenylbutyrate resulted in the inhibition of MDR-Tb in macrophages whilst enhancing the intracellular inhibitory effect of RIF and INH through the induction of LL-37 antimicrobial gene and LC3-dependent autophagy. Furthermore, the combination of vitamin D3+PBA+INH was at least 125 times more potent in reducing the intracellular MDR tuberculosis than INH alone (Rao Muvva et al., 2021).

2.5.3. Bacterial Ghosts (BGs)

BGs are immunostimulants found to enhance the host immunity against *M.tb*. BGs are intact cytoplasm-free *escherichia coli* envelopes, initially used as a bacterial vaccine and adjunct therapy in cancer immunotherapy (Lim et al., 2019). BGs are activators of macrophages which results in an augmented nitric oxide production and potent induction of DCs for effector immune T lymphocytes proliferation and corresponding cytokines production (Michalek et al., 2017). The BGs employ pathways partially dependent on TLR-4 and significantly increase the activator markers, CD80, CD86, CD54, CD40, CCR7, and MHC II on bone marrow-derived macrophages and DCs. A coherent reduction in bacterial burden with a corresponding increase in important lung cytokines are demonstrated. Consequently, the BGs was used in combination with bedaquiline, a WHO-recommended first-line therapy for the treatment of RIF-resistant or multidrug-resistant tuberculosis, with its use in South Africa, dating back to 2007 (Ndjeka and Ismail, 2020). In the same study, combination use with delamid was investigated, which is also used in RIF-resistant or multidrug-resistant tuberculosis since 2015 in SA (Mohr et al., 2018). BGs use PAMPs on their cell wall that includes TLR ligands such as LPS, peptidoglycan, glycolipids, flagellin, and lipoproteins to activate the innate system and cause a pro-inflammatory cascade. This intervention was found to be very effective in bacterial control, a 4 BG weekly dosing regimen was found necessary to achieve optimal bacterial load reduction (Lim et al., 2019).

In an adjunctive use with second-line anti-TB treatment, it was found that pulmonary bacterial loads were reduced to a greater extent when BGs were combined with bedaquiline and delamanid groups compared to drugs alone groups. Although it showed synergism with other drugs, it is of importance to note that BG treatment did not enhance killing efficacy in INH, telacebec, and linezolid-treated mice (Lim et al., 2019). With such prospects identified in this field of research, more studies on other anti-TB drugs may be employed, especially the first-line drugs, to improve their efficacy in reducing bacterial load. The possible lack of synergism in the use of INH with BGs may be due to another study stating that host cell activation through nitrosative stress induces tolerance to first-line drugs, which includes INH, therefore since BGs induces nitric oxide production and activation in macrophages, the efficacy of INH may thus be affected (Liu et al., 2016).

2.5.4. [6]-Gingerol

Ginger extracts have anti-inflammatory and antioxidant properties and have been suggested for use as anti-tuberculous therapy as ginger essential oils show specific anti-mycobacterial activity against mycobacterial species (Baldin et al., 2019; R. A. Kulkarni and Deshpande, 2016). [6]-Gingerol is a very potent pharmacologically active ingredient of ginger with simultaneous host and pathogen-directed therapy which restricts *M.tb* growth in lungs, spleen, and liver. [6]-Gingerol displays activity against dormant stains and MDR and XDR drug-resistant strains *in vivo*. Its minimum inhibitory concentration (MIC) for *M.tb* strains, MDR, and XDR was 12 $\mu g.ml^{-1}$, 30 $\mu g.ml^{-1}$, and 50 $\mu g.ml^{-1}$, respectively. Moreover, [6]-Gingerol also demonstrated exceptional killing in Phosphate Buffer Saline (PBS) starved dormant bacilli, known to be resistant to all first-line drugs at a MIC of 1.5 $\mu g.ml^{-1}$. As an adjunct therapy, it enhanced the anti-tubercular effect of INH in pulmonary tuberculosis. In the spleen, a reduction in bacterial load was complemented with an increase in host Th1/Th17 immune response due to its ability to influence intracellular signalling in host macrophages. A significant rise in CD4 and CD8 T cells by inducing the prevalence of IFN-γ and IL-17 was observed and in the p38 MAPK signalling pathway, [6]-Gingerol, induced the phosphorylation of p38 MAPK in peritoneal macrophages (Bhaskar et al., 2020).

2.5.5. Allicin

Like ginger, garlic has been known to have strong antibacterial activity, against Gram positive bacteria, and Gram negative bacteria, including mycobacteria (Bakri and Douglas, 2005; Dwivedi et al., 2019). The main antimicrobial component of garlic is allicin, an oxygenated sulfur compound, thio-2-propene-1-sulfinic acid S-allyl ester (Curtis et al., 2004). In a dose-dependent manner, allicin reduced the bacterial load of MDR and XDR strains in macrophages

without tampering with the cell viability. Allicin prevents *M.tb* internalization to macrophages by possibly blocking its adhesion to ICAM (Dwivedi et al., 2019; Son et al., 2006). In addition to its anti-mycobacterial effect, it has been shown to have significant anti-tubercular immune responses in the lungs. In comparison to INH, allicin had a modest effect on CD4 and CD8 cells prevalence, whilst reversing the adverse effect of INH on T cells which dampens the immune system. IL-20 and IFN-γ production was also enhanced, whilst promoting Th1 protective effects against *M.tb* (Dwivedi et al., 2019).

In the examination of pro-and anti-inflammatory cytokines, allicin is an inducer of IL-1β (through Stress-activated protein kinases (SAPK)/ JNK pathway) and IL-12, and an inhibitor of TNF-α and IL-10. MAPK and SAPK/JNK signalling are important for pro-and anti-inflammatory pathways. There was an enhanced SAPK/JNK phosphorylation in allicin-treated macrophages after 15 min, whilst p38- MAPK phosphorylation was significantly inhibited (Dwivedi et al., 2019). This, therefore, indicates allicin elevated protective pro-inflammatory cytokines as and had a modest effect on anti-inflammatory cytokines, which is important to prevent fibrosis and tissue damage. The effect of allicin thus holds prospective treatment for both drug-resistant and drug-sensitive TB.

2.5.6. Phyllantus niruri L. (Euphorbiaceae)

Phyllanthus niruri L. (P. niruri) also known as Euphorbiaceae is a herbal species among the rich medicinal plant category that has been studied worldwide. Its various pharmacological properties allow it to function as an antibacterial, anti-hyperglycemia, anti-viral, diuretic, hepatoprotector, and immunomodulator (Lee et al., 2016; Tjandrawinata et al., 2017). More recently a study by Putri and teammates on the herbal plant showed that P. niruri aqueous extract stimulated the proliferation of peripheral blood mononuclear cells, improving macrophages' phagocytic activity and enhancing NO release (Putri et al., 2018). In the case of TB, studies have shown that *P. niruri* extracts stimulate the secretion of IFN-γ, maintaining elevated cytokine levels for up to 2-6 months after therapy (Tjandrawinata et al., 2017). Furthermore, the aqueous extract elevated TNF-α, a dual effect composed of an initial decrease followed by an increase in the last 4 months of therapy (Tjandrawinata et al., 2017). It suppressed human IL-10 secretion in patients with moderate or severe radiological lesions, also improving radiological outcomes. Recent studies in TB reports that in severe to advance TB, $CD8^+$ is increased with a decreased $CD4^+$ / $CD8^+$ ratio. This ratio is thus used as an indicator to assess the immunity of a TB patient (Yongmei et al., 2015). These findings compliments and correlate with results found by Raveinal, whereby after one month of treatment, the $CD4^+$ count and $CD4^+$ / $CD8^+$ ratio was elevated indicating immunity cover in TB patients (Raveinal, 2003; Tjandrawinata et al., 2017).

In addition to the aforementioned effects, it is also found to speed up the conversion of sputum acid-fast bacilli within 1 week of treatment (Tjandrawinata et al., 2017). Apart from *P. niruri*, other herbal plants moiety including *Piper nigrum L.* and *Piper lungum L.* from Piperine; *Cinnamomum verum. J. Presl* from Cinnamon tree, *Tinospora cordifolia (Thunb.) Miers* from *Guduchi* and *Shorea robusta Roth* from Sal (*Shorea robusta L.*) have shown potent anti-mycobacterial and immunomodulatory functions in combating TB. Most recently, the n-hexane fraction of a plant species, *Eugenia astringens* has shown a great immunomodulatory effect by suppressing the secretion of inflammatory cytokines and the production of NO by the inhibition of nitric oxide synthase in macrophages. Furthermore, it was found to have a good enough antitubercular activity to show prospects for the development of a new TB drug (Santiago-Carvalho et al., 2022). With more studies on the safety, tolerability, and efficacy of these complementary medicines, they may present importance in use as adjunctive therapy for the treatment of TB (Sarangi et al., 2021).

2.5.7. Etanercept

Etanercept is a TNF-α inhibitor. The inhibition of TNF has been employed in various other inflammatory conditions such as rheumatoid arthritis, Crohn's disease, and ulcerative colitis (Feldmann, 2002). However, the use of anti-TNF antibodies in chronic diseases causes modification in B and T cells that could result in the reactivation of latent TB infections through cell death and granuloma disintegration, increasing extracellular bacteria and its proliferation (Bourigault et al., 2013; Egen et al., 2008; Garcia et al., 2011). This is because granulomas also act as a niche that allows the *M.tb* to survive in its latent stage awaiting a decline in the immunity for reactivation in the host (Allué-Guardia et al., 2021). A study showing a combinational use of Etanercept with anti-Tb drugs promoted the safety of TNF-inhibitors with regards to its TB reactivating potential and the efficacy of the anti-TB drugs (RIF and INH) administration in TB. The pulmonary bacterial load, lung pathology, and treatment duration were reduced when used in conjunction with etanercept than alone (Bourigault et al., 2013). This effect is due to improved access to TB infected cells of the anti TB drugs, especially necrotic TB granuloma. Therefore, although TNF-α inhibitor alone may be detrimental in TB infections, their combinatory use with INH/RIF may enhance the efficacy of the traditional anti-TB drugs.

2.5.8. Carbamazepine

Autophagy occurs in macrophages infected with *M.tb* which stimulates a pro-inflammatory cascade. Carbamazepine, an anti-epileptic, has shown alternative action from inhibiting sodium and calcium firing, causing autophagy independently of mammalian target of

rapamycin (mTOR), by acting as an activator of adenosine monophosphate-activated protein kinase (AMPK) and suppressor of inositol triphosphate (IP3). In infected macrophages *in vitro*, carbamazepine increased TNFα and IL-8 release. *In vivo*, infected mice treated with carbamazepine enhanced TNF-α, IL-12, and IL-27 production as well as enhanced production of DCs and macrophages' MHC class II surface expression. In addition to the innate immune response, the adaptive immune response also demonstrated an upregulation of memory T cells and IFN-γ-secreting T cells, whilst downregulating the IL-10 regulatory T cells (Schiebler et al., 2015). The mTOR-independent autophagy may be attributed to known triggers of the pathway, which carbamazepine produces, like its ability to reduce calcium, thus decreasing ATP production, which increases phosphorylation of AMPK and ULK1 (Alers et al., 2012; Cárdenas et al., 2010; Egan et al., 2011; Schiebler et al., 2015). The ripple effect of this cascade is a reduction in the MDR-TB burden.

2.5.9. Anti-Inflammatories

Drugs like NSAIDs, corticosteroids, and zileuton have all demonstrated adjunctive benefits against *M.tb*. Low-dose aspirin in addition to its cardioprotective effects in the prevention of vascular diseases has been found to enhance the synthesis of 15-epi-lipoxin A4 and upregulates its receptor, FPRL1, and ALX. 15-Epi-lipoxin A4 is responsible for stimulating antiadhesive NO prevention of leukocyte migration and interaction, consequently inhibiting the innate immune response (Morris et al., 2009). Secondly, excess lipoxin tends to increase susceptibility to TB. For this reason, aspirin, like glucocorticosteroids, shows benefit in high-LTA4H expressing patients as an adjunctive treatment to standard antitubercular therapy. Correspondingly, aspirin also supports the vitamin D pathway by increasing vitamin D-binding protein levels. It is suggestive that zileuton, a 5-lipoxygenase inhibitor may show benefits for both high-LTA4H expressing and low-LTA4H expressing patients, by inhibiting both lipoxin and leukotriene, which stimulates prostaglandin E2, altering the TB prognosis favourably (Tobin and Ramakrishnan, 2013). Prednisolone and dexamethasone act on intracellular genes, inhibiting phospholipase A2 production of prostaglandins and leukotrienes, thus acting as an anti-inflammatory and immunologic down regulator (Donovan et al., 2018), including controlling hypersensitivity to anti-TB drugs (Thompson, 1969). Low-dose corticosteroids has proven effective in reducing pericardial constriction and hospitalization (Mayosi et al., 2014).

2.5.10. Phosphodiesterase-Inhibitors (PDE-I)

Phosphodiesterase inhibitors control the immune response by increasing intracellular cyclic adenosine monophosphate (cAMP) (Page and Spina, 2011). Its unique mechanism of inhibiting chronic inflammation whilst enhancing anti-bacterial responses makes it relevant in

TB as well as extra-pulmonary TB (Young et al., 2020). Drugs like sildenafil and cilostazol, PDE-5, and PDE-3 inhibitors, respectively, may be used adjunctively with anti-TB drugs. Cilostazol decreases TNF-α and thus its resultant activation of nuclear factor-κB (NF-κB) and THP-1 human monocytic cells' gene expression of pro-inflammatory cytokines (Hattori et al., 2009; Maiga et al., 2012). Cilostazol and sildenafil in addition to anti-TB chemotherapy enhance the host's ability to combat TB, decreasing the duration of the standard anti-TB regimen from 6 months to 5 months (Maiga et al., 2012, 2013). PDE-3 receptors are found in macrophages, platelets endothelial cells, and pulmonary smooth muscle cells, PDE-5 are prominent in pulmonary smooth muscles of pulmonary vessels, whilst PDE-4 are found in neutrophils, eosinophils, macrophages, and endothelial cells (Szczypka and Obmińska-Mrukowicz, 2010). PDE-4i is different from PDE-5i and PDE-3i because the PDE-4 receptor hydrolyses cAMP. PDE-5 demonstrates a high affinity for cGMP and PDE3 affinity for both cAMP and cGMP (Courtade et al., 1975). In the use of CC-11050 (PDE-4i), an analog of thalidomide, the bacterial load, and lung pathology were decreased in combinatory use with INH (Subbian et al., 2016). PDE-I therefore provides adjunctive benefits when used with anti-TB drugs.

2.5.11. Statins

Statins are used in dyslipidemia, acting as a reversible 3-hydroxy3-methylglutaryl-CoA reductase inhibitor, decreasing the hepatic synthesis of VLDL, the LDL-cholesterol precursor whilst also increasing the LDL-receptors on cell surfaces to catabolise and clear circulating LDL-cholesterol. In addition to that, they have been found to have potent anti-inflammatory properties, resulting in reduced tissue damage (Mortensen et al., 2005). This is done by downregulation of the expression of TNF-α, IL-1β, IL-6, IFN-γ, and IL-8 from lymphocytes and the upregulation of transcription factor Kruppel-like factor (KLF), which is responsible for the suppression of inflammation (Jain and Ridker, 2005; Xu et al., 2017). In a study performed on a mouse model, Simvastatin was found to amplify the anti-TB activities of INH, RIF, and PZN (Skerry et al., 2014). Epidemiological studies also complement these findings, showing that the frequency of active TB incidence in statin users is reduced as compared to non-statin users, suggesting a lower risk of active TB incidence whilst taking statins (Lai et al., 2016). More recently, pravastatin, simvastatin, and fluvastatin adjunctively improved the anti-TB activities of the first-line drugs INH, RIF, and PZN in THP-1 cells. Pravastatin was the least toxic, acting by modulating phagosomal maturation characteristics in macrophages, decreasing phagosomal acidification and proteolytic activity (Dutta et al., 2020). For this reason, a randomized clinical trial, Statins as Adjunctive Therapy for TB (StAT-TB) is present

been studied to determine whether pravastatin adjunctive therapy shortens the duration of therapy and improves lung function in TB (Dutta et al., 2020).

2.5.12. Verapamil

Verapamil is a calcium channel blocker, an efflux pump inhibitor used in the treatment of cardiovascular disorders including hypertension and angina (Angus et al., 1982; Hangai-Hoger et al., 2005). In *M.tb* the efflux pump is associated with resistance allowing the bacteria to withstand extreme conditions (Poole, 2007). The resistance results in the reduction of its intracellular antimicrobial concentrations and the susceptibility of the organism thereof. Verapamil uses in Tb infected mice have demonstrated a reduction in the duration of treatment, suggesting it is a great prospective adjunctive therapy in TB treatment (Gupta et al., 2013). In combinatory studies of verapamil and bedaquiline, it has been found that the bacterial load was reduced (Gupta et al., 2015; Xu et al., 2017). Other benefits of verapamil as an adjunct therapy include increasing the bioavailability of bedaquiline (Xu et al., 2017), and the disruption of the dynamic membrane of the *Mycobacterium* (Chen et al., 2018). More recently, in adjunctive use with rifampicin, the downregulation of some efflux pumps related genes was evident which is indicative of the inhibitory activity of verapamil (Caleffi-Ferracioli et al., 2019). These findings, therefore, create prospective inception for the use of efflux pump inhibitors in treating *M.tb*.

2.5.13. Metformin

Metformin is a Type-2 diabetic medication. It is commercially approved as a biguanide that reduces basal and postprandial plasma glucose by reducing glucose production through gluconeogenesis and glycogenolysis and stimulates intracellular glycogen synthesis, and insulin sensitivity for peripheral glucose uptake. Apart from its glycemic control function, it has been found to significantly reduce the risk of acquiring TB in patients with diabetes mellitus (X. Yu et al., 2019). This mechanism is believed to be through the activation of adenosine monophosphate (AMP)-activated protein kinases responsible for sensing cellular energy levels, which in turn may act as a pathway for the activation of autophagy for clearance of *M.tb* (Bento et al., 2015; Hur and Lee, 2015). Metformin reduces *M.tb* growth through the induction of mitochondrial ROS production. When used adjunctively with standard anti-TB drugs, it is found to reduce inflammatory tissue pathology and stimulate the secretion of IFN-γ from $CD8^+$ and $CD4^+$ T-cell populations, whilst inhibiting the activity of chronic inflammatory genes (Kim and Yang, 2017; Singhal et al., 2014). Although some studies have indicated the efficacy of metformin in improving sputum culture conversion after 2 months of treatment, new clinical studies as well as in 2022 are being conducted to validate its efficacy in sputum conversion

ratio from positive to negative in patients with pulmonary TB on standard anti-TB treatment with metformin, as well as the safety and tolerability of the combination. The most recent study showed no fastening in the sputum culture conversion but found that excess inflammation was reduced therefore minimizing lung tissue damage (Padmapriydarsini et al., 2021).

2.5.14. Kv1.3 Inhibitors

Kv1.3 inhibition has been shown to favour T_{CM} cell proliferation which is important for prolonged and enhanced immunity against TB. Curcumin, Clofazimine and Luteolin are amongst the drugs known to inhibit Kv1.3 and possibly augment the BCG vaccine efficacy (Faisal et al., 2022; Lian et al., 2013; Singh et al., 2016, 2020). Curcumin is the main natural polyphenol found in turmeric a member of the ginger family, Zingiberaceae, a herb known for its antioxidant, antimicrobial, anti-inflammatory, anti-mutagenic and anti-cancer properties (Hewlings and Kalman, 2017). Curcumin shows further immunomodulatory properties through NLRs by regulating NF-kB activation, suppressing the production of pro-inflammatory IFN-γ, TNF-α, IL-1, and IL-8 cytokines and inducing anti-inflammatory IL-2 cytokine proliferation. Curcumin promotes apoptosis and autophagy in macrophages. They also produce IFN-γ and IL-22 increasing the activity of phagolysosome fusion responsible for the inhibition of *M.tb* proliferation. In addition to its immunomodulatory effect, it has hepatoprotective properties, with a study showing beneficial combinatory use with Isoniazid in reducing inflammatory lesions and hepatotoxicity caused by isoniazid (Bai et al., 2016; Faisal et al., 2022; Tousif et al., 2017). Clofazimine is a re-purposed anti-leprosy drug shown to enhance Th1 and Th17 response and the release of pro-inflammatory IFN-γ, TNF-α, and IL-2, IL-6, IL-12, IL-17, and IL-22 in BCG vaccination and enhances host-protection as compared to BCG alone by enhancing T_{CM}: T_{EM} cell ratio (Singh et al., 2016). Luteolin is a natural flavonoid, derived from the various plants and vegetables such as broccoli, green pepper, thyme, carrots, olive oil and peppermint (López-Lázaro, 2009; Shimoi et al., 1998). Due to its biological safety, it presents ease of use with vaccination. Luteolin like clofazimine demonstrates potent Th1 and Th17 response and is found to activate macrophage stimulatory molecules such as CD11B, CD11C, CD80 and CD86; therefore, improving its bactericidal activity (Singh et al., 2020). These drugs, therefore, demonstrate a prospective advantage in vaccine development and enhancement for the treatment of TB.

Table 2.2: Host-directed immunomodulatory agents in clinical trials for the treatment of tuberculosis.

Agent/s	**Objective**	**Phase**	**Study Parameters**	**Trial No.**
Azithromycin An initial azithromycin loading dose of 500 mg followed by Azithromycin 250 mg once daily for 28 days	Investigating the immunomodulatory effect of azithromycin in tuberculosis patients receiving standard therapy	2	To determine whether -Azithromycin enhances the resolution of systemic inflammation in patients with drug-susceptible pulmonary TB receiving standard treatment. -Azithromycin on top of standard treatment in patients with drug-susceptible pulmonary TB reduces airway inflammation and reduces tissue degradation and remodelling -Azithromycin shortens the time to sputum conversion.	NCT03160638
Everolimus 0.5 MG Auranofin 6	Investigating the safety and preliminary efficacy of the 4	2	To determine whether: -auranofin, everolimus,	NCT02968927

MG Vitamin D3 CC-11050	HDT drug candidates in comparison to rifabutin-modified TB therapy.		and vitamin D result in experiencing suspected unexpected serious adverse reactions (SUSARs). -CC-11050 results in experiencing treatment-emergent serious adverse events (SAEs).	
Vitamin D3 9,600 IU/day for 8 weeks	Investigating the immunomodulatory properties of Vit D after TB	2	To determine: -the Inflammation Score on PET-CT (a biomarker responsible for predicting the risk of TB recurrence in patients taking anti-TB treatment) at 8-week. -Concentration of inflammatory mediators. -the rate of sputum culture conversion.	NCT03011580
Vitamin D 3 treatment arms of 600,	Investigating the immunomodulatory properties	Not applicable	To determine: -immune response assessed by superoxide	NCT01992263

2000, and 4000 IU vitamin D), compared to placebo, for 12 months	of Vit D		bursts and proteolytic capacities of macrophages and monocytes.	
Vitamin D3 10,000 IU once weekly for 3 years	Investigating the ability of Vitamin D3 to reduce the risk of acquisition of latent tuberculosis infection.	3	To determine the: - safety - efficacy - ability to prevent the acquisition of latent infection - incidence of active TB - incidence of lung complications	NCT02880982
Ibuprofen 400mg/day/2 months	Investigating the immunomodulatory properties, safety, and efficacy of Ibuprofen as adjunctive therapy for the Treatment of XDR	2	To determine its effect on -microbiological efficacy -radiological efficacy -clinical efficacy -safety	NCT02781909

	Tuberculosis.		-the quality of life	
N-acetyl cysteine 1200 mg BID for months 1-4 followed by 2 months of standard TB treatment alone	Investigating sputum culture conversion and immunomodulatory effects.	2	To determine -the rate of sputum culture conversion -normalization ability of cellular glutathione in tuberculosis (TB) -its potential effects on lung and immune function	NCT03702738
Pravastatin A standard Tb regimen of INH 300 mg, RIF 450 mg (weight <50 kg) or 600 mg (weight >50 kg), PZN 20-25 mg/kg, and EMB 15-20 mg/kg daily for 14 days PLUS escalating doses of	Investigating the safety, tolerability, and efficacy of pravastatin	2	A 2-stage trial whereby stage 1 determines: -safety -tolerability, as well as -pharmacokinetics (PK) And stage 2 determines: -ability of pravastatin to shorten the time to sputum culture	NCT03456102

pravastatin (40 mg - 160 mg)			conversion -improve lung function	
Acetylsalicylic acid (ASA) and Ibuprofen (IBU). -TB treatment + acetylsalicylic acid 300mg twice daily during the first 4 weeks of TB treatment followed by acetylsalicylic acid 300mg once daily for an additional 4 weeks. -TB treatment + ibuprofen 400mg twice daily during the first 4 weeks of TB	Investigating the adjunctive use of the HDT agents with standard anti-TB treatment compared with standard anti-Tb treatment in drug-sensitive (DS) and multi-drug resistant (MDR) TB patients	2b	To determine -the rate of negative sputum culture conversion. -improvement or resolution of clinical signs and symptoms at end of treatment. -improvement of lung function impairment	NCT04575519

treatment followed by ibuprofen 400mg once daily for an additional 4 weeks.				
Etoricoxib and TB vaccine (H56:IC31) Etoricoxib was given for 20 weeks and H56:IC31 was given as two immunizations on day 84 and day 140.	Investigating the safety and immune effect of the use of etoricoxib alone, H56:IC31 alone, and the combinatory use of both in addition to standard anti-TB drugs.	1	To determine whether: -etoricoxib will improve the patient's immune system and boost TB vaccine responses. -to study and identify immune regulatory mechanisms and biomarkers responsible for noticed outcomes	NCT02503839
Metformin 500 mg oral tablet for 6 months	Investigating the acid-fast bacillus sputum conversion ratio from positive to negative in pulmonary TB patients	1	To determine whether: acid-fast bacillus converts to negative when taking metformin after the second week, second, fifth, and sixth	NCT05215990

			month.	
Metformin 500 mg tablet followed by 500 mg tablet twice daily for 11 weeks	Investigating the safety and tolerability of metformin in people with HIV and TB co-infection.	2	To determine whether metformin -improves respiratory health -improves HIV outcomes -improves TB treatment outcomes -improves time to sputum conversion	NCT04930744

2.6. FUTURE PERSPECTIVES AND CONCLUSION

Even though over the years, advancements have been made in the treatment of TB, very few new drugs have been developed to contribute to fighting the disease. For this reason, drug repurposing to obtain host-directed mechanisms of action from drugs not originally approved for TB has demonstrated conducive and prospective possibilities in alleviating the disease. The repurposed biological agents act by modulating pro-inflammatory mediators, enhancing immune response efficacy, macrophage phagocytic activity, and/or disruption of granuloma (Young et al., 2020). Since these mechanisms are host cell-targeted, it further reduces the possibility of resistance.

HDT allows the application of PRRs and PAMPs to elicit an anti-tubercular immunomodulatory response (Pahari et al., 2017). With more studies on PAMPs binding to PRRs, more adjunctive therapy may be established, allowing the implementation of the bests adjunct therapy into established treatment regimens. Such implementation will allow the reduction in dose of the adjunct therapy as well as of standard anti-TB, reduction in the duration of therapy, thus reducing

toxicity, improving patient compliance, and reducing drug resistance. Most recently, monocytes and macrophages miRNA are readily accessible biomarkers for early diagnosis of TB as well as for possible therapeutic targeting. miRNA can act as immunomodulators for innate mechanisms such as apoptosis and autophagy. Therefore, multidisciplinary clinical studies incorporating factors like age, gender, and disease stage may assist in gaining better insight into the value of miRNA as potent agents in HDT (Dockrell et al., 2022).

Although many theoretical and *in vitro* studies show promising outcomes, the corresponding clinical studies have shown some varying results due to various additional factors in clinical trials such as age, dose selection, lifestyle variations of subjects, ethnicity, co-infection, and genetic morphisms (Kolloli and Subbian, 2017; Zumla et al., 2013). Newer clinical studies are looking into considering these such as trial NCT04930744 which takes co-infection with HIV as a variability factor. With newer multicentred randomized trials considering these factors by ensuring more meticulous inclusion and exclusion criteria, we may look to get closer to the most possibly safe and effective way of treating TB.

2.7. REFERENCES

Abdelaziz, M. H., Abdelwahab, S. F., Wan, J., Cai, W., Huixuan, W., Jianjun, C., Kumar, K. D., Vasudevan, A., Sadek, A., and Su, Z. (2020). Alternatively activated macrophages; a double-edged sword in allergic asthma. Journal of Translational Medicine, 18, 1–12.

Abel, B., Thieblemont, N., Quesniaux, V. J. F., Brown, N., Mpagi, J., Miyake, K., Bihl, F., and Ryffel, B. (2002). Toll-Like Receptor 4 Expression Is Required to Control Chronic *Mycobacterium tuberculosis* Infection in Mice. The Journal of Immunology, 169(6), 3155.

Ahn, C., Oh, K.-H., Kim, K., Lee, K. Y., Lee, J. G., Oh, M. D., Kim, Y., Han, J. S., Kim, S., and Lee, J. S. (2003). Effect of peritoneal dialysis on plasma and peritoneal fluid concentrations of isoniazid, pyrazinamide, and rifampin. Peritoneal Dialysis International, 23(4), 362–367.

Akira, S., Uematsu, S., and Takeuchi, O. (2006). Pathogen Recognition and Innate Immunity. Cell, 124(4), 783–801.

Alers, S., Löffler, A. S., Wesselborg, S., and Stork, B. (2012). Role of AMPK-mTOR-Ulk1/2 in the regulation of autophagy: cross talk, shortcuts, and feedbacks. Molecular and Cellular Biology, 32(1), 2–11.

Allawadhi, P., Singh, V., Khurana, I., Rawat, P. S., Renushe, A. P., Khurana, A., Navik, U., Allwadhi, S., Kumar Karlapudi, S., Banothu, A. K., and Bharani, K. K. (2021). Decorin as a possible strategy for the amelioration of COVID-19. Medical Hypotheses, 152, 110612.

Allué-Guardia, A., García, J. I., and Torrelles, J. B. (2021). Evolution of Drug-Resistant *Mycobacterium tuberculosis* Strains and Their Adaptation to the Human Lung Environment. Frontiers in Microbiology, 12, 612675

Altamimi, M. A., Hussain, A., Imam, S. S., Alshehri, S., Singh, S. K., and Webster, T. J. (2020). Transdermal delivery of isoniazid loaded elastic liposomes to control cutaneous and systemic tuberculosis. Journal of Drug Delivery Science and Technology, 59, 101848.

Angus, J. A., Brazenor, R. M., and le Duc, M. A. (1982). Verapamil: a selective antagonist of constrictor substances in dog coronary artery: implications for variant angina. Clinical and Experimental Pharmacology and Physiology. Supplement, 6, 15–28.

Anusiem, C. A., Brown, S. A., Ezejiofor, N. A., Barikpoar, E., and Orisakwe, O. E. (2018). Isoniazid pharmacokinetics in the presence of ofloxacin and norfloxacin antibiotics. American Journal of Therapeutics, 25(4), e397–e404.

Bafica, A., Scanga, C. A., Feng, C. G., Leifer, C., Cheever, A., and Sher, A. (2005). TLR9 regulates Th1 responses and cooperates with TLR2 in mediating optimal resistance to *Mycobacterium tuberculosis*. The Journal of Experimental Medicine, 202(12), 1715–1724.

Bai, X., Oberley-Deegan, R. E., Bai, A., Ovrutsky, A. R., Kinney, W. H., Weaver, M., Zhang, G., Honda, J. R., and Chan, E. D. (2016). Curcumin enhances human macrophage control of *Mycobacterium tuberculosis* infection. Respirology, 21(5), 951–957.

Bakri, I. M., and Douglas, C. W. I. (2005). Inhibitory effect of garlic extract on oral bacteria. Archives of Oral Biology, 50(7), 645–651.

Baldin, V. P., de Lima Scodro, R. B., Fernandez, C. M. M., Ieque, A. L., Caleffi-Ferracioli, K. R., Siqueira, V. L. D., de Almeida, A. L., Gonçalves, J. E., Cortez, D. A. G., and Cardoso, R. F. (2019). Ginger essential oil and fractions against *Mycobacterium spp*. Journal of Ethnopharmacology, 244, 112095.

Bekele, A., Gebreselassie, N., Ashenafi, S., Kassa, E., Aseffa, G., Amogne, W., Getachew, M., Aseffa, A., Worku, A., and Raqib, R. (2018). Daily adjunctive therapy with vitamin D 3 and phenylbutyrate supports clinical recovery from pulmonary tuberculosis: a randomized controlled trial in Ethiopia. Journal of Internal Medicine, 284(3), 292–306.

Bento, C. F., Empadinhas, N., and Mendes, V. (2015). Autophagy in the fight against tuberculosis. DNA and Cell Biology, 34(4), 228–242.

Bhaskar, A., Kumari, A., Singh, M., Kumar, S., Kumar, S., Dabla, A., Chaturvedi, S., Yadav, V., Chattopadhyay, D., and Dwivedi, V. P. (2020). [6]-Gingerol exhibits potent anti-mycobacterial and immunomodulatory activity against tuberculosis. International Immunopharmacology, 87, 106809.

Bickel, M. (1993). The role of interleukin-8 in inflammation and mechanisms of regulation. Journal of Periodontology, 64(5 Suppl), 456–460.

Bourigault, M.-L., Vacher, R., Rose, S., Olleros, M. L., Janssens, J.-P., Quesniaux, V. F. J., and Garcia, I. (2013). Tumor necrosis factor neutralization combined with chemotherapy enhances

Mycobacterium tuberculosis clearance and reduces lung pathology. American Journal of Clinical and Experimental Immunology, 2(1), 124.

Caleffi-Ferracioli, K. R., Cardoso, R. F., de Souza, J. V. P., Murase, L. S., Canezin, P. H., Scodro, R. B. L., LD Siqueira, V., and Pavan, F. R. (2019). Modulatory effects of verapamil in rifampicin activity against *Mycobacterium tuberculosis*. Future Microbiology, 14(3), 185–194.

Campbell, G. R., and Spector, S. A. (2012). Vitamin D inhibits human immunodeficiency virus type 1 and *Mycobacterium tuberculosis* infection in macrophages through the induction of autophagy. PLoS Pathogens, 8(5), e1002689.

Caon, T., Campos, C. E. M., Simões, C. M. O., and Silva, M. A. S. (2015). Novel perspectives in the tuberculosis treatment: Administration of isoniazid through the skin. International Journal of Pharmaceutics, 494(1), 463–470.

Cárdenas, C., Miller, R. A., Smith, I., Bui, T., Molgó, J., Müller, M., Vais, H., Cheung, K.-H., Yang, J., and Parker, I. (2010). Essential regulation of cell bioenergetics by constitutive InsP3 receptor Ca2+ transfer to mitochondria. Cell, 142(2), 270–283.

Chan, H. C. S., Shan, H., Dahoun, T., Vogel, H., and Yuan, S. (2019). Advancing drug discovery via artificial intelligence. Trends in Pharmacological Sciences, 40(8), 592–604.

Chen, C., Gardete, S., Jansen, R. S., Shetty, A., Dick, T., Rhee, K. Y., and Dartois, V. (2018). Verapamil targets membrane energetics in *Mycobacterium tuberculosis*. Antimicrobial Agents and Chemotherapy, 62(5), e02107-17.

Chiriac, A., Ferariu, D., Solovan, C., Brzezinski, P., and Feldman, S. R. (2014). Improvement in severe psoriasis associated with isoniazid treatment. Dermatology Online Journal, 20(5).

Chodisetti, S. B., Gowthaman, U., Rai, P. K., Vidyarthi, A., Khan, N., and Agrewala, J. N. (2015). Triggering through Toll-like receptor 2 limits chronically stimulated T-helper type 1 cells from undergoing exhaustion. The Journal of Infectious Diseases, 211(3), 486–496.

Coban, C., Igari, Y., Yagi, M., Reimer, T., Koyama, S., Aoshi, T., Ohata, K., Tsukui, T., Takeshita, F., and Sakurai, K. (2010). Immunogenicity of whole-parasite vaccines against Plasmodium falciparum involves malarial hemozoin and host TLR9. Cell Host and Microbe, 7(1), 50–61.

Cohen, A., Mathiasen, V. D., Schön, T., and Wejse, C. (2019). The global prevalence of latent tuberculosis: a systematic review and meta-analysis. European Respiratory Journal, 54(3).

Courtade, E. T., Tsuda, T., Thomas, C. R., and Dannenberg, A. M. (1975). Capillary density in developing and healing tuberculous lesions produced by BCG in rabbits. A quantitative study. The American Journal of Pathology, 78(2), 243.

Coussens, A., Timms, P. M., Boucher, B. J., Venton, T. R., Ashcroft, A. T., Skolimowska, K. H., Newton, S. M., Wilkinson, K. A., Davidson, R. N., and Griffiths, C. J. (2009). 1α, 25-dihydroxyvitamin D3 inhibits matrix metalloproteinases induced by *Mycobacterium tuberculosis* infection. Immunology, 127(4), 539–548.

Curtis, H., Noll, U., Störmann, J., and Slusarenko, A. J. (2004). Broad-spectrum activity of the volatile phytoanticipin allicin in extracts of garlic (Allium sativum L.) against plant pathogenic bacteria, fungi and Oomycetes. Physiological and Molecular Plant Pathology, 65(2), 79–89.

Deretic, V., Singh, S., Master, S., Harris, J., Roberts, E., Kyei, G., Davis, A., de Haro, S., Naylor, J., and Lee, H. (2006). *Mycobacterium tuberculosis* inhibition of phagolysosome biogenesis and autophagy as a host defence mechanism. Cellular Microbiology, 8(5), 719–727.

Divangahi, M., Mostowy, S., Coulombe, F., Kozak, R., Guillot, L., Veyrier, F., Kobayashi, K. S., Flavell, R. A., Gros, P., and Behr, M. A. (2008). NOD2-deficient mice have impaired resistance to *Mycobacterium tuberculosis* infection through defective innate and adaptive immunity. The Journal of Immunology, 181(10), 7157–7165.

Dockrell, H. M., Pinheiro, R. O., and Serrano, C. J. (2022). Monocyte and Macrophage miRNA: Potent Biomarker and Target for Host-Directed Therapy for Tuberculosis. Immunological Biomarkers for Tuberculosis.

Doležal, M., Zitko, J., and Jampílek, J. (2012). Pyrazinecarboxylic acid derivatives with antimycobacterial activity. Understanding Tuberculosis-New Approaches to Fighting Against Drug Resistance, 1.

Donald, P. R., and McIlleron, H. (2009). Chapter 59 - Antituberculosis drugs. In H. S. Schaaf, A. I. Zumla, J. M. Grange, M. C. Raviglione, W. W. Yew, J. R. Starke, M. Pai, and P. R. Donald (Eds.), Tuberculosis (pp. 608–617). W.B. Saunders. https://doi.org/https://doi.org/10.1016/B978-1-4160-3988-4.00059-7

Donovan, J., Phu, N. H., Mai, N. T. H., Dung, L. T., Imran, D., Burhan, E., Ngoc, L. H. B., Bang, N. D., Giang, D. C., and Ha, D. T. M. (2018). Adjunctive dexamethasone for the treatment of HIV-infected adults with tuberculous meningitis (ACT HIV): study protocol for a randomised controlled trial. Wellcome Open Research, 3.

Dutta, N. K., Bruiners, N., Zimmerman, M. D., Tan, S., Dartois, V., Gennaro, M. L., and Karakousis, P. C. (2020). Adjunctive host-directed therapy with statins improves tuberculosis-related outcomes in mice. The Journal of Infectious Diseases, 221(7), 1079–1087.

Dwivedi, V. P., Bhattacharya, D., Singh, M., Bhaskar, A., Kumar, S., Fatima, S., Sobia, P., van Kaer, L., and Das, G. (2019). Allicin enhances antimicrobial activity of macrophages during *Mycobacterium tuberculosis* infection. Journal of Ethnopharmacology, 243, 111634.

Egan, D. F., Shackelford, D. B., Mihaylova, M. M., Gelino, S., Kohnz, R. A., Mair, W., Vasquez, D. S., Joshi, A., Gwinn, D. M., and Taylor, R. (2011). Phosphorylation of ULK1 (hATG1) by AMP-activated protein kinase connects energy sensing to mitophagy. Science, 331(6016), 456–461.

Egen, J. G., Rothfuchs, A. G., Feng, C. G., Winter, N., Sher, A., and Germain, R. N. (2008). Macrophage and T cell dynamics during the development and disintegration of mycobacterial granulomas. Immunity, 28(2), 271–284.

Faisal, E. G., Amirah, S., Maulana, S., Komariah, M., and Platini, H. (2022). Role of Curcumin as a Potential Immunomodulator to Adjunct Tuberculosis Treatment in Indonesia. Open Access Macedonian Journal of Medical Sciences, 10(F), 326–331.

Fatima, S., Bhaskar, A., and Dwivedi, V. P. (2021). Repurposing Immunomodulatory Drugs to Combat Tuberculosis. Frontiers in Immunology, 12, 1149.

Feldmann, M. (2002). Development of anti-TNF therapy for rheumatoid arthritis. Nature Reviews Immunology, 2(5), 364–371.

Fernandes, G. F. dos S., Salgado, H. R. N., and Santos, J. L. dos. (2017). Isoniazid: a review of characteristics, properties and analytical methods. Critical Reviews in Analytical Chemistry, 47(4), 298–308.

Friedland, J. S. (2010). Chapter 30 - Tuberculosis and other mycobacterial infections. In J. Cohen, S. M. Opal, and W. G. Powderly (Eds.), Infectious Diseases (Third Edition) (pp. 309–327). Mosby. https://doi.org/https://doi.org/10.1016/B978-0-323-04579-7.00030-7

Gantner, B. N., Simmons, R. M., Canavera, S. J., Akira, S., and Underhill, D. M. (2003). Collaborative induction of inflammatory responses by dectin-1 and Toll-like receptor 2. The Journal of Experimental Medicine, 197(9), 1107–1117.

Garcia, I., Olleros, M. L., Quesniaux, V. F. J., Jacobs, M., Allie, N., Nedospasov, S. A., Szymkowski, D. E., and Ryffel, B. (2011). Roles of soluble and membrane TNF and related ligands in mycobacterial infections: effects of selective and non-selective TNF inhibitors during infection. Advances in TNF Family Research, 187–201.

Geijtenbeek, T. B. H., and Gringhuis, S. I. (2009). Signalling through C-type lectin receptors: shaping immune responses. Nature Reviews Immunology, 9(7), 465–479.

Geijtenbeek, T. B. H., and Gringhuis, S. I. (2016). C-type lectin receptors in the control of T helper cell differentiation. Nature Reviews Immunology, 16(7), 433–448.

Gocke, A. R., Lebson, L. A., Grishkan, I. v, Hu, L., Nguyen, H. M., Whartenby, K. A., Chandy, K. G., and Calabresi, P. A. (2012). Kv1. 3 deletion biases T cells toward an immunoregulatory phenotype and renders mice resistant to autoimmune encephalomyelitis. The Journal of Immunology, 188(12), 5877–5886.

González, O., Blanco, M. E., Iriarte, G., Bartolomé, L., Maguregui, M. I., and Alonso, R. M. (2014). Bioanalytical chromatographic method validation according to current regulations, with a special focus on the non-well defined parameters limit of quantification, robustness and matrix effect. Journal of Chromatography A, 1353, 10–27.

Gopal, R., Rapaka, R. R., and Kolls, J. K. (2017). Immune reconstitution inflammatory syndrome associated with pulmonary pathogens. European Respiratory Review, 26(143).

Gringhuis, S. I., den Dunnen, J., Litjens, M., van der Vlist, M., and Geijtenbeek, T. B. H. (2009). Carbohydrate-specific signaling through the DC-SIGN signalosome tailors immunity to *Mycobacterium tuberculosis*, HIV-1 and Helicobacter pylori. Nature Immunology, 10(10), 1081–1088. https://doi.org/10.1038/ni.1778

Gringhuis, S. I., den Dunnen, J., Litjens, M., van het Hof, B., van Kooyk, Y., and Geijtenbeek, T. B. B. H. (2007). C-Type Lectin DC-SIGN Modulates Toll-like Receptor Signaling via Raf-1 Kinase-Dependent Acetylation of Transcription Factor NF-κB. Immunity, 26(5), 605–616.

Gupta, S., Tyagi, S., Almeida, D. v, Maiga, M. C., Ammerman, N. C., and Bishai, W. R. (2013). Acceleration of tuberculosis treatment by adjunctive therapy with verapamil as an efflux inhibitor. American Journal of Respiratory and Critical Care Medicine, 188(5), 600–607.

Gupta, S., Tyagi, S., and Bishai, W. R. (2015). Verapamil increases the bactericidal activity of bedaquiline against *Mycobacterium tuberculosis* in a mouse model. Antimicrobial Agents and Chemotherapy, 59(1), 673–676.

H, I. C. (2005). International Conference on Harmonization: Validation of analytical procedures: Text and Methodology Q2 (R1). ICH Harmonised Tripartite Guideline Rockville, MD, USA.

Hangai-Hoger, N., Tsai, A. G., Friesenecker, B., Cabrales, P., and Intaglietta, M. (2005). Microvascular oxygen delivery and consumption following treatment with verapamil. American Journal of Physiology-Heart and Circulatory Physiology, 288(4), H1515–H1520.

Harishankar, M., Anbalagan, S., and Selvaraj, P. (2016). Effect of vitamin D3 on chemokine levels and regulatory T-cells in pulmonary tuberculosis. International Immunopharmacology, 34, 86–91.

Harmon, R. C. (2007). Pyrazinamide. In S. J. Enna and D. B. Bylund (Eds.), xPharm: The Comprehensive Pharmacology Reference (pp. 1–5). Elsevier. https://doi.org/https://doi.org/10.1016/B978-008055232-3.62492-4

Hattori, Y., Suzuki, K., Tomizawa, A., Hirama, N., Okayasu, T., Hattori, S., Satoh, H., Akimoto, K., and Kasai, K. (2009). Cilostazol inhibits cytokine-induced nuclear factor-κB activation via AMP-activated protein kinase activation in vascular endothelial cells. Cardiovascular Research, 81(1), 133–139.

Hewlings, S. J., and Kalman, D. S. (2017). Curcumin: A review of its effects on human health. Foods, 6(10), 92.

Hoit, B. D. (2017). Pathophysiology of the Pericardium. Progress in Cardiovascular Diseases, 59(4), 341–348.

Horváth, C. (2013). High-performance liquid chromatography: advances and perspectives. ed. C. S. Horvath, Academic Press, New York, Volume 2, 1980.

Howlett, P., du Bruyn, E., Morrison, H., Godsent, I. C., Wilkinson, K. A., Ntsekhe, M., and Wilkinson, R. J. (2020). The immunopathogenesis of tuberculous pericarditis. Microbes and Infection, 22(4–5), 172–181.

Hsu, Y.-M. S., Zhang, Y., You, Y., Wang, D., Li, H., Duramad, O., Qin, X.-F., Dong, C., and Lin, X. (2007). The adaptor protein CARD9 is required for innate immune responses to intracellular pathogens. Nature Immunology, 8(2), 198–205.

Hur, K. Y., and Lee, M. (2015). New mechanisms of metformin action: Focusing on mitochondria and the gut. Journal of Diabetes Investigation, 6(6), 600–609.

Ishihara, T., Ferrans, V. J., Jones, M., Boyce, S. W., Kawanami, O., and Roberts, W. C. (1980). Histologic and ultrastructural features of normal human parietal pericardium. The American Journal of Cardiology, 46(5), 744–753.

Isiguzo, G., Du Bruyn, E., Howlett, P., and Ntsekhe, M. (2020). Diagnosis and management of tuberculous pericarditis: what is new? Current Cardiology Reports, 22, 1–8.

Jain, M. K., and Ridker, P. M. (2005). Anti-inflammatory effects of statins: clinical evidence and basic mechanisms. Nature Reviews Drug Discovery, 4(12), 977–987.

Janeway, C. A. (1989). Approaching the asymptote? Evolution and revolution in immunology. Cold Spring Harbor Symposia on Quantitative Biology, 54, 1–13.

Jégouzo, S. A. F., Harding, E. C., Acton, O., Rex, M. J., Fadden, A. J., Taylor, M. E., and Drickamer, K. (2014). Defining the conformation of human mincle that interacts with mycobacterial trehalose dimycolate. Glycobiology, 24(12), 1291–1300.

Junginger, H. (1996). Drug absorption enhancement, concepts, possibilities, limitations and trends. Journal of Drug Targeting, 4(1), 51–52.

Kaufmann, S. H. E. (2001). How can immunology contribute to the control of tuberculosis? Nature Reviews Immunology, 1(1), 20–30.

Kawai, T., and Akira, S. (2010). The role of pattern-recognition receptors in innate immunity: update on Toll-like receptors. Nature Immunology, 11(5), 373–384.

Kawasaki, T., and Kawai, T. (2014). Toll-like receptor signaling pathways. Frontiers in Immunology, 461.

Keane, J., Gershon, S., Wise, R. P., Mirabile-Levens, E., Kasznica, J., Schwieterman, W. D., Siegel, J. N., and Braun, M. M. (2001). Tuberculosis associated with infliximab, a tumor necrosis factor α–neutralizing agent. New England Journal of Medicine, 345(15), 1098–1104.

Kerrigan, A. M., and Brown, G. D. (2011). Syk-coupled C-type lectins in immunity. Trends in Immunology, 32(4), 151–156.

Khan, N., Pahari, S., Vidyarthi, A., Aqdas, M., and Agrewala, J. N. (2016). NOD-2 and TLR-4 signaling reinforces the efficacy of dendritic cells and reduces the dose of TB drugs against *Mycobacterium tuberculosis*. Journal of Innate Immunity, 8(3), 228–242.

Kim, Y.-R., and Yang, C.-S. (2017). Host-directed therapeutics as a novel approach for tuberculosis treatment. Journal of Microbiology and Biotechnology, 27(9).

Kinjyo, I., Hanada, T., Inagaki-Ohara, K., Mori, H., Aki, D., Ohishi, M., Yoshida, H., Kubo, M., and Yoshimura, A. (2002). SOCS1/JAB is a negative regulator of LPS-induced macrophage activation. Immunity, 17(5), 583–591.

Kolloli, A., and Subbian, S. (2017). Host-directed therapeutic strategies for tuberculosis. Frontiers in Medicine, 4, 171.

Kroth, R., Argenta, D. F., Conte, J., Amaral, B. R., and Caon, T. (2020). Transbuccal delivery of isoniazid: *Ex vivo* permeability and drug-surfactant interaction studies. American Association of Pharmaceutical Scientists PharmSciTech, 21, 1–12.

Kulkarni, R. A., and Deshpande, A. R. (2016). Anti-inflammatory and antioxidant effect of ginger in tuberculosis. Journal of Complementary and Integrative Medicine, 13(2), 201–206.

Lai, C.-C., Lee, M. G., Lee, S.-H., Hsu, W.-T., Chang, S.-S., Chen, S.-C., and Lee, C.-C. (2016). Statin treatment is associated with a decreased risk of active tuberculosis: an analysis of a nationally representative cohort. Thorax, 71(7), 646–651.

Lakshmi, D., and Jacob, J. T. (2018). Validated Degradation studies for the estimation of Pyrazinamide, Ethambutol, Isoniazid and Rifampacin in a fixed dose combination by UPLC. Research Journal of Pharmacy and Technology, 11(7), 2869–2875.

Law, B. (2000). Basic Drugs: Liquid Chromatography. Touchstone, 613, 665.

Lee, K. Y. (2019). M1 and M2 polarization of macrophages: a mini-review. Journal of Medical and Biological Engineering, 2(1), 1-5.

Lee, N. Y. S., Khoo, W. K. S., Adnan, M. A., Mahalingam, T. P., Fernandez, A. R., and Jeevaratnam, K. (2016). The pharmacological potential of Phyllanthus niruri. Journal of Pharmacy and Pharmacology, 68(8), 953–969.

Lee, S. M. Y., Kok, K.-H., Jaume, M., Cheung, T. K. W., Yip, T.-F., Lai, J. C. C., Guan, Y., Webster, R. G., Jin, D.-Y., and Peiris, J. S. M. (2014). Toll-like receptor 10 is involved in induction of innate immune responses to influenza virus infection. Proceedings of the National Academy of Sciences, 111(10), 3793–3798.

Lian, Y., Yang, X., Wang, Z., Yang, Y., Yang, Y., Shu, Y., Cheng, L., and Liu, K. (2013). Curcumin serves as a human kv1. 3 blocker to inhibit effector memory T lymphocyte activities. Phytotherapy Research, 27(9), 1321–1327.

Lim, J., Koh, V. H. Q., Cho, S. S. L., Periaswamy, B., Choi, D. P. S., Vacca, M., de Sessions, P. F., Kudela, P., Lubitz, W., and Pastorin, G. (2019). Harnessing the immunomodulatory properties of bacterial ghosts to boost the anti-mycobacterial protective immunity. Frontiers in Immunology, 10, 2737.

Lin, P. L., Myers, A., Smith, L., Bigbee, C., Bigbee, M., Fuhrman, C., Grieser, H., Chiosea, I., Voitenek, N. N., and Capuano, S. v. (2010). Tumor necrosis factor neutralization results in disseminated disease in acute and latent *Mycobacterium tuberculosis* infection with normal granuloma structure in a cynomolgus macaque model. Arthritis and Rheumatism: Official Journal of the American College of Rheumatology, 62(2), 340–350.

Lin, Y., Ritchea, S., Logar, A., Slight, S., Messmer, M., Rangel-Moreno, J., Guglani, L., Alcorn, J. F., Strawbridge, H., and Park, S. M. (2009). Interleukin-17 is required for T helper 1 cell immunity and host resistance to the intracellular pathogen Francisella tularensis. Immunity, 31(5), 799–810.

Liu, P. T., Stenger, S., Tang, D. H., and Modlin, R. L. (2007). Cutting edge: vitamin D-mediated human antimicrobial activity against *Mycobacterium tuberculosis* is dependent on the induction of cathelicidin. The Journal of Immunology, 179(4), 2060–2063.

Liu, Y., Tan, S., Huang, L., Abramovitch, R. B., Rohde, K. H., Zimmerman, M. D., Chen, C., Dartois, V., VanderVen, B. C., and Russell, D. G. (2016). Immune activation of the host cell induces drug tolerance in *Mycobacterium tuberculosis* both *in vitro* and *in vivo*. Journal of Experimental Medicine, 213(5), 809–825.

López-Lázaro, M. (2009). Distribution and biological activities of flavonoid luteolin. Mini Reviews in Medicinal Chemistry, 9(1), 31–59.

Maiga, M., Agarwal, N., Ammerman, N. C., Gupta, R., Guo, H., Maiga, M. C., Lun, S., and Bishai, W. R. (2012). Successful shortening of tuberculosis treatment using adjuvant host-directed therapy with FDA-approved phosphodiesterase inhibitors in the mouse model. Public Library of Science One, 7(2), e30749.

Maiga, M., Ammerman, N. C., Maiga, M. C., Tounkara, A., Siddiqui, S., Polis, M., Murphy, R., and Bishai, W. R. (2013). Adjuvant host-directed therapy with types 3 and 5 but not type 4 phosphodiesterase inhibitors shortens the duration of tuberculosis treatment. The Journal of Infectious Diseases, 208(3), 512–519.

Majeed, S., Radotra, B. D., and Sharma, S. (2016). Adjunctive role of MMP-9 inhibition along with conventional anti-tubercular drugs against experimental tuberculous meningitis. International Journal of Experimental Pathology, 97(3), 230–237.

Martineau, A. R., Honecker, F. U., Wilkinson, R. J., and Griffiths, C. J. (2007). Vitamin D in the treatment of pulmonary tuberculosis. The Journal of Steroid Biochemistry and Molecular Biology, 103(3–5), 793–798.

Martinez, F. O., and Gordon, S. (2014). The M1 and M2 paradigm of macrophage activation: time for reassessment. F1000prime Reports, 6.

Mayosi, B. M., Ntsekhe, M., Bosch, J., Pandie, S., Jung, H., Gumedze, F., Pogue, J., Thabane, L., Smieja, M., and Francis, V. (2014). Prednisolone and *Mycobacterium* indicus pranii in tuberculous pericarditis. New England Journal of Medicine, 371(12), 1121–1130.

Mebazaa, A., ben Hadid, R., Cheikh Rouhou, R., Trojjet, S., el Euch, D., Mokni, M., Zitouna, M., and ben Osman, A. (2009). Hidradenitis suppurativa: a disease with male predominance in Tunisia. Acta Dermatovenerol Alp Pannonica Adriat, 18(4), 165–172.

Mehta, S., Mugusi, F. M., Bosch, R. J., Aboud, S., Urassa, W., Villamor, E., and Fawzi, W. W. (2013). Vitamin D status and TB treatment outcomes in adult patients in Tanzania: a cohort study. British Medical Journal Open, 3(11), e003703.

Meraviglia, S., el Daker, S., Dieli, F., Martini, F., and Martino, A. (2011). γδ T cells cross-link innate and adaptive immunity in *Mycobacterium tuberculosis* infection. Clinical and Developmental Immunology, 2011.

Meyer, V. R. (2013). Practical high-performance liquid chromatography. id Chromatography, 5th ed.; John Wiley and Sons: St. Gallen, Switzerland.

Michalek, J., Hezova, R., Turanek-Knötigova, P., Gabkova, J., Strioga, M., Lubitz, W., and Kudela, P. (2017). Oncolysate-loaded Escherichia coli bacterial ghosts enhance the stimulatory capacity of human dendritic cells. Cancer Immunology, Immunotherapy, 66(2), 149–159.

Mily, A., Rekha, R. S., Kamal, S. M., Akhtar, E., Sarker, P., Rahim, Z., Gudmundsson, G. H., Agerberth, B., and Raqib, R. (2013). Oral intake of phenylbutyrate with or without vitamin D3upregulates the cathelicidin LL-37 in human macrophages: a dose finding study for treatment of tuberculosis. BioMed Cental Pulmonary Medicine, 13(1), 1–8.

Mily, A., Rekha, R. S., Kamal, S. M. M., Arifuzzaman, A. S. M., Rahim, Z., Khan, L., Haq, M. A., Zaman, K., Bergman, P., and Brighenti, S. (2015). Significant effects of oral phenylbutyrate and vitamin D3 adjunctive therapy in pulmonary tuberculosis: a randomized controlled trial. Public Library of Science One, 10(9), e0138340.

Miyazaki, T., Pride, H. P., and Zipes, D. P. (1990). Prostaglandins in the pericardial fluid modulate neural regulation of cardiac electrophysiological properties. Circulation Research, 66(1), 163–175.

Mohr, E., Hughes, J., Reuter, A., Duran, L. T., Ferlazzo, G., Daniels, J., de Azevedo, V., Kock, Y., Steele, S. J., and Shroufi, A. (2018). Delamanid for rifampicin-resistant tuberculosis: a retrospective study from South Africa. European Respiratory Journal, 51(6).

Montoya, D., Inkeles, M. S., Liu, P. T., Realegeno, S., B. Teles, R. M., Vaidya, P., Munoz, M. A., Schenk, M., Swindell, W. R., and Chun, R. (2014). IL-32 is a molecular marker of a host defense network in human tuberculosis. Science Translational Medicine, 6(250), 250ra114-250ra114.

Moreland, R. B., Goldstein, I., Kim, N. N., and Traish, A. (1999). Sildenafil citrate, a selective phosphodiesterase type 5 inhibitor: research and clinical implications in erectile dysfunction. Trends in Endocrinology and Metabolism, 10(3), 97–104.

Morris, T., Stables, M., Hobbs, A., de Souza, P., Colville-Nash, P., Warner, T., Newson, J., Bellingan, G., and Gilroy, D. W. (2009). Effects of low-dose aspirin on acute inflammatory responses in humans. The Journal of Immunology, 183(3), 2089–2096.

Mortensen, E. M., Restrepo, M. I., Anzueto, A., and Pugh, J. (2005). The effect of prior statin use on 30-day mortality for patients hospitalized with community-acquired pneumonia. Respiratory Research, 6(1), 1–7.

Mu, X., Ubagai, T., Kikuchi-Ueda, T., Tansho-Nagakawa, S., Nakano, R., Kikuchi, H., and Ono, Y. (2013). Effects of erythromycin and rifampicin on immunomodulatory gene expression and cellular function in human polymorphonuclear leukocytes. Chemotherapy, 59(6), 395–401.

Ndjeka, N., and Ismail, N. A. (2020). Bedaquiline and clofazimine: successes and challenges. The Lancet Microbe, 1(4), e139–e140.

Organization, W. H. (2020). World Health Organization Global Tuberculosis Report 2020. World Health Organization, 232.

Orme, I. M., and Basaraba, R. J. (2014). The formation of the granuloma in tuberculosis infection. Seminars in Immunology, 26(6), 601–609.

Padmapriydarsini, C., Mamulwar, M., Mohan, A., Shanmugam, P., Gomathy, N. S., Mane, A., Singh, U. B., Pavankumar, N., Kadam, A., and Kumar, H. (2021). Randomized Trial of Metformin With Anti-Tuberculosis Drugs for Early Sputum Conversion in Adults With Pulmonary Tuberculosis. Clinical Infectious Diseases. 75(3), 425-434.

Page, C. P., and Spina, D. (2011). Phosphodiesterase inhibitors in the treatment of inflammatory diseases. Phosphodiesterases as Drug Targets, 391–414.

Pahari, S., Kaur, G., Aqdas, M., Negi, S., Chatterjee, D., Bashir, H., Singh, S., and Agrewala, J. N. (2017). Bolstering immunity through pattern recognition receptors: a unique approach to control tuberculosis. Frontiers in Immunology, 8, 906.

Palsson-McDermott, E. M., Doyle, S. L., McGettrick, A. F., Hardy, M., Husebye, H., Banahan, K., Gong, M., Golenbock, D., Espevik, T., and O'neill, L. A. J. (2009). TAG, a splice variant of the adaptor TRAM, negatively regulates the adaptor MyD88–independent TLR4 pathway. Nature Immunology, 10(6), 579–586.

Păunescu, E. (1970). *In vivo* and *in vitro* suppression of humoral and cellular immunological response by rifampicin. Nature, 228(5277), 1188–1190.

Peng, J., Yuan, Q., Lin, B., Panneerselvam, P., Wang, X., Luan, X. L., Lim, S. K., Leung, B. P., Ho, B., and Ding, J. L. (2010). SARM inhibits both TRIF-and MyD88-mediated AP-1 activation. European Journal of Immunology, 40(6), 1738–1747.

Poole, K. (2007). Efflux pumps as antimicrobial resistance mechanisms. Annals of Medicine, 39(3), 162–176.

Pradhan, S., Madke, B., Kabra, P., and Singh, A. L. (2016). Anti-inflammatory and immunomodulatory effects of antibiotics and their use in dermatology. Indian Journal of Dermatology, 61(5), 469.

Putri, D. U., Rintiswati, N., Soesatyo, M. H. N. E., and Haryana, S. M. (2018). Immune modulation properties of herbal plant leaves: Phyllanthus niruri aqueous extract on immune cells of tuberculosis patient-*in vitro* study. Natural Product Research, 32(4), 463–467.

Ramasamy, V., Mayosi, B. M., Sturrock, E. D., and Ntsekhe, M. (2018). Established and novel pathophysiological mechanisms of pericardial injury and constrictive pericarditis. World Journal of Cardiology, 10(9), 87.

Ramírez-Pérez, S., Hernández-Palma, L. A., Oregon-Romero, E., Anaya-Macías, B. U., García-Arellano, S., González-Estevez, G., and Muñoz-Valle, J. F. (2020). Downregulation of inflammatory cytokine release from Il-1β and Lps-stimulated Pbmc orchestrated by St2825, a Myd88 dimerisation inhibitor. Molecules, 25(18), 4322.

Rao Muvva, J., Ahmed, S., Rekha, R. S., Kalsum, S., Groenheit, R., Schön, T., Agerberth, B., Bergman, P., and Brighenti, S. (2021). Immunomodulatory agents combat multidrug-resistant tuberculosis by improving antimicrobial immunity. The Journal of Infectious Diseases, 224(2), 332–344.

Raveinal, R. (2003). The effect of natural immunomodulator (Phyllanti herb extract) administration on cellular immune response of patients with pulmonary tuberculosis. Padang: University of Andalas.

Regan, T., Nally, K., Carmody, R., Houston, A., Shanahan, F., MacSharry, J., and Brint, E. (2013). Identification of TLR10 as a key mediator of the inflammatory response to Listeria monocytogenes in intestinal epithelial cells and macrophages. The Journal of Immunology, 191(12), 6084–6092.

Rekha, R. S., Rao Muvva, S. S. V. J., Wan, M., Raqib, R., Bergman, P., Brighenti, S., Gudmundsson, G. H., and Agerberth, B. (2015). Phenylbutyrate induces LL-37-dependent autophagy and intracellular killing of *Mycobacterium tuberculosis* in human macrophages. Autophagy, 11(9), 1688–1699.

Robinson, P. S., Huang, T.-F., Kazam, E., Iozzo, R. v, Birk, D. E., and Soslowsky, L. J. (2005). Influence of decorin and biglycan on mechanical properties of multiple tendons in knockout mice. Journal of Biomechanical Engineering, 127(1), 181–185.

Rodriguez, E. R., and Tan, C. D. (2017). Structure and anatomy of the human pericardium. Progress in Cardiovascular Diseases, 59(4), 327–340.

Romero, M. M., Basile, J. I., Corra Feo, L., López, B., Ritacco, V., and Alemán, M. (2016). Reactive oxygen species production by human dendritic cells involves TLR2 and dectin-1 and is essential for efficient immune response against Mycobacteria. Cellular Microbiology, 18(6), 875–886.

Russell, M. S., Dudani, R., Krishnan, L., and Sad, S. (2009). IFN-γ expressed by T cells regulates the persistence of antigen presentation by limiting the survival of dendritic cells. The Journal of Immunology, 183(12), 7710–7718.

Saiga, H., Shimada, Y., and Takeda, K. (2011). Innate immune effectors in mycobacterial infection. Clinical and Developmental Immunology, 2011.

Salahuddin, N., Ali, F., Hasan, Z., Rao, N., Aqeel, M., and Mahmood, F. (2013). Vitamin D accelerates clinical recovery from tuberculosis: results of the SUCCINCT Study [Supplementary Cholecalciferol in recovery from tuberculosis]. A randomized, placebo-controlled, clinical trial of vitamin D supplementation in patients with pulmonary tuberculosis'. BioMed Central Infectious Diseases, 13(1), 1–11.

Santiago-Carvalho, I., Simão, T. L. B. V., Calixto, S. D., de Albuquerque, T. C., Konno, T. U. P., Salgado, R. M., Muzitano, M. F., Pinto, S. C., and Lasunskaia, E. (2022). Antitubercular and immunomodulatory activities of Eugenia astringens n-hexane fraction. Phytomedicine Plus, 2(2), 100236.

Sarangi, A., Das, B. S., Patnaik, G., Sarkar, S., Debnath, M., Mohan, M., and Bhattacharya, D. (2021). Potent anti-mycobacterial and immunomodulatory activity of some bioactive molecules of Indian ethnomedicinal plants that have the potential to enter in TB management. Journal of Applied Microbiology, 131(4), 1578–1599.

Sarathy, J. P., Liang, H. H., Weiner, D., Gonzales, J., Via, L. E., and Dartois, V. (2017). An *in vitro* caseum binding assay that predicts drug penetration in tuberculosis lesions. Journal of Visualized Experiments, 123, e55559.

Sarker, S. D., and Nahar, L. (2015). Applications of high performance liquid chromatography in the analysis of herbal products. In Evidence-Based Validation of Herbal Medicine (pp. 405–425). Elsevier.

Saroj, P., Verma, M., and Jha, K. K. (2012). An overview on immunomodulation. Journal of Advanced Scientific Research, 3(1).

Schiebler, M., Brown, K., Hegyi, K., Newton, S. M., Renna, M., Hepburn, L., Klapholz, C., Coulter, S., Obregón-Henao, A., and Henao Tamayo, M. (2015). Functional drug screening reveals anticonvulsants as enhancers of mTOR-independent autophagic killing of *Mycobacterium tuberculosis* through inositol depletion. EMBO Molecular Medicine, 7(2), 127–139.

Schoeman, J. F., Springer, P., van Rensburg, A. J., Swanevelder, S., Hanekom, W. A., Haslett, P. A. J., and Kaplan, G. (2004). Adjunctive thalidomide therapy for childhood tuberculous meningitis: results of a randomized study. Journal of Child Neurology, 19(4), 250–257.

Schoenen, H., Bodendorfer, B., Hitchens, K., Manzanero, S., Werninghaus, K., Nimmerjahn, F., Agger, E. M., Stenger, S., Andersen, P., and Ruland, J. (2010). Cutting edge: Mincle is essential for recognition and adjuvanticity of the mycobacterial cord factor and its synthetic analog trehalose-dibehenate. The Journal of Immunology, 184(6), 2756–2760.

Schönfeld, N., Bergmann, T., Vesenbeckh, S., Mauch, H., Bettermann, G., Bauer, T. T., and Rüssmann, H. (2012). Minimal inhibitory concentrations of first-line drugs of multidrug-resistant tuberculosis isolates. Lung India: Official Organ of Indian Chest Society, 29(4), 309.

Shabetai, R. (2003). The pericardium (Vol. 249). Springer Science and Business Media.

Sharma, M., Sharma, S., Roy, S., Varma, S., and Bose, M. (2007). Pulmonary epithelial cells are a source of interferon-γ in response to *Mycobacterium tuberculosis* infection. Immunology and Cell Biology, 85(3), 229–237.

Shenje, J., Adimora-Nweke, F.I., Ross, I.L., Ntsekhe, M., Wiesner, L., Deffur, A., McIlleron, H.M., Pasipanodya, J., Gumbo, T. and Mayosi, B.M. (2015). Poor Penetration of Antibiotics into Pericardium in Pericardial Tuberculosis. EBioMedicine, 2(11), 1640–1649.

Shimoi, K., Okada, H., Furugori, M., Goda, T., Takase, S., Suzuki, M., Hara, Y., Yamamoto, H., and Kinae, N. (1998). Intestinal absorption of luteolin and luteolin 7-O-β-glucoside in rats and humans. Federation of European Biochemical Societies Letters, 438(3), 220–224.

Singh, D. K., Dwivedi, V. P., Ranganathan, A., Bishai, W. R., van Kaer, L., and Das, G. (2016). Blockade of the Kv1. 3 K+ channel enhances BCG vaccine efficacy by expanding central memory T lymphocytes. The Journal of Infectious Diseases, 214(9), 1456–1464.

Singh, D. K., Dwivedi, V. P., Singh, S. P., Kumari, A., Sharma, S. K., Ranganathan, A., Kaer, L. van, and Das, G. (2020). Luteolin-mediated Kv1. 3 K+ channel inhibition augments BCG vaccine efficacy against tuberculosis by promoting central memory T cell responses in mice. Public Library of Science Pathogens, 16(9), e1008887.

Singhal, A., Jie, L., Kumar, P., Hong, G. S., Leow, M. K.S., Paleja, B., Tsenova, L., Kurepina, N., Chen, J., and Zolezzi, F. (2014). Metformin as adjunct antituberculosis therapy. Science Translational Medicine, 6(263), 263ra159-263ra159.

Skerry, C., Pinn, M. L., Bruiners, N., Pine, R., Gennaro, M. L., and Karakousis, P. C. (2014). Simvastatin increases the *in vivo* activity of the first-line tuberculosis regimen. Journal of Antimicrobial Chemotherapy, 69(9), 2453–2457.

Son, E.-W., Mo, S.-J., Rhee, D.-K., and Pyo, S. (2006). Inhibition of ICAM-1 expression by garlic component, allicin, in gamma-irradiated human vascular endothelial cells via downregulation of the JNK signaling pathway. International Immunopharmacology, 6(12), 1788–1795.

Steinmann, J., Halldórsson, S., Agerberth, B., and Gudmundsson, G. H. (2009). Phenylbutyrate induces antimicrobial peptide expression. Antimicrobial Agents and Chemotherapy, 53(12), 5127–5133.

Subbian, S., Tsenova, L., Holloway, J., Peixoto, B., O'Brien, P., Dartois, V., Khetani, V., Zeldis, J. B., and Kaplan, G. (2016). Adjunctive phosphodiesterase-4 inhibitor therapy improves antibiotic response to pulmonary tuberculosis in a rabbit model. EBioMedicine, 4, 104–114.

Sundar, S. (2023). In-silico transcriptome analysis of antibiotic-treated *Mycobacterium tuberculosis* identifies novel antibiotic resistance factors. Indian Journal of Tuberculosis.

Suo, J., Chang, C.-E., Lin, T. P., and Heifets, L. B. (1988). Minimal inhibitory concentrations of isoniazid, rifampin, ethambutol, and streptomycin against *Mycobacterium tuberculosis* strains isolated before treatment of patients in Taiwan. American Journal of Respiratory and Critical Care Medicine, 138(4), 999–1001.

Szczypka, M., and Obmińska-Mrukowicz, B. (2010). Modulating effects of nonselective and selective phosphodiesterase inhibitors on lymphocyte subsets and humoral immune response in mice. Pharmacological Reports, 62(6), 1148–1158.

Tanne, A., Ma, B. O., Boudou, F., Tailleux, L., Botella, H., Badell, E., Levillain, F., Taylor, M. E., Drickamer, K., and Nigou, J. (2009). A murine DC-SIGN homologue contributes to early host defense against *Mycobacterium tuberculosis*. Journal of Experimental Medicine, 206(10), 2205–2220.

Thoma-Uszynski, S., Kiertscher, S. M., Ochoa, M. T., Bouis, D. A., Norgard, M. v, Miyake, K., Godowski, P. J., Roth, M. D., and Modlin, R. L. (2000). Activation of toll-like receptor 2 on human dendritic cells triggers induction of IL-12, but not IL-10. The Journal of Immunology, 165(7), 3804–3810.

Thompson, J. E. (1969). The management of hypersensitivity reactions to antituberculosis drugs. Medical Journal of Australia, 2(21), 1058–1063.

Tjandrawinata, R., Susanto, L., and Nofiarny, D. (2017). The use of Phyllanthus niruri L. as an immunomodulator for the treatment of infectious diseases in clinical settings. Asian Pacific Journal of Tropical Disease, 7, 132–140.

Tobin, D. M., and Ramakrishnan, L. (2013). TB: the Yin and Yang of lipid mediators. Current Opinion in Pharmacology, 13(4), 641–645.

Tousif, S., Singh, D. K., Ahmad, S., Moodley, P., Bhattacharyya, M., van Kaer, L., and Das, G. (2014). Isoniazid Induces Apoptosis of Activated CD4+ T Cells. Journal of Biological Chemistry, 289(44), 30190–30195.

Tousif, S., Singh, D. K., Mukherjee, S., Ahmad, S., Arya, R., Nanda, R., Ranganathan, A., Bhattacharyya, M., van Kaer, L., and Kar, S. K. (2017). Nanoparticle-formulated curcumin prevents posttherapeutic disease reactivation and reinfection with *Mycobacterium tuberculosis* following isoniazid therapy. Frontiers in Immunology, 8, 739.

Tukvadze, N., Sanikidze, E., Kipiani, M., Hebbar, G., Easley, K. A., Shenvi, N., Kempker, R. R., Frediani, J. K., Mirtskhulava, V., and Alvarez, J. A. (2015). High-dose vitamin D3 in adults with pulmonary tuberculosis: a double-blind randomized controlled trial. The American Journal of Clinical Nutrition, 102(5), 1059–1069.

Turvey, S. E., and Broide, D. H. (2010). Innate immunity. Journal of Allergy and Clinical Immunology, 125(2), S24–S32.

Underhill, D. M., Ozinsky, A., Smith, K. D., and Aderem, A. (1999). Toll-like receptor-2 mediates mycobacteria-induced proinflammatory signaling in macrophages. Proceedings of the National Academy of Sciences, 96(25), 14459–14463.

Van Crevel, R., and Hill, P. C. (2017). Tuberculosis. Infectious Diseases, 2-Volume Set, 271-284.e1.

van der Does, A. M., Kenne, E., Koppelaar, E., Agerberth, B., and Lindbom, L. (2014). Vitamin D3 and phenylbutyrate promote development of a human dendritic cell subset displaying enhanced antimicrobial properties. Journal of Leukocyte Biology, 95(6), 883–891.

van der Paardt, A.-F., Wilffert, B., Akkerman, O. W., de Lange, W. C. M., van Soolingen, D., Sinha, B., van der Werf, T. S., Kosterink, J. G. W., and Alffenaar, J.-W. C. (2015). Evaluation of macrolides for possible use against multidrug-resistant *Mycobacterium tuberculosis*. European Respiratory Journal, 46(2), 444–455.

Walker, N. F., Clark, S. O., Oni, T., Andreu, N., Tezera, L., Singh, S., Saraiva, L., Pedersen, B., Kelly, D. L., and Tree, J. A. (2012). Doxycycline and HIV infection suppress tuberculosis-induced matrix metalloproteinases. American Journal of Respiratory and Critical Care Medicine, 185(9), 989–997.

Wang, N., Liang, H., and Zen, K. (2014). Molecular mechanisms that influence the macrophage M1–M2 polarization balance. Frontiers in Immunology, 5, 614.

Wang, X., Grace, P. M., Pham, M. N., Cheng, K., Strand, K. A., Smith, C., Li, J., Watkins, L. R., and Yin, H. (2013). Rifampin inhibits Toll-like receptor 4 signaling by targeting myeloid differentiation protein 2 and attenuates neuropathic pain. The Federation of American Societies for Experimental Biology Journal, 27(7), 2713–2722.

Werninghaus, K., Babiak, A., Groß, O., Hölscher, C., Dietrich, H., Agger, E. M., Mages, J., Mocsai, A., Schoenen, H., and Finger, K. (2009). Adjuvanticity of a synthetic cord factor analogue for subunit *Mycobacterium tuberculosis* vaccination requires FcRγ–Syk–Card9–dependent innate immune activation. Journal of Experimental Medicine, 206(1), 89–97.

Whittaker, E., Nicol, M. P., Zar, H. J., Tena-Coki, N. G., and Kampmann, B. (2018). Age-related waning of immune responses to BCG in healthy children supports the need for a booster dose of BCG in TB endemic countries. Scientific Reports, 8(1), 1–10.

Xu, Y., Xu, S., Liu, P., Koroleva, M., Zhang, S., Si, S., and Jin, Z. G. (2017). Suberanilohydroxamic acid as a pharmacological Kruppel-Like Factor 2 activator that represses vascular inflammation and atherosclerosis. Journal of the American Heart Association, 6(12), e007134.

Yamasaki, S., Ishikawa, E., Sakuma, M., Hara, H., Ogata, K., and Saito, T. (2008). Mincle is an ITAM-coupled activating receptor that senses damaged cells. Nature Immunology, 9(10), 1179–1188.

Yonekawa, A., Saijo, S., Hoshino, Y., Miyake, Y., Ishikawa, E., Suzukawa, M., Inoue, H., Tanaka, M., Yoneyama, M., and Oh-Hora, M. (2014). Dectin-2 is a direct receptor for mannose-capped lipoarabinomannan of mycobacteria. Immunity, 41(3), 402–413.

Yongmei, Y. I. N., Jie, Q. I. N., Yaping, D. A. I., Fanwei, Z., Hao, P. E. I., and Jun, W. (2015). The CD4+/CD8+ ratio in pulmonary tuberculosis: systematic and meta-analysis article. Iranian Journal of Public Health, 44(2), 185.

Young, C., Walzl, G., and du Plessis, N. (2020). Therapeutic host-directed strategies to improve outcome in tuberculosis. Mucosal Immunology, 13(2), 190–204.

Yu, X., Li, L., Xia, L., Feng, X., Chen, F., Cao, S., and Wei, X. (2019). Impact of metformin on the risk and treatment outcomes of tuberculosis in diabetics: a systematic review. BioMed Central Infectious Diseases, 19(1), 1–11.

Zhang, W., Ge, Y., Cheng, Q., Zhang, Q., Fang, L., and Zheng, J. (2018). Decorin is a pivotal effector in the extracellular matrix and tumour microenvironment. Oncotarget, 9(4), 5480.

Ziglam, H. M., Daniels, I., and Finch, R. G. (2004). Immunomodulating activity of rifampicin. Journal of Chemotherapy, 16(4), 357–361.

CHAPTER THREE

SURFACE MODIFIED DRUG DELIVERY SYSTEM FOR TUBERCULOSIS INTERVENTION

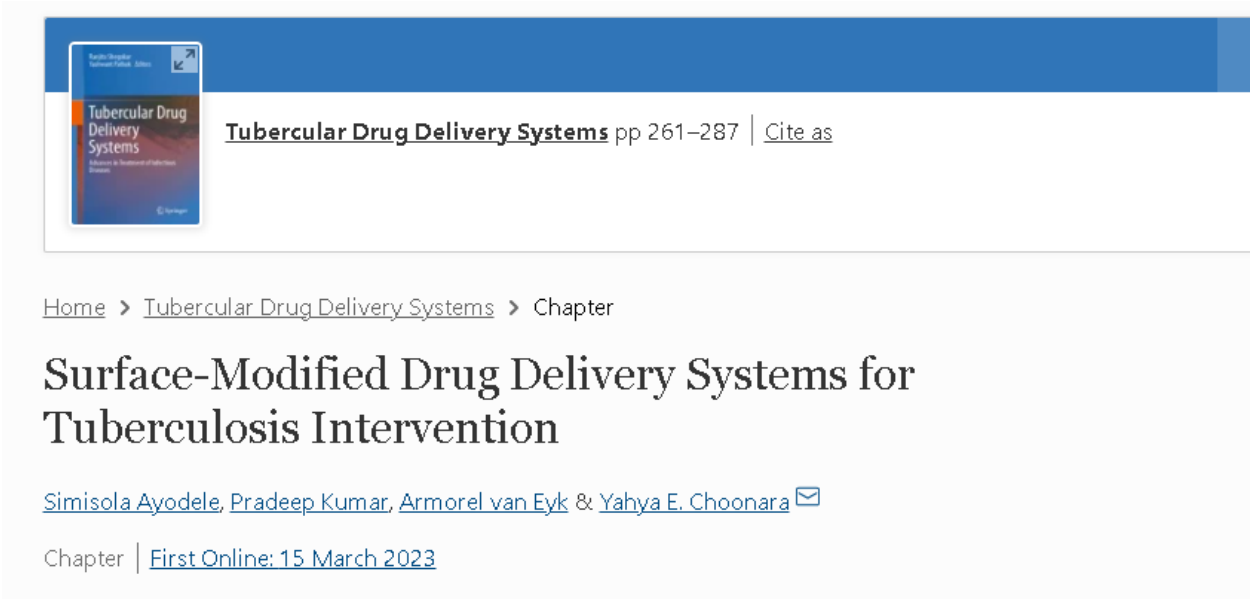

Tuberculosis (TB) presents as the second most lethal infectious disease after HIV/AIDs and has presented difficulty in treatment over the years, due to prolonged duration of therapy and side-effects of the drugs resulting in patient non-compliance and the development of multi-drug resistance (MDR) strains. To prevent these train of events, anti-TB drugs incorporated in nanosystems may reduce side effects by delivering the drug selectively into infection reservoirs such as macrophages, which may assist in clearing the TB bacilli faster, and reducing the duration of therapy. The rapid development in nanosciences has improved the targeted delivery of therapeutics, offering great benefits in the treatment of chronic diseases. Nanosystems demonstrate great prospect, by specific and selective targeting, supported by their ability to be surface functionalised with targeting ligands. This chapter will therefore demonstrate the state-of-the-art in the development of surface-modified nanotechnology incorporated with anti-TB therapeutics.

3.1. INTRODUCTION

Even with enhanced research and decades of dedication towards finding the solution for the best treatment of tuberculosis (TB) whilst ensuring efficacy and safety, TB is still considered cataclysmic in nature, ranking 1st in mortality by a single infectious agent in the world (MacNeil et al., 2019). In 2019, it was reported that 1.4 million people died from the disease. The mortality rate has been found to drop by 9% between 2015 and 2019 by 2% annually but is still less than half the milestone 20% target set between the years 2015 and 2020 in correlation with the United Nations Sustainable Development Goals (SDGs) and World Health Organization (WHO) goals to end TB by 2030 and 2035, respectively (WHO, 2015; WHO, 2020). With this target in place and our reports not on track, it is evident that more interventions and efforts are needed to achieve these goals. These interventions will need to improve the 6 monthly duration of treatment and patient compliance which are causes of treatment failure and MDR strains (Dye, 2006). MDR strains require second-line drugs which take a longer period of 9-12 months to treat, increasing the possibility of patient incompliance and mortality.

With TB maintaining its notable mortality rate over the past decades, it has become more evident that the conventional anti-TB therapeutic regimen with no enhancing delivery system alone, may not be sufficient to end TB in the set periods due to the limitations it poses. Targeted drug delivery systems are looked up to as a method to counter these limitations and enhance the therapeutic efficacy of these drugs by enhancing drug permeability, decreasing resistance, providing controlled drug release, increasing potency whilst decreasing dosage amount, frequency and the potential for adverse effects (Sarkar et al., 2021).

The conventional anti-TB drugs poorly permeate the hydrophobic lipoarabinomannan rich envelope of *Mycobacterium tuberculosis* (*M.tb*), which also includes a hydroxyl fatty acid, mycolic acid which is bound to arabinogalactan, granting it a very hydrophobic character (Sarkar et al., 2021). Out of the 4 standard anti-TB drugs, isoniazid (INH), pyrazinamide (PZA) and ethambutol (EMB) are all hydrophilic making them impermeable to these cell walls. Rifampicin (RIF) is the only lipophilic drug and most structurally complex of all standard anti-TB drugs. Studies suggest that lipophilic derivatives were more active against replicating mycobacteria than its hydrophilic companions (Piccaro et al., 2015), it was found that the application of lipophilic compounds such as bedaquiline, rifapentine, clofazimine, PA-824, sutezolid and the new nitroimidazole called TBA-354 on rats, resulted in sterilization from *M.tb* in 6-8 weeks in comparison to RIF+INH+PZA which took 6 months (Williams et al., 2012; and Piccaro et al., 2015). Additionally, only lipophilic

compounds killed both dormant H12/H19 cells and A5/H5 cells (Piccaro et al., 2015). Based on such a background, a drug delivery system that enhances permeability and internalization of hydrophilic drugs may be required to improve therapeutic outcomes.

Targeted drug delivery systems will allow the encompassing of pulmonary therapeutic advancement and also extrapulmonary tuberculosis therapeutic advancement which contributes to 16% of TB cases and is the most difficult to treat (WHO, 2020). Central Nervous System (CNS) manifestations of TB is the most prominent form of extrapulmonary TB, with worse therapeutic outcomes than pulmonary TB due to a lack of an effective system to ensure drug delivery to require site of action. From the first line, only INH and PZA show sufficient CSF bioavailability but RIF and EMB have been shown to have poorer CSF bioavailability, thus requiring a higher dose for therapeutic relevance consequently causing an increased severity in the possible adverse effects like cerebral haemorrhage and visual impairment, respectively. Fluoroquinolones, a second-line agent also have good bioavailability in the CSF. New generational fluoroquinolones have also proven to be greatly efficacious in the treatment of MDR-TB, like gatifloxacin due to its low incidence of resistance (Zhang et al., 2014). On the other hand, streptomycin demonstrates minimal efficacy whereby at high doses may increase the risk of nephrotoxicity and ototoxicity.

Nanotechnology is an extensively studied method of delivery in recent years. The nanospheres' small-sized property of nanoparticles allow the particle to be able to travel uninterruptedly across the human body (Patra et al., 2018). Nanomedicine has gained more medical relevance over time due to its ability to bind to a drug or even encapsulate it whilst simultaneously attaching unto its surface, functionalizing proteins to promote targeted controlled delivery of the drug. Surface modification of the delivery system brings about a more specific targeted delivery which is also accompanied by theranostics, the integration of therapy and diagnosis. Dendrimers are typical examples of nanoparticles well known for their entrapment and surface attaching capabilities. Their very small size of 2-10 nm and multiple functional group sites on its surface, allows binding of drugs and ligands for targeted-controlled drug delivery (Kaur et al., 2015; and Singh et al., 2016). Carbon nanotubes are another synthetic nano-biotechnology of size 1-100 nm with great prospects in the nano-field due to the ease of surface modification with drug and functional ligands based on the desire for enhanced site-specific delivery (Pabreja et al., 2014).

Nanosensors modification on nanoparticles further allows diagnosis apart from treatment. In the case of poly (ethylene glycol)-modified poly (amidoamine) dendrimers encapsulating gold nanoparticles, a system that employs both imaging functions of cancer diagnosis and treatment (Haba et al., 2007), using gold nanoparticles are used as biomarkers and tumour labels in detection assays (Patra et al., 2018). Combination studies of nano-systems and natural products have gained prominence over the last decades for the treatment of various conditions. This green nanotechnology allows the incorporation of nanoparticles with natural products, decreasing the development of toxicity encountered from biosynthetic processes which result in side effects (Lam et al., 2017). These methods have been greatly appreciated, leading to the FDA approval of liposomes and micelles, the forebearers of nanoparticle-based therapy (Shi et al., 2008).

The CD206/mannose receptors are predominantly expressed on the surface of macrophages and dendritic cells acting as a pattern recognition receptor (PRR) which is recognised by mannose-binding lectin receptors that bind to glycoproteins found on the surface pathogens like *M.tb*. The M2 macrophage which are responsible for the resolution of inflammation, protection from excessive inflammation and tissue repair, express more CD206 receptor in comparison to M1 macrophages (Hussell and Bell, 2014). The CD206 receptor, unfortunately, stands as the site of exploitation by *M.tb* to facilitate infection in macrophages (Kang et al., 2005). In addition to that, soluble forms of CD206, (sCD206) are found in the periphery and can recognise mannosylated carbohydrates and cause an effect on the innate and immune response (Su et al., 2005). The CD206 receptor can therefore be used as a therapeutic target for the treatment of *M.tb*.

This concept has therefore created a path using mannosylated-nanostructured lipid carrier (NLC) for active targeting of the CD206 on macrophages (Vieira, et al., 2018; and Pi et al., 2019) and mannose microstructured modified liposomes (Chono et al., 2008). A definite increase in the uptake of the particles was observed in rats' alveolar macrophages after pulmonary administration. Furthermore, plasma concentrations of encapsulated drugs are found to be decreased in comparison to free drugs indicating increased specificity and selectivity of the delivery system. In the study of liposomes at a size range of 90–125 nm, a positive correlation was observed between the concentrations of mannose on the surface and a more notable cellular uptake (Wijagkanalan et al., 2008). In the presence of excess solubilised mannan, the uptake of the nanoparticles also decreased due to receptor overload, further confirming the specificity of mannose to CD206 receptor (Wijagkanalan et al., 2008).

HIV/AIDs is an important cause of the continuation of TB, which has contributed to the mortality and morbidity rates of TB (Sharma et al., 2005). A slight contributing factor to the increased mortality and morbidity includes intestinal malabsorption of anti-TB drugs, mainly RIF and ETB (Smith, 2003). Since RIF is taken over 6 months, it is important for it to have good bioavailability, due to its lipophilic nature, but unfortunately demonstrates low aqueous solubility and low intestinal absorption (Mariappan and Singh, 2003). This is because, in gastric acidic conditions, RIF is hydrolysed into even lesser soluble forms such as 3-formyl rifampicin and 1-amino-4-methyl piperazine (Sosnik et al., 2010). In fixed-dose combinations, the intragastric reaction of RIF with INH also forms an insoluble hydrazone (Singh et al., 2000).

Enhancing drug bioavailability and targeted treatment will increase drug effectiveness and decrease treatment duration, improve patient compliance, and minimize the dose required to obtain a therapeutic effect. These are the goals for the pharmaceutical industry making targeted encapsulated drug delivery systems great prospects in achieving this goal (Sosnik et al., 2010).

3.2. NANOTECHNOLOGIES IN TUBERCULOSIS

Nanosystems generally have various structural and functional properties, therefore modification is possible, to achieve the required outcome by changing the compositions of the system. These modifications include the drug, polymeric materials, functional groups and even excipients (Garg et al., 2015). Nanosystems' success is easily measured by their physicochemical abilities and their permeation abilities across anatomical barriers that unloaded drugs hardly pass through (Singh et al., 2016). Drug encapsulation within nano-sized carriers reduces drug elimination from the intracellular medium facilitated by resistant-mediated efflux pumps that is prevalent in various pathologies including cancer, HIV, and hepatitis. Nanotechnology thus has the prospects to overcome or decrease drug resistance.

3.3. POLYMERIC NANOSYSTEMS

Polymeric nanoparticles (PNPs) present great prospects in the treatment of diseases due to their intricate structure that allows surface modification. They have been substantially investigated to improve drug solubility, stability and targeting, which ultimately improves drug bioavailability at the required site of action (Sosnik et al., 2010). Polymeric nanoparticles are mainly subclassified into 2 broad groups, namely nanocapsules and nanospheres. Nanocapsules comprises drugs incorporated with hydrophilic/ hydrophobic solvents bounded by a polymeric membrane, whilst nanospheres is a solid network, a model that allows even distribution of drug across variable

pores in its structure. PNPs high loading capacity of both hydrophilic and hydrophobic drugs and its viability across various routes of administration makes it a prominent delivery system for drug entrapment (Brannon-Peppas, 1995). Opsonization and phagocytosis are two mechanisms for eliminating PNP from the body. This clearance method could also present advantageously in the treatment of TB since the body clears TB in the same way. Furthermore, to prolong blood circulation periods, promising outcomes have been identified by the modification of nanosystems with highly hydrophilic chains such as poly(ethylene glycol) (PEG) (Sosnik et al., 2010).

3.3.1. Modified Polymeric Nanoparticles

Lectin surface-modified poly(lactic-co-glycolic acid) (PLGA) nanoparticles enhanced targeted delivery of anti-tubercular drugs across pulmonary and gastro-intestinal mucosa (Sharma et al., 2004). The process employed the use of carbodiimide, which yields the formation of amide bonds between the amines of lectin; wheat germ agglutinin (WGA), and carboxylic acid groups of PLGA. This surface grafting method yielded a coupling efficiency of 60-70%, whereby 3–3.5 mg lectin bound per mg of PLGA by acting as bioadhesive drug carriers, causing the drug residence time in plasma of RIF, INH and PZA to be improved. The WGA-coating allowed RIF to be retained in plasma for 6-7 days, instead of 4-6 days in uncoated particles. PZA and INH were retained for 13-14 days instead of 8-9 days. In the liver, spleen and lungs, the drugs were all detectable for 15 days, minimising the chance of drug resistance. In SGF and SIF, only 3-5% drug was released, stipulating its targeting ability and stability in the GIT, but the glycosylated structures in the GIT, allowed immobility on the system using the surface grafted lectin recognizable by GI mucosa and lung mucosa. The dosing frequency was also revealed to decrease the dose required to reach undetectable mycobacteria colony-forming units from 45 doses in the conventional free drugs compared to 3 doses of oral/nebulized lectin-coated nanoparticles administered fortnightly (Sharma et al., 2004).

A more interesting concept of polymeric nanoparticles involves the use of the polymer poly(ethylene oxide) monomethyl ether-block-poly(ε - caprolactone) with a förster resonance energy transfer system sensor which allows perceptible assessment of the delivery system drug release. There was an observed enhanced release of drug from polymer *in vivo* for cells that retained the system than *in vitro* dialysis tubes. Furthermore, *in vitro* assays showed that apart from the antimicrobial effect of RIF, blank NPs also exhibited antimicrobial effects against *Mycobacterium fortuitum* (Trousil et al., 2017).

Polymeric nanoparticles together with liposomes (LPs) may form a hybrid nano-carrier, called solid lipid nanoparticles (SLNPs), a solid lipid core, surrounded by surfactants to improve the drug stability and loading capacity of LPs (Abed and Couvreur, 2014). To practicalize these concepts, a WGA-conjugated SLNP has been studied for the enhancement of RIF delivery. The nanoparticles consisted of glyceryl monostearate (GMS) and stearic acid (SA), of which the SA introduced free carboxylic acid to the surface of the nanoparticles, whilst forming together with GMS, the internal part of the lipid. The nanosystem was synthesised by a process of simple emulsification, before solvent evaporation followed by a carbodiimide reaction for WGA conjugation as in Figure 3.1 below (Pooja et al., 2015).

The entrapment efficacy of RIF into the nanosystem was 68.71%, consequently, it was noted that the entrapment had no significant effect on the particle size and zeta potential of the system. The WGA allowed a high binding efficacy unto intestinal mucus glycoproteins of 93.06% compared to polymeric nanoparticles, since lipids have the ability to bind to mucin, which promoted a more controlled release, from 20 h in pure RIF to a biphasic release throughout 120 h with an initial burst release of 37.1% in the first 24 h and 76.9% release after 120 h. The system presented toxicity by showing a positive haemagglutinin test, which could be explained by the binding of the lectin conjugated system (WGA) to the carbohydrate moiety on red blood cells (RBC). In the presence of excess N-acetyl glucosamine (NAG), this toxicity was prevented, altering binding of the system to RBCs (Pooja et al., 2015).

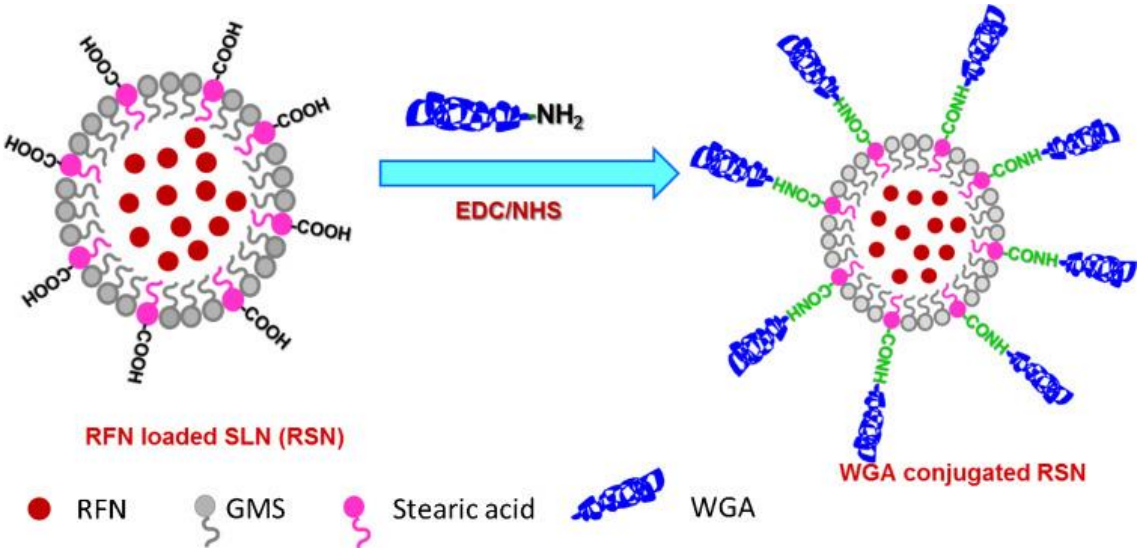

Figure 3.1: Schematic diagram showing the arrangement of rifampicin (RFN) and lipids (stearic acid and glyceryl monostearate (GMS)) in the nanoparticles followed by conjugation of wheat germ agglutinin (WGA) on the surface. Keywords: ethyl carbodiimide (EDC), N-hydroxys.

To survive in GI acidic medium, the RIF degradation, in the presence of INH was decreased, SLNPs, made up of Compritol® ATO 888/ polysorbate 80. The nanosystem synthesised by microemulsification method was found to minimize the drug's interaction. Results obtained indicated that RIF-loaded SLNPs promoted 60% degradation protection induced by free INH at acidic pH while a 74.7% degradation protection was achieved when both the agents were incorporated separately into SLNPs (Singh et al., 2013).

A RIF-loaded SLNPs coated with chitosan, with the lipid phase composed of cetyl palmitate synthesised by ultrasonication method, demonstrated improved mucoadhesive properties *in vitro*, increasing retention time of system in the alveolar and improving RIF permeability across alveolar epithelial cells due to the chitosan coating. This platform may be a prospective system for the enhancement of aerosol drug delivery (Vieira et al., 2018b). Apart from RIF, INH has also been incorporated in similar strategies, whereby chitosan was more soluble in gastric pH of 1.2 compared to intestinal pH of 7.4, the acidic pH favoured the swelling of the polymer and solubility of the drug, due to the basic nature of INH, it solubilizes at acidic pH (Banik et al., 2012). An initial burst release in the first 3 h of 50% of the drug due to the adsorbed drug on the surface of the nanoparticles was observed.

Employing biomaterial, PLGA and PEG, a PLGA-PEG-PLGA triblock copolymer synthesised by a water-oil-water double emulsification technique for the delivery of INH, loaded by sonication

with a drug loading efficiency and drug content of (12.8–18.67%) and (6.4–8.9%), respectively, improved bioavailability of INH by 28 folds. The nitrogen atom of INH binds to the carbonyl oxygen of the polymer, causing INH to be loaded on the surface of the core-shell. This effect resulted in an initial 2 hr burst release of INH from the surface. Due to the emulsification technique of nanoparticle synthesis, an additional small burst release occurred due to the interstitial space in the core-shell, and subsequently, a third stage controlled release from individual nanoparticles as in Figure 3.2 below. The sustained release is said to be present for up to a period of 124 h (Gajendiran et al., 2013).

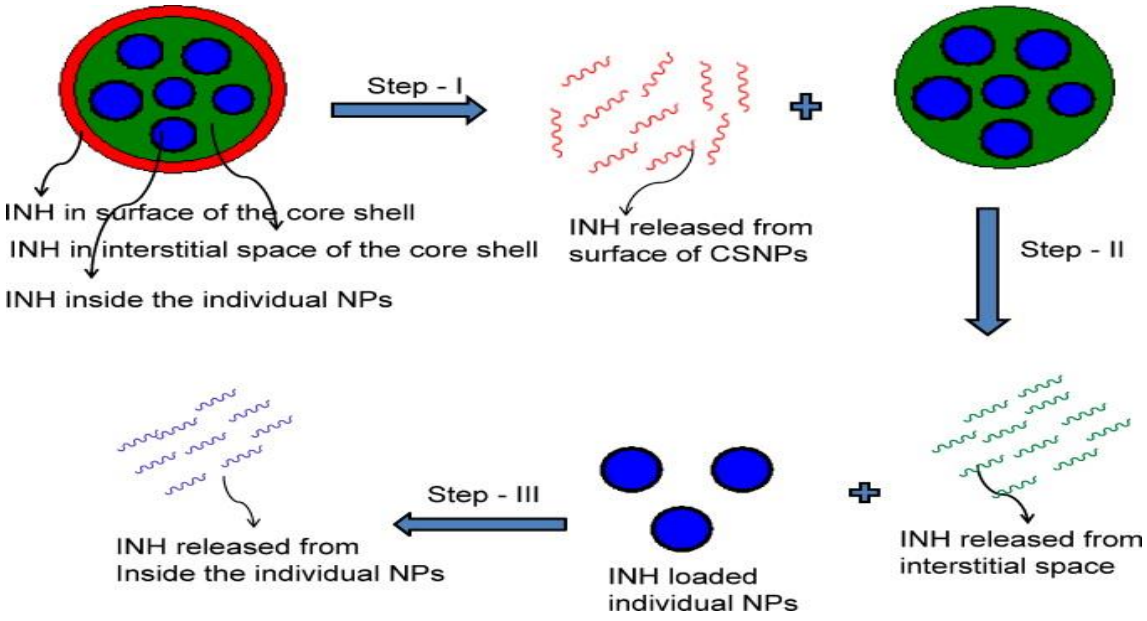

Figure 3.2: Mechanism of drug release of PLGA-PEG-PLGA triblock copolymer synthesised by water-oil-water double emulsification. Figure obtained with permission from (Gajendiran et al., 2013).

Another approach looked towards the synthesis of RIF-, INH- and PZA-loaded PLGA nebulized nanoparticles for pulmonary delivery, with a mass median aerodynamic diameter (MMDA) of 1.88µm, indicating the respirability of the nanoparticles, showing plasma detection 6 h post-administration. Due to the prolonged half-life of the system, loaded anti-TB drugs had a higher AUC than both IV and oral free drugs bioavailability. When compared to nebulised free drugs the bioavailability increases by 51.0-, 20.0- and 28.0-fold for RIF, INH and PZA, respectively, indicating the significance of the PLGA nanoparticles. Furthermore, the drug residence time in the body was 11 days for drug incorporated nanosystems as compared to 24 h for free unloaded drugs. The retarded elimination of the drug allowed a dosing regimen of 5 doses of nanoparticles administered every 10 days showing equal therapeutic efficacy as 46 oral daily doses (Pandey et

al., 2003). A similar approach with the only difference of nanoparticles being alginate nebulised nanoparticles demonstrated, faster plasma detection at 3 h and a drug residence time up to 14 days, whereby 3 doses of nanoparticles administered every 15 days for 45 days was as effective in clearing *M.tb* bacilli of lung and spleen as 45 oral daily doses of the free drugs (Zahoor et al., 2005).

A RIF/PLGA nanoparticle, incorporated in mannitol microspheres enhanced the uptake by NR8383 macrophage cells in the lungs, with the mannitol microspheres affecting its uptake from 13.5% in RIF/PLGA nanoparticle to 47.1% in a microsphere, RIF/PLGA nanoparticle (Ohashi et al., 2009).

3.3.2. Modified Polymeric Micelles

Polymeric micelles are self-assembled nanocarriers, made of a hydrophobic core, representing the drug reservoir, and an outer hydrophilic shell, usually PEG, which acts on the surface as an opsonization and elimination preventative method (Sosnik et al., 2010). The two components form an amphiphilic stimuli-responsive system that incorporates hydrophobic drugs, loading it, for improved targeted delivery (Sosnik et al., 2010). Drugs loaded in the inner core are consequently protected from the environment chemical and biological degradation. Polymeric micelles have a slow disassembly process depending on the molecular weight, HLB of the polymer and properties of the encapsulating drug, making it a more stable delivery system compared to conventional micelles.

In relation to TB, a study investigated the incorporation of RIF, a large hydrophobic drug within various poly(ethylene oxide)–poly(propylene oxide) (PEO–PPO) block copolymers, which includes linear poloxamers and branched poloxamines. The solubilization was found to be minimal (~2 folds of RIF alone), due to the size of the core in comparison to the RIF molecule. With the flexibility of synthesis, modification of the polymer by linking mono and bifunctional PEG precursors of different molecular weight with polycaprolactone which improves the HLB and enlarges the core cause improved solubilization to (~5-7 folds of RIF alone) (Sosnik et al., 2010). A thermo-responsive poly(ε-caprolactone-coglycolide)–poly(ethylene glycol)-poly(ε-caprolactone-co-glycolide) block synthesised by ring-opening polymerization copolymer loaded with RIF presented with an unimproved solubility of 2 $mg.ml^{-1}$ but presented the slow release of drug over 32 days which could present a partway in the development of a depot injection (Jiang et al., 2007).

The use of enantiomeric pure micelles was outclassed by an evenly mixed molar ratio of monomethoxy PEG poly (ethylene glycol)–poly(L-lactide) (MPEG-PLLA) and monomethoxy PEG poly(ethylene glycol)-poly(D-lactide) (MPEG-PDLA) block copolymers, improving RIF loading capacity and release in comparison to the single polymer micelles. *In vitro* studies showed a fast initial release of 50% after 4-8 h, then became sustained afterwards to release 100% of the drug in 48 h. It is important to also note that although there was a burst release, there was no free drug on the shell of the micelles. The release rate was inversely proportional to the contents of the polylactic acid (PLA) segment in the stereo complex block copolymers (Chen et al., 2007).

In another design, chitosan was employed to modify spherical PLA micelles, which upon entrapment of RIF, resulted in a size increase from a range of (154-181) nm to (163–210) nm. *In vitro* release demonstrated a 35% burst release within the first 5 h, followed by a slow sustained release until 5 days (Wu et al., 2009).

Furthermore, in other studies involving other anti-TB drugs, encapsulating INH, PZA and RIF. A poly(ethylene glycol)-poly(aspartic acid) (PEG-PASP) copolymer with INH embedded in it, resulting in 5.6 times decrease in mycobacteria tuberculosis MIC compared to the drug alone (Silva et al., 2001). The same micelles had a level of drug conjugated between 65.02%-85.70% and were with a size of 78.2 nm, 84.2 nm and 98.9 nm, for INH, PZA and RIF, respectively. Due to a decreased diameter and hydrophilic surface, these systems have minimised renal filtration and reticular system elimination (Sosnik et al., 2010).

3.3.3. Modified Dendrimers

Dendrimers are exemplary types of lipid-based polymeric drug delivery systems that are monodispersed and can easily be surface modified to desired targeting goals. Dendrimers are very small macromolecular synthetic nanosystems ranging from 2 and 10 nm, which allow the attachment of various and multiple functional groups on their external surface, which can be used for treatment and diagnosis (Singh et al., 2016; and Mignani et al., 2018). This presence of multiple terminal groups causes dendrimers to be less viscous than other linear polymers, highly soluble, reactive, and miscible (Kumar et al., 2015; and Singh et al., 2016). Dendrimers are therefore candidates in reducing toxicity, enhancing solubility and bioavailability of anti-TB drugs. They are special because as their diameter increases linearly, the number of surface groups increase exponentially (Mignani et al., 2018).

The dendrimers' macromolecular structure can be divided into 4 main components, which includes (a) central core moiety, responsible for the molecular arrangement, size and shape, (b) interior layers which consist of patterns of repeating branches attached to the core, which increases based on the generation causing surface groups to increase exponentially. These branches form (c) void spaces which act as room for molecular cargos. The outer surface is made of (d) terminal functional groups used in targeted delivery (Mignani et al., 2018).

A generational 1 dendrimer would have 8 terminal amino groups, whilst a Gen 2 dendrimer would exponentially increase to 16 terminal groups and gen 5 dendrimer therefore would have 128 terminal groups (Mignani et al., 2018). These terminal groups, therefore, act as sites for the attachment of functionalizing groups. Dendrimers are adjustable pH based systems, which retain the drug at a blood pH of 7.4 and release the drug at acidic pH, in correlation with a TB infected macrophage which is a pH of ~4.5. For this reason, dendrimers present themselves as very prospective candidates for the incorporation and functionalization of anti-TB drugs presenting a form of targeted delivery. The various types of dendrimers differ based on their size and the number of terminal functional groups. The main materials used comprise PAMAM dendrimers, poly-ether hydroxyl-amine (PEHAM) dendrimers, PPI dendrimers, carbosilane dendrimers, and phosphorus-based dendrimers (Majoral et al., 2018).

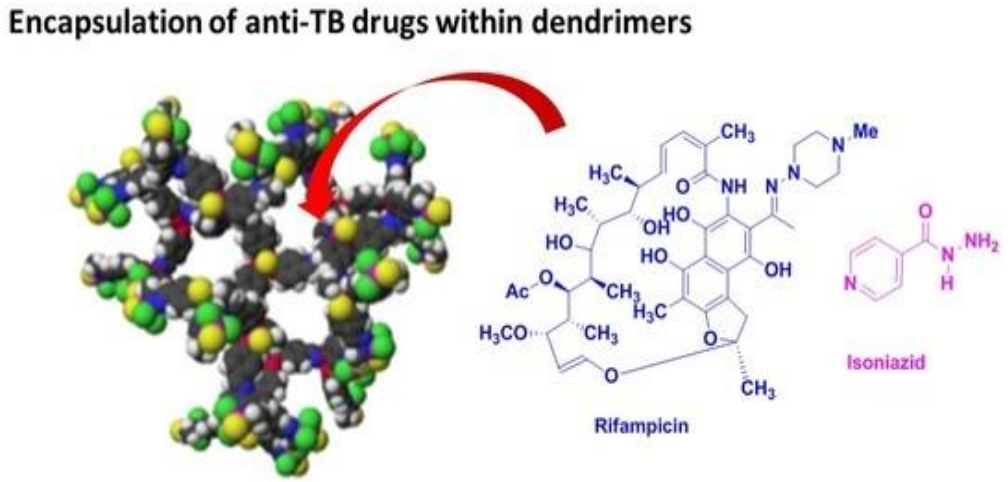

Figure 3.3: Schematic representation of the use of dendrimers as nanocarriers for the delivery of anti-tuberculosis drugs. Figure obtained with permission from (Mignani et al., 2018).

About TB, studies incorporating anti-TB drugs as in Figure 3.3 has been explored. Mannose functionalised ethylene diamine poly(propylene imine) (EDA-PPI) 5th gen dendrimers with 64 amino groups on the surface for targeted delivery of RIF to alveolar macrophages has been

performed (Kumar et al., 2006). The core of the particle was composed of EDA and its surface was grafted with ~30-D-mannose groups. Since RIF hydrolysed in pH of 4-5 (gastric pH) into less soluble compounds, the use of dendrimers with mannose will allow leptin receptors on phagocytic cells the recognition of the system and its uptake, consequently enhancing the uptake of the drugs found in the void space (Majoral et al., 2018). Although the solubility of the nanosystem is decreased from 50 $mg.ml^{-1}$ to 5 $mg.ml^{-1}$ in unmannoslyted RIF loaded dendrimers compared with mannosylated RIF. The mannose functionalised dendrimer still possesses an aqueous solubility twice that of RIF alone. Noncovalent interactions were observed between RIF and the mannosylated dendrimer, whilst hydrogen and hydrophobic interactions occur between RIF and the core. Haemolytic toxicity limitations were observed in the G5 EDA-PPI dendrimers, though it was observed that the unmannosylated dendrimers were haemolytic, their toxicity was decreased by functionalising with mannose from 15.6% to 2.8% due to a minimized interaction of the charged peripheral amino groups with cells. This serves as a prelude to the requirement of modification of their surface by functional groups to inhibit its cationic and subsequent haemolytic effect since these effects will preclude the effect from the use of unfunctionalized dendrimers (Majoral et al. 2018).

In relation to anti-TB drugs, a study on vero cells, used in cell studies indicated negligible cytotoxic effect as 100 $ug.ml^{-1}$, with RIF-loaded mannosylated dendrimer (G5 EDA-PPI) having ~85% viability better than RIF alone at ~50%. In mannosylated dendrimers, RIF stayed entrapped for ~5 days in comparison to less than 10 h in PPI dendrimers. Furthermore, mannosylated dendrimers undergo drug release at a pH of 5, the same required condition in phagolysosomes like infected macrophages. The target delivery of the system using mannose improves the intracellular concentration of the drug, improves cellular viability whilst improving the therapeutic efficacy of lipophilic drugs life RIF (Majoral et al., 2018).

Taking into consideration the same method, the authors describe the formulation of G4 and G5 PPI dendrimers, which is PEGlatyed instead of mannose. In addition to the cytotoxic effects of primary amino group terminal bearing PPI and PAMAM dendrimers, they have also been found to be cleared rapidly if administered intravenously (Lee et al., 2005). In contrast, PEG is water-soluble, thermostable, chemically inert, unhydrolysed, and not deteriorative, making it non-toxic and biocompatible (Vijayaraj Kumar et al., 2007). Therefore, the incorporation of PEG into the surface of polymeric micelles such as dendrimers suppresses the interaction of the delivery system with plasma proteins and cells, prolonging their blood elimination half-life (Vijayaraj Kumar et al., 2007).

The incorporation of RIF, known for its short half-life, solubility difficulty into PEGylated ethylene diamine (EDA)-PPI dendrimers, resulted in a slower release of the drug, with G4 non-PEGylated releasing 97.3 % of RIF in 36 h, whilst G4 PEGylated released half of that in 36 h and 93.1% in 96h. In G5 non-PEGylated released 94.6% of RIF in 48 h and G5 PEGylated released half of that in 48 h and 93.4% after 120 h. This is because as the generation increases, the hydrophobic interactions of the core increase, therefore these interactions with RIF as well as the doubling up of the terminal groups from 32 to 64 contributed to its delayed release profile. With regards to its haemolytic toxicity, dendrimers generally have (~14.6–20.3%) RBC haemolysis, and PEG significantly decreased it to less than 3% due to minimised interaction between quaternary ammonium groups in the terminal end of dendrimers and RBCs (Vijayaraj Kumar et al., 2007).

Furthermore, on G5 PEGylated dendrimer, encapsulation efficacy of RIF more recently was found to be ~99% by P. Dineshkumar and co-workers, with a comparable drug release rate of 81% after 120 h and 98% after 72 hr in non-PEGylated, with inhibition of RBC haemolysis by less than 2.5% (Dineshkumar et al., 2017). Westran albino rats studies performed *in vivo* comparing the pharmacokinetic properties of RIF encapsulated G5 PEGylated dendrimer and RIF alone showed that over 120 h, the presence of RIF alone was not observed after 6 h. In correspondence with *In vitro* studies, RIF encapsulated G5 PEGylated dendrimer was retained in plasma for 120 h. Even after its storage for 3 months at -40 °C, the release of the drug system was unaltered, ensuring improved AUC, and drug residence time (Singh et al., 2016; and Mignani et al., 2018).

INH is another drug that has been incorporated into dendrimers. An INH G1.5 PAMAM dendrimers were synthesised using the dialysis method. Drug release study showed controlled 93.25% release of INH over a period of 24 h. A zero-order kinetic was demonstrated (Karthikeyan et al., 2016; and Singh et al., 2016). Dendrimers show great prospect in the incorporation of both high molecular weight, hydrophilic and hydrophobic chemical entities that have low solubility and low half-life.

3.4. NANOTECHNOLOGICAL ADVANCES FOR MDR AND XDR TB

TB resistance has emerged over the years and proven to be a challenging aspect of TB to manage, with patient noncompliance in first-line therapy, recurrently causing therapeutic failure. Furthermore, the resistant TB-bacilli may also be contracted through person-2-person transmission. With nanotechnology striving to enhance patient compliance in the first-line therapy, which reduces the emergence of resistant TB, a strong urge to improve treatment of present individuals with MDR and XDR-TB, assures nanotechnology an opening to be a prospective

breakthrough for this aim. According to the world health organisation, Fluoroquinolones are considered the main therapeutic pathway to counter MDR, particularly moxifloxacin (MOX), which is recommended for the 'shorter MDR-TB regimen' by WHO, even though its shortcomings include lack of patient compliance due to its associated hepatotoxicity.

Nanoencapsulation may be a good attempt to counter the shortcomings of MOX, by reducing its side-effect, with studies indicating that modification of NPs with hydrophilic polymers such as PEG and water-soluble chitosan deters the accumulation of MOX in the liver due to their 'brush-like configuration (Mustafa et al., 2016). Polyisobutylcyanoacrylate and gelatin synthesised nanoparticles incorporating RIF+MOX also targeted improved cellular immune response in murine alveolar macrophages by increasing intracellular pro-inflammatory cytokines (Sarfraz et al., 2016).

Bedaquiline showed complete encapsulation as well as a surface binding capacity on different diblock copolymers, which includes poly(lactic-co-glycolic acid) (PLGA), poly(lactic-co-hydroxymethyl glycolic acid) (PLHMGA) and poly(lactic-co-benzyloxymethyl glycolic acid) (PLBMGA) which are all surface modified by the hydrophilic mPEG, (Ritsema et al., 2018). This causes a burst release of 30–42% within the first hour, and a sustained release thereafter up to 100% within ~3-7 days (Ritsema et al., 2018). Modification of NPs to make a lipid-polymer hybrid NPs also shows prospective advantages in second-line drugs. A study incorporating INH and CPX in a lipid-polymer hybrid NPs, composed of (i) soy lecithin (LC), used to construct the shell of lipid particles for electrostatic interaction with oppositely charged polymers, (ii) PEGylated DSPE (1,2-distearoyl-sn-glycero-3-phosphoethanolamine), responsible for modifying the system to escape the recognition by the reticuloendothelial system (RES) (Thevenot et al., 2007), which wraps the polymeric core matrix made of PLGA and by altering the lipid component, concurrently provides targeting variety with a controlled release on the targeting effect. This system improved *in vitro* cellular uptake of CPX into J774A.1 cell (Bhardwaj et al., 2016). *In vivo*, the drug accumulation from nanocarriers in lungs was significantly more than unloaded free drugs.

3.5. MODIFIED NANO-SYSTEM FOR ACTIVE TARGETING TO *M. TB* RESERVOIRS

As much as surface modification of a delivery system may be passive and be present to stabilize drugs, protect drugs, and prevent rapid elimination. It may also be actively directed to the specific site of action in a ligand-receptor interaction mechanism as in Figure 3.4 that may exist between the nanocarrier and cell/tissue in the body. These ligands are generally coated, complexed or modified onto the surface of the nanosystem.

Since macrophages remains a significant factor in the pathogenesis of *M.tb*, acting as a reservoir of the *M.tb* bacilli, as well as in latent infections, active targeting would look to specify drug delivery towards alveolar macrophages in pulmonary TB, and lymph nodes in extrapulmonary TB. Consequently, increasing site bioavailability and minimizing side effects of the drug without having to increase the dose.

The pattern recognition receptors on macrophages give a site of exploitation for a ligand for targeted delivery. These receptors include toll-like receptors (TLRs), C-type lectin receptors (CLRs), NOD-like receptors (NLRs), and DC-specific intercellular adhesion molecule-3-grabbing non-integrin (DC-SIGN). The most researched ligand is mannose, which is recognisable by CLRs found on macrophage surfaces. Mannose has presented prospective results; whereby cationic mannose lipid NPs significantly improve the uptake of the nanosystem in alveolar macrophages *in vitro* and *in vivo*. It is further understood that the cationic nature of the system allows NP-plasma protein interaction and aggregation in the alveolar macrophages, causing its improved lung deposition (Grotz et al., 2018).

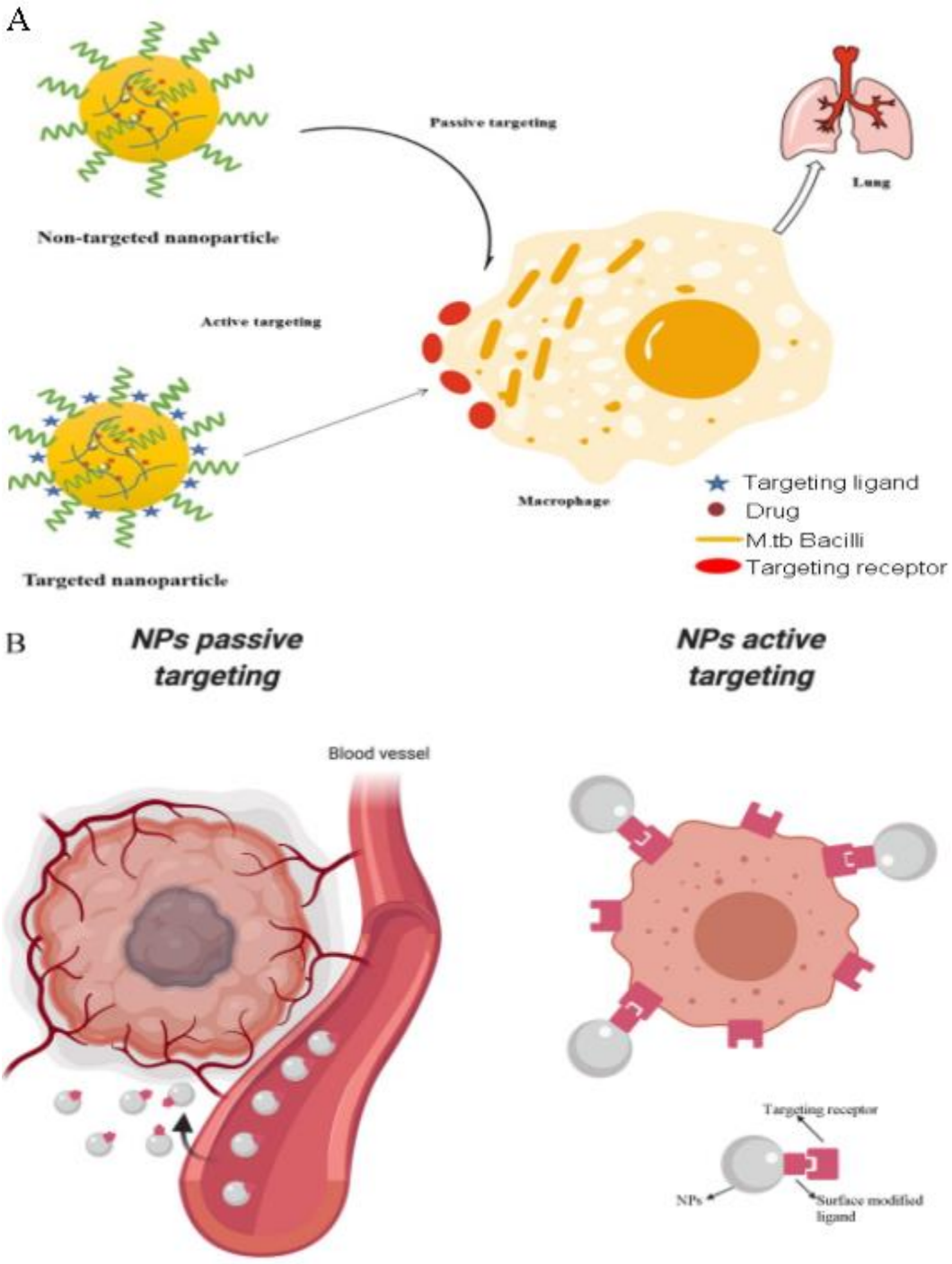

Figure 3.4: Schematic representation of (a) macrophage targeted by surface-modified nanoparticles. Figure adapted with permission from (Pawde et al., 2020). (b) active and passive uptake of nanoparticles. Figure adapted with open access.

Solid lipid NPs functionalized with mannose and loaded with RIF and INH, individually have shown similar outcomes. In a fluorescent RIF-loaded mannosylated SLNPs, made of glycerol tripalmitate (lipid phase) and surfactant (Tween® 80) in double deionized water (aqueous phase) with an entrapment efficacy of 90%, the internalization of RIF into THP-1 differentiated macrophages were improved, with the system remaining bio-compatible at concentrations less than 57 ug.ml^{-1} of which RIF bactericidal concentration is 3.2 µg.ml^{-1} (Yamori et al., 1992). 80% or more of the drug remained entrapped in the system after contact with pulmonary simulated conditions for up to 8 h and can release the drug in infected cells in a pH-dependent manner, with a faster drug release at acidic pH, which supports its suitability for pulmonary delivery, with diminished degradation and improvement in bioavailability. The NPs cell entry took place quickly within 15 min of administration (Vieira et al., 2018a). With regards to INH, and SLNP, synthesised by a modified solvent emulsification-evaporation method employing a w/o/w double emulsion technique. The 500 nm system was composed of Witepsol® E85 forming the lipid phases and stearylamine (SA) which contributed to the system by surfacing amine groups for the attachment of mannose to form a lipid matrix which showed enhanced internalisation of the system even based on mere adsorption of mannose to the surface of the particles. The fluorescent M-SLNP system enhances *in vitro* uptake of INH into dTHP-1 than the unfunctionalised SLNP (Costa et al., 2018).

Pi et al., 2019 synthesized a novel 50–300 nm mannosylated and PEGylated graphene oxide nanocarrier for selective targeting and delivery of RIF to mucosal CD14+ macrophages (derived from *M.tb*- infected rhesus macaques) via mannose receptor-mediated endocytosis. Results indicated that selectivity for macrophages was established, with a higher concentration of RIF as compared to T and B cells due to low mannose-binding, c type lectin receptors on their surface. Subsequently, drug release in the macrophages was attributed to acidic lysosomic condition, causing a burst release to enhance intracellular killing of *M.tb*.

A 272 nm lactoferrin (Lf) conjugated RIF-loaded SLNPs with an encapsulation efficacy of 66% was synthesised. It is composed of tristearin, soya lecithin and stearylamine. Most drugs remain in the nanoparticles upon administration in the blood which decreases RIF toxicity. IV administration of free drugs resulted in 0.4% RIF concentration in the lungs after 4 h and undetectable levels after 24 h. In unfunctionalized SLNP, 15.6% and 2.1% RIF concentration was recovered at 4 h and 24 h, respectively, whilst in Lf conjugated SLNPs, a staggering 47.7% and 35.3% RIF concentration was recovered after 4 h and 24 h, respectively, a 3 fold increase in drug load in lung tissue in functionalized nanoparticle as compared to that of unfunctionalized

nanoparticles, indicating the significance of the Lf specificity to the lung even when administered systemically and not locally/nebulised, due to the abundance of Lf recognising receptors in the lungs. Upon fluorescence imaging, the alveolar macrophages were distinctly filled with the nanosystem (Shilpi et al., 2015).

A similar approach has been applied, whereby methyl α-d-mannopyranoside was engineered on an SLNP to deliver rifampicin, synthesised through melt emulsification technique combining cholesteryl myristate with palmitic acid (PA set) or tripalmitin (TP set) and functionalised with methyl α-d-mannopyranoside. Maretti et al. synthesised SLNP demonstrated good cytotoxicity and cell internalisation ability into J774 murine macrophage cell line, whilst making possible drug preservation in SLNPs along the respiratory tract prior to macrophage internalisation. Although favourable results were achieved, the particles cohesiveness hampered respirability, especially when SLNPs were functionalized, causing the need for better-balanced amphiphiles with -d-mannose residues prior to further investigation that can protect powder against moisture in the environment enhancing particle de-aggregation and lowering powder cohesiveness (Maretti et al., 2017).

Aside from monosaccharides, mannose, other ligands on other polymeric platforms have been experimented with. The study of a flower-like poly(epsilon-caprolactone)- poly (ethylene glycol)-poly(epsilon-caprolactone) polymeric micelles encapsulating RIF functionalised by hydrolysed galactomannan (GalM-h), a polysaccharide of mannose and galactose both recognised by CLRs, to form a complex polymeric NP, coated with GalM-h/chitosan, with drug encapsulation efficacy of 12.9 times that of unfunctionalised NP. The presence of GalM-h was confirmed by an agglutination assay with concanavalin A, whilst its uptake and internalization into RAW 264.7 murine macrophages were observed by fluorescence microscopy, with the polysaccharide significantly improving the intracellular concentration of RIF (Moretton et al., 2013).

Furthermore, on mannose functionalized nanocarriers, Pawde et al., 2020 also demonstrated using chitosan-based bioadhesive nanoparticles loaded with clofazimine, the effect of mannose functionalization, an excellent enhanced therapeutic efficacy in terms of inhibition and anti-mycobacterial activity by 46 folds as compared to free clofazimine. The nanosystem with a particle size ranging between 132–184 nm and an encapsulation efficacy of 95% demonstrated great *in vitro* release, showing a burst release, whereby 30–40% of the drug is released in the first 5 h followed by sustained release between 10-72 h, after which 70.98% of drugs in mannose functionalized nanoparticles are released (Chaubey and Mishra, 2014).

In the insight of a different ligand class from mannose, hyaluronic acid (HA) has been investigated, recognizable by its receptors such as CD44 and TLR -2 and -4, via MyD88 to activate NF-κB and induce proinflammatory cytokine gene expression (Lee-Sayer et al., 2015). The expression of these receptors on alveolar macrophages allows HA use for active targeting and drug delivery (Grassin-Delyle et al., 2020). A targeted delivery system for RIF, comprised of the incorporation of HA into tocopherol/ succinate (TS) micelles, increasing the *in vitro* uptake of RIF in murine alveolar macrophages (AMs) (MH-S cells) by phagocytosis, in a dose and energy-dependent manner. Concurrently, the micelles were up taken through CD-44 receptor-mediated endocytosis. The MH-S cells were activated, which in turn further improved the RIF-HA-TS uptake. The cytokine secreting activity demonstrated the enhanced secretion of Th1 cytokines due to the presence of the nanosystem in comparison to free drugs (Gao et al., 2015).

Carneiro et al., 2019 synthesised an oleic acid tuftsin-modified peptide (pTUF-OA) to be used as a ligand unto an SLNP as in Figure 3.5 below. The peptide is composed of threonine, lysine, proline and arginine amino acids and an oleic acid molecule. The SLNP is composed of a lipid phase of stearic and oleic acid and a surfactants mixture composed of Phospholipon 80H and Tween 80. *In vitro* pulmonary simulated condition, indicating an initial 10% burst release of drug for 2 h followed by a slow sustained release. Cell viability of over 70% was established in J774 A.1 cells as compared to a 60% cell viability of free RIF, improving the RIF treatment drawback with regards to toxicity. A 2-fold improved MIC of 0.48 $ug.ml^{-1}$ for RIF loaded peptide NP, as compared to 1 $ug.ml^{-1}$ for free RIF due to the enhanced penetration of NP across the mycobacteria cell wall. The enhanced internalization was attributed to the specific tuftsin binding receptor, which could possibly be neuropilin-1 (Nrp1) (Nissen et al., 2013) on the surface of the macrophages, higher contact surface and hydrophobic nature of the NP.

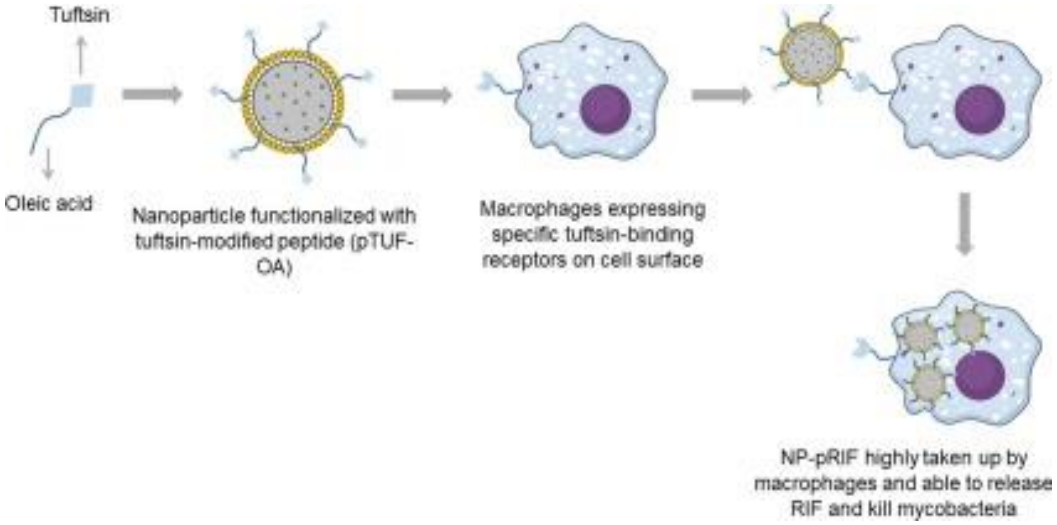

Figure 3.5: Diagram showing oleic acid- tuftsin-modified peptide functionalization unto rifampicin loaded nanoparticles for active targeting of macrophages. Figure obtained with permission from (Carneiro et al., 2019).

Other ligands with limited studies, includes O-stearoyl amylopectin, (O-SAP), and methylated bovine serum albumin, (MBSA) that have a specific affinity for macrophages and selectivity for type 1 and 2 scavenger receptor, respectively. A RIF-loaded aerosolized egg phosphatidylcholine (PC)- and cholesterol (Chol) based liposome coated with these ligands demonstrated rapid attainment of high concentration of drug in alveolar macrophages over an extended period of time as compared to free drugs. O-SAP-coated liposomes demonstrated better accumulation in macrophages, with 10.8% of O-SAP liposomes retained in the lungs after 24 h compared to 8.2% MBSA liposomes. Although the delivery system shows prospective use, the fast elimination, and uptake by RES is a challenge that still needs to be overcome.

In extrapulmonary TB, fluoroquinolones with a low incidence of resistance, gatifloxacin (GAT) have been incorporated into nanoparticles and functionalized for the treatment of CNS tuberculosis. Marcianes et al. 2017, synthesised a PLGA 502 nanoparticle surface modified with polysorbate 80 or labrafil. Labrafil is a more lipophillic surfactant in comparison to polysorbate 80, therefore facilitates more access of nanoparticles to the CNS but has a low entrapment efficacy, giving polysorbate 80 the advantage as a modifier. The distribution into the brain, lungs and liver were evaluated using rhodamine-loaded PLGA nanoparticles in male Wistar rats. *In vivo* fluorescence studies indicated a significant increase in rhodamine concentration in the cerebral cortex and hippocampus at 30 and after 60 min, indicating correspondence to the expected effect of gatifloxacin loaded nanoparticles suggesting prolonged encapsulation of drug after delivery, as >80% of GAT was still encapsulated after 30 min, allowing enhanced drug residence time for the

exertion of therapeutic efficacy. The non-ionic surfactant potentially reduces cellular drug efflux (Chen et al., 2015). In the cortex rhodamine concentration in the cortex was 10 folds higher when incorporated into the nanosystem than in solution. The transportation of the nanocarrier across the BBB may be attributed to polysorbate 80, allowing adsorption of ApoA1, ApoB, and/or ApoE onto the surface of the low-density lipoprotein and other related receptors on the BBB as observed in polysorbate 80-coated poly butyl cyanoacrylate NPs, leading to endocytosis thereafter, transcytosis of the NP (Ramge et al., 2000, Kreuter, 2013). No significant cytotoxicity was experienced with regards to cell viability and neuron survival. A greater distribution of NP was observed in the lung as compared to the liver after 30 min, which is advantageous in targeting the *M.tb* bacilli, from its origin. After 60 min the concentration had decreased in both lungs and liver. *In vitro* studies of GAT release showed a biphasic release, with rapid release occurring within the first 10 h, followed by controlled release (Marcianes et al., 2017). The Gat-loaded PLGA NPs functionalized with polysorbate 80 present a prospective system for the treatment of CNS TB.

Another instance of gatifloxacin use in surface-modified PLGA microparticles for active targeting to macrophages demonstrated the author's synthesis of PLGA microparticles using PLGA 502H and underwent surface modification using labrafil. Labrafil actively increases the phagocytosis of PLGA 502H microparticles by macrophages as it makes the surface more lipophilic. Lipophilic surfaces are readily phagocytosed than hydrophilic surfaces since the same nanosystem without labrafil remained not phagocytosed after 5 h due to the formulation having a more hydrophilic surface. The internalization of the nanosystem occurred by the formation of a membrane-bound vesicle via protrusion of the cell membrane, causing invagination of the macrophage membrane and the possibility of phagosome development and phagocytosis. With a high encapsulation efficacy of 89.6%, the system was noticed in macrophages after 3 h and remained in macrophages for at least 48 h, showing suitability for the treatment of MDR-TB. *In vitro* studies showed a biphasic release of GAT, a rapid release in the first 3 days, followed by slow release (Marcianes et al., 2020).

Most recently, the enzyme mimetic activity of magnetic iron oxide nanoparticles has shown benefit in the delivery of anti-TB drugs. INH is a prodrug that is activated when exposed to KatG enzyme or catalase and peroxidase, for this reason, the absence of catalase and peroxidase or a KatG gene mutation, which is by large the most common mutations in INH resistant MTBs is an important factor to take note of in treatment (WHO, 2018). Magnetic iron oxide nanoparticles have intrinsic peroxidase-like and catalase-like enzymatic activity, showing a prospective combinatory effect against *M.tb*. A study incorporating INH in a lipoamino acid surface-modified magnetic

nanoparticle with an average size of 12.93 nm demonstrated a reduced INH MIC from 1.26 ug.ml^{-1} to 1.08 µg.ml^{-1} when incorporated in the nanoparticle. In the use of unmodified nanoparticles, a more impressive MIC of 0.87 µg.ml^{-1} was noticed, but due to the possible unintended effect of uncoated magnetic nanoparticles, it is preferable to coat it, since lipoamino acid may mimic the structure of the cell membrane (Fait et al., 2017) and prevent unintended interaction with plasma proteins in the body. Furthermore, the presence of a lipophilic structure enhances drug efficacy especially in the lung, the most prominent site for TB infection.

A study demonstrating the anti-*M.tb* effect of gallium (III) (Ga)-based compounds, types of drugs in development, when incorporated in nanoparticles was performed. Choi et al., 2017 synthesised various nanoparticles, comprising RIF, gallium incorporated in NPs made of Pluronic F127, mannose/folic acid conjugated F127, dendrimer, and poloxamer 188. It was very interesting to note that Ga loaded folate- or mannose-functionalized block copolymers provided sustained Ga release for 15 days whilst significantly inhibiting *M.tb* (H37Rv) microbial growth in THP-1 cells for the same period. Ga(III) concentration in folate conjugated NPs was 2.5 and 10 folds compared to the mannose-NPs and free GA, respectively, by acting on folate receptor β (FRβ) (Chandrupatla et al., 2019). In addition to the delivery and inhibition of *M.tb*, Ga was also found to block the phagosome maturation process by interrupting *M.tb*-mediated suppression of Gal3.

An active targeted system presents unique advantages and more studies, including extended *in vivo* studies will confirm and assure the complete prospects of the delivery system. Furthermore, studies incorporating the delivery of combinatorial anti-TB drugs as performed in the standard regimen, or studies with the combination of anti-TB drugs and repurposed drugs in the active target nanosystems may have possible enhanced benefits to counter the progress of the disease. These strategies may be administered by various routes of administration, such as the pulmonary route for pulmonary TB, and IV or intraperitoneal for extrapulmonary tuberculosis (Grotz et al., 2018).

3.6. FUTURE PERSPECTIVES

The extensive studies over the years on nanotechnology have continuously gained grounds in its impressive ability to overcome physicochemical limitations, of solubility and stability, by addition virtue of its nano-size range, whilst enhancing the bioavailability of required anti-TB drugs. This size also contributes to enhancing drug permeation across membranes and cellular uptake, with its functionalization allowing specificity and selectivity to the required cell. For pulmonary TB, many studies on the administration of the medicines through the oral route for the administration

of the free anti-TB drugs have been performed. More recently, pulmonary TB therapy, employing the use of nanosystems, is showing a prospective alternative to the oral route, with pulmonary administration of drugs generally gaining awareness due to its non-invasiveness, reduced side effects, and evasion of the hepatic first-pass metabolism, and the large alveoli surface area. Furthermore, since most TB is pulmonary, it will be administered directly to the required site of action (Grotz et al., 2018).

Although the need to optimize the even distribution of nanocarriers across the lung remains a key parameter, another feature to consider is the aerodynamic behaviour of the nanoparticles in relation to the rapid clearance from the respiratory system. Methods to improve mucoadhesion and mucus penetration as present in polymers like chitosan and pluronic needs to be investigated (Dong et al., 2020). In comparison to mucoadhesive formulations with identical particle size, the mucus-penetrating nanoparticles for the administration of baicalein permitted deeper penetration, cellular absorption, enhanced drug distribution in airways, and superior local distribution and bioavailability. As a result, there's a chance that pluronic and other mucus-penetrative polymers might be used to make nanosystems for pulmonary TB therapies.

More interestingly, the approach of active targeting using ligand-receptor pattern recognition demonstrates a promising preferential approach for internalization into *M.tb* reservoirs whilst optimizing the pharmacotherapy. Discovering and exploring other surface ligands apart from mannose and HA that may act as keys for pattern recognition on the receptors on *M.tb* reservoirs, such as toll-like receptors (TLRs), C-type lectin receptors (CLRs), NOD-like receptors (NLRs), that are normally used for the entrapment of the microbes need to be explored with the concept of drug internalization. With more promising *in vivo* data, a greater insight will allow pre-clinical studies to determine its possible use clinically. Only then will the prospect of acquiring a commercially viable nanoformulation become a possibility.

Table 3.1: Overview table showing types of surface modified drug delivery systems employed in the treatment of tuberculosis.

TYPE OF NANOCARRIER	DRUG	PARTICLE SIZE DISTRIBUTION	SURFACE MODIFIER	METHOD EMPLOYED	TARGETING CELLS/ ORGAN	REF.
PASSIVE DRUG DELIVERY SYSTEMS						
Cetyl palmitate SLNP	Rifampicin	333-355 nm	Chitosan	Hot ultrasonication method	-	Vieira et al., 2018
Compritol® ATO 888	Rifampicin Isoniazid	141.2 ± 13.5nm 120.0 ± 0.7 nm	Polysorbate 80	Microemulsification method	-	Singh et al., 2013
Ethylene diamine poly(propylene imine) (EDA-PPI) 4th and 5th gen dendrimers	Rifampicin	-	PEG	Double Michael addition and exhaustive amidation reactions	-	Vijayaraj Kumar et al., 2007 Dineshkumar et al., 2017
Glyceryl monostearate (GMS) and stearic acid (SA) containing SLNP	Rifampicin	30-200 nm	FITC labelled WGA	Emulsification followed by a solvent evaporation method.	-	Pooja et al., 2015
PLA micelles	Rifampicin	163–210 nm	Chitosan	Swern oxidation	-	Wu et al., 2009
PLGA nanoparticles	Rifampicin Isoniazid	350-400 nm	Lectin: Wheat germ	Two-step amide bond linkage using carbodiimide	-	Sharma et al., 2004

	Pyrazinamide		agglutinin (WGA)			
PLGA nanoparticles	Moxifloxacin	50-200 nm	PEG-Water Soluble Chitosan	Solvent-emulsion evaporation method	-	Mustafa et al., 2016
PLGA-PEG-PLGA triblock copolymer	Isoniazid	150–400 nm	Isoniazid	Water-oil-water double emulsification technique	-	Gajendiran et al., 2013
Poly(ethylene glycol)-poly(aspartic acid) (PEG-PASP) copolymer	Rifampicin Isoniazid Pyrazinamide	239-293 nm	PEG	Condensation using EDC	-	Silva et al., 2001
Poly (ethylene glycol)–poly(L-lactide) (MPEG-PLLA) and poly(ethylene glycol)-poly(D-lactide) (MPEG-PDLA) block copolymers	Rifampicin	40 to 120 nm	Monomethoxy PEG	Ring-opening polymerization of L-lactide and D-lactide in the presence of monomethoxy PEG, respectively	-	Chen et al., 2007
Poly(ethylene oxide) monomethyl ether-block-poly(ε - caprolactone)	Rifampicin	20-60 nm	Förster resonance energy transfer (FRET) sensor	Ring-opening copolymerization	-	Trousil et al., 2017

Poly(lactic-co-glycolic acid) (PLGA), poly(lactic-co-hydroxymethyl glycolic acid) (PLHMGA) and poly(lactic-co-benzyloxymethyl glycolic acid) (PLBMGA) copolymer	Bedaquiline	241 - 290 nm	mPEG	Ring-opening polymerization	-	Ritsema et al., 2018
Poly(ε-caprolactone-coglycolide)–poly(ethylene glycol)-poly(ε-caprolactone-co-glycolide)	Rifampicin	-	PEG	Ring-opening polymerization of ε-caprolactone and glycolide in the presence of PEG	-	Jiang et al., 2007
Soy lecithin (LC) and DSPE (1,2-distearoyl-sn-glycero-3-phosphoethanolamine)	Isoniazid Ciprofloxacin	11.81 ± 1.2 nm 172.23 ± 2.31 nm	PEG	w-o-w double-emulsification-solvent-evaporation method	-	Bhardwaj et al., 2016
ACTIVE-TARGETING DRUG DELIVERY SYSTEM						
Chitosan-based bioadhesive nanoparticles	Clofazimine	132–184 nm	Mannose	Solvent evaporation method	Macrophages	Pawde et al., 2020
Cholesteryl myristate with palmitic acid (PA	Rifampicin	0.72 ± 0.02 μm to 1.38 ± 0.19 μm	Methyl α-d-mannopyranoside	Melt emulsification technique	Respiratory tract, J774	Maretti et al., 2017

set) or tripalmitin (TP set)					murine macrophage	
Egg phosphatidylcholine (PC)- and cholesterol (Chol)	Rifampicin	3.85 ± 0.59 μm	O-stearoyl amylopectin, (O-SAP), and methylated bovine serum albumin	Cast film method	Alveolar macrophages	Vyas et al., 2004
Ethylene diamine poly(propylene imine) (EDA-PPI) 5th gen dendrimers	Rifampicin	Less than 5 μm	Mannose	Double Michael addition and exhaustive amidation reactions	Alveolar macrophages	Majoral et al., 2018
Graphene oxide nanocarrier	Rifampicin	50–300 nm	Mannose and PEG	EDC amide bond formation	Mucosal CD14+ macrophages	Pi et al., 2019
Magnetic nanoparticles	Isoniazid	Average of 12.93 nm	Lipoamino acid	Coprecipitation method	Lungs	Zargarnezhad et al., 2020
PLGA microparticles	Gatifloxacin	3-5 μm	Labrafil	Solvent evaporation-extraction method	Macrophages	Marcianes et al., 2020
PLGA nanoparticles	Gatifloxacin	194.9±5.7 nm	Rhodamine and polysorbate 80	Acetone-water nanoprecipitation method	Brain cortex	Marcianes et al., 2017

PLGA nanoparticles	Rifampicin	3.2 µm	Mannitol (MAN) microspheres	Spray drying using four-fluid nozzle spray drier	NR8383 Lungs macrophage cells	Ohashi et al., 2009
Pluronic F127	Rifampicin and Gallium	~300 nm	Mannose	Solvent evaporation method and DCC amide bond linkage	THP-1 Cells	Choi et al., 2017
Poly(epsilon-caprolactone)-poly(ethylene glycol)-poly(epsilon-caprolactone)	Rifampicin	263 and 340 nm bimodal distribution	Galactomannan	Ionotropic gelation.	RAW 264.7 murine macrophages	Moretton et al., 2013
Stearic and oleic acid, Phospholipon 80H and Tween 80	Rifampicin	-	Oleic acid-Tuftsin-modified peptide (pTUF-OA)	Peptide synthesis and purification through ion-exchange chromatography and microemulsion technique	Macrophage and microglial	Carneiro et al., 2019
Tocopherol/ succinate (TS) micelles	Rifampicin	212–294.6 nm	Hyaluronic acid (HA)	-	Alveolar macrophages (AMs)	Gao et al., 2015
Tristearin, soya lecithin and stearyl amine.	Rifampicin	272 nm	Lactoferrin (Lf)	Solvent injection	Lungs	Shilpi et al., 2015

Witepsol® E85 forming the lipid phases and stearylamine (SA)	Isoniazid	500 nm	Mannose	Solvent emulsification-evaporation method	dTHP-1 cells	Costa et al., 2018

3.7. CONCLUSION

To get back on track with the UN SDGs and WHO goals to end TB by 2030 and 2035, respectively, nanotechnology systems need to be thoroughly scrutinized to obtain all possible benefits as carriers of anti-TB therapy. The improved clinical outcome will counter and concurrently treat MDR TB, therefore curbing the spread and severity of the disease. A combination of toxicity studies, biomaterial approval by regulatory affairs, and enhanced pre-clinical studies will bring us closer to the world of commercially available specific and selective nano-targeted therapies. This will allow dose reduction and dose frequency which will enhance patient compliance, whilst decreasing treatment cost. Moreover, simply incorporating nanoformulation with present conventional anti-TB drugs is more cost-effective, timesaving, and more beneficial to low and middle-income countries than the research and development of a new chemical entity with better therapeutic efficacy.

3.8. REFERENCES

Abed, N., and Couvreur, P. (2014). Nanocarriers for antibiotics: A promising solution to treat intracellular bacterial infections. International journal of antimicrobial agents, 43(6), 485-496.

Banik, N., Hussain, A., Ramteke, A., Sharma, H. K., and Maji, T. K. (2012). Preparation and evaluation of the effect of particle size on the properties of chitosan-montmorillonite nanoparticles loaded with isoniazid. The Royal Society of Chemistry Advances, 2(28), 10519-10528.

Bhardwaj, A., Mehta, S., Yadav, S., Singh, S. K., Grobler, A., Goyal, A. K., and Mehta, A. (2016). Pulmonary delivery of antitubercular drugs using spray-dried lipid–polymer hybrid nanoparticles. Artificial cells, Nanomedicine, and Biotechnology, 44(6), 1544-1555.

Brannon-Peppas, L. (1995). Recent advances on the use of biodegradable microparticles and nanoparticles in controlled drug delivery. International Journal of Pharmaceutics, 116(1), 1-9.

Carneiro, S. P., Carvalho, K. V., Soares, R. D. D. O. A., Carneiro, C. M., de Andrade, M. H. G., Duarte, R. S., and Dos Santos, O. D. H. (2019). Functionalized rifampicin-loaded nanostructured lipid carriers enhance macrophages uptake and antimycobacterial activity. Colloids and Surfaces B: Biointerfaces, 175, 306-313.

Chandrupatla, D. M., Molthoff, C. F., Lammertsma, A. A., van der Laken, C. J., and Jansen, G. (2019). The folate receptor β as a macrophage-mediated imaging and therapeutic target in rheumatoid arthritis. Drug Delivery and Translational Research, 9(1), 366-378.

Chaubey, P., and Mishra, B. (2014). Mannose-conjugated chitosan nanoparticles loaded with rifampicin for the treatment of visceral leishmaniasis. Carbohydrate Polymers, 101, 1101-1108.

Chen, H.H., Huang, W.C., Chiang, W.H., Liu, T.I., Shen, M.Y., Hsu, Y.H., Lin, S.C. and Chiu, H.C., (2015). pH-Responsive therapeutic solid lipid nanoparticles for reducing P-glycoprotein-mediated drug efflux of multidrug resistant cancer cells. International Journal of Nanomedicine, 10, 5035.

Chen, L., Xie, Z., Hu, J., Chen, X., and Jing, X. (2007). Enantiomeric PLA–PEG block copolymers and their stereocomplex micelles used as rifampin delivery. Journal of Nanoparticle Research, 9(5), 777-785.

Choi, S. R., Britigan, B. E., Moran, D. M., and Narayanasamy, P. (2017). Gallium nanoparticles facilitate phagosome maturation and inhibit growth of virulent *Mycobacterium tuberculosis* in macrophages. Public Library of Science One, 12(5), e0177987.

Chono, S., Tanino, T., Seki, T., and Morimoto, K. (2008). Efficient drug targeting to rat alveolar macrophages by pulmonary administration of ciprofloxacin incorporated into mannosylated liposomes for treatment of respiratory intracellular parasitic infections. Journal of Controlled Release, 127(1), 50-58.

Costa, A., Sarmento, B., and Seabra, V. (2018). Mannose-functionalized solid lipid nanoparticles are effective in targeting alveolar macrophages. European Journal of Pharmaceutical Sciences, 114, 103-113.

Dineshkumar, P., Panneerselvam, T., Deepti Brundavani, K., Selvaraj, K., and Vijayaraj Kumar, P. (2017). Formulation of rifampicin loaded PEGylated 5.0 G EDA-PAMAM dendrimers as effective long-duration release drug carriers. Current Drug Therapy, 12(2), 115-126.

Dong, W., Ye, J., Zhou, J., Wang, W., Wang, H., Zheng, X., Yang, Y., Xia, X. and Liu, Y. (2020). Comparative study of mucoadhesive and mucus-penetrative nanoparticles based on phospholipid complex to overcome the mucus barrier for inhaled delivery of baicalein. Acta Pharmaceutica Sinica B, 10(8), 1576-1585.

Dye, C. (2006). Global epidemiology of tuberculosis. The Lancet, 367(9514), 938-940.

Fate, M.E., Hermet, M., Comelles, F., Clapés, P., Alvarez, H.A., Prieto, E., Herlax, V., Morcelle, S.R. and Bakás, L. (2017). Microvesicle release and micellar attack as the alternative mechanisms involved in the red-blood-cell-membrane solubilization induced by arginine-based surfactants. RSC advances, 7(60), 37549-37558.

Gajendiran, M., Gopi, V., Elangovan, V., Murali, R. V., and Balasubramanian, S. (2013). Isoniazid loaded core shell nanoparticles derived from PLGA–PEG–PLGA tri-block copolymers: *in vitro* and *in vivo* drug release. Colloids and Surfaces B: Biointerfaces, 104, 107-115.

Gao, Y., Sarfraz, M. K., Clas, S. D., Roa, W., and Löbenberg, R. (2015). Hyaluronic acid-tocopherol succinate-based self-assembling micelles for targeted delivery of rifampicin to alveolar macrophages. Journal of Biomedical Nanotechnology, 11(8), 1312-1329.

Garg, T., Rath, G., R Murthy, R., D Gupta, U., G Vatsala, P., and K Goyal, A. (2015). Current nanotechnological approaches for an effective delivery of bioactive drug molecules to overcome drug resistance tuberculosis. Current Pharmaceutical Design, 21(22), 3076-3089.

Grassin-Delyle, S., Abrial, C., Salvator, H., Brollo, M., Naline, E., and Devillier, P. (2020). The role of toll-like receptors in the production of cytokines by human lung macrophages. Journal of Innate Immunity, 12(1), 63-73.

Grotz, E., Tateosian, N., Amiano, N., Cagel, M., Bernabeu, E., Chiappetta, D. A., and Moretton, M. A. (2018). Nanotechnology in tuberculosis: state of the art and the challenges ahead. Pharmaceutical Research, 35(11), 1-22.

Haba, Y., Kojima, C., Harada, A., Ura, T., Horinaka, H., and Kono, K. (2007). Preparation of poly (ethylene glycol)-modified poly (amido amine) dendrimers encapsulating gold nanoparticles and their heat-generating ability. Langmuir, 23(10), 5243-5246.

Hussell, T., and Bell, T. J. (2014). Alveolar macrophages: plasticity in a tissue-specific context. Nature Reviews Immunology, 14(2), 81-93.

Jiang, Z., You, Y., Deng, X., and Hao, J. (2007). Injectable hydrogels of poly (ε-caprolactone-co-glycolide)–poly (ethylene glycol)–poly (ε-caprolactone-co-glycolide) triblock copolymer aqueous solutions. Polymer, 48(16), 4786-4792.

Kang, P.B., Azad, A.K., Torrelles, J.B., Kaufman, T.M., Beharka, A., Tibesar, E., DesJardin, L.E. and Schlesinger, L. S. (2005). The human macrophage mannose receptor directs *Mycobacterium tuberculosis* lipoarabinomannan-mediated phagosome biogenesis. The Journal of Experimental Medicine, 202(7), 987-999.

Karthikeyan, R., Koushik, O. S., and Kumar, V. P. (2016). Surface modification of cationic dendrimers eases drug delivery of anticancer drugs. Journal of Nanoscience and Nanotechnology, 10, 108.

Kaur R, Garg T, Goyal AK, and Rath G. (2015). Development, optimization and evaluation ofelectrospun nanofibers: tool fortargeted vaginal delivery of antimicrobials against urinary tract infections. Curr Drug Deliv 22, 328–334.

Kreuter, J. (2013). Mechanism of polymeric nanoparticle-based drug transport across the blood-brain barrier (BBB). Journal of Microencapsulation, 30(1), 49-54.

Kumar, A., Garg, T., Sarma, G. S., Rath, G., and Goyal, A. K. (2015). Optimization of combinational intranasal drug delivery system for the management of migraine by using statistical design. European Journal of Pharmaceutical Sciences, 70, 140-151.

Kumar, P. V., Asthana, A., Dutta, T., and Jain, N. K. (2006). Intracellular macrophage uptake of rifampicin loaded mannosylated dendrimers. Journal of Drug Targeting, 14(8), 546-556.

Lam, P. L., Wong, W. Y., Bian, Z., Chui, C. H., and Gambari, R. (2017). Recent advances in green nanoparticulate systems for drug delivery: efficient delivery and safety concern. Nanomedicine, 12(4), 357-385.

Lee, C. C., MacKay, J. A., Fréchet, J. M., and Szoka, F. C. (2005). Designing dendrimers for biological applications. Nature Biotechnology, 23(12), 1517-1526.

Lee-Sayer, S. S., Dong, Y., Arif, A. A., Olsson, M., Brown, K. L., and Johnson, P. (2015). The where, when, how, and why of hyaluronan binding by immune cells. Frontiers in Immunology, 6, 150.

MacNeil, A., Glaziou, P., Sismanidis, C., Maloney, S., and Floyd, K. (2019). Global epidemiology of tuberculosis and progress toward achieving global targets—2017. Morbidity and Mortality Weekly Report, 68(11), 263.

Majoral, J. P., Zablocka, M., Caminade, A. M., Balczewski, P., Shi, X., and Mignani, S. (2018). Interactions gold/phosphorus dendrimers. Versatile ways to hybrid organic–metallic macromolecules. Coordination Chemistry Reviews, 358, 80-91.

Marcianes, P., Negro, S., García-García, L., Montejo, C., Barcia, E., and Fernández-Carballido, A. (2017). Surface-modified gatifloxacin nanoparticles with potential for treating central nervous system tuberculosis. International Journal of Nanomedicine, 12, 1959.

Marcianes, P., Negro, S., Barcia, E., Montejo, C., and Fernández-Carballido, A. (2020). Potential active targeting of gatifloxacin to macrophages by means of surface-modified PLGA microparticles destined to treat tuberculosis. American Association of Pharmaceutical Scientists, 21(1), 1-14.

Maretti, E., Costantino, L., Rustichelli, C., Leo, E., Croce, M.A., Buttini, F., Truzzi, E. and Iannuccelli, V. (2017). Surface engineering of Solid Lipid Nanoparticle assemblies by methyl α-d-mannopyranoside for the active targeting to macrophages in anti-tuberculosis inhalation therapy. International Journal of Pharmaceutics, 528(1-2), 440-451.

Mariappan, T. T., and Singh, S. (2003). Regional gastrointestinal permeability of rifampicin and isoniazid (alone and their combination) in the rat. The International Journal of Tuberculosis and Lung Disease, 7(8), 797-803.

Mignani, S., Tripathi, R. P., Chen, L., Caminade, A. M., Shi, X., and Majoral, J. P. (2018). New ways to treat tuberculosis using dendrimers as nanocarriers. Pharmaceutics, 10(3), 105.

Moretton, M. A., Chiappetta, D. A., Andrade, F., Das Neves, J., Ferreira, D., Sarmento, B., and Sosnik, A. (2013). Hydrolyzed galactomannan-modified nanoparticles and flower-like polymeric micelles for the active targeting of rifampicin to macrophages. Journal of Biomedical Nanotechnology, 9(6), 1076-1087.

Mustafa, S., Devi, V. K., and Pai, R. S. (2017). Effect of PEG and water-soluble chitosan coating on moxifloxacin-loaded PLGA long-circulating nanoparticles. Drug Delivery and Translational Research, 7(1), 27-36.

Nissen, J. C., Selwood, D. L., and Tsirka, S. E. (2013). Tuftsin signals through its receptor neuropilin-1 via the transforming growth factor beta pathway. Journal of Neurochemistry, 127(3), 394-402.

Ohashi, K., Kabasawa, T., Ozeki, T., and Okada, H. (2009). One-step preparation of rifampicin/poly (lactic-co-glycolic acid) nanoparticle-containing mannitol microspheres using a four-fluid nozzle spray drier for inhalation therapy of tuberculosis. Journal of Controlled Release, 135(1), 19-24.

Pabreja, S., Garg, T., Rath, G., and Goyal, A. K. (2016). Mucosal vaccination against tuberculosis using Ag85A-loaded immunostimulating complexes. Artificial Cells, Nanomedicine, and Biotechnology, 44(2), 532-539.

Pandey, R., Sharma, A., Zahoor, A., Sharma, S., Khuller, G. K., and Prasad, B. (2003). Poly (DL-lactide-co-glycolide) nanoparticle-based inhalable sustained drug delivery system for experimental tuberculosis. Journal of Antimicrobial Chemotherapy, 52(6), 981-986.

Patra, J.K., Das, G., Fraceto, L.F., Campos, E.V.R., del Pilar Rodriguez-Torres, M., Acosta-Torres, L.S., Diaz-Torres, L.A., Grillo, R., Swamy, M.K., Sharma, S. and Habtemariam, S. (2018). Nano based drug delivery systems: recent developments and future prospects. Journal of Nanobiotechnology, 16(1), 1-33.

Pawde, D.M., Viswanadh, M.K., Mehata, A.K., Sonkar, R., Poddar, S., Burande, A.S., Jha, A., Vajanthri, K.Y., Mahto, S.K., Dustakeer, V.A. and Muthu, M.S., (2020). Mannose receptor targeted bioadhesive chitosan nanoparticles of clofazimine for effective therapy of tuberculosis. Saudi Pharmaceutical Journal, 28(12), 1616-1625.

Pi, J., Shen, L., Shen, H., Yang, E., Wang, W., Wang, R., Huang, D., Lee, B.S., Hu, C., Chen, C. and Jin, H., (2019). Mannosylated graphene oxide as macrophage-targeted delivery system for enhanced intracellular *M. tuberculosis* killing efficiency. Materials Science and Engineering: C, 103, 109777.

Piccaro, G., Poce, G., Biava, M., Giannoni, F., and Fattorini, L. (2015). Activity of lipophilic and hydrophilic drugs against dormant and replicating *Mycobacterium tuberculosis*. The Journal of Antibiotics, 68(11), 711-714.

Pooja, D., Tunki, L., Kulhari, H., Reddy, B. B., and Sistla, R. (2015). Characterization, biorecognitive activity and stability of WGA grafted lipid nanostructures for the controlled delivery of Rifampicin. Chemistry and Physics of Lipids, 193, 11-17.

Ramge, P., Unger, R. E., Oltrogge, J. B., Zenker, D., Begley, D., Kreuter, J., and Von Briesen, H. (2000). Polysorbate-80 coating enhances uptake of polybutylcyanoacrylate (PBCA)-nanoparticles by human and bovine primary brain capillary endothelial cells. European Journal of Neuroscience, 12(6), 1931-1940.

Ritsema, J.A.S., Herschberg, E.M.A., Borgos, S.E., Løvmo, C., Schmid, R., Te Welscher, Y.M., Storm, G. and van Nostrum, C.F. (2018). Relationship between polarities of antibiotic and polymer matrix on nanoparticle formulations based on aliphatic polyesters. International Journal of Pharmaceutics, 548(2), 730-739.

Sanità, G., Carrese, B., and Lamberti, A. (2020). Nanoparticle surface functionalization: How to improve biocompatibility and cellular internalization. Frontiers in Molecular Biosciences, 7, 381.

Sarfraz, M., Shi, W., Gao, Y., Clas, S. D., Roa, W., Bou-Chacra, N., and Löbenberg, R. (2016). Immune response to antituberculosis drug-loaded gelatin and polyisobutyl-cyanoacrylate nanoparticles in macrophages. Therapeutic Delivery, 7(4), 213-228.

Sarkar, K., Kumar, M., Jha, A., Bharti, K., Das, M., and Mishra, B. (2021). Nanocarriers for tuberculosis therapy: Design of safe and effective drug delivery strategies to overcome the therapeutic challenges. Journal of Drug Delivery Science and Technology, 102850.

Sharma, A., Sharma, S., and Khuller, G. K. (2004). Lectin-functionalized poly (lactide-co-glycolide) nanoparticles as oral/aerosolized antitubercular drug carriers for treatment of tuberculosis. Journal of Antimicrobial Chemotherapy, 54(4), 761-766.

Shi, X., Sun, K., and Baker Jr, J. R. (2008). Spontaneous formation of functionalized dendrimer-stabilized gold nanoparticles. The Journal of Physical Chemistry C, 112(22), 8251-8258.

Shilpi, S., Vimal, V. D., and Soni, V. (2015). Assessment of lactoferrin-conjugated solid lipid nanoparticles for efficient targeting to the lung. Progress in Biomaterials, 4(1), 55-63.

Silva, M., Lara, A. S., Leite, C. Q. F., and Ferreira, E. I. (2001). Potential Tuberculostatic Agents: Micelle-Forming Copolymer Poly (ethylene glycol)-Poly (aspartic acid) Prodrug with Isoniazid. Archiv der Pharmazie: An International Journal Pharmaceutical and Medicinal Chemistry, 334(6), 189-193.

Singh, H., Bhandari, R., and Kaur, I. P. (2013). Encapsulation of Rifampicin in a solid lipid nanoparticulate system to limit its degradation and interaction with Isoniazid at acidic pH. International Journal of Pharmaceutics, 446(1-2), 106-111.

Singh, J., Garg, T., Rath, G., and Goyal, A. K. (2016). Advances in nanotechnology-based carrier systems for targeted delivery of bioactive drug molecules with special emphasis on immunotherapy in drug resistant tuberculosis–a critical review. Drug Delivery, 23(5), 1676-1698.

Singh, N., Gautam, S. P., Singh, H. L., Dhiman, A., Siddiqui, G., and Verma, A. (2016). Isonizid loaded dendrimer based nano carriers for the delivery of anti-tuberculosis. Indian Journal of Pharmaceutical Sciences 3, 519-529.

Singh, S., Mariappan, T. T., Sharda, N., Kumar, S., and Chakraborti, A. K. (2000). The reason for an increase in decomposition of rifampicin in the presence of isoniazid under acid conditions. Pharmacy and Pharmacology Communications, 6(9), 405-410.

Smith, I. (2003). *Mycobacterium tuberculosis* pathogenesis and molecular determinants of virulence. Clinical Microbiology Reviews, 16(3), 463-496.

Sosnik, A., Carcaboso, Á. M., Glisoni, R. J., Moretton, M. A., and Chiappetta, D. A. (2010). New old challenges in tuberculosis: potentially effective nanotechnologies in drug delivery. Advanced Drug Delivery Reviews, 62(4-5), 547-559.

Su, Y., Bakker, T., Harris, J., Tsang, C., Brown, G.D., Wormald, M.R., Gordon, S., Dwek, R.A., Rudd, P.M. and Martinez-Pomares, L. (2005). Glycosylation influences the lectin activities of the macrophage mannose receptor. Journal of Biological Chemistry, 280(38), 32811-32820.

Thevenot, J., Troutier, A. L., David, L., Delair, T., and Ladavière, C. (2007). Steric stabilization of lipid/polymer particle assemblies by poly (ethylene glycol)-lipids. Biomacromolecules, 8(11), 3651-3660.

Trousil, J., Filippov, S.K., Hrubý, M., Mazel, T., Syrová, Z., Cmarko, D., Svidenská, S., Matějková, J., Kováčik, L., Porsch, B. and Konefał, R. (2017). System with embedded drug release and nanoparticle degradation sensor showing efficient rifampicin delivery into macrophages. Nanomedicine: Nanotechnology, Biology and Medicine, 13(1), 307-315.

Vieira, A. C., Chaves, L. L., Pinheiro, M., Lima, S. A. C., Ferreira, D., Sarmento, B., and Reis, S. (2018). Mannosylated solid lipid nanoparticles for the selective delivery of rifampicin to macrophages. Artificial Cells, Nanomedicine, and Biotechnology, 46(sup1), 653-663.

Vieira, A.C., Chaves, L.L., Pinheiro, S., Pinto, S., Pinheiro, M., Lima, S.C., Ferreira, D., Sarmento, B. and Reis, S. (2018). Mucoadhesive chitosan-coated solid lipid nanoparticles for better management of tuberculosis. International Journal of Pharmaceutics, 536(1), 478-485.

Vijayaraj Kumar, P., Agashe, H., Dutta, T. and Jain, N.K., (2007). PEGylated dendritic architecture for development of a prolonged drug delivery system for an antitubercular drug. Current Drug Delivery, 4(1), 11-19.

Wijagkanalan, W., Kawakami, S., Takenaga, M., Igarashi, R., Yamashita, F., and Hashida, M. (2008). Efficient targeting to alveolar macrophages by intratracheal administration of mannosylated liposomes in rats. Journal of Controlled Release, 125(2), 121-130.

Williams, K., Minkowski, A., Amoabeng, O., Peloquin, C.A., Taylor, D., Andries, K., Wallis, R.S., Mdluli, K.E. and Nuermberger, E.L. (2012). Sterilizing activities of novel combinations lacking first- and second-line drugs in a murine model of tuberculosis. Antimicrobial Agents and Chemotherapy, 56(6), 3114-3120.

World Health Organization. (2015). Implementing the end TB strategy: the essentials (No. WHO/HTM/TB/2015.31). World Health Organization.

WHO (2018) Treatment guidelines for isoniazid-resistant tuberculosis. (Accessed on 11/15/2021) at https://www.who.int/tb/publications/2018/FAQ_TB_policy_recommendations_guidelines.pdf

World Health Organization Global tuberculosis report (2020). Licences: CC BY-NC SA 3.0 IGO.

Wu, Y., Li, M., and Gao, H. (2009). Polymeric micelle composed of PLA and chitosan as a drug carrier. Journal of Polymer Research, 16(1), 11-18.

Yamori, S., Ichiyama, S., Shimokata, K., and Tsukamura, M. (1992). Bacteriostatic and bactericidal activity of antituberculosis drugs against *Mycobacterium tuberculosis*, *Mycobacterium* avium-*Mycobacterium* intracellulare complex and *Mycobacterium* kansasii in different growth phases. Microbiology and Immunology, 36(4), 361-368.

Zahoor, A., Sharma, S., and Khuller, G. K. (2005). Inhalable alginate nanoparticles as antitubercular drug carriers against experimental tuberculosis. International Journal of Antimicrobial Agents, 26(4), 298-303.

Zhang, Z., Lu, J., Wang, Y., Pang, Y., and Zhao, Y. (2014). Prevalence and molecular characterization of fluoroquinolone-resistant *Mycobacterium tuberculosis* isolates in China. Antimicrobial Agents and Chemotherapy, 58(1), 364-369.

CHAPTER FOUR

PRELIMINARY STUDIES: RP-HPLC METHOD VALIDATION AND *EX VIVO* PERMEATION STUDIES OF ISONIAZID AND PYRAZINAMIDE ACROSS PORCINE PERICARDIUM

4.1. INTRODUCTION

High-performance liquid chromatography (HPLC) is an analytical tool employed for cost-effective analysis in the pharmaceutical industry for the reasonable and reliable quantitative and qualitative analysis of a compound/s in a mixture. The method of analysis uses a concept wrapped around the energetics of interactions between the sorbent (stationary phase) and solute molecules and the sorbent and solvent molecules (mobile phase) known as the 'adsorption milieu' (Horváth, 2013).

Reverse Phase- HPLC is the most used liquid chromatographic separational method which employs the use of an immobilized non-polar stationary phase, and a relatively polar mobile phase that results in non-polar solutes eluting later as compared to polar solutes (Meyer, 2013). The delayed elution is due to the van der Waal dispersion force between the non-polar compound and the hydrocarbon groups attached to the silica, resulting in an extended retention of the compound. The stationary phase is usually porous and made up of either C8 or C18 straight chain alkyl group modified silica-based sorbent. The mobile phase is usually composed of a mixture of water and other miscible organic solvents such as acetonitrile, isopropanol, methanol, or tetrahydrofuran (Sarker and Nahar, 2015).

Unreacted silanols are always present in amounts as much as 60% of the stationary phase despite the use of forcing conditions during the bonding stage. These unreacted silanols are polar and acidic, allowing them to react to solutes through hydrogen bonding and problematically, if ionized, act as an ion exchange site with basic molecules. The higher the pKa of the compound, the lower the steric hindrance around the basic centre (e.g., pyridine), causing greater interaction with these silanols (Law, 2000). For this reason, instead of water, a buffer may at times be used to improve chromatography and reduce peak tailing by suppressing the ionization of the compound or the ionization of free unreacted silanols on the stationary phase (Sarker and Nahar, 2015).

The pericardium is a fibrous tissue layer composed of compact collagen fibres and short elastin fiber, responsible for stress relaxation and diastolic pressure control (Hoit, 2017; Shabetai, 2003).

It also consists of a mesothelial layer which is metabolically active, providing immunologic and fibrinolytic activities by producing endothelin, prostaglandin E2, eicosanoids, and prostacyclin (Hoit, 2017; Miyazaki et al., 1990). The pericardium lines a space known as the pericardial cavity containing the pericardial fluid, an ultrafiltrate of plasma that comes from epicardial and parietal pericardial capillaries and drains into the lymphatic system on the epicardial surface of the heart and in the parietal pericardium (Rodriguez and Tan, 2017). Rare mast cells and mononuclear cells have also been identified in the pericardial layer (Ishihara et al., 1980; Rodriguez and Tan, 2017). Pinocytic vesicles are present on the inner surface of the pericardium towards the pericardial cavity. The mesothelial cell presents with abundant microvilli and on its lateral surface, a highly interlocked surface showing cell junctions and desmosomes. The transport of fluids and proteins is said to occur due to the irregular invaginations of the plasma membrane, multivesicular bodies, and coated and uncoated vesicles (Rodriguez and Tan, 2017). The porcine pericardium is similar to the human pericardium including its thickness, therefore presents good models for experimental use to determine the outcome of the research on human pericardium (Morticelli et al., 2013).

For the treatment of tuberculosis pericarditis, the standard anti-tuberculosis combination therapy, comprising rifampicin, isoniazid, pyrazinamide and ethambutol has been used for decades even though they collectively have a limited ability to penetrate the pericardium at adequate non-protein bound concentrations. Their use has been maintained due to a lack of comparative effectiveness studies (Isiguzo et al., 2020a; Shenje, 2015). *In vitro* and *in vivo* studies have both confirmed that only isoniazid of all four drugs would penetrate the pericardium and have bactericidal effects (Sarathy et al., 2017; Shenje, 2015). In these studies, rifampicin was found to have delayed, decreased penetration across the pericardium, high clearance from the pericardial fluid and a low unbound concentration due to protein content in the pericardium being as high as the plasma, considering a 90% rifampicin protein binding (Sarathy et al., 2017; Shenje, 2015). Ethambutol was found to have 30% protein binding, but irrespectively, had a low pericardial concentration due to inherent poor pericardial penetration (Shenje, 2015). Pyrazinamide had an initial delay in permeation but eventually had a similar concentration between the pericardial fluid and plasma, indicating that the compound penetrates well, but due to its acidic-dependent bactericidal abilities with zero microbial kill at pH ≥ 6.8, it was calculated to be below the MIC at pH of 7.34 (the pH of TB- infected pericardial fluid) (Shenje, 2015). Isoniazid, like pyrazinamide, had a similar concentration between the pericardial fluid and plasma, suggesting good permeation. Furthermore, since isoniazid is only 10% protein bound, the unbound-protein median peak

concentration was found to be 64 times higher than the median MIC ($p<0.001$). The lack of effectiveness of rifampicin, and possibly pyrazinamide, therefore, is concerning since both drugs are the main drugs amongst the combination associated with a sterilizing effect against *M.tb* (Shenje, 2015). For this study, the two drugs with good permeation ability, isoniazid and pyrazinamide have been investigated for their permeability across porcine pericardium and quantified on HPLC.

Isoniazid, chemically identified as pyridine-4-carbohydrazide, is a hydrazide of isonicotinic acid. Its structure is shown in Figure 4.1. Isoniazid is tuberculostatic in resting bacilli and bactericidal in rapidly dividing bacilli (Anusiem et al., 2018). It is a prodrug that is converted and activated by mycobacterial catalase-peroxidase KatG to isonicotinic acyl radical which couples with NADH to form a nicotinoyl-NAD adduct (Sundar, 2023). This adduct inhibits Inh A enzyme which is involved in the synthetic pathway of mycolic acid, a key component of the mycobacterial cell wall (Sundar, 2023). Isoniazid has a plasma half-life dependent on whether the patient is a slow or fast acetylator, ranging from 1–3 h (Van Crevel and Hill, 2017), with a MIC of <1 $\mu g.ml^{-1}$ in susceptible *M.tb* and 1-8 $ug.ml^{-1}$ in resistant tuberculosis (Schönfeld et al., 2012; Suo et al., 1988). It has a pKa of 1.82 at 20 °C (Fernandes et al., 2017).

Pyrazinamide (Figure 4.2) is chemically identified as pyrazine-2-carboxamide. It is a tuberculostatic first-line drug, which is converted by pyrazinamidase to pyrazinoic acid in the bacilli where it interferes with fatty acid synthase FAS I, preventing the bacteria from lipogenesis required for growth and replication. Pyrazinoic acid is only active under acidic conditions, active at or below pH 5.6 (Doležal et al., 2012; Harmon, 2007). The MIC of pyrazinamide is much higher than that of isoniazid and is also influenced by pH; a MIC of 20 $\mu g.ml^{-1}$ has been reported on 7H10 agar, but in liquid media, the MIC varied from 50 $\mu g.ml^{-1}$ at pH 5.5 to 400 $\mu g.ml^{-1}$ at pH 5.95 for susceptible TB (Donald and McIlleron, 2009). Pyrazinamide has a plasma half-life of ~ 10 h (Friedland, 2010) and a pKa of 0.5 (Ahn et al., 2003).

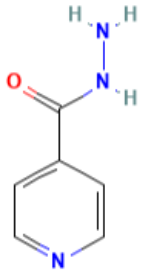

Figure 4.1: Chemical structure of isoniazid (https://pubchem.ncbi.nlm.nih.gov/)

Figure 4.2: Chemical structure of pyrazinamide (https://pubchem.ncbi.nlm.nih.gov/)

4.2. MATERIALS AND METHOD

4.2.1. Materials

Isoniazid (INH) and pyrazinamide (PZA) reference standards were procured from Sigma Aldrich Inc. (St. Louis, Missouri, United States). Analytical grade reagents and solvents, like methanol (HPLC grade), acetonitrile (HPLC grade), triethylamine (TEA), Milli Q water, potassium dihydrogen orthophosphate and orthophosphoric acid were used. All reagents and compounds used for HPLC were filtered (0.45 µm) before use.

4.2.2. Method Development and Validation

4.2.2.1. Preparation of Standards and Phosphate Buffer for Mobile Phase

Phosphate buffer was prepared by weighing 20 mg of potassium dihydrogen orthophosphate (KH_2PO_4) and dissolving it in 1000 ml Milli-Q® water. Triethylamine (10 ml) was added to this mixture and the pH of the subsequent solution was adjusted to 7.4 with 10% (v/v) orthophosphoric acid.

The mobile phase was prepared by mixing 90 ml of phosphate buffer prepared above, 8.5 ml of methanol and 1.5 ml acetonitrile. Isoniazid and pyrazinamide (20 mg each) were mixed separately in 10 ml of mobile phase and further diluted down using a dilution factor of 0.1 (10%) to form 200 $ug.ml^{-1}$ of each stock solution which were filtered through a 0.45 µm syringe filter and stored in the refrigerator below 4 °C.

4.2.2.2. Running Conditions

A UPLC method described by Lakshmi and Jacob, 2018 employing the use of a X Bridge 3x50 mm, 3.7 µm C18 column using a mobile phase consisting of triethylamine and potassium dihydrogen ortho phosphate pH 7.4 [Sol A]: Methanol and acetonitrile in a ratio of 85:15 adjusted with [Sol B] in the ratio 90:10, 0.5 $ml.min^{-1}$ flow rate with a PDA detector was used for this study. The method was originally used for the detection of rifampicin, isoniazid, pyrazinamide and ethambutol (Lakshmi and Jacob, 2018) and was adopted, adjusted, and used to detect isoniazid and pyrazinamide on HPLC. Both compounds were separately dissolved in the proposed mobile phase and tested for their lambda max on a UV-Vis spectrometer. Thereafter the flow rate was adjusted from 0.5 $ml.min^{-1}$ to 1 $ml.min^{-1}$ since a HPLC apparatus would be used as compared to a UPLC. Symmetrical peaks were identified for both isoniazid and pyrazinamide, thereafter method validation was conducted. The chromatographic apparatus and conditions employed were as follows (Table 4.1):

Table 4.1: Instrumentation and chromatography conditions for the detection of isoniazid and pyrazinamide.

Parameter	Isoniazid	Pyrazinamide
Instrument	A Perkin Elmer Flexar HPLC system, consisting of a binary pump, autosampler, column oven and a UV/Vis detector. The system was equipped with Chromera® software for data acquisition and analysis (Perkin Elmer Inc., Waltham, Massachusetts, USA).	
Column	Phenomenex Kinetex C18 RP LC Column with dimensions of 150 x 4.6 mm and particle size of 5 µm.	

Mobile Phase	An organic phase (A) of methanol: acetonitrile (85:15) and an aqueous phase (B) made of triethylamine (10 ml) and potassium phosphate buffer (20 mg in 1000 ml) adjusted with orthophosphoric acid to a pH of 7.4. The phosphate buffer was filtered using a vacuum pump through a 0.45-µm membrane. Pumped across the HPLC at a ratio of 10:90 (A: B)	
Flow rate	1 $ml.min^{-1}$	
Detection wavelength	263 nm	270 nm
Injection Volume	20 µl	
Run time	3 min	3.5 min
Column Temperature	20 °C	25 °C
Elution technique	Isocratic	

4.2.2.3. Validation Parameters

4.2.2.3.1. Linearity

Linearity is the ability of a method to obtain analytical values that are directly proportional to the concentration of sample analytes in a set range. The acceptance criterion for linearity is that the correlation coefficient (R^2) should be ≥ 0.990 for the least squares method of the analysis of the line. The %RSD should be ≤ 5% at all standard concentrations (H.I.C, 2005). The LOD and LOQ were estimated by comparing the blank chromatography signal-to-noise ratio to a chromatograph with a 3x times signal-to-noise ratio and 10x signal-to-noise ratio for LOD and LOQ, respectively (H.I.C, 2005).

The linearity of isoniazid and pyrazinamide were separately performed by linear regression analyses of the graph of the peak area versus concentration (μg.ml^{-1}) to obtain a linear equation (Equation 4.1).

$$y = mx + c \quad (4.1)$$

Where:

$y =$ Peak area of analyte

$m =$ Slope

$x =$ Concentration of analyte (μg.ml^{-1})

$c =$y-intercept

Standard solutions were diluted from the stock solution prepared as described in section 4.2.2.1.2 to prepare calibration curve standards of 5 μg.ml^{-1}, 10 μg.ml^{-1}, 20 μg.ml^{-1}, 50 μg.ml^{-1}, 100 μg.ml^{-1} and 150 μg.ml^{-1}. These working standards were separately analysed in triplicate.

4.2.2.3.2. Precision

Precision is the measure of the extent of repeatability of a method under normal operating conditions.

4.2.2.3.2.1. Intraday Precision

Three samples (10 µg.ml^{-1}, 50 µg.ml^{-1}, and 100 µg.ml^{-1}) were used to determine intraday precision. Samples were injected in triplicate in the morning and afternoon (8 h apart) on the same day. The acceptance criteria for intra-day precision are set to be a % relative standard deviation (RSD) ≤ 2.0.

4.2.2.3.2.2. Interday Precision

Three samples (10 µg.ml^{-1}, 50 µg.ml^{-1}, and 100 µg.ml^{-1}) were used to determine inter-day precision. Samples were injected in triplicate for 3 consecutive days. The acceptance criteria for intra-day precision are set to be a % relative standard deviation (RSD) ≤ 2.0.

4.2.2.3.3. Accuracy

Accuracy is the measure of agreement between value found and value present in the sample analyte. It is a measured as the %recovery of analyte by assay after spiking in a blind study (H, 2005). For quality of analytical results, three different standard concentrations were formed by spiking phosphate buffer saline (PBS) (pH 7.4) with 25 µg.ml^{-1} standard solution from each drug to obtain the following final concentrations: 5 µg.ml^{-1}, 7.5 µg.ml^{-1}, and 15 µg.ml^{-1} for each drug. The concentrations are three different levels of target concentration (50%, 75% and 150%) as per the ICH guideline. These standards were analysed in replicates (n=6). The acceptance criteria for accuracy are between 98-102%.

4.2.2.3.4. Robustness

Robustness is the ability of a method to provide reliable results despite slight variation in analytical conditions (González et al., 2014). Robustness of the method was performed on 10 µg.ml^{-1}, 50 µg.ml^{-1}, and 100 µg.ml^{-1} by adjusting mobile phase, temperature, and flow rate (standards were injected n=6). The mobile phase was adjusted by ±1% of the organic component, temperature was adjusted by ±1 °C and flow rate was adjusted by ± 0.1 ml.min^{-1} and tested to note its variation in % recovery. The change in retention time and the area change were evaluated (RSD ≤ 2%).

4.2.2.3.5. Stability

Stability of the analyte in mobile phase was tested by placing 10 µg.ml^{-1}, 50 µg.ml^{-1}, and 100 µg.ml^{-1} standards at room temperature, 4 °C and -20 °C, tested weekly until significant change occurred. The acceptance criteria for recovery are set to be between 98-102%. This allows the

analyst to know the time frame a sample can be kept from day of preparation until the time it degrades by 2%.

4.2.3. Collection and Treatment of Porcine Pericardial Tissue

Porcine pericardial tissue was collected from animals euthanized for other purposes at the University of the Witwatersrand Central Animal Unit. For this study, an ethics waiver for the use of porcine tissue was obtained from the University of the Witwatersrand Animal Research Ethics Committee (waiver number: AREC-101210-002) (Appendix A).

The pericardial tissue was immediately placed in PBS, pH 7.4 and within an hour sectioned into strips, placed into cryovials, snap frozen and stored in liquid nitrogen (-195 °C).

4.2.4. *Ex Vivo* Diffusion Studies

Porcine pericardial tissue was thawed for 10 min in PBS, after which the tissue was sectioned into approximately 1 cm^2 each. Tissue sections were mounted in PermeGear in-line flow-through diffusion cells (exposed area 0.039 cm^2), part of a PermeGear 7-in-line Flow-through Diffusion system (PermeGear Inc, Hellertown, USA). The tissue sections were equilibrated for 10 min in PBS (pH 7.4) at 37 °C in both the donor and receptor compartments of the diffusion cells before each permeability experiment started. To set up the experiment at infinite dosing conditions, PBS in the various donor compartments was replaced with 1 $mg.ml^{-1}$ of isoniazid or 1 $mg.ml^{-1}$ pyrazinamide. Phosphate buffer saline was pumped through the receptor chambers at a rate of 1.5 $ml.hr^{-1}$ at 37 °C and elutes were collected using a fraction collector at 2 h intervals for 24 h. The study was repeated three times. After collection, eluents were analysed on the HPLC. Cumulative amount per area ($\mu g.cm^{-2}$) vs time graph was constructed and the steady-state flux rates ($\mu g.cm^{-2}.min^{-1}$), Equation 4.2) and lag phase (min) were obtained from the regression of the linear portion of the cumulative amount per area versus time graph and the x-axis intercepts, respectively. The apparent permeability coefficient was calculated from the steady-state flux (Equation 4.3).

$$= \mathrm{Q}/\left(\mathrm{A} \times \mathrm{t}\right) \tag{4.2}$$

$$\mathrm{P} = \mathrm{J}/(\mathrm{Cdoner} - \mathrm{Creceptor}) \tag{4.3}$$

whereby;

J is the steady-state flux, Q is the quantity of substance crossing the membrane (in µg), A is the membrane area exposed (in cm^2) and t is the time of exposure (in min).

P is the apparent permeability coefficient, Cdonor is the Concentration in the donor compartment of the flow-through cell at t=0 h and Creceptor is the Concentration in the receptor compartment of the flow-through cell. The experiment was conducted under sink conditions and infinite dosing, and as such, the Cdonor (0 h) ≈ Creceptor (t=24 h). Sink condition is when the concentration of the permeant in the receptor chamber is less than 10% of that in the donor compartment. Infinite dosing is an experimental condition that assumes that there is no change in the Cdonor (permeant) concentration throughout the experiment.

4.3. RESULTS

4.3.1. RP-HPLC Method Development and Validation

4.3.1.1. Method Development

The adopted UPLC method worked on the Perkin Elmer Flexar system containing the Phenomenex Kinetex C18 RP LC Column used in the study. Peaks that were obtained were narrow and symmetrical with a retention time of 2.261 min and 2.789 min for isoniazid and pyrazinamide, respectively (Figure 4.3a and 4.3b). For proper elution, the column was equilibrated using 90:10 water: organic phase (containing methanol 85:15 acetonitrile) for 10 min before interchanging the water with phosphate buffer and equilibrating for 20 min to prevent crystallization between the buffer and organic phase. To prevent blockage of the column, a mobile phase of buffer containing as little as 20 mg/1000 ml of potassium dihydrogen orthophosphate and 10 ml/1000 ml triethylamine adjusted to a pH of 7.4 using orthophosphoric acid was used in conjunction with methanol and acetonitrile in a ratio 90:8.5:1.5 (v/v) to make up the mobile phase.

(a)

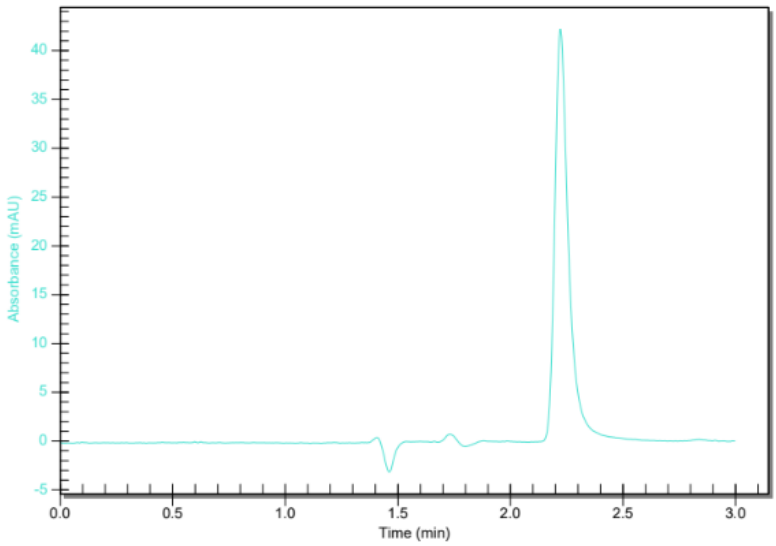

(b)

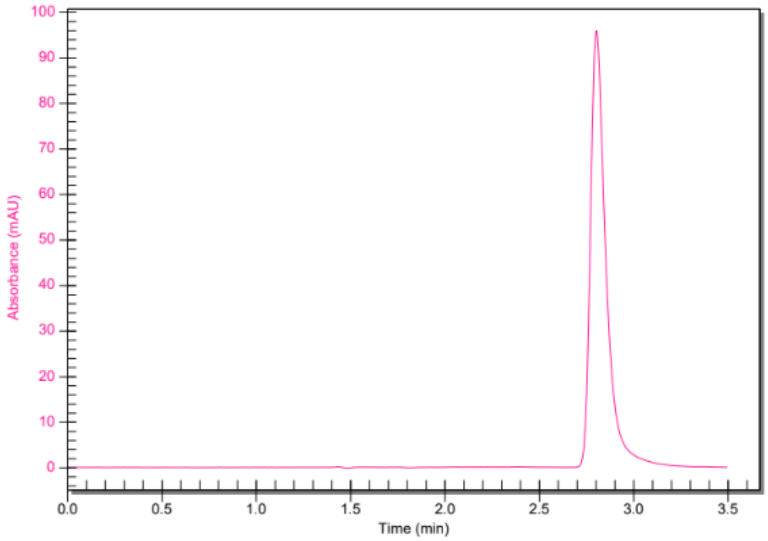

Figure 4.3: RP-HPLC chromatogram with a run time of 3 min and 3.5 min for (a) isoniazid (5 µg.ml^{-1}) and (b) pyrazinamide (5 µg.ml^{-1}), respectively, using a mobile phase of 90:10 (phosphate buffer: organic phase (containing methanol 85:15 acetonitrile)) at a flow rate of 1 ml.min^{-1} for (a) isoniazid, with a retention time of 2.261 min at a detection wavelength of 263 nm and (b) pyrazinamide, with a retention time of 2.789 min at a detection wavelength of 270 nm .

4.3.1.2. Method Validation

4.3.1.2.1. Linearity

The linear regression curves displayed the suitability of the method within the prescribed concentration range (5-150 µg.ml^{-1}) for both isoniazid and pyrazinamide with the correlation of determination (R^2) = 0.9996 and 0.9993, respectively, as can be seen in Figure 4.4 and 4.5 below and detailed in Table 4.2 and 4.3. The LOD and LOQ were found to be 0.01 µg.ml^{-1} and 0.03 µg.ml^{-1}, respectively, for isoniazid using signal-to-noise ratio as can be seen in Figure 4.6. The LOD and LOQ were found to be 0.06 ug.ml^{-1} and 0.19 µg.ml^{-1}, respectively, for pyrazinamide as can be seen in Figure 4.6.

(a)

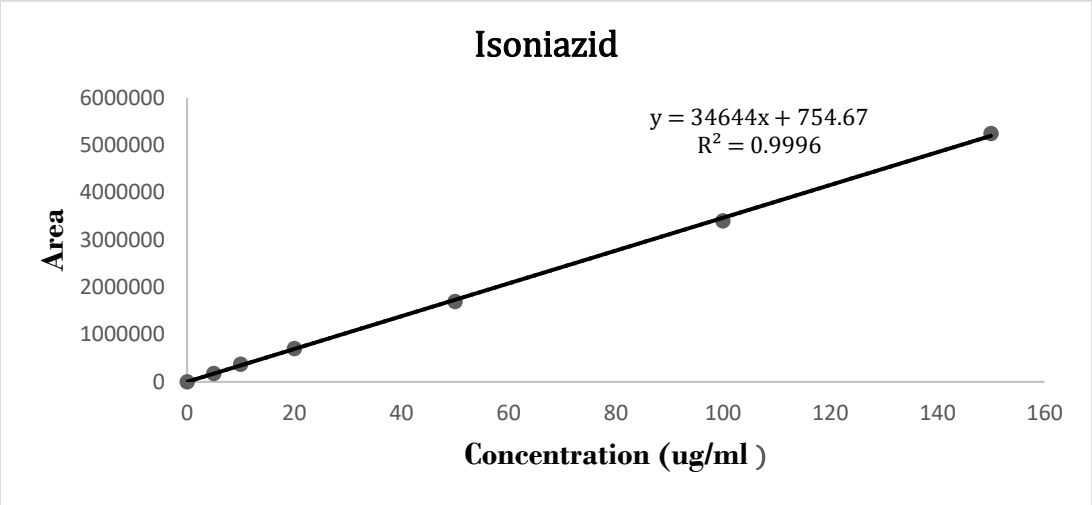

.

(b)

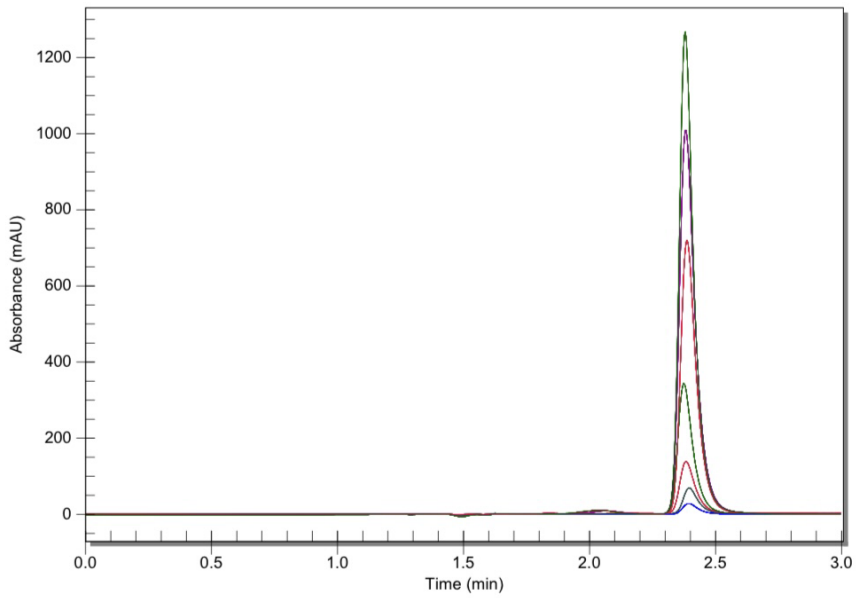

Figure 4.4: Diagram showing (a) a standard curve of isoniazid done in triplicates (each standard was injected 3 times), (b) Overlay of isoniazid standard curve peaks.

(a)

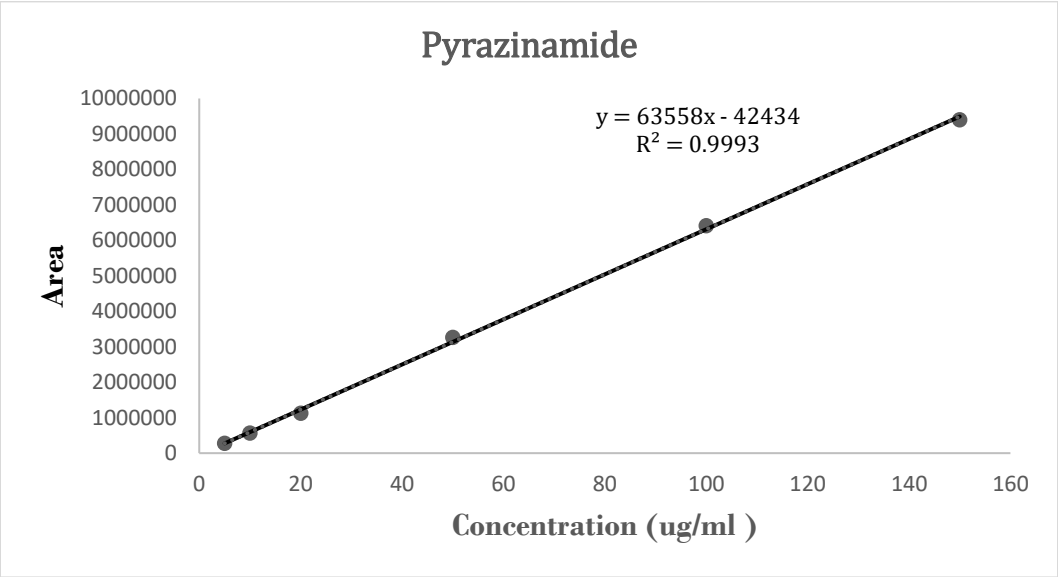

(b)

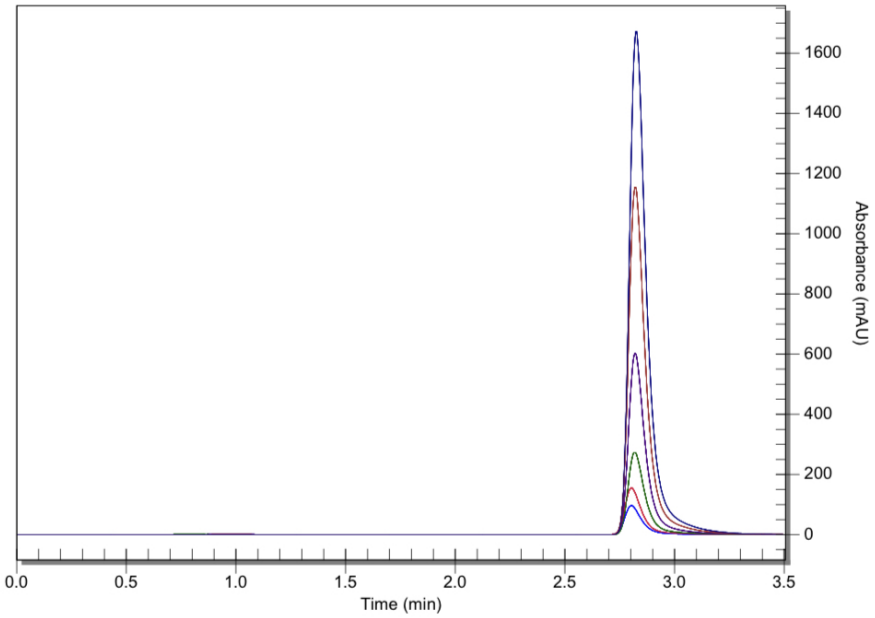

Figure 4.5: Diagram showing (a) a standard curve of pyrazinamide done in triplicates (each standard was injected 3 times), (b) overlay of pyrazinamide standard curve peaks.

(a)

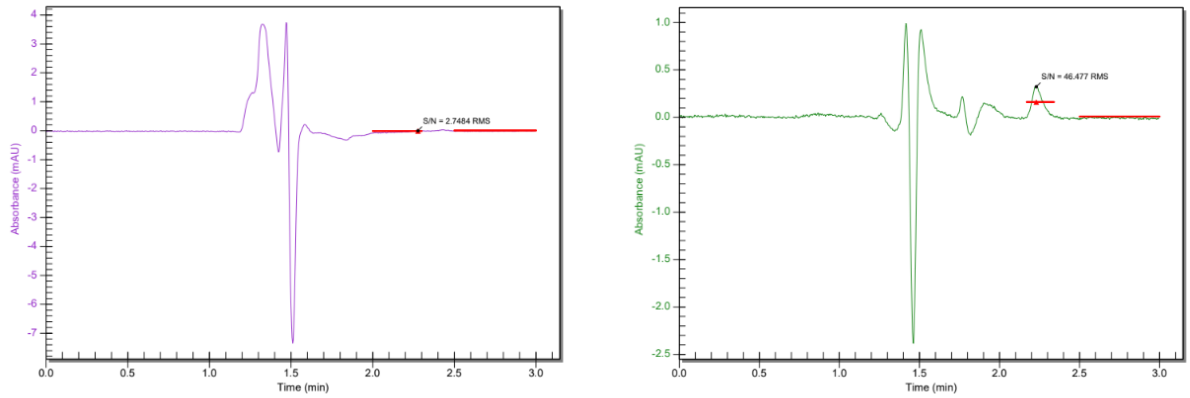

(b)

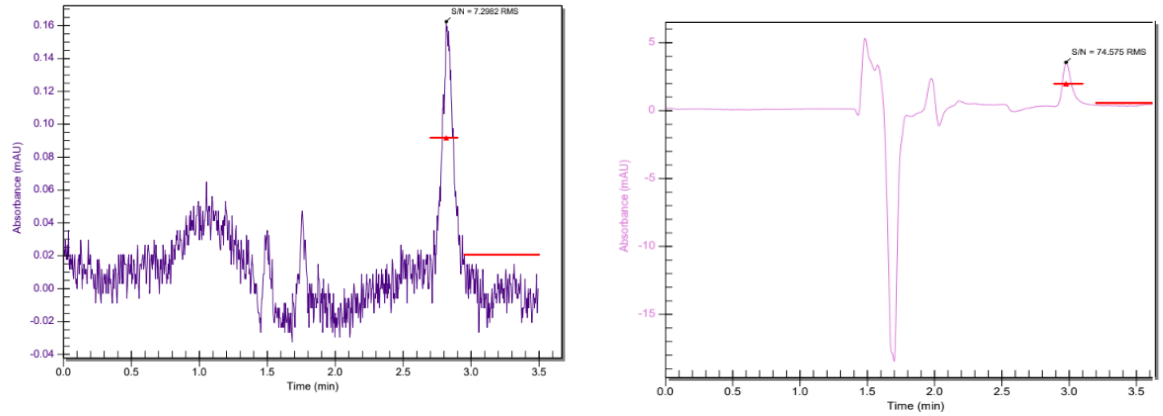

Figure 4.6: Chromatogram showing the signal-to-noise ratio of a blank peak and a peak 10x its signal-to-noise ratio for (a) isoniazid and (b) pyrazinamide.

Table 4.2: Linearity of isoniazid established from three independent standard curves using the established RP-HPLC method. Each analyte concentration was done in triplicate.

Concentration ($\mu g.ml^{-1}$)	Std.Curve 1 Mean Peak area (±SD)	Std.Curve 2 Mean Peak area (±SD)	Std.Curve 3 Mean Peak area (±SD)	Overall Mean Peak Area (Overall SD)	%RSD
5	178618.03 (298.24)	176495.95 (755.72)	176558.97 (17.57)	177224.31 (985.84)	0.55

10	388662.47 (1329.22)	363299.68 (744.45)	378049.64 (1155.06)	376670.59 (10400.13)	2.76
20	708488.64 (2648.53)	705246.08 (3461.55)	709761.15 (269.48)	707831.95 (1900.86)	0.27
50	1728725.08 (5165.24)	1725566.71 (8592.82)	1647613.52 (8452.44)	1700635.10 (37514.08)	2.21
100	3484994.58 (3022.74)	3414065.17 (1869.20)	3310301.11 (16708.47)	3403120.28 (71736.99)	2.11
150	5325444.83 (22126.90)	5269219.43 (16970.71)	5141725.03 (26712.92)	5245463.09 (76861.40)	1.47

Table 4.3: Linearity of pyrazinamide established from three independent standard curves using the established RP-HPLC method. Each analyte concentration was done in triplicate.

Concentration ($\mu g.ml^{-1}$)	Std.Curve 1 Mean Peak area (±SD)	Std.Curve 2 Mean Peak area (±SD)	Std.Curve 3 Mean Peak area (±SD)	Overall Mean Peak area (Overall SD)	%RSD
5	278491.62 (460.04)	278812.60 (397.30)	277539.45 (158.77)	278281.22 (540.64)	0.19
10	591375.00 (431.48)	553349.25 (372.21)	550774.28 (1823.72)	565166.18 (18562.23)	3.28
20	1183923.38 (895.55)	1100838.12 (4687.57)	1086962.60 (4645.93)	1123908.04 (42813.66)	3.81
50	3205458.99 (20738.87)	3223170.26 (2515.97)	3343737.27 (3750.94)	3257455.51 (61437.39)	1.89
100	6260884.67 (1561.19)	6522895.47 (2490.36)	6451238.14 (7298.41)	6411672.76 (110563.65)	1.72

150	9294245.45 (4388.36)	9531073.25 (4831.65)	9376856.22 (1790.68)	9400724.97	1.04

4.3.1.2.2. Precision

The inter-day and intra-day precision showed reproducibility over 3 days in the detection of both compounds, with a %RSD of <2% for all selected standard concentrations, which is within the acceptance criteria (Table 4.4).

Table 4.4: Precision determined for the established HPLC method from three independent standard concentrations. Each analyte concentration was repeated six times.

Drug	Concentration ($\mu g.ml^{-1}$)	Intraday Precision		Interday Precision			
				Day 2		Day 3	
		Mean Peak Area (±SD)	%RSD	Mean Peak Area (±SD)	%RSD	Mean Peak Area (±SD)	%RSD
INH	10	362608.88 (250.47)	0.095	362272.36 (235.70)	0.142	362473.30 (183.72)	0.114
	50	1732359.35 (686.47)	0.197	1732700.69 (1352.44)	0.206	1730004.29 (3884.79)	0.128
	100	3416987.88 (2095.96)	0.043	3411933.39 (2309.15)	0.031	3411276.29 (1137.87)	0.041
PZA	10	557400.81 (711.46)	0.514	552865.18 (347.87)	0.062	548013.87 (194.64)	0.688
	50	3214446.65 (603.45)	0.192	3207554.24 (8125.27)	0.344	3214943.87 (4804.40)	0.181

	100	6506848.13 (2861.33)	0.344	6503105.55 (9206.15)	0.215	6530546.11 (17345.29)	0.083

INZ: Isoniazid; PZA: Pyrazinamide, %RSD; % Relative Standard Deviation

4.3.1.2.3. Accuracy

The method was efficient, with an overall 100.28% and 99.86% recovery for isoniazid and pyrazinamide with a %RSD of 0.93% and 1.31% (n=6) after spiking of PBS with 25 $\mu g.ml^{-1}$, respectively, as detailed in Table 4.5.

Table 4.5: Accuracy of the established HPLC method from three independent standard concentrations. Each analyte concentration was repeated six times.

Drug	Level, %	Concentration ($\mu g.ml^{-1}$)	Amount recovered (SD) ($\mu g.ml^{-1}$)	Recovery (SD), %	RSD, %
INH	50	5	5.01 (0.022)	101.14 (0.380)	1.13
	75	7.5	7.43 (0.011)	99.16 (0.138)	0.84
	150	15	15.08 (0.111)	100.53 (0.743)	0.81
PZA	50	5	5.09 (0.008)	102.00 (0.165)	1.99
	75	7.5	7.45 (0.003)	99.34 (0.046)	0.66
	150	15	14.81 (0.021)	98.71 (0.138)	1.29

INH: Isoniazid; PZA: Pyrazinamide

4.3.1.2.4. Robustness

The robustness of the HPLC method was investigated by varying small variations in the following running conditions: flow rate, temperature, and the organic mobile phase component. The results can be observed in Tables 4.6 and 4.7 below. A slight alteration in temperature for isoniazid caused a very slight shift in the retention time and peak area detected, with a recovery range of 98.0-101.7%. A slight increase in temperature for pyrazinamide resulted in a peak area detected, with a recovery range of 99.9-100.3%, however, the area detected was slightly less stable with a slight temperature decrease, with a recovery range of 94.4-109.2%. As the flow rate decreased, elution occurred later by a difference of 11.14% and 9.65% for isoniazid and pyrazinamide, respectively. The % recovery of both compounds increased to a range of 106.7-111.3% and 108.0-110.2% for isoniazid and pyrazinamide, respectively. As the flow rate increased, elution occurred earlier by a difference of 9.10% and 10.08% for isoniazid and pyrazinamide, respectively. The % recovery of both compounds decreased to a range of 90.5-94.5% and 87.7-90.9% for isoniazid and pyrazinamide, respectively. As the mobile phase ratio of organic: aqueous decreases, the peak eluted later by a difference of 7.13% and 4.18% for isoniazid and pyrazinamide, respectively. The % recovery of both compounds increased. A slight increase with a recovery of 99.5-103.6 % for isoniazid was noticed, whilst a distinct increase was noted with a recovery of 108.0-108.6 % for pyrazinamide. As the mobile phase ratio of organic: aqueous increases, the peak eluted earlier by a difference of 4.48% and 5.69% for isoniazid and pyrazinamide, respectively. The % recovery of both compounds increased. A notable difference with a recovery of 84.5-90.5% for isoniazid was noticed, whilst a slight decrease was noted with a recovery of 97.5-98.2% for pyrazinamide.

Table 4.6: Robustness determined for the established isoniazid HPLC method from three independent standard concentrations by varying flow rate, temperature, and organic mobile phase component. Each analyte concentration was repeated six times.

Condition	Isoniazid				
	Mean Peak Area (±SD)	Amount recovered. ($\mu g.ml^{-1}$)	% Recovery	Mean RT (SD)	Mean RT %RSD
FR: 1 $ml.min^{-1}$ MP: 10:90 T: 20 °C Isoniazid	364844.91 (2724.03)	10.12 (0.05)	-	2.235 (0.002)	
	1645553.18 (4459.42)	47.27 (0.10)	-		
	3277696.86 (8062.66)	94.60 (0.20)	-		
FR change: 0.9 $ml.min^{-1}$	388402.38 (3968.25)	10.81 (0.09)	106.7 (0.89)	2.484 (0.004)	11.14
	1829683.89 (3770.22)	52.61 (0.08)	111.3 (0.17)		
	3513591.89 (2827.98)	101.44 (0.05)	107.2 (0.05)		
FR change: 1.1 $ml.min^{-1}$	345480.65 (1956.49)	9.56 (0.03)	94.5 (0.30)	2.0318 (0.005)	9.10
	1543842.28 (3945.68)	44.32 (0.09)	93.8 (0.19)		
	2967571.07 (2734.45)	85.61 (0.05)	90.5 (0.05)		

T change: 19 °C isoniazid 24 °C pyrazinamide	360286.56 (2683.37)	9.99 (0.05)	98.7 (0.49)	2.265 (0.003)	1.34
	1674019.95 (2249.63)	48.09 (0.04)	101.7(0.08)		
	3211213.86 (4458.44)	92.67 (0.10)	98.0 (0.11)		
T change 1: 21 °C isoniazid 26 °C pyrazinamide	367838.32 (261.92)	10.21 (0.005)	100.9 (0.05)	2.236 (0.002)	0.04
	1674233.00 (8216.47)	48.10 (0.21)	101.8 (0.44)		
	3235913.20 (7572.72)	93.39 (0.19)	98.7 (0.20)		
MP change: 9:91 (A: B)	377023.99 (2330.29)	10.48 (0.04)	103.5 (0.40)	2.395 (0.010)	7.13
	1704661.94 (2744.37)	48.98 (0.05)	103.6 (0.11)		
	3260783.05 (1764.21)	94.11 (0.02)	99.5 (0.02)		
MP change: 11:89 (A: B)	310585.07 (3629.55)	8.55 (0.08)	84.5 (0.79)	2.135 (0.001)	4.48
	1489157.50 (5187.80)	42.73 (0.12)	90.4 (0.25)		
	2967571.07 (7327.94)	85.61 (0.18)	90.5 (0.19)		

FR: Flow rate; T: Temperature; MP: Mobile phase; RT: Retention time; %RSD: % Relative standard deviation from normal conditions

Table 4.7: Robustness determined for the established pyrazinamide HPLC method from three independent standard concentrations by varying flow rate, temperature, and organic mobile phase component. Each analyte concentration was repeated six times.

Condition	Pyrazinamide				
	Mean Peak Area (±SD)	Amount recovered. (±SD) ($\mu g.ml^{-1}$)	% Recovery	Mean RT (SD)	Mean RT %RSD
FR: 1 $ml.min^{-1}$ MP: 10:90 T: 25 °C pyrazinamide	736755.20 (1762.42) (FR 1 $ml.min^{-1}$)	10.92 (0.02)	-	2.820 (0.002)	
	665318.01 (1019.40) (T 25 °C and MP 10:90)	9.80 (0.01)			
	3554335.54 (2787.24) (FR 1$ml.min^{-1}$)	55.26 (0.04)	-		
	3282356.21 (4712.61) (T 25 °C and MP 10:90)	50.98 (0.07)			
	6984244.76 (3853.06) (FR 1 $ml.min^{-1}$)	109.22 (0.05)	-		

	6484923.32 (7472.73) (T 25 °C and MP 10:90)	101.36 (0.11)			
FR change: 0.9 ml.min^{-1}	791983.94 (3848.92)	11.79 (0.05)	108.0 (0.46)	3.092 (0.006)	9.65
	3914164.19 (1114.47)	60.92 (0.01)	110.2 (0.02)		
	7673501.53 (14216.78)	120.06 (0.22)	109.9 (0.18)		
FR change: 1.1 ml.min^{-1}	651381.79 (7885.34)	9.58 (0.11)	87.7 (1.01)	2.536 (0.009)	10.08
	3229786.60 (3472.87)	50.15 (0.05)	90.8 (0.10)		
	6352272.20 (1655.87)	99.28 (0.02)	90.9 (0.02)		
T change: 19 °C isoniazid 24 °C pyrazinamide	722834.44 (3191.17)	10.71 (0.04)	109.2 (0.37)	2.833 (0.003)	0.46
	3281901.86 (7969.89)	50.97 (0.11)	100.0 (0.22)		
	6126418.17 (4488.87)	95.72 (0.06)	94.4 (0.06)		
T change 1: 21 °C isoniazid	665854.50 (1020.58)	9.81 (0.009)	100.1 (0.09)	2.75 (0.007)	2.35

26 °C pyrazinamide	3278886.64 (1671.37)	50.92 (0.02)	99.9 (0.04)		
	6501491.07 (3375.54)	101.62 (0.05)	100.3 (0.05)		
MP change: 9:91 (A: B)	715140.37 (2301.46)	10.58 (0.03)	108.0 (0.28)	2.94 (0.006)	4.18
	3559456.95 (4348.77)	55.34 (0.06)	108.6 (0.11)		
	7014056.99 (15962.91)	109.69 (0.24)	108.2 (0.22)		
MP change: 11:89 (A: B)	710235.14 (4055.01)	9.62 (0.06)	98.2 (0.62)	2.62 (0.008)	5.69
	3215436.07 (7969.81)	49.92 (0.12)	97.9 (0.24)		
	6323989.16 (16249.03)	98.83 (0.25)	97.5 (0.25)		

FR: Flow rate; T: Temperature; MP: Mobile phase; RT: Retention time; %RSD: % Relative standard deviation from normal conditions

4.3.1.2.5. Stability

Both compounds showed greater stability when frozen at -20 °C. After 3 freeze-thaw cycles over 3 weeks, the standards showed insignificant changes in recovered isoniazid and pyrazinamide concentrations as indicated in Table 4.8 and 4.9, respectively. Pyrazinamide demonstrated better stability, as isoniazid degraded quicker when stored in the fridge (4 °C) as compared to pyrazinamide. Both compounds may be stored for at least one week before analyses at either room temperature (25 °C), fridge (4 °C) or freezer (-20 °C).

Table 4.8: Stability of the established isoniazid HPLC method from three independent standard concentrations. Each analyte concentration was repeated six times.

Parameters		Isoniazid								
	Condition °C	25	4	-20	25	4	-20	25	4	-20
W0	Rec ($\mu g.ml^{-1}$)	9.36			44.85			91.44		
	%RV	-			-			-		
W1	Rec ($\mu g.ml^{-1}$) (SD)	9.24 (0.12)	9.18 (0.18)	9.34 (0.02)	44.32 (0.33)	44.86 (0.01)	44.31 (0.54)	91.51 (0.06)	90.90 (0.54)	91.49 (0.05)
	%RV	98.68	98.02	99.74	98.84	100.03	98.82	100.08	99.41	100.06
W2	Rec ($\mu g.ml^{-1}$) (SD)	9.24 (0.12)	7.66 (1.70)	9.19 (0.17)	43.98 (0.87)	43.63 (1.22)	44.53 (0.32)	87.17 (4.27)	81.28 (10.16)	91.09 (0.35)
	%RV	98.69	81.78	98.17	98.06	97.28	99.30	95.34	88.89	99.62

W3	Rec ($\mu g.ml^{-1}$) (SD)	8.70 (0.66)	-	8.99 (0.37)	44.66 (0.19)	-	43.97 (0.88)	82.86 (8.58)	-	90.18 (1.26)
	%RV	92.89	-	96.01	99.59	-	98.06	90.62	-	98.62

W0: Initial concentration; W1; Week 1; W2; Week 2; W3; Week 3; QC: Quality Control; LQC: Lower quality control; MQC: Middle quality control; HQC: Higher quality control; Rec: Recovery; %RV: %Recovery

Table 4.9: Stability of the established pyrazinamide HPLC method from three independent standard concentrations. Each analyte concentration was repeated six times.

Parameters		Pyrazinamide								
	Condition °C	25	4	-20	25	4	-20	25	4	-20
W0	Rec ($\mu g.ml^{-1}$)	9.37	9.97		51.38	51.10		103.30	99.17	
	%RV	-			-			-		
W1	Rec ($\mu g.ml^{-1}$) (SD)	9.33 (0.04)	9.97 (0.00)	9.98 (0.01)	50.92 (0.46)	51.48 (0.38)	51.01 (0.09)	103.04 (0.26)	99.29 (0.12)	99.50 (0.33)
	%RV	99.49	99.96	100.09	99.10	100.75	99.81	99.75	100.12	100.33
W2	Rec ($\mu g.ml^{-1}$) (SD)	9.37 (0.00)	9.54 (0.43)	9.96 (0.01)	50.09 (1.29)	50.87 (0.23)	51.14 (0.04)	103.09 (0.21)	101.62 (2.45)	99.37 (0.20)
	%RV	100.01	95.71	99.85	97.48	99.55	100.08	99.80	102.46	100.20

W3	Rec ($\mu g.ml^{-1}$) (SD)	9.39 (0.02)	9.69 (0.28)	10.04 (0.07)	51.87 (0.49)	51.05 (0.05)	51.23 (0.13)	103.53 (0.23)	102.34 (3.17)	99.71 (0.54)
	%RV	100.16	97.15	100.71	100.95	99.90	100.24	100.22	103.20	100.54

W0: Initial concentration; W1; Week 1; W2; Week 2; W3; Week 3; Rec: Recovery; %RV: %Recovery

4.3.2. Diffusion Studies

Similar amounts of isoniazid and pyrazinamide permeated across the pericardium although the permeation behavior was found to be vastly different as shown in Figure 4.7 below. The chromatogram of the eluents from the control (PBS) across the pericardium peaks of placebo (no drug in PBS) showed no interference with the isoniazid and pyrazinamide peaks in PBS as in Figure 4.8 and 4.9, respectively, below. A steady state was already reached after 2 h for both isoniazid and pyrazinamide. The rate increased linearly with time as the compounds diffused across the tissue up to approximately 20 h and then decreased slightly. Isoniazid presented with great variability of diffusion resulting in 3 levels, i.e., high diffusion, medium diffusion and low diffusion as compared to pyrazinamide which presented with 1 level of diffusion across the tissue. The average steady-state fluxes (standard deviation) were calculated to be 1.187 (±0.039) $\mu g.cm^{-2}.min^{-1}$ (3.045 (±0.062), 1.367 (±0.049), and 0.224 (±0.023) $\mu g.cm^{-2}.min^{-1}$ for high diffusion, medium diffusion, and low diffusion, respectively), and 1.261 (±0.022) $\mu g.cm^{-2}.min^{-1}$ for isoniazid and pyrazinamide, respectively. The apparent permeability coefficient was calculated to be 4.718 x 10^{-5} $cm.min^{-1}$ and 3.466 x 10^{-5} $cm.min^{-1}$ for isoniazid and pyrazinamide, respectively, across porcine pericardium.

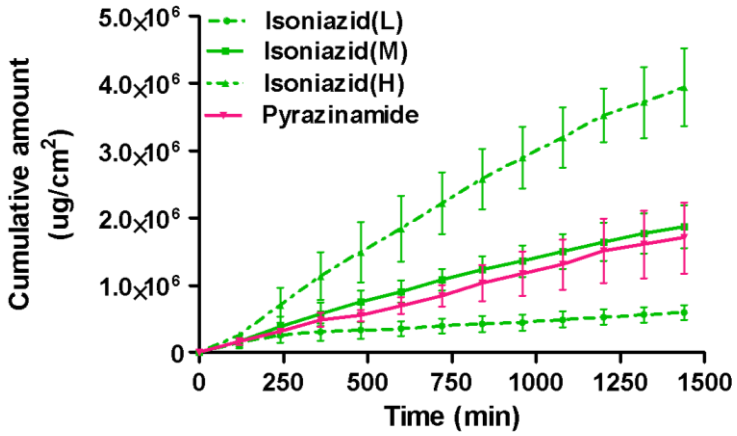

Figure 4.7: *Ex vivo* isoniazid and pyrazinamide diffusion results across porcine pericardium showing cumulative amount vs time graph (n=14) for each drug. Error bars = standard error of mean.

(a)

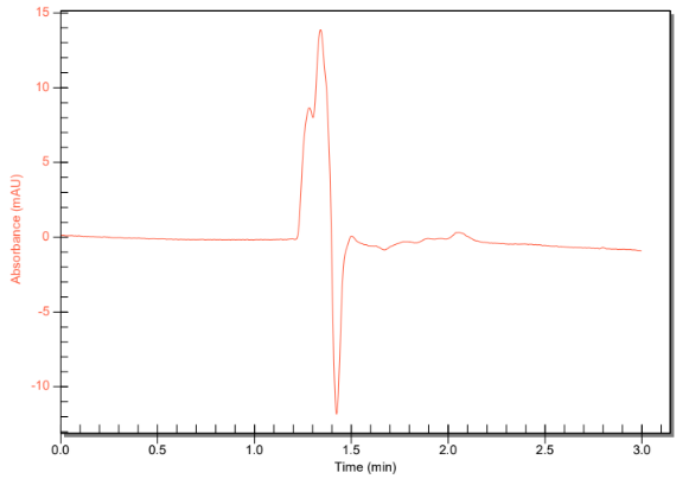

(b)

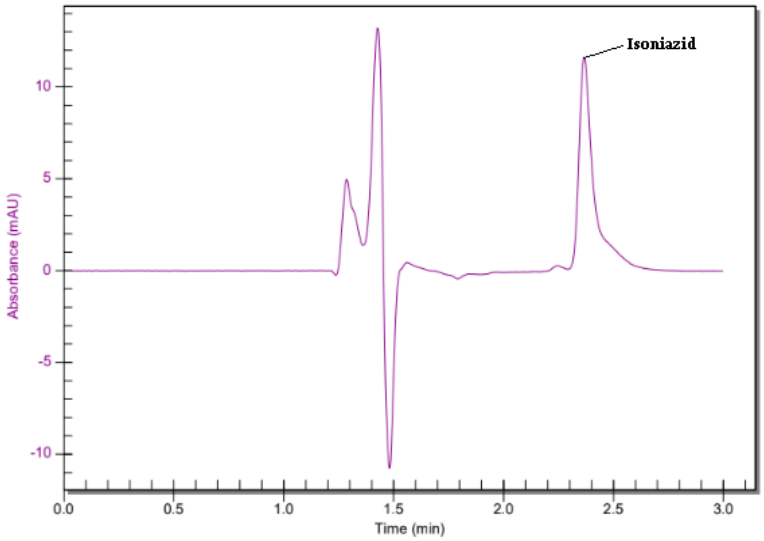

Figure 4.8: RP-HPLC Chromatograms of the eluents collected during the *ex vivo* studies across porcine pericardium for (a) control (PBS) and (b) isoniazid in phosphate buffer saline pH 7.4.

(a)

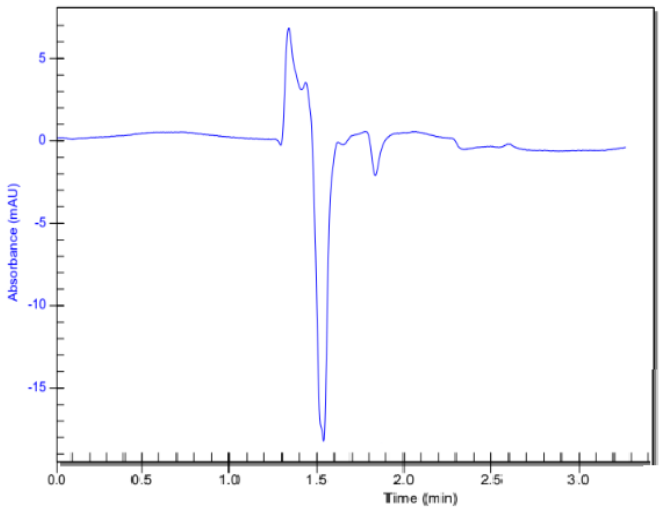

(b)

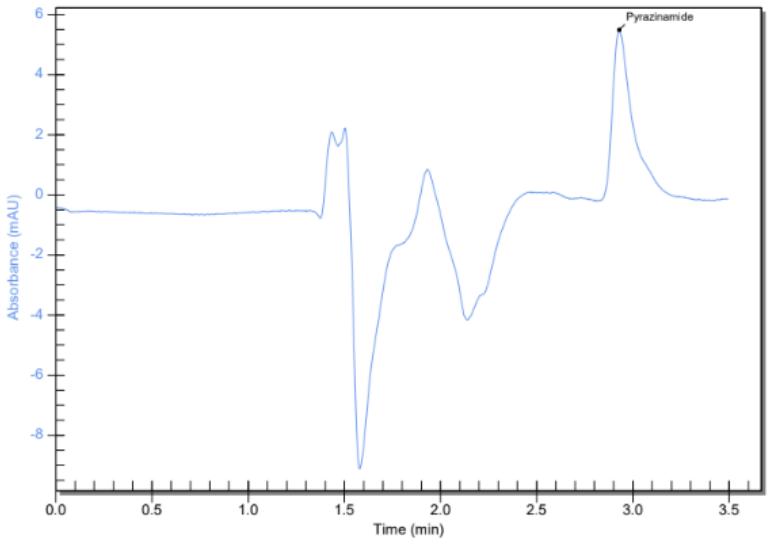

Figure 4.9: RP-HPLC chromatograms of the eluents collected during the *ex vivo* studies across porcine pericardium for (a) control (PBS) and (b) pyrazinamide in phosphate buffer saline pH 7.4.

4.4. DISCUSSION

The RP-HPLC method for the detection of both isoniazid and pyrazinamide was found to be linear (%RSD <2%), accurate and precise. The peaks eluted quicker for isoniazid and later for pyrazinamide as compared to the original method, due to the use of a different apparatus and column. The method was robust and only showed slight variation in minor changes in temperature. A slight alteration in flow rate (± 0.1 $ml.min^{-1}$) as expected, influenced the retention time of the compounds. A slight alteration in the organic mobile phase changed the recovery of isoniazid as compared to a more aqueous mobile phase, whilst a more aqueous mobile phase significantly changed the recovery of pyrazinamide as compared to a more organic mobile phase. Both isoniazid and pyrazinamide remained stable under various storage conditions for at least a week, allowing enough time for the experiment and analysis of the HPLC. The MP allowed the validation of an economical, highly sensitive, reliable, accurate and transient method. The methods were used successfully in the detection and quantification of both isoniazid and pyrazinamide diffusion across porcine pericardium.

Studies on the diffusion behaviour of isoniazid and pyrazinamide across the pericardium are lacking and as such, this study is currently the only research indicating the compounds' diffusion across this tissue. Anti-TB drugs need to permeate the pericardium for the effective treatment of TBP. An understanding of the diffusion pathway may bring us closer to finding the most effective treatment for TBP.

Isoniazid is a small molecule with a molecular weight of 137.14 $g.mol^{-1}$ and a log P (P: octanol/water partial coefficient) value of -0.7 (PubChem) making it a hydrophilic drug. *Ex vivo* transbuccal studies on isoniazid have been reported to have a steady state flux of 49.16 $\mu g.cm^{-2}.hr^{-1}$ (0.819 $\mu g.cm^{-2}.min^{-1}$) (Kroth et al., 2020). The buccal mucosa transports drugs via the transcellular and paracellular routes (Junginger, 1996). Since isoniazid is hydrophilic, the passive transcellular pathway is reported as the most important pathway for absorption (Kroth et al., 2020). *Ex vivo* transdermal studies on isoniazid have reported isoniazid to have a steady state flux of 16.28 ± 3.20 $\mu g.cm^{-2}.hr^{-1}$ (0.271 $\mu g.cm^{-2}.min^{-1}$) (Caon et al., 2015) which is like the lower diffusion steady state of 0.224 $\mu g.cm^{-2}.min^{-1}$. Isoniazid is although said to permeate the skin through the follicular pathway and internalization of the vesicle with the dermal cells (intracellular route) (Altamimi et al., 2020; Caon et al., 2015). Isoniazid permeated across the pericardium at a mean steady-state flux of 1.187 (±0.039) $\mu g.cm^{-2}.min^{-1}$, like the reported permeation of 0.819 $\mu g.cm^{-2}.min^{-1}$ across buccal mucosa. Isoniazid showed great variation in diffusion across the

pericardium and may suggest a multi-diffusion pathway, using both paracellular and intracellular pathways as reported in the buccal mucosa and skin, respectively (Altamimi et al., 2020; Caon et al., 2015; Kroth et al., 2020). The pericardium is a thinner membrane as compared to other tissues, which is possibly why it generally had a higher steady-state flux. Although the limited studies may suggest similar diffusion behaviour between the tissues, more studies are required to confirm this.

Pyrazinamide is also a small molecule with a molecular weight of 123.11 $g.mol^{-1}$, slightly smaller than isoniazid and slightly less hydrophilic with a log P value of -0.6 (pubchem). From the literature, limited studies have been performed on pyrazinamide drug alone regarding its permeability across tissues. Pyrazinamide had a very slightly higher steady-state flux of 1.261 (±0.022) $\mu g.cm^{-2}.min^{-1}$ as compared to 1.187 (±0.039) $\mu g.cm^{-2}.min^{-1}$ of isoniazid because the size, structure, and solubility is close. The slight increase observed in pyrazinamide may be due to its slightly smaller molecular size. Compared to isoniazid, pyrazinamide was observed to diffuse with a narrow range. Due to its hydrophilic nature, pyrazinamide is expected to diffuse through the paracellular pathway. Further studies are required to identify or explain the reason for the variation.

Ionized forms of isoniazid (pKa: 2.36, 3.35 and 13.61) and pyrazinamide (pKa: -0.68 and 13,06) are not found in pH 7.4, with 100% unionized form present at this pH as shown in Figure 4.10. For this reason, an ionized form of both drugs is not present to possibly hinder the permeation of the drug, further supporting why the drugs were found to successfully permeate across porcine pericardium (Khan et al., 2017).

(a)

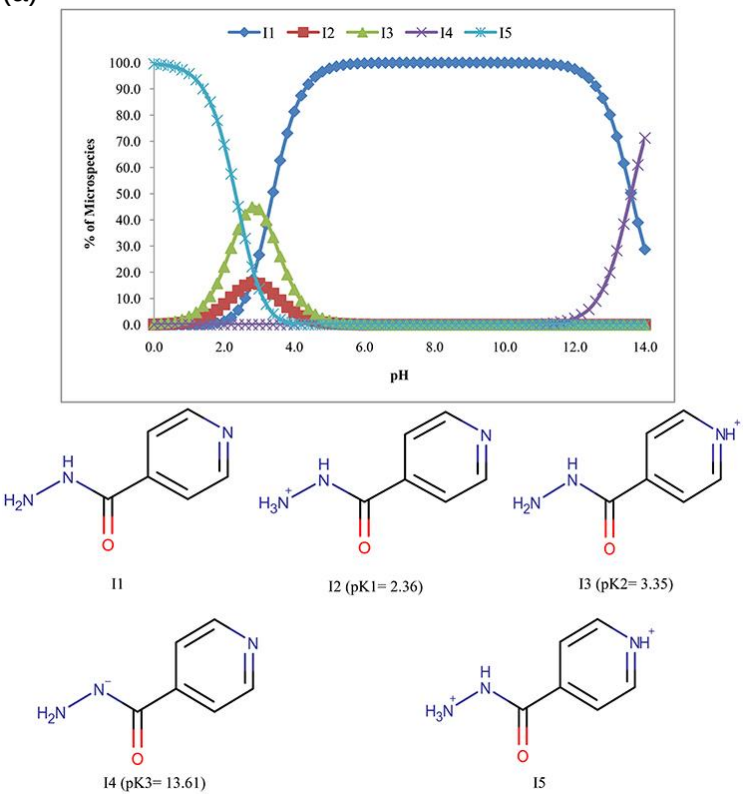

(b)

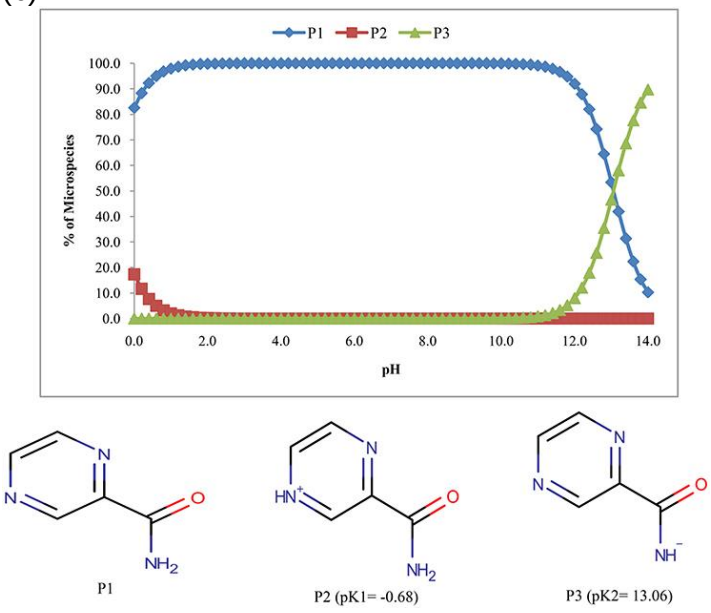

Figure 4.10: pH metric data showing ionization distribution of (a) isoniazid (I) and (b) pyrazinamide (P) across pH 0-14 (Khan et al., 2017).

4.5. CONCLUSION

An easy and rapid method for the detection and quantification of isoniazid and an equally easy and rapid method for the detection and quantification of pyrazinamide at a physiological pH of 7.4 were successfully developed. They were subsequently used for the quantification of isoniazid and pyrazinamide permeants across porcine pericardium. Both drugs permeated across the pericardium at pH 7.4, but only isoniazid has anti-tubercular effects at this pH. Pericardial tissue studies on rifampicin and ethambutol need to be investigated to understand their diffusion pattern to obtain more understanding required to ultimately ensure anti-TB drugs are successfully delivered across the pericardium for the treatment of TBP.

4.6. REFERENCES

Ahn, C., Oh, K.H., Kim, K., Lee, K. Y., Lee, J. G., Oh, M. D., Kim, Y., Han, J. S., Kim, S., and Lee, J. S. (2003). Effect of peritoneal dialysis on plasma and peritoneal fluid concentrations of isoniazid, pyrazinamide, and rifampin. Peritoneal Dialysis International, 23(4), 362–367.

Altamimi, M. A., Hussain, A., Imam, S. S., Alshehri, S., Singh, S. K., and Webster, T. J. (2020). Transdermal delivery of isoniazid-loaded elastic liposomes to control cutaneous and systemic tuberculosis. Journal of Drug Delivery Science and Technology, 59, 101848.

Anusiem, C. A., Brown, S. A., Ezejiofor, N. A., Barikpoar, E., and Orisakwe, O. E. (2018). Isoniazid pharmacokinetics in the presence of ofloxacin and norfloxacin antibiotics. American Journal of Therapeutics, 25(4), e397–e404.

Caon, T., Campos, C. E. M., Simões, C. M. O., and Silva, M. A. S. (2015). Novel perspectives in the tuberculosis treatment: Administration of isoniazid through the skin. International Journal of Pharmaceutics, 494(1), 463–470.

Doležal, M., Zitko, J., and Jampílek, J. (2012). Pyrazinecarboxylic acid derivatives with antimycobacterial activity. Understanding Tuberculosis-New Approaches to Fighting Against Drug Resistance, 1.

Donald, P. R., and McIlleron, H. (2009). Chapter 59 - Antituberculosis drugs. In H. S. Schaaf, A. I. Zumla, J. M. Grange, M. C. Raviglione, W. W. Yew, J. R. Starke, M. Pai, and P. R. Donald (Eds.), Tuberculosis (pp. 608–617). W.B. Saunders. https://doi.org/https://doi.org/10.1016/B978-1-4160-3988-4.00059-7

Fernandes, G. F. dos S., Salgado, H. R. N., and Santos, J. L. dos. (2017). Isoniazid: a review of characteristics, properties and analytical methods. Critical Reviews in Analytical Chemistry, 47(4), 298–308.

Friedland, J. S. (2010). Chapter 30 - Tuberculosis and other mycobacterial infections. In J. Cohen, S. M. Opal, and W. G. Powderly (Eds.), Infectious Diseases (Third Edition) (pp. 309–327). Mosby. https://doi.org/https://doi.org/10.1016/B978-0-323-04579-7.00030-7

González, O., Blanco, M. E., Iriarte, G., Bartolomé, L., Maguregui, M. I., and Alonso, R. M. (2014). Bioanalytical chromatographic method validation according to current regulations, with a special focus on the non-well defined parameters limit of quantification, robustness and matrix effect. Journal of Chromatography A, 1353, 10–27.

H, I. C. (2005). International Conference on Harmonization: Validation of analytical procedures: Text and Methodology Q2 (R1). ICH Harmonised Tripartite Guideline Rockville, MD, USA.

Harmon, R. C. (2007). Pyrazinamide. In S. J. Enna and D. B. Bylund (Eds.), xPharm: The Comprehensive Pharmacology Reference (pp. 1–5). Elsevier. https://doi.org/https://doi.org/10.1016/B978-008055232-3.62492-4

Hoit, B. D. (2017). Pathophysiology of the Pericardium. Progress in Cardiovascular Diseases, 59(4), 341–348.

Horváth, C. (2013). High-performance liquid chromatography: advances and perspectives.

Ishihara, T., Ferrans, V. J., Jones, M., Boyce, S. W., Kawanami, O., and Roberts, W. C. (1980). Histologic and ultrastructural features of normal human parietal pericardium. The American Journal of Cardiology, 46(5), 744–753.

Isiguzo, G., Du Bruyn, E., Howlett, P., and Ntsekhe, M. (2020). Diagnosis and management of tuberculous pericarditis: what is new? Current Cardiology Reports, 22, 1–8.

Junginger, H. (1996). Drug absorption enhancement, concepts, possibilities, limitations and trends. Journal of Drug Targeting, 4(1), 51–52.

Khan, M. F., Rita, S. A., Kayser, M. S., Islam, M. S., Asad, S., Bin Rashid, R., Bari, M. A., Rahman, M. M., Al Aman, D. A. A., and Setu, N. I. (2017). Theoretically guided analytical method development and validation for the estimation of rifampicin in a mixture of isoniazid and pyrazinamide by UV spectrophotometer. Frontiers in Chemistry, 5, 27.

Kroth, R., Argenta, D. F., Conte, J., Amaral, B. R., and Caon, T. (2020). Transbuccal delivery of isoniazid: Ex vivo permeability and drug-surfactant interaction studies. AAPS PharmSciTech, 21, 1–12.

Lakshmi, D., and Jacob, J. T. (2018). Validated Degradation studies for the estimation of Pyrazinamide, Ethambutol, Isoniazid and Rifampacin in a fixed dose combination by UPLC. Research Journal of Pharmacy and Technology, 11(7), 2869–2875.

Law, B. (2000). Basic Drugs: Liquid Chromatography. Touchstone, 613, 665.

Meyer, V. R. (2013). Practical high-performance liquid chromatography. John Wiley and Sons.

Miyazaki, T., Pride, H. P., and Zipes, D. P. (1990). Prostaglandins in the pericardial fluid modulate neural regulation of cardiac electrophysiological properties. Circulation Research, 66(1), 163–175.

Morticelli, L., Thomas, D., Roberts, N., Ingham, E., and Korossis, S. (2013). Investigation of the suitability of decellularized porcine pericardium in mitral valve reconstruction. J Heart Valve Dis, 22(3), 340–353.

Rodriguez, E. R., and Tan, C. D. (2017). Structure and anatomy of the human pericardium. Progress in Cardiovascular Diseases, 59(4), 327–340.

Sarathy, J. P., Liang, H. H., Weiner, D., Gonzales, J., Via, L. E., and Dartois, V. (2017). An in vitro caseum binding assay that predicts drug penetration in tuberculosis lesions. JoVE (Journal of Visualized Experiments), 123, e55559.

Sarker, S. D., and Nahar, L. (2015). Applications of high performance liquid chromatography in the analysis of herbal products. In Evidence-Based Validation of Herbal Medicine (pp. 405–425). Elsevier.

Schönfeld, N., Bergmann, T., Vesenbeckh, S., Mauch, H., Bettermann, G., Bauer, T. T., and Rüssmann, H. (2012). Minimal inhibitory concentrations of first-line drugs of multidrug-resistant tuberculosis isolates. Lung India: Official Organ of Indian Chest Society, 29(4), 309.

Shabetai, R. (2003). The pericardium (Vol. 249). Springer Science and Business Media.

Shenje, J. (2015). Ifeoma Adimora-Nweke F, Ross IL, et al. Poor Penetration of Antibiotics into Pericardium in Pericardial Tuberculosis. EBioMedicine, 2(11), 1640–1649.

Sundar, S. (2023). In-silico transcriptome analysis of antibiotic-treated *Mycobacterium tuberculosis* identifies novel antibiotic resistance factors. Indian Journal of Tuberculosis.

Suo, J., Chang, C.-E., Lin, T. P., and Heifets, L. B. (1988). Minimal inhibitory concentrations of isoniazid, rifampin, ethambutol, and streptomycin against *Mycobacterium tuberculosis* strains isolated before treatment of patients in Taiwan. American Journal of Respiratory and Critical Care Medicine, 138(4), 999–1001.

Van Crevel, R., and Hill, P. C. (2017). Tuberculosis. Infectious Diseases, 2-Volume Set, 271-284.e1. https://doi.org/10.1016/B978-0-7020-6285-8.00031-9.

CHAPTER FIVE

PREFORMULATION STUDIES: BEDAQUILINE'S HPLC METHOD DEVELOPMENT, VALIDATION AND ITS DESIGN, PREPARATION, AND CHARACTERIZATION IN POTENTIAL NANOSYSTEMS FOR THE TREATMENT OF TUBERCULOSIS PERICARDITIS

5.1. INTRODUCTION

The tuberculosis pericarditis (TBP) drug of choice is oral isoniazid 300 mg once daily; oral rifampin 600mg once daily; oral pyrazinamide 15–30 mg/kg per day (up to 2 g/day) given as a single dose; either oral ethambutol 15–25 mg/kg once daily or intramuscular streptomycin 20–40 mg/kg (up to 1g) given once daily. Prolonged treatment is often required when drug resistance emerges. In cases where the organism is resistant to isoniazid, it is treated with rifampicin, ethambutol, and pyrazinamide for 6 months. In the case of resistance to rifampicin and isoniazid, at least 18-24 months of therapy would be required (Pankuweit et al., 2005).

Drug resistance is primarily driven by low drug concentration (Pasipanodya et al., 2013), and due to the lack of permeation across the pericardium of the drugs of choice against TBP, the probability of resistance development increases. Bedaquiline is a drug with improved bactericidal activity against MDR-XRD-TB and thus presents a viable option for the treatment of TBP. Recent studies have shown that Bedaquiline used concurrently with an optimized drug regimen in South African patients with rifampicin-resistant tuberculosis (TB) and resistance to fluoroquinolones and/or injectable drugs (extensively drug-resistant (XDR) and preXDR-TB) have shown a high rate of successful treatment outcomes (Ndjeka et al., 2018).

Due to its side effect profile, which includes an increased risk of QT prolongation, and hepatic-related adverse events associated with increased levels of aminotransferase. Bedaquiline use is limited as a last resort option (Chahine et al., 2014). Recent studies have found that the use of QT-prolonging drugs alone or in combination, is relatively safe. Clinically significant QT changes were observed in only 10/60 patients with no patient showing clinical events (Yoon et al., 2017).

Due to the low permeation of the standard anti-TB antibiotics across the pericardium, strategies to enhance the permeation, such as increasing drug concentration or finding alternative drugs need to be investigated. The encapsulation of more than one drug into a nanosystem may lead to variations in drug loading and encapsulation efficacy of each drug. This could lead to either the inadequate or excess loading of the drug into a nanosystem due to competitive loading. For this

reason, a single drug is preferred for encapsulation in a nanosystem. Since rifampicin, isoniazid, pyrazinamide and ethambutol all work concurrently in the treatment of tuberculosis due to the risk of resistance, it may prove difficult to encapsulate these drugs simultaneously into one nanosystem. Furthermore, the lack of permeation across the pericardium at an effective concentration of any drug among the four increases the likelihood of resistance.

Over the years, nanotechnology has been studied, displaying various physiochemical properties that result in advantages that improve drug function. The improvement of pharmacokinetic and pharmacodynamic properties of a drug places nanotechnology at the forefront of research as a good candidate for the targeted delivery of drugs e.g., antibiotics. These properties include the protection of drugs in the systemic circulation and their selective release at the required site. This results in less drug being required and the minimization of side effects of the active moiety (Kadian, 2018; Sajja et al., 2009; Singh et al., 2011; Vineela and Krishna, 2014). Additionally, nanotechnology may allow the enhancement of drug permeation across a membrane as required in the case of TBP. Nanotechnology thus can be considered an ideal means for the delivery of drugs with limited use due to their side effects e.g., bedaquiline.

This chapter therefore evaluates and expands on the parameters required for the formulation of the preferred nanosystem that will enhance the permeation of drugs across the pericardium. Secondly, it describes the development and validation of an HPLC for the detection and quantification of bedaquiline encapsulated in a nanosystem and at a physiological pH of 7.4 after permeation across the pericardium.

5.2. MATERIALS AND METHODS

5.2.1. Materials

The materials employed in this study were of the highest purity grade and were purchased from Sigma-Aldrich (Pty) Ltd (St. Louis, Missouri, United States). This included the following: ferric chloride hexahydrate ($FeCl_3 \cdot 6H2O$), ferrous chloride tetrahydrate ($FeCl_2 \cdot 4H2O$), sodium hydroxide (NaOH), nitrogen gas, ethanol, ammonia 25%, tetraethyl orthosilicate (TEOS), (3-aminopropyl)triethoxysilane (APTES), hydrochloric acid, fluorescein isothiocyanate (FITC), 1-ethyl-3-(3-dimethylaminopropyl)carbodiimide (EDC), N-hydroxysuccinimide (NHS), chitosan medium molecular weight, chitosan oligosaccharide lactate (COS) (Mw 5 kDa), mannan oligosaccharide (MN) from *Saccharomyces cerevisiae*, tween 80, dichloromethane (DCM), sodium tripolyphosphate (sTPP), bedaquiline (BDQ), ethanol, phenol, sulfuric acid (H_2SO_4),

methanol (HPLC grade), acetonitrile (HPLC grade), potassium dihydrogen orthophosphate, triethylamine, orthophosphoric acid, phosphate buffer saline (PBS) tablets, sodium lauryl sulphate (SLS).

5.2.2. Synthesis of Superparamagnetic Iron Oxide Nanoparticles (SPIONs) Incorporated Nanosystem

SPIONs are nanoparticles with theranostic properties and have mostly been studied for their use in cancer treatments (Saesoo et al., 2018; Zhu et al., 2017). It has been reported that in the presence of an external magnetic field, SPIONs enhance the permeations of drugs across epithelial membranes (Mondalek et al., 2006), therefore SPIONs were synthesized to facilitate the *ex vivo* diffusion of bedaquiline, which is insoluble in aqueous solution, across porcine pericardial tissue. SPIONs are mostly synthesized by chemical co-precipitation of iron salts, Fe^{2+} and Fe^{3+} in the presence of a base such as ammonia/ sodium hydroxide (Nnadozie and Ajibade, 2022). Naked SPIONs have been reported to have biocompatibility issues due to their interaction with red blood cells resulting in hemolysis (Janko et al., 2017). *In vivo and in vitro* studies have reported SiO_2, a suitable coating around SPIONs to improve its biocompatibility in the body (Romano et al., 2022). In this synthesis, Iron oxide nanoparticles were synthesized by co-precipitation in the presence of NaOH and coated using silica precursors, TEOS and APTES. Refer to Appendix H

5.2.3. Synthesis of Bedaquiline-Loaded Chitosan-Mannan Complexes and Size Determinations

Chitosan has permeation-enhancing properties (Bernkop-Schnürch and Dünnhaupt, 2012; Sadeghi et al., 2008), different molecular weights and pH-based solubilities. They are known to improve the solubility of poorly water-soluble drugs (Shu and Zhu, 2000; Trapani et al., 2009), and thus would be an ideal agent in improving the solubility and dissolution properties of drugs like bedaquiline. Therefore, chitosan and chitosan oligosaccharide were employed at different ratios and synthetic conditions as presented in Table 5.1 below to determine the effect on the size and potential of a novel nanosystem. In summary, chitosan/COS together with MN were added into 10 ml water and stirred for 30 min. Tween 80 was added and stirred until homogeneous. Bedaquiline was dissolved in DCM, added dropwisely and allowed to stir at 1500 rpm for 20 min. sTPP was dissolved in distilled water, filtered through a 0.22 µm filter, and added into the solution at a drop rate of 0.2 $ml.min^{-1}$. The solution was thereafter allowed to stir for 24 h. The suspension

was then homogenized and/or sonicated, frozen for 24 h at -90 °C and lyophilized for 12 h thereafter.

Table 5.1: Summary of the ratios of polymers, solvent and excipients that were combined during the synthesis of the chitosan-mannan-bedaquiline-loaded nanosystem.

Batch No.	COS (mg)	MN (mg)	Tween 80 (ml)	Bedaquiline amount (mg)	DCM (ml)	sTPP (mg)	Homogenizer	Probe sonication (x 10^6 Joules)	Probe sonication (% Amplitude)	Probe sonication time (min)
A	20									
B	20	5 mg								
C	200	-	0.1	20	2	7.5	-	0.5	30	5
D	200	50	0.1	20	1	12.5	-	0.5	30	5
E	200	1	0.2	10	2	12.5	-	0.5	30	10
F	100	1	0.2	5	2	12.5	-	0.5	30	10
G	200	50 mg	0.1	20	2	7.5	-	0.5	30	5
H	200	50	0.2	5	5	7.5	-	3.6	40	5
I	200	50	0.2	5	5	7.5	2000 rpm for 10 min	3.6	40	2
J	200	50	0.2	5	5	7.5	2000 rpm for 20 min	4.8	40	2
K	200	50	0.2	5	5	7.5	2000 rpm for 10 min	4.8	40	2

5.2.4. Determination of Particle Size and Zeta Potential of COS-MN-BDQ NPs

A nano zetasizer instrument (NanoZS, Malvern Panalytical, Malvern, UK) was used to obtain the average hydrodynamic size of the nanoparticles and the surface zeta potential of the nanoparticles by dynamic light scattering and electrophoretic light scattering, respectively. The suspension (0.1 ml) was diluted into 10 ml of distilled water. The resultant samples (1 ml) were transferred into disposable cuvettes to determine the hydrodynamic size and polydispersity index while 0.8 ml was transferred into zeta potential disposable folded capillary cells (DTS 1070) for surface charge analysis at 25 °C.

Samples of Individual BDQ, MN, COS, and BDQ-loaded COS-MN nanoparticles were analyzed at 110 psi pressure in a range of 4000–650 cm^{-1} over 20 scans to obtain relevant spectra.

5.2.5. Method Validation for Evaluation of Mannan Loading Content

Conjugated MN was investigated using a colourimetric assay by using a phenol-sulfuric acid method. Using a Nanophotometer UV/Vi's spectrophotometer NP80 (Implen, Munchen, Germany), the total sugar was spectrophotometrically measured at 490 nm, the wavelength at which hexoses and their methylated derivatives show maximum absorption (Carrión-Prieto et al., 2018). Unloaded nanoparticles were synthesised following the same method without adding bedaquiline. The supernatant and washing solution for a drug-loaded and drug-free system were collected and used to quantify unconjugated MN by a phenol-sulfuric acid method. Briefly, 1 ml of 5% phenol was added into 2 ml of supernatant solution, followed by a rapid addition of 5 ml 96% H_2SO_4 and heated at 90 °C for 5 min, followed by 20 min of cooling. The drug-free supernatant was used as the blank. The absorbance was then measured and extrapolated from a standard curve of 1 $\mu g.ml^{-1}$, 5 $\mu g.ml^{-1}$, 10 $\mu g.ml^{-1}$, 15 $\mu g.ml^{-1}$ and 20 $\mu g.ml^{-1}$ of MN. The conjugated MN was calculated by the following formula (Equation 5.1):

$$\frac{\text{Total mannan added} - \text{Unloaded mannan}}{\text{Total mannan added}} \text{ x } 100\% \qquad (5.1)$$

5.2.6. Method Development and Validation for the Detection of Bedaquiline on HPLC

5.2.6.1. Materials

Bedaquiline (BDQ) reference standards were procured from Sigma Aldrich Inc. (St. Louis, Missouri, United States). Analytical grade reagents and solvents, like methanol (HPLC grade), acetonitrile (HPLC grade), triethylamine (TEA), Milli Q water, potassium dihydrogen orthophosphate and orthophosphoric acid were used. All reagents and compounds used for HPLC were filtered (0.45 µm) before use.

5.2.6.2. Chemical Properties of Analyte

Bedaquiline is chemically identified as 1R,2S)-1-(6-Bromo-2-methoxy-3-quinolyl)-4-dimethylamino-2-(1-naphthyl)-1-phenylbutan-2-ol as shown in Figure 5.1 below. It is a diarylquinoline with tuberculocidal activity approved for the treatment of multi-drug resistant tuberculosis. It works by inhibiting the proton pump of *M.tb* ATP synthase. It also forms 2 major metabolites N- monodesmethyl (M2) and N-didesmethyl-bedaquiline (M3), with an *in vitro* potency of about 5- and 187-fold less than that of bedaquiline, respectively. It has a MIC of 0.03 $mg.l^{-1}$ against *M.tb* H37Rv and 0.12 $mg.l^{-1}$ against a range of *M.tb* clinical isolates (Alajlani, 2022). Bedaquiline has also been found to be slightly more potent against dormant *M.tb* strains as compared to rifampicin and isoniazid. It has a half-life of ~5.5 months. Bedaquiline is a positively charged molecule with pKa values of 1.57 (imine); 8.91 (amine); and 13.61 (hydroxyl) (*Committee for Medicinal Products for Human Use (CHMP) Assessment Report SIRTURO.*, 2013).

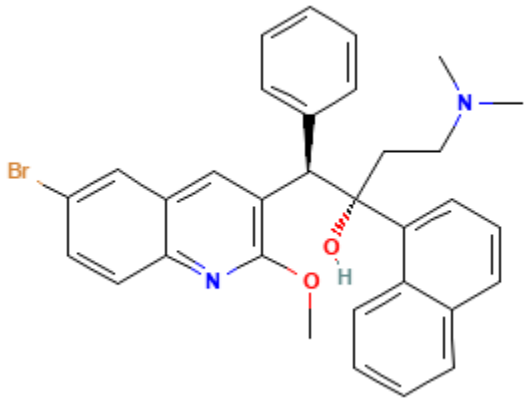

Figure 5.1: Chemical structure of bedaquiline (https://pubchem.ncbi.nlm.nih.gov/).

5.2.6.3. Preparation of Standards and Phosphate Buffer for Mobile Phase

Phosphate Buffer was prepared by weighing 20 mg of potassium dihydrogen orthophosphate (KH_2PO_4) and dissolving it in 1000 ml Milli-Q® water. Triethylamine (10 ml) was added to this mixture and the pH of the subsequent solution was adjusted to 7.4 with 10% (v/v) orthophosphoric acid.

The mobile phase was prepared by mixing 5 ml of phosphate buffer prepared above, with 80.8 ml of methanol and 14.2 ml of acetonitrile. Bedaquiline (10 mg) was dissolved in 10 ml of mobile phase and further diluted down using a dilution factor of 0.1 (10%) to form 100 $ug.ml^{-1}$ of stock solution.

5.2.6.4. Running Conditions

Various methods have been developed and validated for the detection of bedaquiline with most employing the use of a high organic phase ratio due to the lipophilic nature of bedaquiline. Preliminary studies using methanol: acetonitrile (85:15): water in a ratio of (90:10) were conducted and no peaks were obtained, therefore phosphate buffer, containing triethylamine and adjusted with orthophosphoric acid to physiological pericardial pH of 7.4, was prepared. The lambda max was determined by dissolving bedaquiline in the proposed mobile phase and obtaining its wavelength on a UV-Vis spectrometer. Running conditions using rations of methanol: acetonitrile (85:15): phosphate buffer at 90:10, 85:15 and 95:5 were tested, and the chosen condition was based on system suitability, characteristics of the peak, and retention time. The chromatographic apparatus and conditions employed are displayed below (Table 5.2):

Table 5.2: Instrumentation and chromatography conditions for the detection of bedaquiline.

Parameter	Conditions
Instrument	A Perkin Elmer Flexar HPLC system, consisting of a binary pump, autosampler, column oven and a UV/Vis detector. The system was equipped with Chromera® software for data acquisition and analysis (Perkin Elmer Inc., Waltham, Massachusetts, USA).

Column	Phenomenex Kinetex C18 RP LC Column with dimensions of 150 x 4.6 mm and particle size of 5 µm.
Mobile Phase	An organic phase of (A): (methanol: acetonitrile (85:15)) and an aqueous phase of (B): (triethylamine (10 ml), and potassium phosphate buffer (20 mg in 1000 ml) adjusted with orthophosphoric acid to a pH of 7.4). The phosphate buffer was filtered using a vacuum pump through a 0.45-µm membrane. Pumped across the HPLC at a ratio of 95:5 (A: B)
Flow rate	1 $ml.min^{-1}$
Detection wavelength	275 nm
Injection Volume	20 µl
Run time	5 min
Column Temperature	25 °C

Elution technique	Isocratic

5.2.6.5. Validation Parameters

5.2.6.5.1. Linearity

The linearity of bedaquiline was performed by linear regression analyses of the graph of the peak area versus concentration (μg.ml^{-1}) to obtain a linear equation (Equation 5.2).

$$y = mx + c \quad (5.2)$$

Where:

y = the peak area of analyte

m = slope

x = the concentration of analyte (μg.ml^{-1})

c = y - intercept

Standard solutions were diluted from the stock solution prepared as described in section 5.2.7.3.2 to prepare working standards of 1 μg.ml^{-1}, 2 μg.ml^{-1}, 5 μg.ml^{-1}, 10 μg.ml^{-1}, 25 μg.ml^{-1} and 50 μg.ml^{-1} concentrations. These standards were separately analysed in triplicate.

5.2.6.5.2. Precision

5.2.6.5.2.1. Intraday Precision

Three standards (1 μg.ml^{-1}, 10 μg.ml^{-1}, and 50 μg.ml^{-1}) were used to determine intraday precision. Standards were injected in triplicate in the morning and afternoon (8 h apart) on the same day. The acceptance criteria for intra-day precision are set to be a % relative standard deviation (RSD) ≤ 2.0.

5.2.6.5.2.2. Interday Precision

Three standards (1 µg.ml^{-1}, 10 µg.ml^{-1}, and 50 µg.ml^{-1}) were used to determine inter-day precision. standards were injected in triplicate for 3 consecutive days. The acceptance criteria for intra-day precision are set to be a % relative standard deviation (RSD) ≤ 2.0.

5.2.6.5.3. Accuracy

For the quality of analytical results determind after *ex vivo* tissue permeation studies, three different standard concentrations were prepared by spiking PBS (pH~7.4) containing 0.2% SLS using a 25 µg.ml^{-1} standard solution to obtain the following final concentrations: 8 µg.ml^{-1}, 10 µg.ml^{-1}, and 12 µg.ml^{-1}. The concentrations are three different levels of target concentration (80%, 100% and 120%) as per the ICH guideline. The standards were analysed in replicates of 6. The acceptance criteria for accuracy are between 98-102%.

5.2.6.5.4. Robustness

The robustness of the method was performed on 1 µg.ml^{-1}, 10 µg.ml^{-1}, and 50 µg.ml^{-1} standard standards by adjusting mobile phase, temperature, and flow rate. The mobile phase was adjusted by ±1% of the organic component, temperature was adjusted by ±1 °C and flow rate was adjusted by ± 0.1 ml.min^{-1} and tested to note its variation in % recovery. Standards were injected 6 times. The change in Rt and the area change were evaluated (RSD ≤ 2%).

5.2.6.5.5. Stability

The stability of the analyte in the mobile phase was tested by placing 1 µg.ml^{-1}, 10 µg.ml^{-1}, and 50 µg.ml^{-1} standards at room temperature, 4 °C and -20 °C, tested weekly until significant change occurred. The acceptance criteria for recovery are between 98-102%. This allows the analyst to know the time frame a sample can be kept from the day of preparation until the time it degrades by 2%.

5.3. RESULTS

5.3.1. Synthesized Superparamagnetic Iron Oxide Nanoparticles (SPIONs) Incorporated Nanosystem Physiochemical and Physiomechanical Properties.

SPIONs coated with silica were successfully synthesized. MN did not attach the surface of the nanosystem. The SPIONs were individually tested to observe permeation across the pericardium. After no permeation of the SPIONs was observed, its study was discontinued and found

unnecessarily to add to the COS-MN-BDQ-NPs. Various ratios of polymers and excipients were employed at different conditions to obtain a COS-MN-BDQ-NPs NP of ~200 nm. The desired NPs were obtained and found to be mostly affected by sonication time, amplitude, and energy. Refer to Appendix H.

5.3.2. COS-MN-BDQ: Assessment of Synthesized Nanosystem at Different Polymeric Ratios and Parameters Regarding Particle Size, Zeta Potential and Morphology.

Chitosan is a natural polymer that can easily be functionalized to obtain the desired targeted results (Garg et al., 2019). It is disadvantaged due to its water insolubility and the requirement of acids, with pKa less than 6.2 to dissolve it, such as acetic acid (de Alvarenga, 2011). Therefore, for the synthesis employing chitosan and mannan, a study has shown the initial synthesis of chitosan followed by mannan functionalization via a carbodiimide chemical reaction using EDC and NHS (Serrasqueiro et al., 2023). Without the use of a chemical reaction, COS, a water-soluble derivative of chitosan does not require acetic acid to dissolve. In this experiment when used concurrently with MN to form a polymer–polymer aqueous two-phase system (Chew et al., 2023), they produced a homogenous solution indicating possible polymer-polymer physical interactions between the polymers. Ratios and parameters were investigated and changed until a stable nanosystem of ~200 nm was obtained (Table 5.3). These sizes were desired as studies have shown that 200 nm cationic nanoparticles had the potential to permeate into lower regions of the buccal epithelium (Morales and Brayden, 2017).

Table 5.3: Table showing particle size and surface potential results of the various ratios of polymers, solvent and excipients that were combined during the synthesis of the chitosan-mannan-bedaquiline loaded nanosystem.

Batch No.	Particle Size (nm)	Surface Potential (mV)	Discussion
A	-	45.4	Chitosan is a cationic polymer
B	-	58.9 ± 4.6	COS: MN in the ratio of 4:1 caused the zeta potential of the polymeric mixture to increase due to the presence of MN.
C	273.3 ± 87.5	30.3 ± 6.3	MN was removed from the synthesis and tween 80 concentration was decreased and found to cause a decrease in the zeta potential of the formulation and an increase in the size of the nanosystem. Excess undissolved bedaquiline was found.

D	331.5 ± 90.7	47.4 ± 7.4	Due to an increase in the sTPP concentration and decrease in DCM volume used to add bedaquiline into the synthesis. Particle size increased and more undissolved drug sediment was found after centrifugation
E	280.1 ± 83.2	35.9 ± 11.7	1 mg of MN as compared to 50 mg of MN caused a decrease in the zeta potential. The drug amount was reduced, and it was observed that less drug was found sedimented and undissolved after centrifugation.
F	136.1 ± 72.2	35.0 ± 12.0	The COS amount was reduced whilst maintaining 1mg of MN and found to cause a significant decrease in the size of the nanosystem. Implying that COS is proportional to the particle size of the nanosystem. The standard deviation of the surface potential though showed that the nanosystem was not closely homogeneous in charge.
G	263.18 ± 98.3	38.0 ± 8.9	An increase in the sonication energy reduced particle size but increased the standard deviation of the surface potential, implying damage to the nanosystem.
H	239.4 ± 91.5	39.3 ± 7.1	An increase in sonication energy and a decrease in sonication time resulted in a decrease in particle size and standard deviation of zeta potential.
I	200.5 ± 53.9	40.8 ± 5.9	The system was homogenized for 10 min, the sonication energy was further increased, and the sonication time decreased, causing a decrease in size to desirable range. The zeta potential std also implied a more homogenous system.
J	477.5 ± 312.2	33.9 ± 10.9	To examine the effect of the homogenizer, the speed time was increased to 20 min, resulting in a drastic increase in the size and standard deviation of the system. This could be due to de-mixing of the mixture before homogenization.
K	189.5 ± 60.5	40.5 ± 4.6	The homogenization time and speed were maintained at 2000 rpm for 10 min, but the sonication energy was increased to 4.8 million joules. The size of the nanosystem decreased to the desired range of 100 nm- 200nm and the narrowest zeta potential was obtained.

5.3.3. Mannan Oligosaccharide UV-Vi's Calibration Curve for the Quantification of Mannan

The linear regression curve (Figure 5.2, Table 5.4) displayed the suitability of the colorimetric assay within the prescribed concentration range (1-20 $\mu g.ml^{-1}$) for the quantification of mannan with a correlation of determination (R^2) = 0.9941.

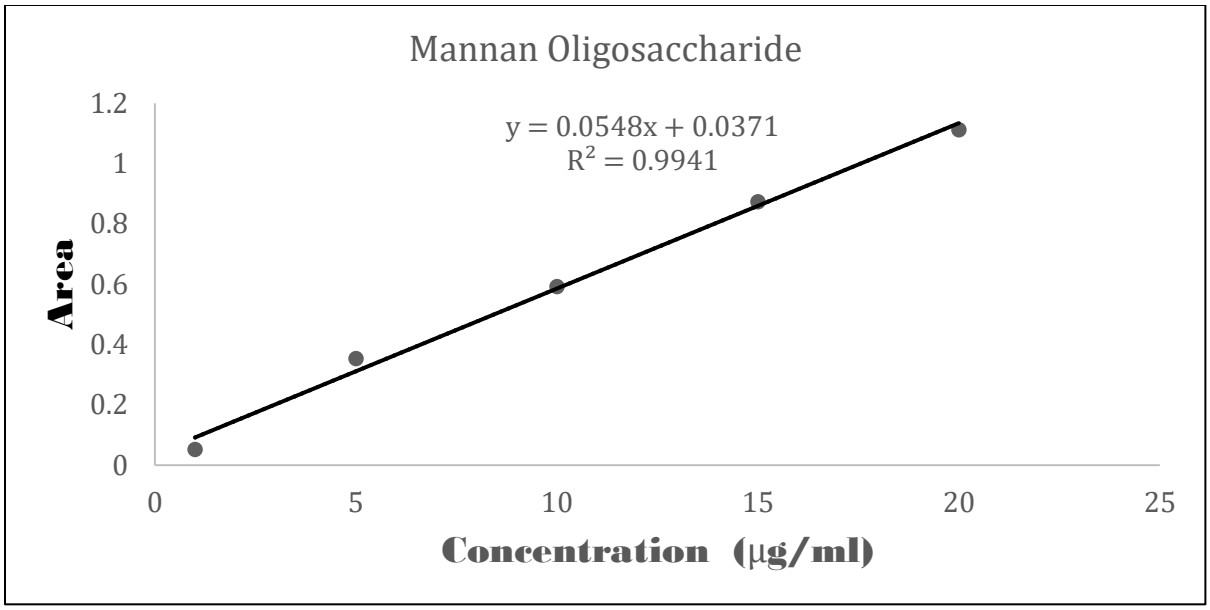

Figure 5.2: Overall linearity of mannan oligosaccharide standard curve done in triplicates using colorimetric assay on a nanophotometer at a wavelength of 490 nm, with each concentration point done 3 times for each experiment.

Table 5.4: Linearity of mannan oligosaccharide established from three different experiments using a nanophotometer. Each analyte concentration was done in triplicate.

Concentration ($ug.ml^{-1}$)	Mean Absorbance 1 (±SD)	Mean Absorbance 2 (±SD)	Mean Absorbance 3 (±SD)	Overall Mean Absorbance (Overall SD)	%RSD
1	0.051 (0.001)	0.051 (0.001)	0.053 (0.001)	0.052 (0.001)	1.825
5	0.353 (0.002)	0.367 (0.001)	0.341 (0.004)	0.354 (0.011)	3.004
10	0.591 (0.001)	0.592 (0.001)	0.592 (0.002)	0.592 (0.000)	0.080
15	0.894 (0.004)	0.844 (0.006)	0.883 (0.002)	0.874 (0.021)	2.455
20	1.117 (0.003)	1.101 (0.001)	1.119 (0.005)	1.112 (0.009)	0.767

5.3.4. RP-HPLC Method Development and Validation for Bedaquiline

5.3.4.1. Method Development

For this method, various mobile phase ratios of 90:10, 85:15 and 95:5 containing (methanol/acetonitrile (85:15): phosphate buffer, pH 7.4) were all tested and showed desirable peaks for the detection of bedaquiline. The mobile phase of 95:5 was chosen since it produced a narrow and symmetrical peak with a retention time of 4.171 min that allowed a run time of less than 5 min (Figure 5.3), low pressure, and a lesser chance of crystallization which was observed to occur as the buffer ratio increased in the system. To prevent crystallization in the column, the column was first equilibrated with 95:5 (methanol/acetonitrile: water) for 10 min. Thereafter, the water was replaced with the prepared phosphate buffer and equilibrated for 30 min at 95:5.

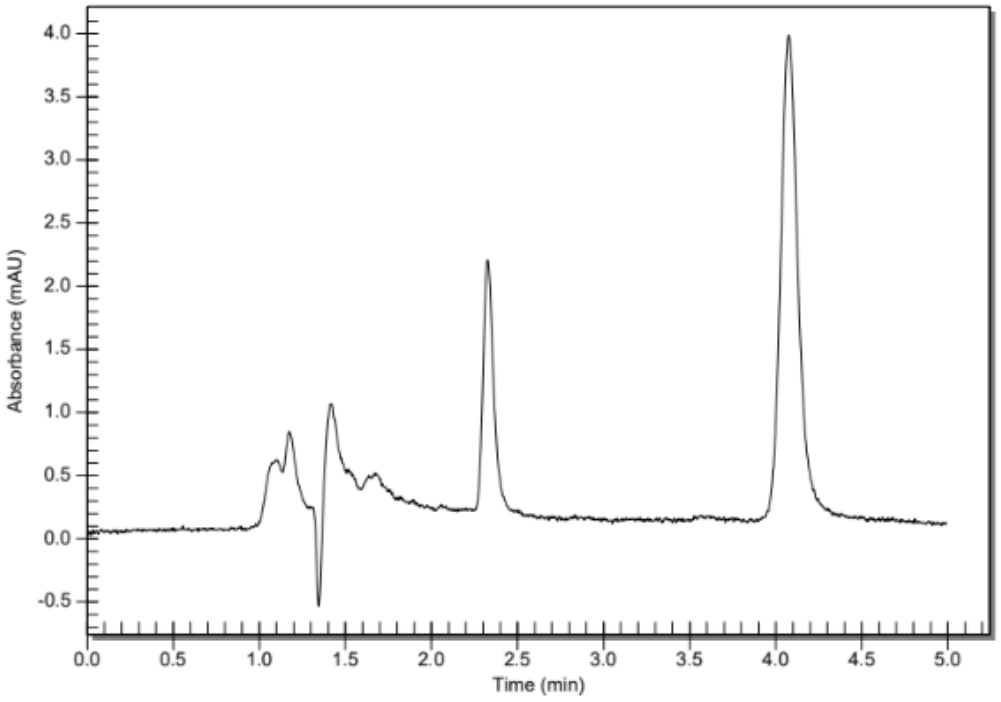

Figure 5.3: RP-HPLC chromatogram with a run time of 5 min and a peak with a retention time of 4.171 min for bedaquiline (1 µg.ml^{-1}) using a mobile phase of 95:5 (organic phase (containing methanol 85:15 acetonitrile): phosphate buffer) at a flow rate of 1 ml.min^{-1} and a detection wavelength of 275 nm.

5.3.4.2. Method Validation

5.3.4.2.1. Linearity

The linear regression curves displayed the suitability of the method within the prescribed concentration range (1-50 $\mu g.ml^{-1}$) for bedaquiline with the correlation of determination (R^2) = 1, (Figure 5.4, Table 5.5). The LOD and LOQ were determined to be 0.05 $\mu g.ml^{-1}$ and 0.15 $\mu g.ml^{-1}$, respectively using signal-to-noise ratio (Figure 5.5).

(a)

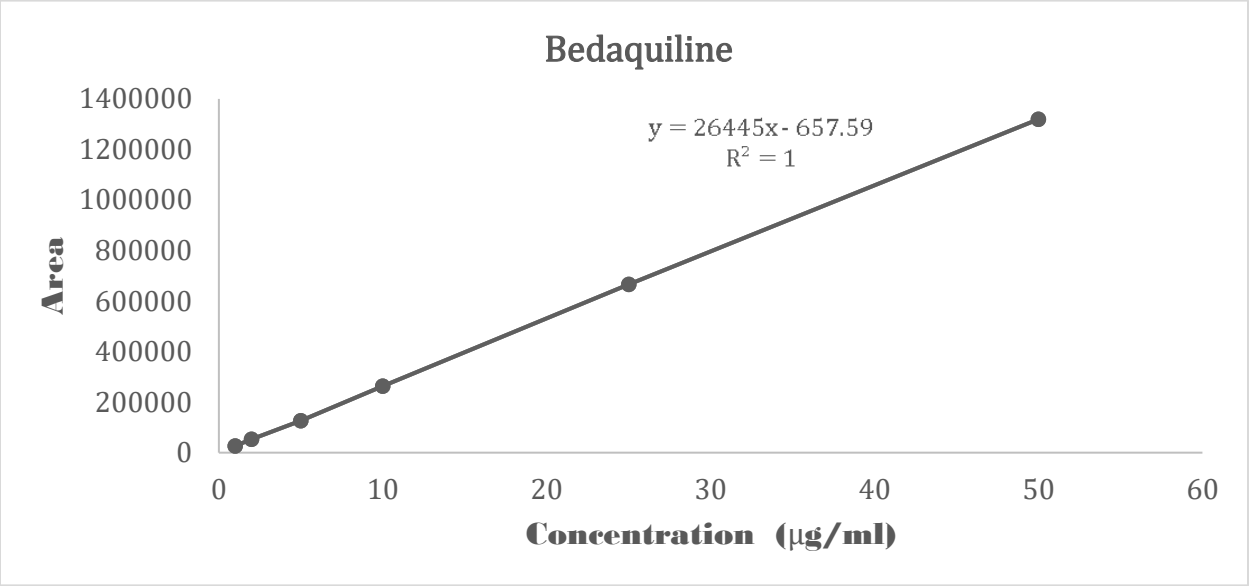

(b)

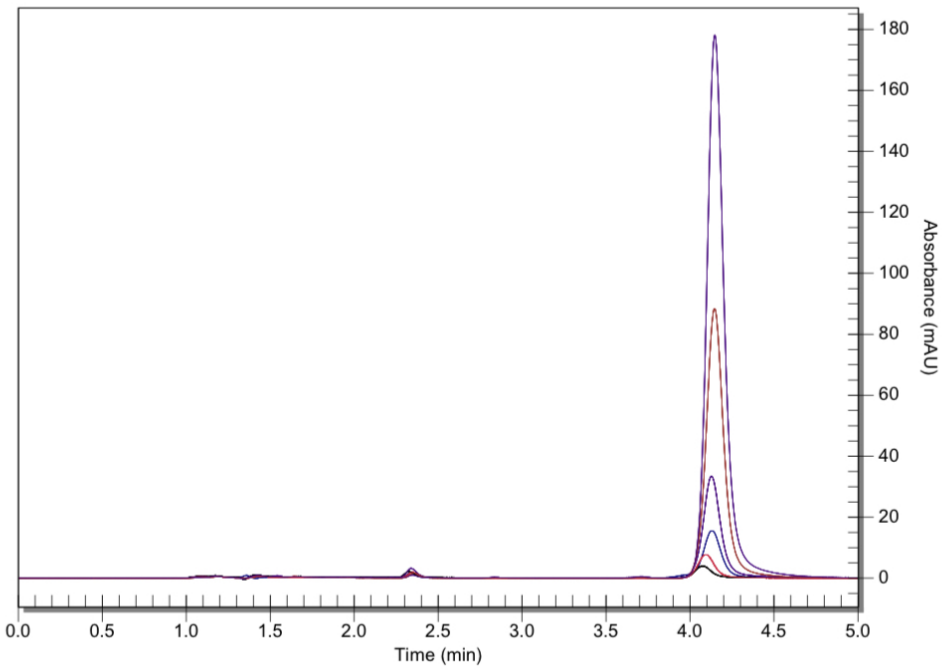

Figure 5.4: Linearity of bedaquiline (a) standard curve of bedaquiline (n=3) (each standard was injected 3 times), (b) overlay of bedaquiline standard curve chromatograms.

(a)

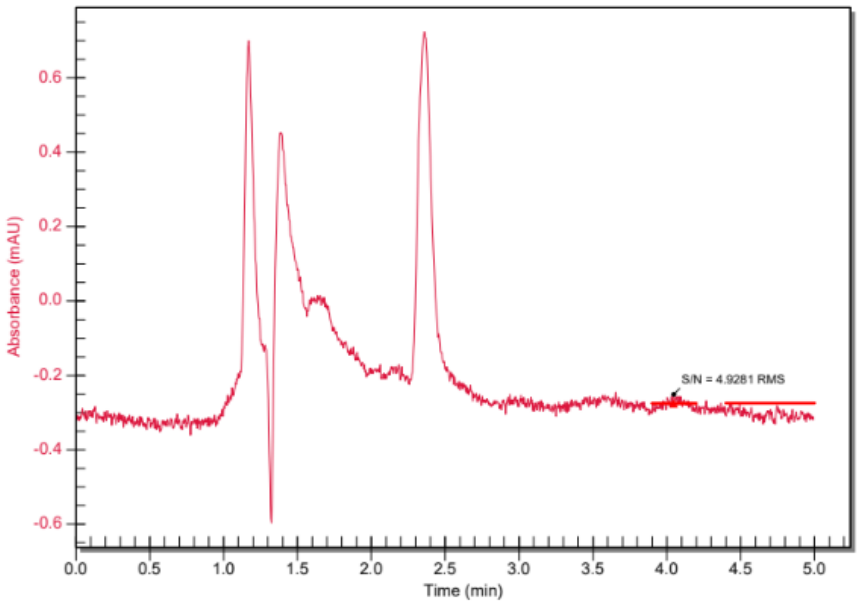

(b)

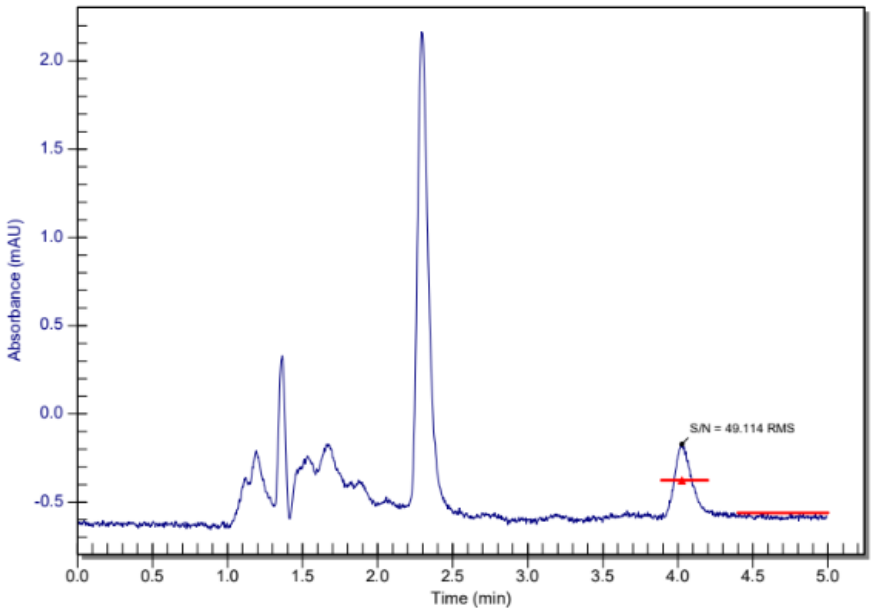

Figure 5.5: RP C18-HPLC chromatograph (a) blank peak signal-to-noise ratio (b) a peak 10x signal-to-noise ratio.

Table 5.5: Linearity of bedaquiline established from three independent standard curves using the established RP C18-HPLC method. Each analyte concentration was done in triplicate.

Concentration ($ug.ml^{-1}$)	Std.Curve 1 Mean Peak area (SD)	Std.Curve 2 Mean Peak area (SD)	Std.Curve 3 Mean Peak area (SD)	Overall Mean Peak Area (SD)	%RSD
1	28972.74 (722.63)	25370.32 (205.15)	26550.40 (147.99)	26964.49 (1499.55)	5.56
2	57405.93 (709.35)	50550.11 (233.54)	51765.03 (157.07)	53240.35 (2986.97)	5.61
5	126958.76 (999.31)	124289.06 (1010.07)	129325.74 (279.57)	126857.85 (2057.45)	1.62
10	253987.42 (405.98)	267336.73 (1456.12)	268280.89 (432.23)	263201.68 (6526.85)	2.48
25	669440.35 (5174.52)	676459.28 (290.18)	651068.14 (384.35)	665655.92 (10705.73)	1.61
50	1300634.92 (10707.34)	1344631.17 (5026.61)	1313333.77 (1835.96)	1319533.29 (18488.61)	1.40

5.3.4.2.2. Precision

The inter-day and intra-day precision showed reproducibility over 3 days in the detection of bedaquiline, with a %RSD of <2% for all selected standard concentrations, which is within the acceptance criteria (Table 5.6).

Table 5.6: Precision determined for the established HPLC method from three independent standard concentrations. Each analyte concentration was repeated six times.

Drug	Concentration ($\mu g.ml^{-1}$)	Intraday Precision		Interday Precision			
		Day 1		Day 2		Day 3	
		Mean Peak Area (SD)	%RSD	Mean Peak Area	%RSD	Mean Peak Area (SD)	%RSD
BDQ	1	362608.88 (250.47)	0.095	362272.36 (235.70)	0.142	362473.30 (183.72)	0.114
	10	1732359.35 (686.47)	0.197	1732700.69 (1352.44)	0.206	1730004.29 (3884.79)	0.128
	50	3416987.88 (2095.96)	0.043	3411933.39 (2309.15)	0.031	3411276.29 (1137.87)	0.041

BDQ: Bedaquiline; %RSD: % Relative standard deviation

5.3.4.2.3. Accuracy

The method was efficient, with an overall recovery of 99.69 % with an RSD of 0.47% (n=6) after a spike of PBS containing 0.2% SLS with 25 $\mu g.ml^{-1}$ bedaquiline, as detailed in Table 5.7.

Table 5.7: Accuracy of the established HPLC method from three independent concentrations. Each analyte concentration was repeated six times.

Drug	Level, %	Concentration ($\mu g.ml^{-1}$)	Amount recovered (SD) ($\mu g.ml^{-1}$)	Recovery (SD), %	RSD (%)
BDQ	80	8.00	7.96 (0.015)	99.45 (0.186)	0.55
	100	10.00	10.02 (0.027)	100.24 (0.267)	0.24
	120	12.00	11.92 (0.005)	99.37 (0.039)	0.63

BDQ: Bedaquiline; SD: Standard deviation; RSD: Relative standard deviation

5.3.4.2.4. Robustness

The developed method is consistent, showing repeatability and specificity in the established running conditions. The robustness of the HPLC method was investigated by small variations in the following conditions: flow rate, temperature, and the organic mobile phase component (Table 5.8). A slight increase in temperature did not alter the retention time (%RSD <2%) and did not alter the peak area detected for bedaquiline significantly, with a recovery range of 96.0-97.8%. However, the retention time decreased by 3.2% and the area detected was slightly less stable with a slight temperature decrease, with a recovery range of 92.0-96.8%. As the flow rate decreased (by 0.1 $ml.min^{-1}$), elution occurred later by a difference of 8.51%. The % recovery increased to a range of 104.3-114.1%. As the flow rate increased (by 0.1 $ml.min^{-1}$), elution occurred earlier by a difference of 10.86%. The % recovery decreased to a range of 89.7-96.2%. As the mobile phase ratio of organic: aqueous decreased, the peak eluted later by a difference of 13.55%. The % recovery decreased slightly to a range of 97.2-98.4%. As the mobile phase ratio of organic: aqueous increased, the peak eluted earlier by a difference of 9.66%. The % recovery was found to be 95.1-101.1%, where the change favoured higher concentrations of 10 $\mu g.ml^{-1}$ and 50 $\mu g.ml^{-1}$ (%RSD <2%).

Table 5.8: Robustness determined for the established HPLC method from three independent standard concentrations by varying flow rate, temperature, and organic mobile phase component. Each analyte concentration was repeated six times.

Condition	Bedaquiline				
	Mean Peak Area (SD)	Amount recovered. ($\mu g.ml^{-1}$)	% Recovery	Mean RT (min) (SD)	Mean RT %RSD
FR: 1 $ml.min^{-1}$ MP: 95:5 T: 25 °C	22149.03 (357.53)	0.86 (0.04)	-	4.16 (0.014)	-
	224328.14 (3339.72)	8.51 (0.15)	-		
	1126410.03 (3203.44)	42.62 (0.15)	-		
FR change: 0.9 $ml.min^{-1}$	23132.39 (282.05)	0.90 (0.04)	104.3 (4.44)	4.52 (0.039)	8.51
	246750.78 (278.72)	9.36 (0.04)	110.0 (0.43)		
	1285761.89 (4065.01)	48.65 (0.18)	114.1 (0.37)		

FR change: 1.1 ml.min^{-1}	19794.46 (394.04)	0.77 (0.04)	89.7 (5.19)	3.71 (0.024)	10.86
	210510.93 (2006.28)	7.99 (0.10)	93.9 (1.25)		
	1084096.45 (2869.08)	41.02 (0.13)	96.2 (0.32)		
T change: 24 °C	20318.04 (131.28)	0.79 (0.03)	92.0 (3.80)	4.13 (0.014)	1.07
	213138.20 (1753.37)	8.08 (0.09)	95.0 (1.11)		
	1090081.38 (1627.26)	41.25 (0.09)	96.8 (0.22)		
T change 1: 26 °C	21477.79 (116.04)	0.84 (0.03)	97.1 (3.57)	4.03 (0.011)	3.20
	215379.26 (248.68)	8.17 (0.03)	96.0 (0.37)		

	1101493.03 (963.25)	41.68 (0.06)	97.8 (0.14)		
MP change: 94:6 (A: B)	21520.981 (227.78)	0.84 (0.03)	97.2 (3.57)	4.72 (0.034)	13.55
	219065.3141 (352.46)	8.31 (0.04)	97.7 (0.48)		
	1108243.451 (1460.23)	41.93 (0.08)	98.4 (0.19)		
MP change: 96:4 (A: B)	21022.98616 (68.23)	0.82 (0.03)	95.1 (3.66)	3.76 (0.011)	9.66
	224131.9622 (197.77)	8.50 (0.03)	99.9 (0.35)		
	1138549.174 (2307.75)	43.08 (0.11)	101.1 (0.26)		

FR: Flow rate; T: Temperature; MP: Mobile phase; RT: Retention time; %RSD: % Relative standard deviation from normal conditions

5.3.4.2.5. Stability

Bedaquiline showed good stability when stored at 4 °C and room temperature in the first week of storage. From week 2 onwards an increase in concentration was observed due to the high percentage of methanol's low vapour pressure causing it to volatilize into air as presented in Table 5.9 below. Bedaquiline demonstrated better stability in the fridge (4 °C) as compared to at room temperature. Both compounds may be stored for at least one week before analyses at either room temperature (25 °C) or fridge (4 °C).

Table 5.9: Stability of the established HPLC method from three independent standard concentrations. Each analyte concentration was repeated six times.

Parameters		Bedaquiline					
	Temperature °C	25	4	25	4	25	4
W0	Rec ($\mu g.ml^{-1}$)	0.98	0.78	10.13	8.76	50.87	42.74
	%RV	-		-		-	
W1	Rec ($\mu g.ml^{-1}$) (±SD)	1.06 (0.08)	0.79 (0.01)	10.55 (0.42)	8.78 (0.02)	52.85 (1.98)	42.23 (0.51)
	%RV	107.80	100.97	104.12	100.28	103.89	98.81
W2	Rec ($\mu g.ml^{-1}$)	1.07 (0.09)	0.86	11.60	9.47	55.84	44.77

	(±SD)		(0.08)	(1.05)	(0.71)	(4.97)	(2.03)
	%RV	108.82	110.68	114.44	108.20	109.77	104.75
W3	Rec ($\mu g.ml^{-1}$) (±SD)	1.27 (0.29)	0.88 (0.10)	14.48 (4.35)	10.24 (1.48)	66.14 (15.27)	49.04 (6.30)
	%RV	128.54	113.09	142.92	116.98	130.01	114.74

W0: Initial concentration; W1; Week 1; W2; Week 2; W3; Week 3; Rec: Recovery; %RV: %Recovery.

5.4. DISCUSSIONS

A search of the literature indicated very few HPLC methods were available for the detection of bedaquiline. Most methods employ the use of a high organic solvent in the presence of an acidic buffer (Momin et al., 2018; Pardhi et al., 2020). Bedaquiline is a water-insoluble drug that can only be eluted in a highly organic mobile phase; therefore 95% organic solvents were used to elute the drug. It can be concluded from the study that the developed method is accurate, precise, and reliable. The developed method in this study is acceptable and sensitive considering no other method could be found in the literature to detect bedaquiline at a physiological pH of 7.4. Flow rate variation is found to significantly affect the recovery of bedaquiline as compared to the effects of temperature and mobile phase variation. The MP allowed the validation of a fast, reliable, accurate and transient method, with a run time of 5 min and retention time of 4.171 min. The method was highly sensitive with a LOD and LOQ of 0.05 $\mu g.ml^{-1}$ and 0.15 $\mu g.ml^{-1}$, respectively.

5.5. CONCLUSION

The most desirable COS-MN-BDQ-NPs were discovered for further studies to be conducted in Chapter 6. The developed method will successfully quantify BDQ permeation from the COS-MN-BDQ-NPs across the pericardium without any interference of excipients/polymers from a synthesized nanosystem as shown in Chapter 6.

5.6. REFERENCES

Alajlani, M. M. (2022). The chemical property position of bedaquiline construed by a chemical global positioning system-natural product. Molecules, 27(3), 753.

Bernkop-Schnürch, A., and Dünnhaupt, S. (2012). Chitosan-based drug delivery systems. European Journal of Pharmaceutics and Biopharmaceutics, 81(3), 463–469.

Carrión-Prieto, P., Martín-Ramos, P., Hernández-Navarro, S., Sánchez-Sastre, L. F., Marcos-Robles, J. L., and Martín-Gil, J. (2018). Furfural, 5-HMF, acid-soluble lignin and sugar contents in C. ladanifer and E. arborea lignocellulosic biomass hydrolysates obtained from microwave-assisted treatments in different solvents. Biomass and Bioenergy, 119, 135–143.

Chahine, E. B., Karaoui, L. R., and Mansour, H. (2014). Bedaquiline: a novel diarylquinoline for multidrug-resistant tuberculosis. Annals of Pharmacotherapy, 48(1), 107–115.

Chew, K. R., Sankaran, R., Chew, K. W., and Show, P. L. (2023). Polymer–polymer interaction. In Principles of Multiple-Liquid Separation Systems (pp. 1–20). Elsevier.

Committee for Medicinal Products for Human Use (CHMP) assessment report SIRTURO. International non-proprietary name: bedaquiline Procedure No. EMEA/H/C/002614/0000. EMA, 2013, 107 p. (2013).

de Alvarenga, E. S. (2011). Characterization and properties of chitosan. Biotechnology of Biopolymers, 91, 48–53.

Garg, U., Chauhan, S., Nagaich, U., and Jain, N. (2019). Current advances in chitosan nanoparticles based drug delivery and targeting. Advanced Pharmaceutical Bulletin, 9(2), 195.

H, I. C. (2005). International Conference on Harmonization: Validation of analytical procedures: Text and Methodology Q2 (R1). ICH Harmonised Tripartite Guideline Rockville, MD, USA.

Hong, T., Yin, J.-Y., Nie, S.-P., and Xie, M.-Y. (2021). Applications of infrared spectroscopy in polysaccharide structural analysis: Progress, challenge and perspective. Food Chemistry: X, 12, 100168.

Janko, C., Zaloga, J., Pöttler, M., Dürr, S., Eberbeck, D., Tietze, R., Lyer, S., and Alexiou, C. (2017). Strategies to optimize the biocompatibility of iron oxide nanoparticles–“SPIONs safe by design”. Journal of Magnetism and Magnetic Materials, 431, 281–284.

Kadian, R. (2018). Nanoparticles: A promising drug delivery approach. Asian J Pharm Clin Res, 11(1), 30–35.

Kulkarni, S. A., Sawadh, P. S., and Palei, P. K. (2014). Synthesis and characterization of superparamagnetic Fe3O4@ SiO2 nanoparticles. Journal of the Korean Chemical Society, 58(1), 100–104.

Momin, M. A. M., Rangnekar, B., and Das, S. C. (2018). Development and validation of a RP-HPLC method for simultaneous quantification of bedaquiline (TMC207), moxifloxacin and pyrazinamide in a pharmaceutical powder formulation for inhalation. Journal of Liquid Chromatography and Related Technologies, 41(8), 415–421.

Mondalek, F. G., Zhang, Y. Y., Kropp, B., Kopke, R. D., Ge, X., Jackson, R. L., and Dormer, K. J. (2006). The permeability of SPION over an artificial three-layer membrane is enhanced by external magnetic field. Journal of Nanobiotechnology, 4, 1–9.

Morales, J. O., and Brayden, D. J. (2017). Buccal delivery of small molecules and biologics: of mucoadhesive polymers, films, and nanoparticles. Current Opinion in Pharmacology, 36, 22–28.

Ndjeka, N., Schnippel, K., Master, I., Meintjes, G., Maartens, G., Romero, R., Padanilam, X., Enwerem, M., Chotoo, S., and Singh, N. (2018). High treatment success rate for multidrug-resistant and extensively drug-resistant tuberculosis using a bedaquiline-containing treatment regimen. European Respiratory Journal, 52(6).

Nnadozie, E. C., and Ajibade, P. A. (2022). Preparation, phase analysis and electrochemistry of magnetite (Fe3O4) and maghemite (γ-Fe2O3) nanoparticles. International Journal of Electrochemical Science, 17(12), 22124.

Pankuweit, S., Ristić, A. D., Seferović, P. M., and Maisch, B. (2005). Bacterial pericarditis: diagnosis and management. American Journal of Cardiovascular Drugs, 5, 103–112.

Pardhi, V., Pant, G., and Flora, S. J. S. (2020). RP-HPLC method development and validation for bedaquiline fumarate to evaluate its forced degradation behaviour and stability in official dissolution media. Future Journal of Pharmaceutical Sciences, 6(1), 1–10.

Pasipanodya, J. G., McIlleron, H., Burger, A., Wash, P. A., Smith, P., and Gumbo, T. (2013). Serum drug concentrations predictive of pulmonary tuberculosis outcomes. The Journal of Infectious Diseases, 208(9), 1464–1473.

Romano, M., González Gómez, M. A., Santonicola, P., Aloi, N., Offer, S., Pantzke, J., Raccosta, S., Longo, V., Surpi, A., and Alacqua, S. (2022). Synthesis and Characterization of a Biocompatible Nanoplatform Based on Silica-Embedded SPIONs Functionalized with Polydopamine. ACS Biomaterials Science and Engineering, 9(1), 303–317.

Sadeghi, A. M. M., Dorkoosh, F. A., Avadi, M. R., Weinhold, M., Bayat, A., Delie, F., Gurny, R., Larijani, B., Rafiee-Tehrani, M., and Junginger, H. E. (2008). Permeation enhancer effect of chitosan and chitosan derivatives: comparison of formulations as soluble polymers and nanoparticulate systems on insulin absorption in Caco-2 cells. European Journal of Pharmaceutics and Biopharmaceutics, 70(1), 270–278.

Saesoo, S., Sathornsumetee, S., Anekwiang, P., Treetidnipa, C., Thuwajit, P., Bunthot, S., Maneeprakorn, W., Maurizi, L., Hofmann, H., and Rungsardthong, R. U. (2018). Characterization of liposome-containing SPIONs conjugated with anti-CD20 developed as a novel theranostic agent for central nervous system lymphoma. Colloids and Surfaces B: Biointerfaces, 161, 497–507.

Sajja, H. K., East, M. P., Mao, H., Wang, Y. A., Nie, S., and Yang, L. (2009). Development of multifunctional nanoparticles for targeted drug delivery and noninvasive imaging of therapeutic effect. Current Drug Discovery Technologies, 6(1), 43–51.

Serrasqueiro, F., Barbosa, A. I., Lima, S. A. C., and Reis, S. (2023). Targeting the Mannose Receptor with Functionalized Fucoidan/Chitosan Nanoparticles Triggers the Classical Activation of Macrophages. International Journal of Molecular Sciences, 24(12), 9908.

Shu, X. Z., and Zhu, K. J. (2000). A novel approach to prepare tripolyphosphate/chitosan complex beads for controlled release drug delivery. International Journal of Pharmaceutics, 201(1), 51–58.

Singh, S., Pandey, V. K., Tewari, R. P., and Agarwal, V. (2011). Nanoparticle based drug delivery system: advantages and applications. Indian J Sci Technol, 4(3), 177–180.

Trapani, A., Sitterberg, J., Bakowsky, U., and Kissel, T. (2009). The potential of glycol chitosan nanoparticles as carrier for low water soluble drugs. International Journal of Pharmaceutics, 375(1–2), 97–106.

Vineela, C. H., and Krishna, K. (2014). Preparation of ibuprofen-loaded Eudragit S100 nanoparticles by solvent evaporation technique. International Journal of Pharma Sciences and Research, 5(7), 375–384.

Yoon, H. Y., Jo, K. W., Nam, G. B., and Shim, T. S. (2017). Clinical significance of QT-prolonging drug use in patients with MDR-TB or NTM disease. The International Journal of Tuberculosis and Lung Disease, 21(9), 996–1001.

Zhao, Y., Wang, J., Fu, Q., Zhang, H., Liang, J., Xue, W., Zhao, G., and Oda, H. (2022). Characterization and Antioxidant Activity of Mannans from Saccharomyces cerevisiae with Different Molecular Weight. Molecules, 27(14), 4439.

Zhu, L., Zhou, Z., Mao, H., and Yang, L. (2017). Magnetic nanoparticles for precision oncology: theranostic magnetic iron oxide nanoparticles for image-guided and targeted cancer therapy. Nanomedicine, 12(1), 73–87.

CHAPTER SIX

SYNTHESIS AND EVALUATION OF NOVEL MANNAN-CHITOSAN OLIGOSACCHARIDE LACTATE NANOPARTICLES FOR THE ENHANCED *EX VIVO* PERMEATION OF BEDAQUILINE ACROSS THE PERICARDIUM FOR THE TREATMENT OF TUBERCULOSIS PERICARDITIS (TO BE PUBLISHED)

ABSTRACT

Amongst the four standard anti-TB drugs, only isoniazid successfully permeates the pericardium at anti-tubercular concentrations. Rifampicin and ethambutol have poor permeation across the pericardium. Although pyrazinamide permeates across the pericardium, it lacks good anti-tubercular activity at a pH of 7.4, making tuberculosis pericarditis a difficult disease to treat with high mortality. Bedaquiline is known to shorten the duration of therapy but has limitations e.g., poor solubility and adverse effects such as prolongation of the QT interval, causing cautious use and close monitoring of its adverse effects and drug interactions. In this study, bedaquiline was incorporated into an inherently targeted nanosystem for host-directed therapy and improved permeation of the drug with the *ex vivo* diffusion studies performed to investigate its penetration. The bedaquiline-loaded chitosan-mannan oligosaccharide lactate nanoparticles were prepared by a one-step ionic gelation probe sonication method. A PermeGear 7-in-line flow-through diffusion system was used for the *ex vivo* diffusion studies across porcine and human Pericardium. The bedaquiline-loaded nanoparticles was placed into the donor compartment. PBS (pH 7.4 with 0.2% sodium lauryl sulphate) was pumped through the receptor compartments at 1.5 $ml.h^{-1}$ (37 °C). Samples of permeants were collected every 2h for 24h and analysed via HPLC. Bedaquiline-loaded nanoparticles with particle size and potential of 192.4 nm and 40.5 mV, respectively were synthesised. The chitosan-mannan bedaquiline-loaded nanoparticles had an encapsulation efficacy of 98.7% and drug loading of 0.6%. Diffusion data indicated a steady state flux of 2.889 and 2.346 $\mu g.cm^{-2}.min^{-1}$ for porcine and human pericardium, respectively. The apparent permeability coefficients were calculated to be 2.66×10^{-4} $cm.min^{-1}$ and 2.16×10^{-4} $cm.min^{-1}$ for porcine and human pericardium, respectively. A stable spherical nanosystem was synthesised. The drug permeation indicated a consistent and linear diffusion pattern across both porcine and human pericardium, additionally approving the porcine pericardium suitable comparable tissue to human tissue for pericardial studies. The nanosystem, therefore, presents a novel and important direction for the treatment of tuberculosis pericarditis with prospectively minimized systemic side effects and host-directed therapy.

6.1. INTRODUCTION

Tuberculosis is primarily understood as a lung disease, but since the emergence of antimicrobial resistance and long duration of treatment, the *Mycobacterium tuberculosis* (*M.tb*) bacilli has demonstrated pernicious effects by haematological and lymphatic spread outside of the lungs, resulting in a variety of extrapulmonary tuberculosis (Baykan et al., 2022). Extrapulmonary tuberculosis (EPTB) accounts for 15%–20% of all TB patients with a mortality rate as high as 2.16 people per 100 days of hospital stay in a clinical study done in Mozambique (Nacarapa et al., 2022; Sharma et al., 2021).

Even though extrapulmonary tuberculosis presents such virulence due to drug resistance, only 17 new systemic antibiotics have been approved by the FDA since 2010, amongst which only 2 were registered for drug-resistant tuberculosis, namely bedaquiline (2012) and protonamid (2019) (Chahine et al., 2022). Extrapulmonary drug resistant -TB is a more severe and prevailing type of tuberculosis, posing a daunting diagnostic and therapeutic challenge (Desai and Joshi, 2019). With the prevalence of multidrug-resistant tuberculosis (MDR-TB) in previously treated cases of EPTB becoming alarming, it is important to develop strategies to curtail the prevalence of the infection, taking into consideration that an MDR-TB patient left untreated or inadequately treated will create another 10-15 new cases of MDR-TB in a year (Kant et al., 2018).

Lymph node tuberculosis encompasses one of the most common types of EPTB, representing approximately half of EPTB cases (Baykan et al., 2022; Ilgazli et al., 2004; Prakasha et al., 2013). Additionally, infection of lymph nodes can cause further EPTB complications as in the case of tuberculosis pericarditis (TBP), caused by the retrograde lymphatic spread of the bacilli from lymph nodes (Gopalaswamy et al., 2021; Isiguzo et al., 2020). TBP is known to have a high burden in southern Africa due to the high prevalence of HIV and its contribution to TBP (Isiguzo et al., 2020).

A limited number of studies have indicated that amongst the four standard anti-TB drugs, only isoniazid successfully permeates the pericardium at anti-tubercular concentrations. Rifampicin and ethambutol have poor permeation across the pericardium. Although pyrazinamide permeates across the pericardium, it lacks good anti-tubercular activity at a pH of 7.4, making TBP a difficult disease to treat with high mortality (Shenjeet al., 2015). Studies have employed the use of nucleic acid amplification, corticosteroids and colchicine therapy to improve diagnosis, treatment, and prevent constrictive pericarditis and decrease mortality, but to little avail (Isiguzo et al., 2020b; Liebenberg et al., 2016; Wiysonge et al., 2008; Yu et al., 2022). Since the high bacillary burden

is closely associated with mortality, for this reason, more research is needed to identify the optimal therapy, dose, duration and delivery system to improve the treatment outcome of TBP.

Due to the difficulty in new drug development and adverse effects associated with the developed drugs, nanotechnology emerges as an important instrument in the targeted delivery to extricate drugs with difficulty in use due to their poor solubility and high toxicity (Baranyai et al., 2021). Bedaquiline (BDQ) is practically insoluble in aqueous media and has side effects as severe as QT prolongation. The incorporation of such drugs into nanoparticles (NPs) will improve drug selectivity and specificity to the required site of action whilst minimising systemic side effects of the drug (Mir et al., 2017).

Chitosan is a biocompatible polymer that has mucoadhesive properties, is enzymatic biodegradable, and has a chemotactic action with concurrent epithelial permeability enhancing properties (Jiménez-Gómez and Cecilia, 2020). Chitosan nanoparticles have previously been employed in the delivery of BDQ (De Matteis et al., 2018; Maddur Taluk, 2022; Rawal et al., 2018). Apart from its general properties, it presents with various pharmacological actions including, antimicrobial, immunostimulant and anti-inflammatory properties, that are advantageous for TB. It has been shown to have enhanced effects when used to transport poorly water-soluble drugs (Gulati et al., 2021).

Chitosan oligosaccharide lactate (COS) is a water-soluble derivative of chitosan. This property allows the synthesis of a nanosystem without having to use an acidic media to solubilise the polymer, shorten the synthetic process and accommodate acid-degrading co-polymers or drugs. COS has anti-inflammatory, anti-microbial, anti-oxidative and tissue regenerative properties and more favourable properties for certain biological interactions as compared to chitosan. The most prominent biological activity COS may have in TB would be its host-directed therapeutic activities. COS have immunomodulatory properties attained through its modulation of nuclear factor kappa B (NF-κB) and mitogen-activated protein kinase (MAPK) pathways, and its activation of the AMP-activated protein kinase (AMPK) pathway (Ignjatović et al., 2018; Muanprasat and Chatsudthipong, 2017).

Chitosan has been reported to have the ability to open tight junctions and improve the paracellular diffusion of chitosan nanoparticles (Pepić et al., 2013, 2010). Cationic polymers such as chitosan are drug absorption enhancers through the reversible loosening of tight junctions (Lemmer and Hamman, 2013; Yeh et al., 2011). Congruent with chitosan properties is the pericardial layer and

its composite. The pericardium is made up of mesothelial cells, a type of epithelial cell with tight junctions, adherence junctions, gap junctions, and desmosomes (Figure 6.1) (Lua and Asahina, 2016; Simionescu and Simionescu, 1977; Ramasamy et al. 2018). For this reason, chitosan nanoparticles present a good strategy for the enhancement of drug permeation across the pericardium. On the other hand, permeation studies using chitosan oligosaccharide lactate (COS) have been conducted and results demonstrated enhanced permeation across the epithelial layer primarily through the transcellular pathway (Luo et al., 2011; Ye et al., 2013).

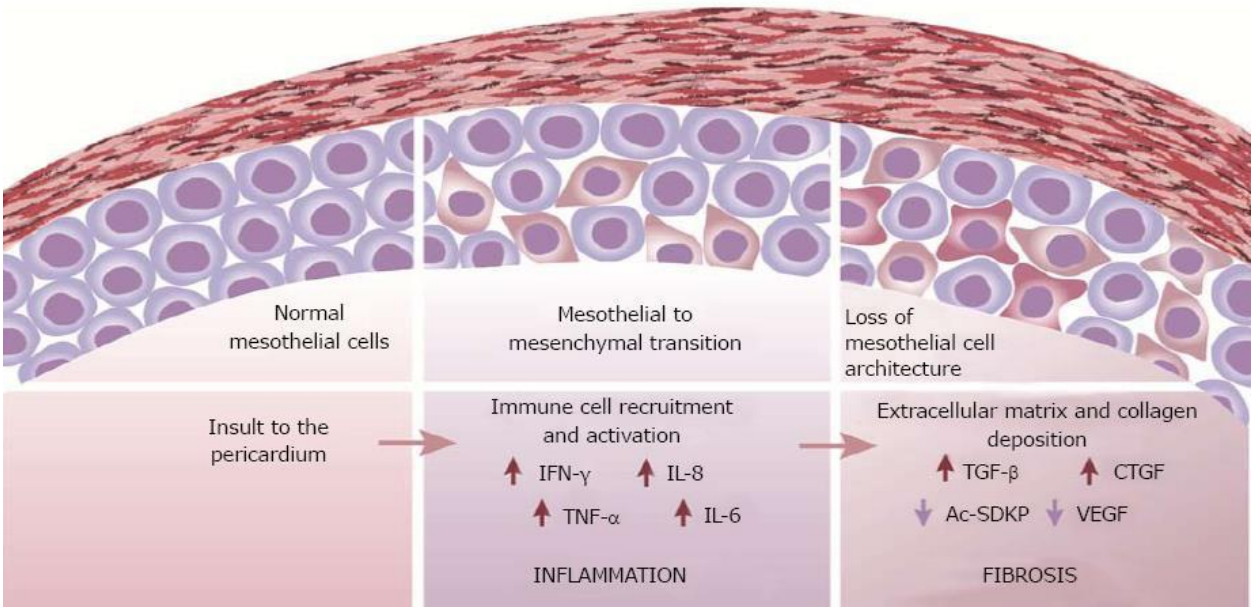

Figure 6.1: Mesothelial cells description at various stages of constrictive pericarditis and its molecular mediators involved in the inflammatory and fibrotic process (Ac-SDKP: N-acetyl-seryl-aspartyl-lysyl- proline; TGF-β: Growth factor β; TNF-α: Tumor necrosis factor-α; CTGF: Connective tissue growth factor; IFN-γ: Interferon-γ; VEGF: Vascular endothelial growth factor (Ramasamy et al., 2018).

Macrophages are primary sites for TB infection, and due to the prominence of macrophages in the pericardial fluid and lymph nodes, they become sites of prolonged bacterial persistence (Ganchua et al., 2018; Verway et al., 2013). Macrophages express various surface receptors allowing specific targets for drugs. The mannose receptor is one of them, allowing recognition of various molecules from the carbohydrate family for receptor-mediated endocytosis (Andrade et al., 2020). *M.Tb* is further known to spread through macrophages in MDR-XDR (Extensively drug-resistant) TB; and for this reason, active targeting of macrophages may present a pathway in curtailing the disease.

Mannan oligosaccharide (MN) from *S. cerevisiae* is a polymer consisting of mannose, which has been employed as a targeting ligand for drug delivery unto CD206/mannose receptors on antigen-presenting cells such as macrophages (Faustino et al., 2021; Park et al., 2007; Vu-Quang et al., 2011). In addition to its targeting abilities, it exhibits techno-functional properties allowing it to act as a viscosity-enhancer and emulsion stabilizer (Singh et al., 2018). Recently, it has been shown to have both anti-oxidative properties (Liu et al., 2018) and biological properties, including inhibition of pathologic adherence, modulation of bacterial growth (Smith et al., 2020) and host-directed properties. Its properties improve host immune response by inducing IL10-producing B cell regulated $CD4^+$ T-cell polarisation, ultimately resulting in the reduction of IFN-y (an anti-inflammatory response) and an increase in IL-4 which contributes to macrophage-induced tissue repair (Bosurgi et al., 2017; Faustino et al., 2021; Lee and Dugoua, 2011; Onitake et al., 2015; Yuan et al., 2019). It additionally hinders the production of pro-inflammatory cytokines such as IL-1β, IL-6 and TNF-α which correlates to the cytokines also found in TBP (Burgess et al., 2002; Tang et al., 2021), suggestive of a prospective immunomodulatory effect in TBP.

Mannan oligosaccharide additionally has epithelial protective properties by enhancing epithelial tight junctions (Chen et al., 2021; Nopvichai et al., 2019), therefore may have a supportive effect in the closing of tight junctions and maintaining epithelial integrity. With the permeation-enhancing properties of COS and the epithelial protective effect of MOS, their combinatory use may lead to a copolymer that may not disrupt the integrity of the pericardium whilst improving the permeation of the drug across it.

Various studies have investigated the incorporation of mannan onto the surface of nanoparticles for receptor-mediated targeting of macrophages (Gupta and Gupta, 2022). Therefore, this study illustrates the novel synthesis of chitosan oligosaccharide -mannan NPs for the active targeting of nanosystems to $Gata6^+$ macrophages (major components of the pericardial immune cell compartment) (Deniset et al., 2019). The nanosystem is expected to enhance the permeation of BDQ across the pericardium. Porcine pericardium and human pericardium are used to determine the similarity and interchangeable use of the tissue for permeability studies. The combination of BDQ, MN and COS (with potential antibacterial activity), could yield a safer and more efficacious treatment for MDR-XDR tuberculosis. This nanosystem was thus synthesised and characterized for all relevant physicochemical and imaging modalities.

6.2. MATERIALS AND METHODS

6.2.1. Materials

The materials employed in this study were of the highest purity grade and were purchased from Sigma-Aldrich (Pty) Ltd (St. Louis, Missouri, United States). They included chitosan oligosaccharide lactate (COS) (Mw 5 kDa), mannan oligosaccharide (MN) from *Saccharomyces cerevisiae*, tween 80, dichloromethane (DCM), sodium tripolyphosphate (sTPP), bedaquiline (BDQ), ethanol, phenol, sulfuric acid (H_2SO_4), methanol (HPLC grade), acetonitrile (HPLC grade), potassium dihydrogen orthophosphate, triethylamine, orthophosphoric acid, phosphate buffer saline (PBS) tablets, sodium lauryl sulphate (SLS).

6.2.2. Synthesis of the BDQ-Loaded COS-MN NPs

The bedaquiline-loaded COS-MN NPs were prepared by a one-step ionic gelation probe sonication method as illustrated in Figure 6.2 (Ko et al., 2002). COS (200 mg) was added into 10 ml of distilled water, followed by the addition of MN (50 mg) into the solution and stirring for 30 min. Tween 80 (200 µl) was added dropwise into the solution until a homogenous solution was obtained. Bedaquiline (5 mg) was dissolved in 5 ml of DCM and the aqueous solution was added to the organic solution, followed by stirring at 1500 rpm for 20 min. sTPP (7.5 mg) was dissolved in 5 ml DW and filtered through a 2.2 µm filter. The sTPP was added dropwise into the prepared bedaquiline solution at a 0.2 $ml.min^{-1}$ drop rate, after which the solution was stirred for 24 h. The resultant solution was then homogenised at 5000 rpm for 10 min. The suspension obtained was sonicated (CV33 VibraCell, Sonics and Materials, Inc., Danbury, CT, USA) for 2 min at 4.8 million Joules and 40% amplitude. The suspension was frozen at -80 °C for 48 h and then subsequently lyophilized for 12 h (FreeZone-50C Benchtop Freeze Dryer, Labconco, Kansas City, MO, USA).

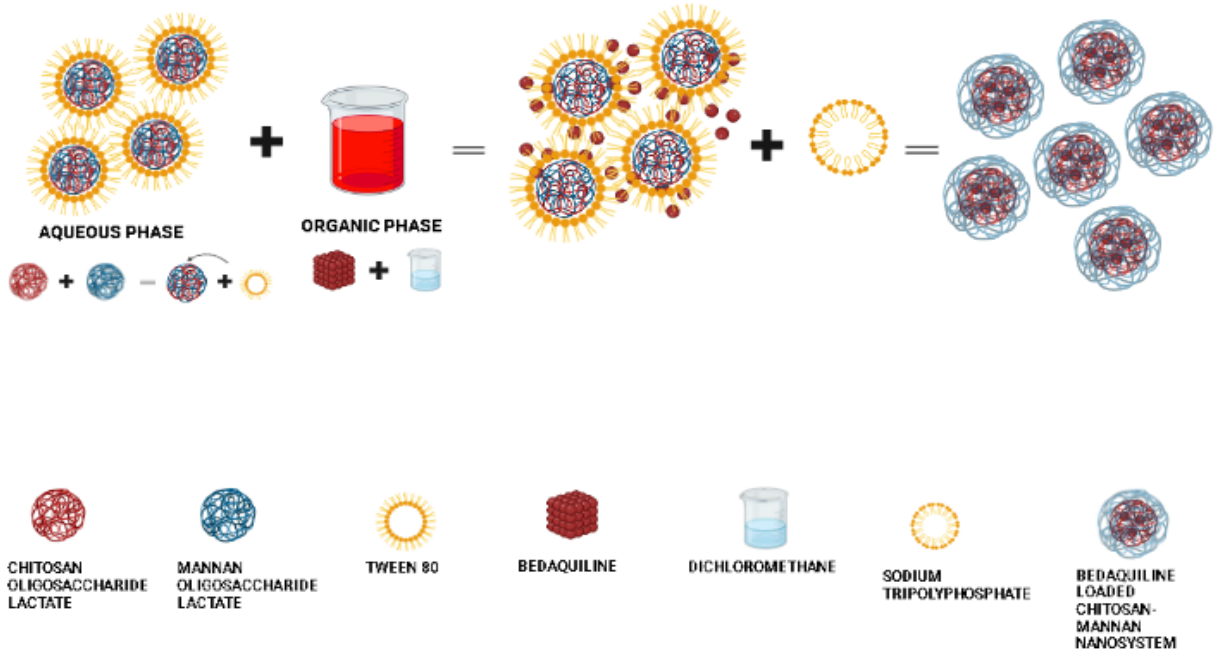

Figure 6.2: A schematic diagram overview showing how the various components combine in the preparation of the chitosan oligosaccharide-mannan-bedaquiline nanoparticles.

6.2.3. Physicochemical and Physicomechanical Characterization of the Synthesized BDQ-Loaded COS-MN NPs

6.2.3.1. Determination of Particle Size, Zeta Potential, and Morphology

A nano zetasizer instrument (NanoZS, Malvern Panalytical, Malvern, UK) was used to obtain the average hydrodynamic size of the nanoparticles and the surface zeta potential of the nanoparticles by dynamic light scattering and electrophoretic light scattering, respectively. The suspension (0.1 ml) was diluted into 10 ml of distilled water. The resultant samples (1 ml) were transferred into disposable cuvettes to determine the hydrodynamic size and polydispersity index while 0.8 ml was transferred into zeta potential disposable folded capillary cells (DTS 1070) for surface charge analysis at 25 °C.

6.2.3.2. Fourier Transform Infrared (FTIR) Spectroscopy.

Fourier transform infrared spectroscopy (Spectrum 100, PerkinElmer Inc., Waltham, MA, USA) was used for comparative analysis of nanoparticles and individual components to identify the difference in the vibrational transition of the chemical bonds in the molecule. The bonds present

will confirm the encapsulation of the drug in the nanosystem. Samples of Individual BDQ, MN, COS, and BDQ-loaded COS-MN nanoparticles were analysed at 110 psi pressure in a range of 4000–650 cm^{-1} over 20 scans to obtain relevant spectra.

6.2.3.3. X-ray Diffraction (XRD) Analysis

The degree of crystalline transition of pristine BDQ, MN, COS, and BDQ-loaded COS-MN nanoparticles was analysed employing X-ray diffractometry (XRD) (Rigaku MiniFlex, Rigaku Inc., Tokyo, Japan). The dry samples of BDQ, MN, COS, and BDQ-loaded COS-MN nanoparticles were mounted onto aluminium sample holders and measured at a current of 40 kV and 15 mA CuKα radiation. The scanning measurement was in the 2θ range of 10°–90°, with a scan rate of $10°.min^{-1}$.

6.2.3.4. Thermogravimetric Analysis (TGA)

The extent of thermal degradation of pristine BDQ, MN, COS and BDQ-loaded COS-MN nanoparticles was evaluated using a thermogravimetric analyser (PerkinElmer, TGA 4000, Llantrisant, Wales, UK). The samples were heated up from 30 °C to 900 °C at a 10 $°C.min^{-1}$ heating rate under a constant and continuous 19.8 $ml.min^{-1}$ nitrogen flow. The thermograms were extrapolated as percentage weight dependent on temperature.

6.2.3.5. Gelling Properties and Texture Analysis of BDQ-Loaded COS-MN NPs

Rheological measurements such as shear viscosity at varying shear rates and frequency shift, for the hydrogel base were performed using the Haake Mars (II) Modular Advanced Rheometer system (Thermoscientific, Waltham, MA USA). This was undertaken using a cone plate geometry (Rotor C35/1, D = mm, 1° Titan) at a gap distance of 0.052 mm. The COS-MN-BDQ-NPs base shear viscosity was determined at varying shear rates at 37 °C. Oscillatory frequency sweeps for COS-MN-BDQ-NPs were performed at a constant shear stress of 1 Pa in the frequency range from 10 to 0.10 Hz, at 37 °C.

The syringeability of the concentrated COS-MN-NPs solution was studied using a texture analyser (TAXT2, Stable Microsystems, UK) in compression mode, whereby the force required to be exerted on the plunger of the syringe to inject the gel was evaluated. The COS-MN-BDQ-NPs gel (1 ml) was drawn into 3 ml syringes and equipped with a 21G needle. A force transducer connected to the texture analyser was employed to measure the force required to push the

plunger of the syringe. The displacement rate was 10 $mm.s^{-1}$, which corresponds to a flow rate of 1 $ml.min^{-1}$.

6.2.4. Evaluation of Mannan Loading Content, BDQ-Loading Capacity and Drug Entrapment Efficacy of BDQ-Loaded COS-MN NPs

Conjugated mannan was investigated using a colourimetric assay by a phenol-sulfuric acid method. Using a Nanophotometer UV/Vis spectrophotometer NP80 (Implen, Munchen, Germany), the total sugar was spectrophotometrically measured at 490 nm, the wavelength at which hexoses and their methylated derivatives show maximum absorption (Carrión-Prieto et al., 2018). Unloaded nanoparticles were synthesised following the same method without adding bedaquiline. The supernatant and washing solution for a drug-loaded and drug-free system were collected and used to quantify unconjugated mannan by a phenol-sulfuric acid method. Briefly, 1 ml of 5% phenol was added into 2 ml of supernatant solution, followed by a rapid addition of 5 ml 96% H_2SO_4 and heated at 90 °C for 5 min, followed by 20 min of cooling. The drug-free system supernatant was used as the blank. The absorbance was then measured and extrapolated from a standard curve of 1 $\mu g.ml^{-1}$, 5 $\mu g.ml^{-1}$, 10 $\mu g.ml^{-1}$, 15 $\mu g.ml^{-1}$ and 20 $\mu g.ml^{-1}$ of MN. The conjugated mannan was calculated by the following formula (Equation 6.1):

$$\frac{\text{Total mannan added} - \text{Unloaded mannan}}{\text{Total mannan added}} \text{ x } 100\% \qquad (6.1)$$

Synthesised nanoparticle entrapment efficiency and drug loading were determined by centrifugal washing (n=3) using 0.2% SLS in water done in triplicate at 12000 rpm 25 °C for 10 min using an Ultracel® Regenerated Cellulose membrane (12kDa MWCO), 15 ml sample volume (Sigma-Aldrich (Pty Ltd (St. Louis, Missouri, United States)). The unreacted supernatant was collected and diluted with methanol: acetonitrile (85:15) and run in triplicate on the HPLC. The obtained results were inserted into equations 6.2 and 6.3 below and used to calculate the percentage.

$$\text{Entrapment efficiency} = \frac{\text{Total amount of drug} - \text{Unloaded drug in supernatant}}{\text{Total amount of drug}} \text{ x } 100\% \qquad (6.2)$$

$$\text{Drug Loading} = \frac{\text{Total amount of drug} - \text{Unloaded drug in supernatant}}{\text{Total weight of formulation}} \text{ x } 100\% \qquad (6.3)$$

6.2.5. *In Vitro* Drug Release Studies

BDQ release profile from the BDQ-loaded COS-MN-NPs was examined at pH 7.4 (pericardial space pH), by loading 105 mg.ml^{-1} NPs dispersed in 0.1 M PBS into semipermeable dialysis membrane tubing (SnakeSkin™, 3500 MWCO) (Sigma Aldrich, St. Louis, MO, USA). The dialysis membrane was then submerged in a 40 ml dissolution medium containing 40 ml of PBS containing 0.2% (w/v) SLS. SLS was used to ensure the solubility of BDQ in dissolution media due to its hydrophobic nature. The dissolution study was performed in a thermostatically stable orbital shaking incubator (Yihder LM-530, Yihder Co., Ltd., Taipei, Taiwan) at 37 °C. At different time intervals (t = 0.5, 1, 2, 4, 8, 12, 24, 48, 72, and 144 h), 1 ml of samples were withdrawn with concurrent replenishing of an equivalent amount of dissolution medium to maintain sink conditions. The released BDQ was quantified using the RP-HPLC method developed and validated in Chapter 5.

6.2.6. Collection and Treatment of Porcine and Human Pericardial Tissue

6.2.6.1. Porcine Pericardial Tissue

Porcine pericardial tissue was collected from animals euthanized for other purposes at the University of the Witwatersrand Central Animal Unit. For this study, an ethics waiver for the use of porcine tissue was obtained from the University of the Witwatersrand Animal Research Ethics Committee (waiver number: AREC-101210-002).

The pericardial tissue was immediately placed in phosphate-buffered saline (PBS, pH 7.4) and within an hour sectioned into strips, placed into cryovials, snap frozen and stored in liquid nitrogen (-195 °C).

6.2.6.2. Human Pericardial Tissue

Healthy pericardial specimens were collected from patients (>18 years of age) who underwent routine cardiac surgery at the Kuils River Netcare Hospital. Tissues collected were designated to be disposed of as medical waste. Ethics approval was obtained for the use of human pericardial tissue from the University of the Witwatersrand Human Research Ethics Committee (Approval number: M230545).

The pericardial tissue was immediately placed in phosphate-buffered saline (PBS, pH 7.4) and within an hour sectioned into strips, placed into cryovials, snap frozen and stored in liquid nitrogen (-195 °C).

6.2.7. *Ex Vivo* Diffusion Studies

Pericardial tissue was thawed for 10 min in PBS, after which the tissue was sectioned into approximately 7 x 1 cm^2 per experiment. Tissue sections were mounted in PermeGear in-line flow-through diffusion cells (exposed area 0.039 cm^2), part of a PermeGear 7-in-line Flow-through Diffusion system (PermeGear Inc, Hellertown, USA). The tissue sections were equilibrated for 10 min in PBS (pH 7.4) containing 0.2% (w/v) SLS at 37 °C in both the donor and receptor compartments of the diffusion cells before each permeability experiment started. PBS in the various donor compartments was replaced with 1 $mg.ml^{-1}$ equivalent concentrations of BDQ-loaded nanoparticles. PBS containing 0.2% (w/v) SLS was pumped through the receptor chambers at a rate of 1.5 $ml.hr^{-1}$ at 37 °C and samples were collected using a fraction collector at 2hr intervals for 24 h. The study was repeated three times. After collection, samples were diluted with Methanol: Acetonitrile (85:15) at a 50:50 ratio and analysed by HPLC. Cumulative amount ($\mu g.cm^{-2}$) versus time graphs were constructed and the steady-state flux rates ($\mu g.cm^{-2}.min^{-1}$), (Equation 6.4) and lag phases (min) were obtained from the linear portion of the slopes of the cumulative curves and the x-axis intercepts, respectively. The apparent permeability coefficient was calculated from the steady-state flux (Equation 6.5).

$$J = Q/(A \times t) \tag{6.4}$$

$$P = \frac{J}{(Cdoner - Creceptor)} \tag{6.5}$$

where;

J is the steady-state flux, Q is the quantity of substance crossing the membrane (in µg), A is the membrane area exposed (in cm^2) and t is the time of exposure (in min).

P is the apparent permeability coefficient, Cdonor is the Concentration in the donor compartment of the flow-through cell and Creceptor is the Concentration in the receptor compartment of the flow-through cell. The experiment was conducted under sink conditions and infinite dosing, and as such, the Cdonor ≈ Creceptor. Sink condition is when the concentration of the permeant in the receptor chamber is less than 10% of that in the donor compartment. Infinite dosing is an experimental condition that assumes that there is no change in the Cdonor (permeant) concentration throughout the experiment.

6.2.8. Tissue Integrity Studies

6.2.8.1. Transepithelial Electrical Resistance

Tissue sections were inserted onto Transwell membrane inserts (6.5 mm, 0.4 µm, 0.33 mm^2) and 0.1 ml PBS was added to the apical side while 0.6 ml PBS was added to the basolateral side into the culture wells. A Millicel® ERS-2 hand-held resistivity meter was used to measure the tissue resistance of membranes before and after permeability experiments.

6.2.8.2. Fourier Transform Infrared (FTIR) Spectroscopy.

FTIR was also used in conjunction with resistance tests to check the tissue integrity of the pericardium before and after 24 h of the *ex vivo* permeation experiment. Samples of porcine pericardium (before and after), and human pericardium (before and after) were analysed at 110 psi pressure in a range of 4000–650 cm^{-1} over 20 scans to obtain relevant spectra.

6.2.9. Statistical Analysis

An unpaired Student *t*-test with Welch's correction was utilised to compare possible differences between the steady state flux values and apparent permeability constants of bedaquiline across the human and porcine pericardial tissues, using a significance level of 5%.

6.3. Results and Discussion

6.3.1. Assessment of BDQ-Loaded COS-MN NPs Regarding Particle Size, Zeta Potential, and Morphology

Chitosan NPs are prepared mainly by ionic gelation, whereby chitosan is dissolved in an acetic acid solution containing Tween 80, followed by the addition of TPP to allow crosslinking of the particles under stirring. Hydrophobic drugs are dissolved in an organic solvent such as dichloromethane and added dropwise into the chitosan solution before cross-linking with TPP (Sharma et al., 2019). Recently bedaquiline-loaded chitosan nanoparticles have been synthesised with improved drug release compared to conventional NPs (Rawal et al., 2018). In this study, water-soluble COS, and MN in the presence of tween 80, without acetic acid were crosslinked with TPP for encapsulation of BDQ.

The average hydrodynamic size and zeta potential were measured as 192.4 nm (Figure 6.3a) and 40.5 mV (Figure 6.3b), respectively, and the overall morphology of the nanosystem was found to be roughly spherically shaped as per smooth electron microscopy imaging (SEM) (Figure 6.3c).

Due to the 5 kV EHT applied on the nanosystem in imaging, the outermost layer of the nanosystem melted, which could be attributed to MN, which is heat sensitive. The size was thus in the desired 100-200 nm size range for macrophage internalization (Pang et al., 2016). Furthermore, the cationic potential and presence of MN will allow high uptake of the nanoparticles by the macrophage's negatively charged sialic acid and mannose receptors, respectively (Cummings, 2022). The nanoparticles' polydispersity index (PDI) was recorded as 0.199, indicating colloidal stability and minimal aggregation in dispersed aqueous media. The PDI and the zeta potential concurrently demonstrated viability as a systemic nano drug-delivery system.

(a)

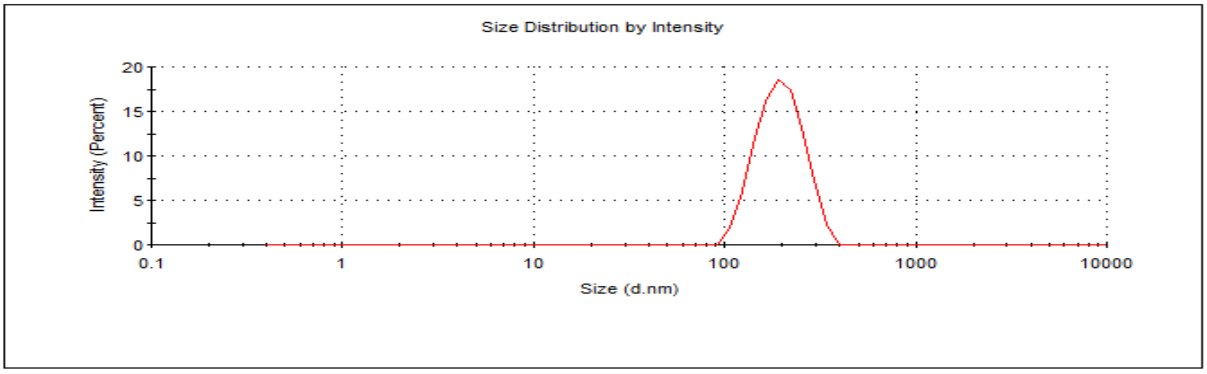

(b)

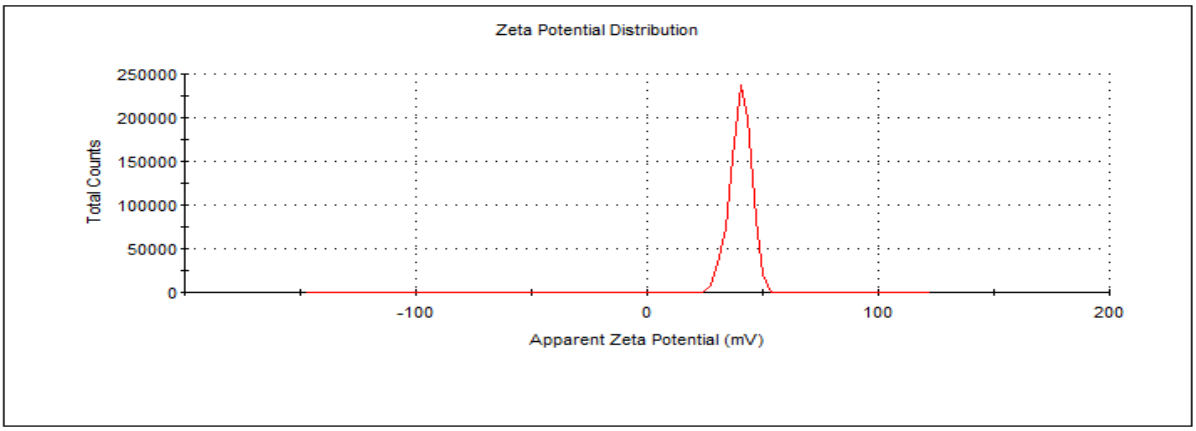

(c)

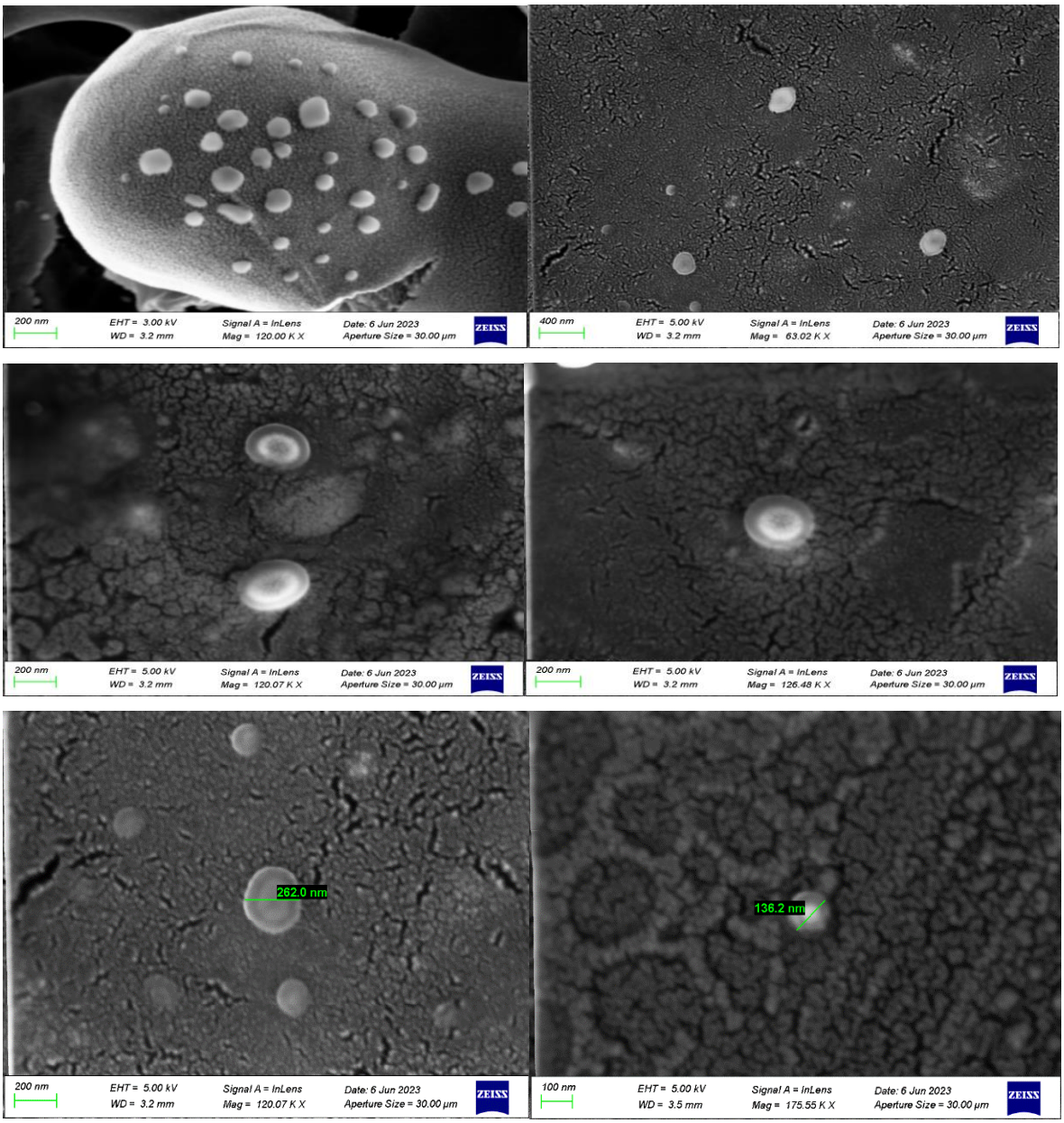

Figure 6.3: (a) A graphical representation of bedaquiline-loaded mannan conjugated chitosan oligosaccharide nanopartices average hydrodynamic size, (b) surface potential and (c) smooth electron microscopy (SEM) images at magnification (top left (120.00kx, EHT=3.00 kV); top right (63.02 Kx, EH 5.00 kV); bottom left (126.48 Kx, EH 5.00 kV); bottom right (120.07 Kx, EHT= 5.00 kV).

6.3.2. Assessment of Functional Transformation of the BDQ-Loaded COS-MN NPs

The FTIR spectra of COS, MN, BDQ and the drug-loaded nanoparticles are depicted in Figure 6.4. The pristine COS exhibited characteristic broad absorption peaks at 3248 cm^{-1} which is

attributed to OH stretch. The CH- stretch appeared at 2883 cm^{-1}, whilst the C=O stretch from the lactate derivative and amide (II) bending appeared at 1618 cm^{-1} and 1586 cm^{-1}, respectively. The 1376 cm^{-1} absorption peak indicates the C-C bending. The intense absorption peaks at 1062 cm^{-1} and 1028 cm^{-1} are attributed to the asymmetric C–O–C bridge and skeletal vibrations characteristic of its saccharide structure (Smitha et al., 2005). These peaks were in correspondence with the observed peaks on the drug-loaded nanosystem: 3338 cm^{-1} (O-H stretch), 2870 cm^{-1} (C-H stretch), 1632 cm^{-1} and 1523 cm^{-1} (C=O stretch and NH_2 bending), 1063 cm^{-1} and 1028 cm^{-1} (asymmetric C–O–C bridge). The shift in the amine and amide peaks indicates cross-linking between COS and sTPP (Mndlovu et al., 2019). The pristine MN exhibited a broad absorption peak at 3320 cm^{-1}, indicative of the OH stretch. The peak at 2929 cm^{-1} represents the symmetric and asymmetric CH- CH-stretching vibrations which are characteristic of polysaccharides (Hong et al., 2021; Zhao et al., 2022). The pyranose ring (C-O-C stretching) of MN is suggested by the 1021 cm^{-1} peak. Absorption peaks at 913 cm^{-1} and 811 cm^{-1}, which are used to access purity, are also characteristics of MN, further indicative of α-glycosidic linkage in the pyranose of MN (Cavagna et al., 2010; Yang and Zhang, 2009; and Yehia et al., 2022). The peaks were in accordance with the observed peaks on the drug-loaded nanosystem: 3338 cm^{-1} (O-H stretch), and 2870 cm^{-1} (C-H stretch) with a higher absorbance due to the co-polymeric complex with COS. The peak at 1643 cm^{-1} on MN (C=O stretching) shifted and became sharper on the loaded nanoparticle to 1735 cm^{-1} indicative of the co-polymeric complexation. Oligosaccharide chains are short and contain 2-10 sugar units (Lan et al., 2020). This complexation may occur by a ring opening and proton transfer from the O–H group of either polymer at the beginning or end of the chain to the O within the pyranose ring of either polymer thereby forming a carbonyl group (C=O) (Ellerbrock and Gerke, 2021). The pristine bedaquiline spectra showed characteristic peaks of ether (1180 cm^{-1} and 1081 cm^{-1}) and aromatic (3054 cm^{-1}, 3028 cm^{-1}, 2975 cm^{-1}, 2946 cm^{-1}, 1614 cm^{-1}, 1596 cm^{-1}, 1455 cm^{-1}, 1250 cm^{-1}) functional groups (Parvathaneni et al., 2021). In the drug-loaded nanoparticles, most peaks disappeared confirming the encapsulation of the nanosystem, with only faint absorbance at 1455 cm^{-1} and 1250 cm^{-1} showing the presence of bedaquiline in the nanosystem. The unloaded nanosystem displayed the same peaks as the loaded nanosystem. The absorbance at 3248 cm^{-1} which is attributed to OH stretch was observed to a greater extent in the unloaded nanosystem. This may be due to the interaction of chitosan with bedaquiline, covering up the bond as compared to the unloaded nanosystem.

(a) (b)

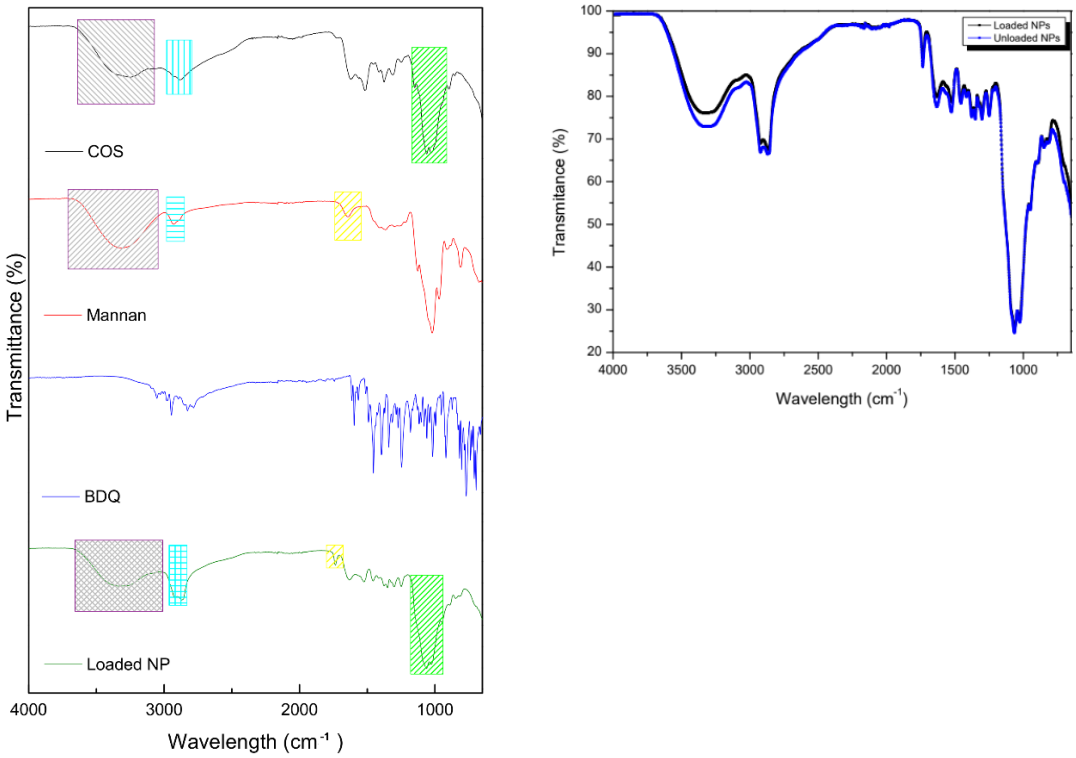

Figure 6.4: Fourier transform infrared spectroscopy images showing (a) the pristine mannan oligosaccharide, chitosan oligosaccharide lactate, bedaquiline, loaded nanoparticles, and (b) unloaded nanoparticles vs drug-loaded nanoparticles.

6.3.3. Determination of Powder Diffraction of BDQ-Loaded COS-MN NPs in Comparison to Individual Compounds

The diffraction patterns in Figure 6.5 show the crystalline nature of pristine BDQ, COS and MN and how they interact to form a nanoparticle. BDQ was observed to be highly crystalline with significant peaks at 2θ-10.5°, 11.5°, 16°, 18°, 20.5°, 24°, and 26.5°. Pristine COS exhibited typical saccharide amorphous peaks at 12° and a semicrystalline peak at 23° (Siafaka et al., 2016). Mannan showed a semi-crystalline peak at 20°, corresponding in intensity with the 21.5° peak on COS-MN BDQ-loaded nanoparticles. The loaded NP peak was a smoother semi-crystalline peak, due to a slight phase change in the crosslinking of MN with COS. The absence of BDQ crystalline peaks on the nanoparticles confirms the complete encapsulation of the drug in the co-polymeric matrix.

(a) (b)

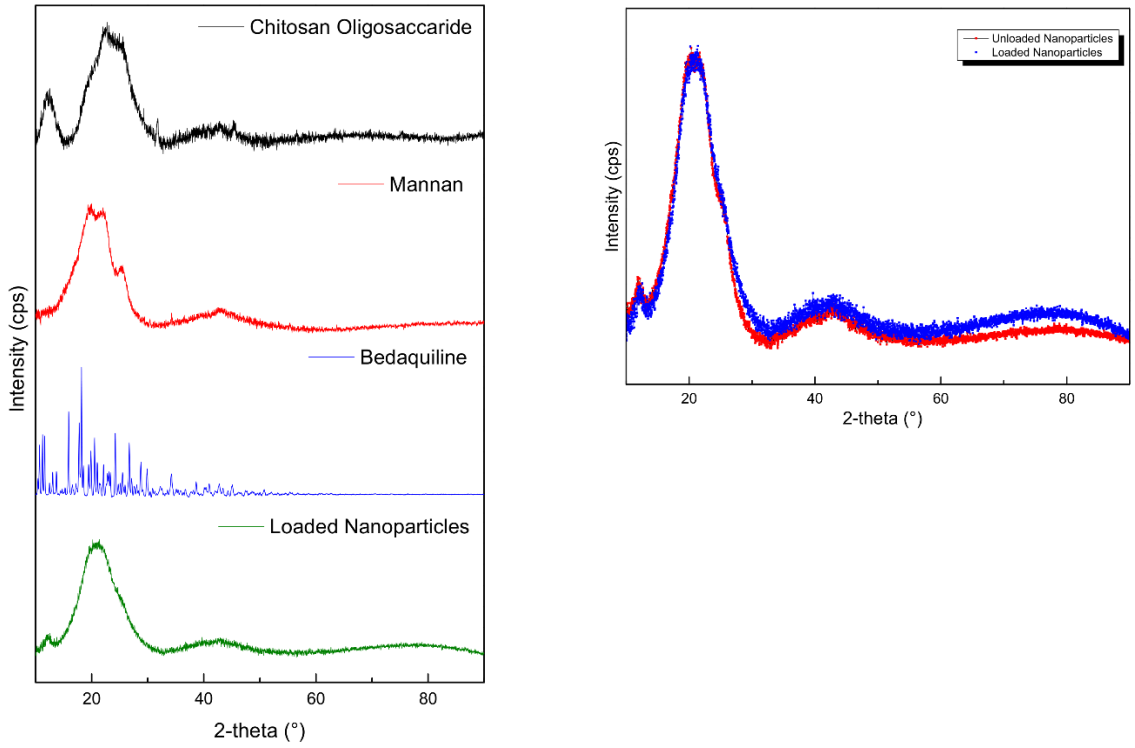

Figure 6.5: X-ray diffraction images of (a) the pristine mannan oligosaccharide, chitosan oligosaccharide lactate, bedaquiline, loaded nanoparticles, and (b) unloaded nanoparticle vs drug-loaded nanoparticles.

6.3.4. Thermo-Behavioural Analysis of BDQ-Loaded COS-MN NPs

As in Figure 6.6, the pristine COS, MN, and drug-loaded NPs showed a conserved weight loss below 100 °C due to dehydration. At 230 °C, 310 °C, and 220 °C, a decline is noticed for COS, MN and BDQ, respectively, indicating significant degradation of the components. The Loaded NPs showed a 2-step degradation at 240 °C and 380 °C corresponding to the loss of COS and MN, respectively. The shift in the exothermic peaks observed in the nanoparticles infers the partial cross-linking between sTPP and COS and interpolymer complexation between COS and MN resulting in a transition in thermal properties, indicative by an increase in the degradation temperature of the respective components. The unloaded nanoparticles showed an initial weight loss between 100 and 200 °C like that observed in COS. This degradation is not as significant in the loaded nanoparticles possibly suggesting the presence of bedaquiline binding to COS thus preventing its degradation.

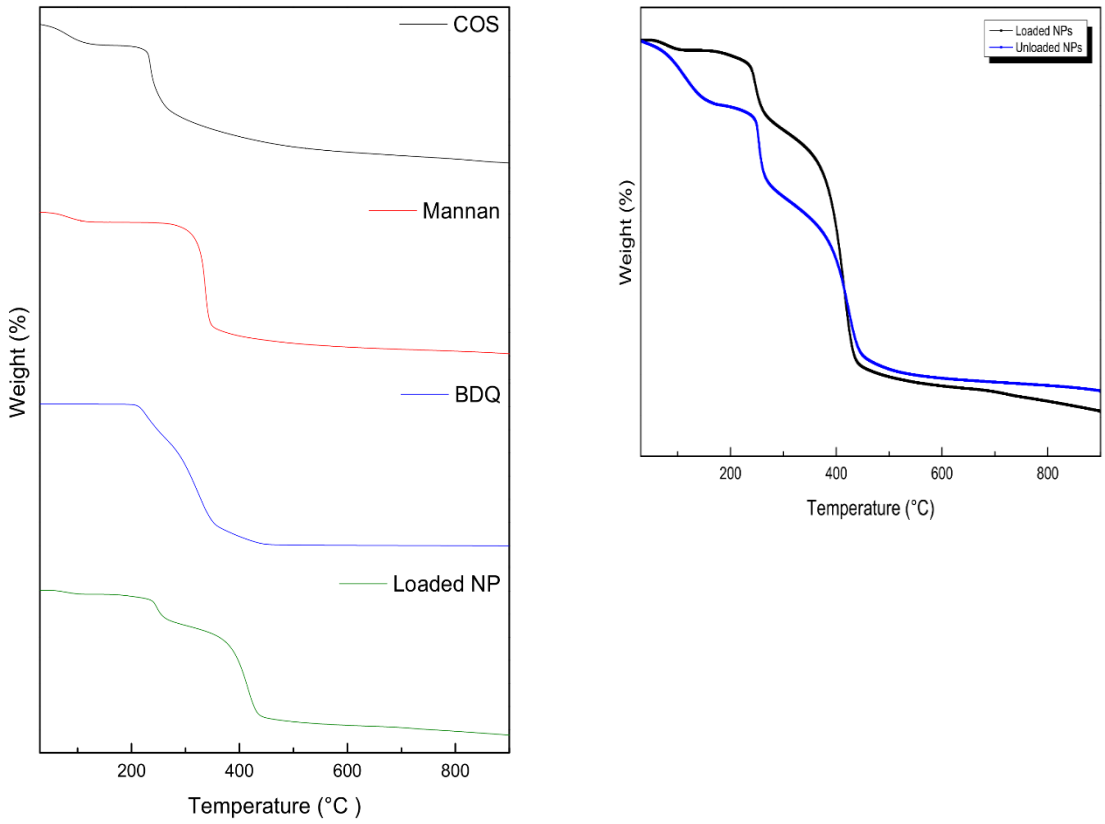

Figure 6.6: Thermogravimetric analysis of (a) the pristine mannan oligosaccharide, chitosan oligosaccharide lactate, bedaquiline loaded nanoparticles, and (b) unloaded nanoparticles vs drug-loaded nanoparticles.

6.3.5. Rheological and Syringeability Properties of BDQ-loaded COS-MN NPs

The nanosystem showed a gel-like behaviour whereby G'>G" as can be observed in Figure 6.7 below. The shear viscosity of COS-MN-NPs at 37 °C with varying shear rates from 0-2000 s^{-1} suggests a shear thinning property in the gel as the viscosity decreases with increasing shear rate. The viscoelastic nature (elastic (G′) and viscous (G″) modulus) of the nanosystem was also evaluated. Higher values of G′ modulus with a higher frequency indicated better gel strength at 37 °C (Badhe et al., 2017). The gel solution is found to be partially diluted as the difference in G′ and viscous G″ get closer to each other at higher frequency values. The viscoelastic modulus ranged from 10.56-52.82 Pa for the gel across the frequency range, showing applicable use in the pericardial space, without significantly affecting the pressure since the effective pericardial pressure is to remain between 0-133.32 Pa (Imazio, 2014).

The syringeability test was performed in triplicate under a flow rate of Q=0.1 ml.s^{-1}. The injection force was found to be 11.94 N well below the maximum force of 79.8 N that can be generated and applied on a syringe by humans (males: 95.4 N, females: 64.1 N) (Vo et al., 2016).

(a) (b)

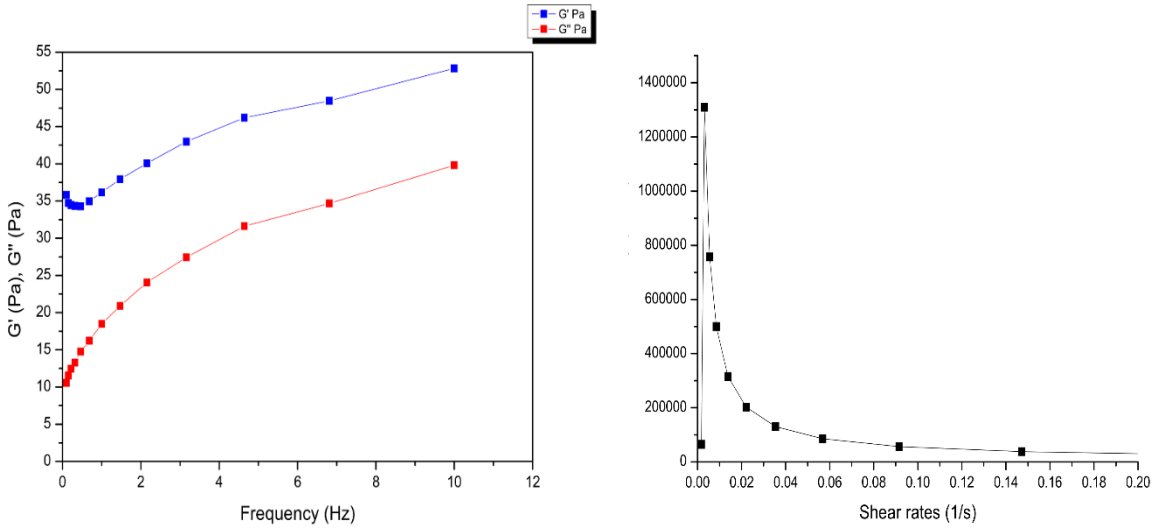

Figure 6.7: Rheological images showing (a) frequency sweep, and (b) viscosity sweep of the nanogel.

6.3.6. Evaluation of Mannan Content, BDQ-Loading Capacity and Drug Entrapment Efficacy of BDQ-Loaded COS-MN NPs

The phenol-sulfuric acid method works by sulfuric acid digestion and dehydration of the polysaccharide mannan to monosaccharide mannose (a hexose sugar), which further reacts with phenol to produce hydroxymethyl furfural, a yellowish-brown coloured mixture (Nielsen, 2010; Rodponthukwaji et al., 2021). In this study, the amount of mannan attached to the nanosystem was calculated to be 94.86%. The BDQ loading capacity was calculated to be 0.6% and the BDQ entrapment efficiency was 98.76% using RP-HPLC.

6.3.7. Evaluation of *In Vitro* Release of BDQ From the BDQ-Loaded COS-MN NPs

The drug release profile of BDQ was evaluated at pH 7.4 in 0.1 M PBS containing 0.2% SLS to mimic the pH of 7.34 of the pericardial fluid of pericardial tuberculosis (Shenje et al., 2015). The BDQ release at pH 7.4 reached a steady state from day 3 of release, with an average of 11.92% of the drug released after 20 days as depicted in Figure 6.8. Since bedaquiline is effective at very low concentrations with as low a MIC of 0.0039-0.25 µg.ml^{-1} (Lopez et al., 2019), the nanosystem

shows the potential to slowly release drugs at effective concentrations over an extended period and possibly result in the treatment of TBP after a single dose/administration.

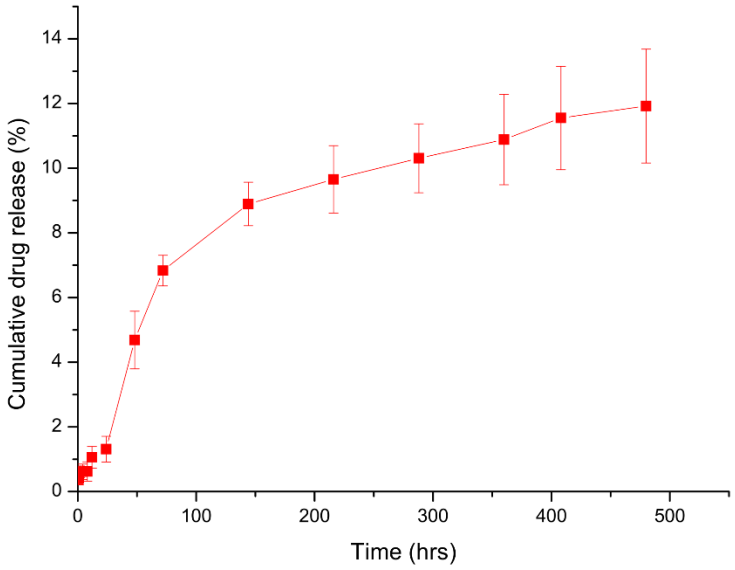

Figure 6.8: *In vitro* dissolution graph of bedaquiline nanoparticles drug release in phosphate buffer saline containing 0.2% sodium lauryl sulphate at pH 7.4 over 20 days (n=3). Error bars= standard error of mean.

6.3.8. Evaluation of *Ex Vivo* Diffusion Study of the BDQ-Loaded COS-MN NPs Across Porcine and Human Pericardium

The RP-HPLC method successfully quantified the amount of bedaquiline that diffused across the pericardium without interference from the nanoparticle components (Figure 6.9). Human and porcine pericardium displayed comparable results in their average cumulative permeation graphs (Figure 6.10). Steady-state flux values were reached as quickly as 2 h across both human and porcine pericardium. The steady-state fluxes were calculated to be 2.889 and 2.346 $\mu g.cm^{-2}.min^{-1}$ for porcine and human pericardium, respectively, the apparent permeability coefficient were calculated to be 2.66×10^{-4} $cm.min^{-1}$ and 2.16×10^{-4} $cm.min^{-1}$ for porcine and human pericardium, respectively. Bedaquiline diffusion across porcine pericardium was found to be slightly higher compared to human pericardium.

The results obtained indicate that the porcine pericardium represents a good model for human pericardium for *ex vivo* diffusion studies as there were no statistically significant differences ($p > 0.05$) (using an unpaired Student *t*-test with Welch's correction) found between the steady state

flux rates and apparent permeability coefficients of bedaquiline between porcine and human pericardial tissue. Both specimens showed a linear diffusion of the bedaquiline nanoparticle, with an instant to speedy steady state establishment, and a constant cumulative drug permeating over time. With poor penetration of standard anti-tuberculosis treatment (ATT) across the pericardium, other interventions needed to be identified to treat the second most lethal version of extrapulmonary tuberculosis, tuberculosis pericarditis. The results obtained in this study therefore clearly indicate prospects of the nanosystem to allow the permeation of bedaquiline at effective concentration consistently.

Bedaquiline is a very lipophilic molecule with a molecular weight of 555.50 $g.mol^{-1}$ and a very high log P value of 7.74 (PubChem). No *ex vivo* permeation studies have been performed on pericardial tissue to determine its correlation of log P to permeation across the tissue to date, but studies on other tissues in the body, have reported that the apparent permeability coefficient and Log P demonstrate a proportional relationship (Lee et al., 2005; Schmitt, 2008), therefore a compound with a high log P (more lipophilic molecule) value is expected to permeate the pericardium better.

The improved permeation and drug release of bedaquiline *ex vivo* as compared to *in vitro* dissolution studies may be attributed to the presence of biofactors in snap-frozen tissues (Svensson et al., 2007). Chitosan/COS is prone to lysosomal biodegradation through hydrolysis (Jiménez-Gómez and Cecilia, 2020; Muanprasat and Chatsudthipong, 2017). Lysosomes are present in all human cells, the improved permeation and release of bedaquiline as evident in the results, may be due to the lysosomal factor on the nanosystem after transcellular permeation since chitosan permeates through paracellular/transcellular pathways (Liang et al., 2017). This may suggest a controlled drug-release polymeric nanosystem whereby drug release occurs by degradation/erosion of the matrix rather than diffusion (Lu et al., 2011; Muanprasat and Chatsudthipong, 2017).

(a)

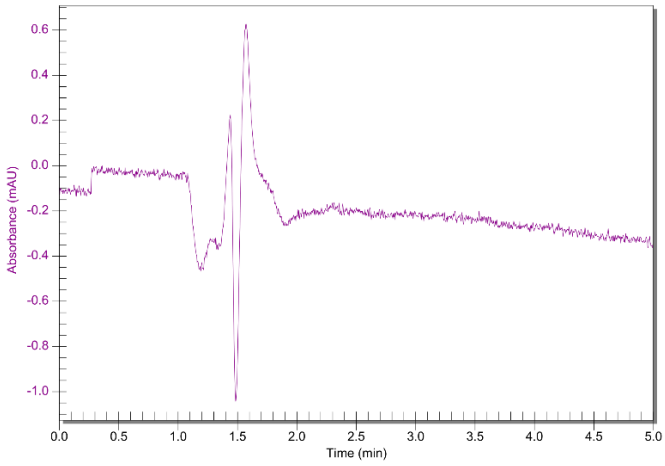

(b)

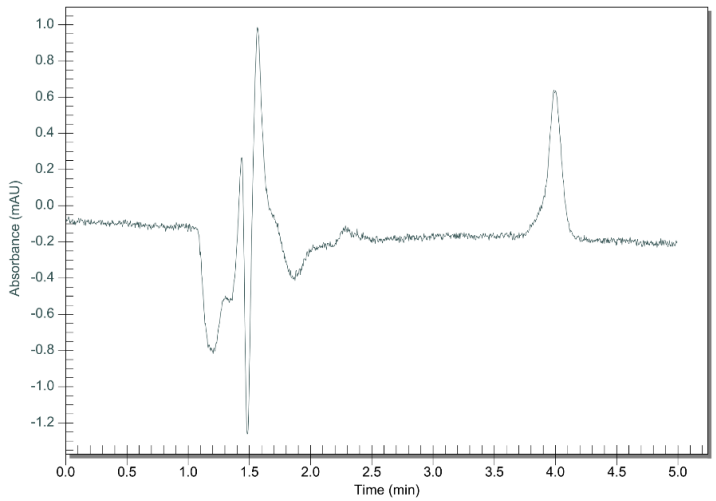

Figure 6.9: RP C18-HPLC chromatograms showing the eluents collected during the *ex vivo* studies across human pericardium for (a) control (unloaded nanosystem) (b) bedaquiline-loaded nanosystem with a retention time of 4.02 for bedaquilinne in phosphate buffer saline pH 7.4 containing 0.2% sodium lauryl sulphate.

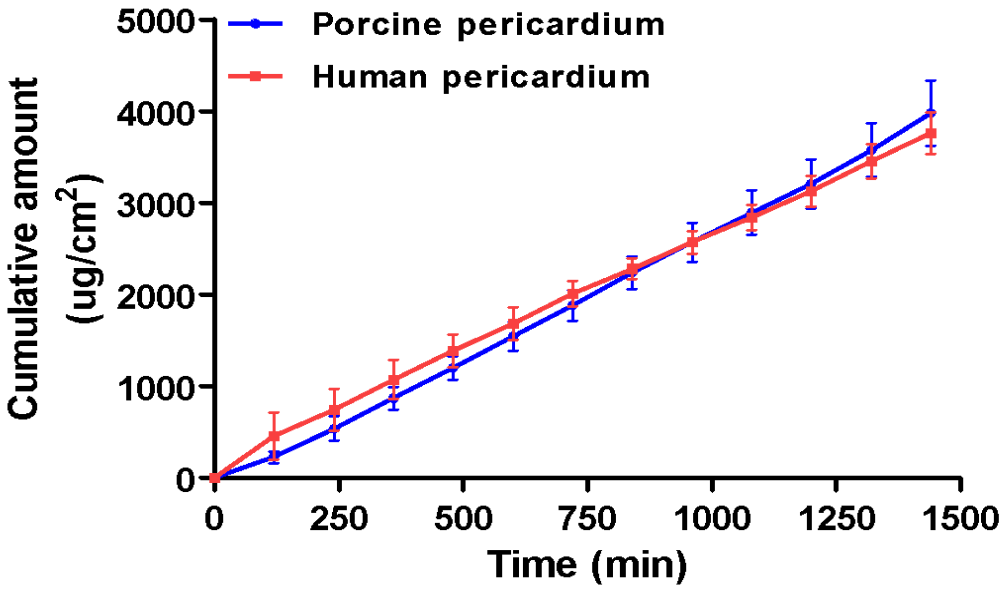

Figure 6.10: Cumulative amount vs time graph of bedaquilline diffusion from the bedaquiline loaded nanosystem across *ex vivo* porcine and human pericardium (n=14). Error bars =standard error of mean. Due to the insolubility of bedaquiline in aqueous media, a bedaquilline aqueous solution was impossible to test across the tissue, therefore necessitating the incorporation of the drug into a nanosystem.

6.3.9. Tissue Integrity Study

The integrity of the porcine and human pericardial tissue over 24 h of exposure to the bedaquiline nanosystem was evaluated using tissue resistance measurements. The transepithelial electrical resistance change across the pericardial tissue before and after the diffusion study (n=3) showed no statistically significant change with a mean percentage difference of 4.43 ± 0.49 % and 2.78 ± 1.14 % ($p > 0.05$) for porcine and human pericardium, respectively (Table 6.1). This implies that the tissue integrity was not affected by the nanosystem or the colleting media throughout the experiment.

Pericardium contains mainly type 1 collagen, glycoproteins and glycosaminoglycans (Rémi et al., 2011). This is concurrent with the characteristic absorption peaks between 3000 cm^{-1} and 2800 cm^{-1} showing a lipid hydrocarbon absorption. The peak at 1630 cm^{-1} is attributed to amide I - C=O stretching of the backbone of the proteins. Furthermore, the peak at 1550 cm^{-1} indicates an amide II bond showing the N-H bending coupled to C-N stretching. The 1454 cm^{-1} peak shows asymmetric and symmetric C-H bending from CH_2 and CH^3 on proteins. The 1400 cm^{-1} peak is indicative of C=O vibrations of COO^- from free amino acids and polypeptides in the pericardial

structure. Amide III from proteins is characterized by the 1338 cm^{-1} peak. The 1033 cm^{-1} peak indicates C-O vibrations from polysaccharides in glycoproteins and glycosaminoglycans (Ami et al., 2016; Zhang et al., 2017). There was immutability in the transmittance of the bonds on the mesothelial pericardial tissue across the range of 4000–650 cm^{-1} over 20 scans before and after the diffusion study (Figure 6.11). There were no statistically significant differences ($p > 0.05$) before and after the diffusion study, suggesting that tissue integrity was not compromised by the nanoparticle or collecting media.

Table 6.1: The transepithelial electrical resistance changes across the membrane before and after the diffusion study for porcine and human pericardium done in triplicate. Each reading was repeated three times.

Mean Electrical resistance Ohm (SD)	Human Pericardium (n=3)			Porcine Pericardium (n=3)		
	(1)	(2)	(3)	(1)	(2)	(3)
Before diffusion study	150.67 (4.64)	166.33 (5.43)	153.00 (5.10)	147.33 (4.99)	151.00 (2.16)	138.33 (5.25)
After diffusion study	147.67 (6.24)	163.00 (2.16)	146.33 (4.50)	152.00 (2.83)	159.00 (2.16)	131.67 (5.25)
Difference (%)	1.99 (1.06)	2.00 (1.97)	4.36 (0.39)	3.17 (1.47)	5.30 (0.00)	4.82 (0.00)
Mean Difference (%)	2.78 (1.14)			4.43 (0.49)		

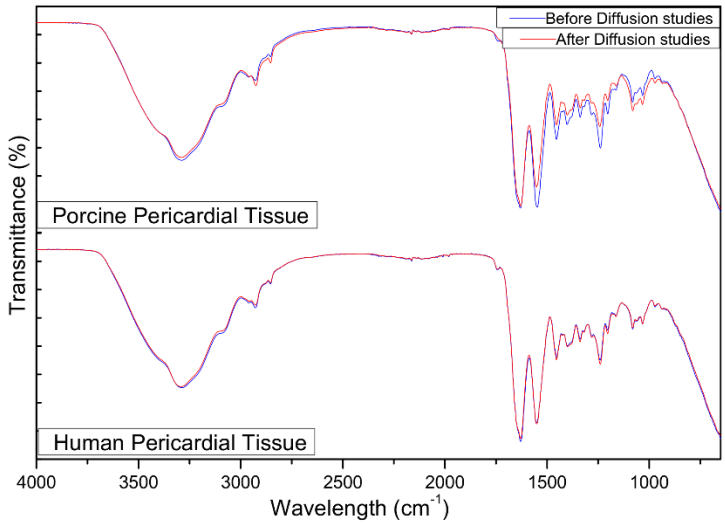

Figure 6.11: Fourier transform infrared spectroscopy images of the porcine and human pericardium before and after 24 h of *ex vivo* diffusion study.

6.4. CONCLUSION

The bedaquiline-loaded chitosan-mannan copolymeric nanosystem was successfully synthesised. The size was verified to be mostly between 100-200 nm using both zeta sizer and SEM. The drug showed complete encapsulation into the nanosystem as per SEM and FTIR and encapsulation efficiency. Mannan enhanced the gelling ability of the nanosystem with further properties to ensure targeted delivery. The excellent permeation and release of the nanosystem *ex vivo* as compared to *in vitro* dissolution studies is possibly due to bio-factors such as enzymatic degradation from the snap frozen *ex vivo* tissue (Svensson et al., 2009). The tissue integrity was maintained however more studies need to be done to confirm the effect of the nanosystem on the barrier. Enzymatic hydrolysis of chitosan by lysosomes, an organelle containing proteolytic enzyme found in pericardial cells may therefore improve the drug release across the pericardium as chitosan is prone to enzymatic biodegradation in the body. Results from the study indicate prospects of bedaquiline's ability to permeate across the pericardium as compared to the standard anti-tuberculosis treatment against tuberculous pericarditis.

6.5. REFERENCES

Ami, D., Lavatelli, F., Rognoni, P., Palladini, G., Raimondi, S., Giorgetti, S., Monti, L., Doglia, S. M., Natalello, A., and Merlini, G. (2016). In situ characterization of protein aggregates in human tissues affected by light chain amyloidosis: a FTIR microspectroscopy study. Scientific Reports, 6(1), 29096.

Andrade, R. G. D., Reis, B., Costas, B., Lima, S. A. C., and Reis, S. (2020). Modulation of macrophages M1/M2 polarization using carbohydrate-functionalized polymeric nanoparticles. Polymers, 13(1), 88.

Badhe, R. V, Bijukumar, D., Chejara, D. R., Mabrouk, M., Choonara, Y. E., Kumar, P., du Toit, L. C., Kondiah, P. P. D., and Pillay, V. (2017). A composite chitosan-gelatin bi-layered, biomimetic macroporous scaffold for blood vessel tissue engineering. Carbohydrate Polymers, 157, 1215–1225.

Baranyai, Z., Soria-Carrera, H., Alleva, M., Millán-Placer, A. C., Lucía, A., Martín-Rapún, R., Aínsa, J. A., and de la Fuente, J. M. (2021). Nanotechnology-based targeted drug delivery: an emerging tool to overcome tuberculosis. Advanced Therapeutics, 4(1), 2000113.

Baykan, A. H., Sayiner, H. S., Aydin, E., Koc, M., Inan, I., and Erturk, S. M. (2022). Extrapulmonary tuberculosıs: an old but resurgent problem. Insights Into Imaging, 13(1), 1–21.

Bosurgi, L., Cao, Y. G., Cabeza-Cabrerizo, M., Tucci, A., Hughes, L. D., Kong, Y., Weinstein, J. S., Licona-Limon, P., Schmid, E. T., and Pelorosso, F. (2017). Macrophage function in tissue repair and remodeling requires IL-4 or IL-13 with apoptotic cells. Science, 356(6342), 1072–1076.

Burgess L, J., Reuter, H., Carstens M, E., Taljaard JJ, F., and Doubell A, F. (2002). Cytokine production in patients with tuberculous pericarditis. The International Journal of Tuberculosis and Lung Disease, 6(5), 439–446.

Carrión-Prieto, P., Martín-Ramos, P., Hernández-Navarro, S., Sánchez-Sastre, L. F., Marcos-Robles, J. L., and Martín-Gil, J. (2018). Furfural, 5-HMF, acid-soluble lignin and sugar contents in C. ladanifer and E. arborea lignocellulosic biomass hydrolysates obtained from microwave-assisted treatments in different solvents. Biomass and Bioenergy, 119, 135–143.

Chahine, E. B., Dougherty, J. A., Thornby, K.-A., and Guirguis, E. H. (2022). Antibiotic approvals in the last decade: are we keeping up with resistance? Annals of Pharmacotherapy, 56(4), 441–462.

Chen, L., Zhang, S., Wu, S., Ren, Z., Liu, G., and Wu, J. (2021). Synergistic protective effect of Konjac Mannan oligosaccharides and Bacillus subtilis on intestinal epithelial barrier dysfunction in Caco-2 cell model and mice model of lipopolysaccharide stimulation. Frontiers in Immunology, 12, 696148.

Cummings, R. D. (2022). The mannose receptor ligands and the macrophage glycome. Current Opinion in Structural Biology, 75, 102394.

De Matteis, L., Jary, D., Lucía, A., García-Embid, S., Serrano-Sevilla, I., Pérez, D., Aínsa, J. A., Navarro, F. P., and De la Fuente, J. M. (2018). New active formulations against M. tuberculosis: Bedaquiline encapsulation in lipid nanoparticles and chitosan nanocapsules. Chemical Engineering Journal, 340, 181–191.

Deniset, J. F., Belke, D., Lee, W.-Y., Jorch, S. K., Deppermann, C., Hassanabad, A. F., Turnbull, J. D., Teng, G., Rozich, I., and Hudspeth, K. (2019). Gata6+ pericardial cavity macrophages relocate to the injured heart and prevent cardiac fibrosis. Immunity, 51(1), 131–140.

Ellerbrock, R. H., and Gerke, H. H. (2021). FTIR spectral band shifts explained by OM–cation interactions. Journal of Plant Nutrition and Soil Science, 184(3), 388–397.

Faustino, M., Durão, J., Pereira, C. F., Pintado, M. E., and Carvalho, A. P. (2021). Mannans and mannan oligosaccharides (MOS) from Saccharomyces cerevisiae–A sustainable source of functional ingredients. Carbohydrate Polymers, 272, 118467.

Ganchua, S. K. C., Cadena, A. M., Maiello, P., Gideon, H. P., Myers, A. J., Junecko, B. F., Klein, E. C., Lin, P. L., Mattila, J. T., and Flynn, J. L. (2018). Lymph nodes are sites of prolonged bacterial persistence during *Mycobacterium tuberculosis* infection in macaques. Public Library of Science Pathogens, 14(11), e1007337.

Gopalaswamy, R., Dusthackeer, V. N. A., Kannayan, S., and Subbian, S. (2021). Extrapulmonary tuberculosis—an update on the diagnosis, treatment and drug resistance. Journal of Respiration, 1(2), 141–164.

Gulati, N., Dua, K., and Dureja, H. (2021). Role of chitosan based nanomedicines in the treatment of chronic respiratory diseases. International Journal of Biological Macromolecules, 185, 20–30.

Gupta, A., and Gupta, G. S. (2022). Applications of mannose-binding lectins and mannan glycoconjugates in nanomedicine. Journal of Nanoparticle Research, 24(11), 228.

Hong, T., Yin, J.-Y., Nie, S.-P., and Xie, M.-Y. (2021). Applications of infrared spectroscopy in polysaccharide structural analysis: Progress, challenge and perspective. Food Chemistry: X, 12, 100168.

Ignjatović, N. L., Sakač, M., Kuzminac, I., Kojić, V., Marković, S., Vasiljević-Radović, D., Wu, V. M., Uskoković, V., and Uskoković, D. P. (2018). Chitosan oligosaccharide lactate coated hydroxyapatite nanoparticles as a vehicle for the delivery of steroid drugs and the targeting of breast cancer cells. Journal of Materials Chemistry B, 6(43), 6957–6968.

Ilgazli, A., Boyaci, H., Basyigit, İ., and Yildiz, F. (2004). Extrapulmonary tuberculosis: clinical and epidemiologic spectrum of 636 cases. Archives of Medical Research, 35(5), 435–441.

Imazio, M. (2014). Pericardial diseases. Evidence-Based Cardiology Consult, 79–89.

Isiguzo, G., Du Bruyn, E., Howlett, P., and Ntsekhe, M. (2020). Diagnosis and management of tuberculous pericarditis: what is new? Current Cardiology Reports, 22, 1–8.

Jiménez-Gómez, C. P., and Cecilia, J. A. (2020). Chitosan: a natural biopolymer with a wide and varied range of applications. Molecules, 25(17), 3981.

Kant, S., Maurya, A. K., Nag, V. L., and Bajpai, J. (2018). Rising trend of drug resistance among extra pulmonary TB in Northern India. European Respiratory Society. 52(suppl 62):PA3681.

Ko, J. A., Park, H. J., Hwang, S. J., Park, J. B., and Lee, J. S. (2002). Preparation and characterization of chitosan microparticles intended for controlled drug delivery. International Journal of Pharmaceutics, 249(1–2), 165–174.

Lan, J., Wang, K., Chen, G., Cao, G., and Yang, C. (2020). Effects of inulin and isomalto-oligosaccharide on diphenoxylate-induced constipation, gastrointestinal motility-related hormones, short-chain fatty acids, and the intestinal flora in rats. Food and Function, 11(10), 9216–9225.

Lee, J. H., Lee, V. J., Yoon, M. K., and Choi, Y. W. (2005). Ex vivo Permeability Characteristics of Porcine Buccal Mucosa to Drugs with Various Polarity. 약제학회지, 35(2), 71–74.

Lee, T., and Dugoua, J.-J. (2011). Nutritional supplements and their effect on glucose control. Current Diabetes Reports, 11, 142–148.

Lemmer, H. J. R., and Hamman, J. H. (2013). Paracellular drug absorption enhancement through tight junction modulation. Expert Opinion on Drug Delivery, 10(1), 103–114.

Liang, J., Yan, H., Puligundla, P., Gao, X., Zhou, Y., and Wan, X. (2017). Applications of chitosan nanoparticles to enhance absorption and bioavailability of tea polyphenols: A review. Food Hydrocolloids, 69, 286–292.

Liebenberg, J. J., Dold, C. J., and Olivier, L. R. (2016). A prospective investigation into the effect of colchicine on tuberculous pericarditis: cardiovascular topics. Cardiovascular Journal of Africa, 27(6), 350–355.

Liu, Y., Huang, G., and Lv, M. (2018). Extraction, characterization and antioxidant activities of mannan from yeast cell wall. International Journal of Biological Macromolecules, 118, 952–956.

Lopez, B., Siqueira de Oliveira, R., Pinhata, J. M. W., Chimara, E., Pacheco Ascencio, E., Puyén Guerra, Z. M., Wainmayer, I., Simboli, N., Del Granado, M., and Palomino, J. C. (2019). Bedaquiline and linezolid MIC distributions and epidemiological cut-off values for *Mycobacterium tuberculosis* in the Latin American region. Journal of Antimicrobial Chemotherapy, 74(2), 373–379.

Lu, X.-Y., Wu, D.-C., Li, Z.-J., and Chen, G.-Q. (2011). Polymer nanoparticles. Progress in Molecular Biology and Translational Science, 104, 299–323.

Lua, I., and Asahina, K. (2016). The role of mesothelial cells in liver development, injury, and regeneration. Gut and Liver, 10(2), 166.

Luo, Q., Zhao, J., Zhang, X., and Pan, W. (2011). Nanostructured lipid carrier (NLC) coated with Chitosan Oligosaccharides and its potential use in ocular drug delivery system. International Journal of Pharmaceutics, 403(1–2), 185–191.

Maddur Taluk, M. D. (2022). Preparation and evaluation of bedaquiline loaded microspheres by solvent evaporation technique. World Journal of Pharmaceutical Research, 11(12), 1432-1444.

Mir, M., Ishtiaq, S., Rabia, S., Khatoon, M., Zeb, A., Khan, G. M., ur Rehman, A., and ud Din, F. (2017). Nanotechnology: from in vivo imaging system to controlled drug delivery. Nanoscale Research Letters, 12, 1–16.

Mndlovu, H., du Toit, L. C., Kumar, P., Marimuthu, T., Kondiah, P. P. D., Choonara, Y. E., and Pillay, V. (2019). Development of a fluid-absorptive alginate-chitosan bioplatform for potential application as a wound dressing. Carbohydrate Polymers, 222, 114988.

Muanprasat, C., and Chatsudthipong, V. (2017). Chitosan oligosaccharide: Biological activities and potential therapeutic applications. Pharmacology and Therapeutics, 170, 80–97.

Nacarapa, E., Munyangaju, I., Osório, D., Zindoga, P., Mutaquiha, C., Jose, B., Macuacua, A., Chongo, B., de-Almeida, M., and Verdu, M.-E. (2022). Extrapulmonary tuberculosis mortality according to clinical and point of care ultrasound features in Mozambique. Scientific Reports, 12(1), 16675.

Nielsen, S. S. (2010). Phenol-sulfuric acid method for total carbohydrates. Food Analysis Laboratory Manual, 47–53.

Nopvichai, C., Charoenwongpaiboon, T., Luengluepunya, N., Ito, K., Muanprasat, C., and Pichyangkura, R. (2019). Production and purification of mannan oligosaccharide with epithelial tight junction enhancing activity. PeerJ, 7, e7206.

Onitake, T., Ueno, Y., Tanaka, S., Sagami, S., Hayashi, R., Nagai, K., Hide, M., and Chayama, K. (2015). Pulverized konjac glucomannan ameliorates oxazolone-induced colitis in mice. European Journal of Nutrition, 54, 959–969.

Pang, L., Qin, J., Han, L., Zhao, W., Liang, J., Xie, Z., Yang, P., and Wang, J. (2016). Exploiting macrophages as targeted carrier to guide nanoparticles into glioma. Oncotarget, 7(24), 37081.

Park, K., Na, K., Lee, Y. S., Chang, W., Park, J., Akaike, T., and Kim, D. K. (2007). Effects of mannosylated glycopolymers on specific interaction to bone marrow hematopoietic and progenitor cells derived from murine species. Journal of Biomedical Materials Research Part A:

An Official Journal of The Society for Biomaterials, The Japanese Society for Biomaterials, and The Australian Society for Biomaterials and the Korean Society for Biomaterials, 82(2), 281–287.

Parvathaneni, V., Elbatanony, R. S., Goyal, M., Chavan, T., Vega, N., Kolluru, S., Muth, A., Gupta, V., and Kunda, N. K. (2021). Repurposing bedaquiline for effective non-small cell lung Cancer (NSCLC) therapy as inhalable cyclodextrin-based molecular inclusion complexes. International Journal of Molecular Sciences, 22(9), 4783.

Pepić, I., Hafner, A., Lovrić, J., Pirkić, B., and Filipović-Grčić, J. (2010). A nonionic surfactant/chitosan micelle system in an innovative eye drop formulation. Journal of Pharmaceutical Sciences, 99(10), 4317–4325.

Pepić, I., Lovrić, J., and Filipović-Grčić, J. (2013). How do polymeric micelles cross epithelial barriers? European Journal of Pharmaceutical Sciences, 50(1), 42–55.

Prakasha, S. R., Suresh, G., D'sa, I. P., Shetty, S. S., and Kumar, S. G. (2013). Mapping the pattern and trends of extrapulmonary tuberculosis. Journal of Global Infectious Diseases, 5(2), 54.

Ramasamy, V., Mayosi, B. M., Sturrock, E. D., and Ntsekhe, M. (2018). Established and novel pathophysiological mechanisms of pericardial injury and constrictive pericarditis. World Journal of Cardiology, 10(9), 87.

Rawal, T., Patel, S., and Butani, S. (2018). Chitosan nanoparticles as a promising approach for pulmonary delivery of bedaquiline. European Journal of Pharmaceutical Sciences, 124, 273–287.

Rémi, E., Khelil, N., Di Centa, I., Roques, C., Ba, M., Medjahed-Hamidi, F., Chaubet, F., Letourneur, D., Lansac, E., and Meddahi-Pellé, A. (2011). Pericardial processing: challenges, outcomes and future prospects. In Biomaterials science and engineering. IntechOpen.

Rodponthukwaji, K., Saengruengrit, C., Tummamunkong, P., Leelahavanichakul, A., Ritprajak, P., and Insin, N. (2021). Facile synthesis of magnetic silica-mannan nanocomposites for enhancement in internalization and immune response of dendritic cells. Materials Today Chemistry, 20, 100417.

Schmitt, W. (2008). General approach for the calculation of tissue to plasma partition coefficients. Toxicology in vitro, 22(2), 457–467.

Sharma, M., Sharma, R., Jain, D. K., and Saraf, A. (2019). Enhancement of oral bioavailability of poorly water soluble carvedilol by chitosan nanoparticles: Optimization and pharmacokinetic study. International Journal of Biological Macromolecules, 135, 246–260.

Sharma, S. K., Mohan, A., and Kohli, M. (2021). Extrapulmonary tuberculosis. Expert Review of Respiratory Medicine, 15(7), 931–948.

Shenje, J., Adimora-Nweke, F. I., Ross, I. L., Ntsekhe, M., Wiesner, L., Deffur, A., McIlleron, H. M., Pasipanodya, J., Gumbo, T., and Mayosi, B. M. (2015). Poor penetration of antibiotics into pericardium in pericardial tuberculosis. EBioMedicine, 2(11), 1640–1649.

Siafaka, P. I., Zisi, A. P., Exindari, M. K., Karantas, I. D., and Bikiaris, D. N. (2016). Porous dressings of modified chitosan with poly (2-hydroxyethyl acrylate) for topical wound delivery of levofloxacin. Carbohydrate Polymers, 143, 90–99.

Simionescu, M., and Simionescu, N. (1977). Organization of cell junctions in the peritoneal mesothelium. The Journal of Cell Biology, 74(1), 98–110.

Singh, S., Singh, G., and Arya, S. K. (2018). Mannans: An overview of properties and application in food products. International Journal of Biological Macromolecules, 119, 79–95.

Smith, H., Grant, S., Parker, J., and Murphy, R. (2020). Yeast cell wall mannan-rich fraction modulates bacterial cellular respiration potentiating antibiotic efficacy. Scientific Reports, 10(1), 21880.

Smitha, B., Sridhar, S., and Khan, A. A. (2005). Chitosan–sodium alginate polyion complexes as fuel cell membranes. European Polymer Journal, 41(8), 1859–1866.

Svensson, M., Borén, M., Skold, K., Fälth, M., Sjogren, B., Andersson, M., Svenningsson, P., Andrén, P.E., 2009. Heat stabilization of the tissue proteome: a new technology for improved proteomics. Journal of Proteome Research, 8(2), 974-981.

Tang, J., Liu, J., Yan, Q., Gu, Z., August, A., Huang, W., and Jiang, Z. (2021). Konjac glucomannan oligosaccharides prevent intestinal inflammation through SIGNR1-mediated regulation of alternatively activated macrophages. Molecular Nutrition and Food Research, 65(20), 2001010.

Verway, M., Bouttier, M., Wang, T.-T., Carrier, M., Calderon, M., An, B.-S., Devemy, E., McIntosh, F., Divangahi, M., and Behr, M. A. (2013). Vitamin D induces interleukin-1β expression: paracrine macrophage epithelial signalling controls M. tuberculosis infection. Public Library of Science Pathogens, 9(6), e1003407.

Vo, A., Doumit, M., and Rockwell, G. (2016). The biomechanics and optimization of the needle-syringe system for injecting triamcinolone acetonide into keloids. Journal of Medical Engineering, 2016, 8.

Vu-Quang, H., Yoo, M.-K., Jeong, H.-J., Lee, H.-J., Muthiah, M., Rhee, J. H., Lee, J.-H., Cho, C.-S., Jeong, Y. Y., and Park, I.-K. (2011). Targeted delivery of mannan-coated superparamagnetic iron oxide nanoparticles to antigen-presenting cells for magnetic resonance-based diagnosis of metastatic lymph nodes in vivo. Acta Biomaterialia, 7(11), 3935–3945.

Wiysonge, C. S., Ntsekhe, M., Gumedze, F., Sliwa, K., Blackett, K. N., Commerford, P. J., Volmink, J. A., and Mayosi, B. M. (2008). Contemporary use of adjunctive corticosteroids in tuberculous pericarditis. International Journal of Cardiology, 124(3), 388–390.

Ye, Y., Xu, Y., Liang, W., Leung, G. P. H., Cheung, K.-H., Zheng, C., Chen, F., and Lam, J. K. W. (2013). DNA-loaded chitosan oligosaccharide nanoparticles with enhanced permeability across Calu-3 cells. Journal of Drug Targeting, 21(5), 474–486.

Yeh, T.-H., Hsu, L.-W., Tseng, M. T., Lee, P.-L., Sonjae, K., Ho, Y.-C., and Sung, H.-W. (2011). Mechanism and consequence of chitosan-mediated reversible epithelial tight junction opening. Biomaterials, 32(26), 6164–6173.

Yu, G., Zhong, F., Zhao, W., Ye, B., Xu, K., and Chen, G. (2022). Head-to-head comparison of the diagnostic value of five tests for constrictive tuberculous pericarditis: five tests for constrictive TBP. International Journal of Infectious Diseases, 120, 25–32.

Yuan, C., Qu, Z.-L., Tang, X.-L., Liu, Q., Luo, W., Huang, C., Pan, Q., and Zhang, X.-L. (2019). *Mycobacterium tuberculosis* mannose-capped lipoarabinomannan induces IL-10-producing B cells and hinders CD4+ Th1 immunity. Iscience, 11, 13–30.

Zhang, X., Shi, J., Ye, X., Ku, Z., Zhang, C., Liu, Q., and Huang, Z. (2017). Coxsackievirus A16 utilizes cell surface heparan sulfate glycosaminoglycans as its attachment receptor. Emerging Microbes and Infections, 6(1), 1–7.

Zhao, Y., Wang, J., Fu, Q., Zhang, H., Liang, J., Xue, W., Zhao, G., and Oda, H. (2022). Characterization and Antioxidant Activity of Mannans from Saccharomyces cerevisiae with Different Molecular Weight. Molecules, 27(14), 4439.

CHAPTER SEVEN

CONCLUSIONS, RESEARCH LIMITATIONS, RECOMMENDATIONS AND FUTURE PERSPECTIVES

7.1. CONCLUSIONS

Amongst numerous communicable diseases that affect humans, Tuberculosis (TB) presents as a very difficult disease to treat due to its unique characteristics that allows it to develop resistance against several antibiotics, and its ability to survive in extreme conditions. The recommendations in the current treatment WHO guidelines may be inadequate to curtail the disease, resulting in the continual prevalence and development of resistance. TB is primarily an infection of the lungs, with the ability to spread to other organs known as EPTB. Recent studies noticed an increase in the amount of EPTB amongst the global cases of TB from 22.6% in 2016 to 27.9% in 2021 (Rolo et al., 2023). These trends make the epidemic a dire global concern for the development of new treatment alternatives or conjuncts.

Tuberculosis pericarditis (TBP) is a type of extrapulmonary tuberculosis that generally requires a longer duration of therapy as compared to pulmonary TB and still presents with a higher mortality despite treatments. This is mainly due to the lack of effective permeation of three-quarters of the drugs recommended in standard treatment regimens.

The use of nanotechnology has over the years reported improvement in drug solubility, bioavailability, and release. These improvements help minimize side effects, dose frequency and duration of treatment. A drug like bedaquiline, with limited use due to its side effect profile and low aqueous solubility, will therefore largely benefit patients when incorporated into a nanosystem. Nanosystems are known to decrease side effects due to a requirement for lower drug administered and improved drug accumulation at disease site. The use of nanosystems thus provides a novel superior delivery system for an existing treatment used in the treatment of TBP and TB as a whole. Due to bedaquiline's potential to cause cardiac toxicity, the nanosystem needs to be investigated and monitored closely because of the proximity of the infection site and the heart. This will provide better understand on the possible advantages or disadvantages of the nanosystem in relation to the drugs side-effect.

For the quantification of the analytes, analytical HPLC methods were developed and validated, all proving simple replicable methods for the detection and quantification of isoniazid, pyrazinamide and bedaquiline. In this study, a novel bedaquiline-loaded chitosan oligosaccharide-mannan co-polymeric nanosystem was prepared to improve bedaquiline's lack of solubility in

aqueous media. It was shown that the nanosystem could be utilized in solubilising bedaquiline in aqueous media for the permeation of the drug across the pericardium for the treatment of TBP. The nanosystem resulted in the improved permeation of bedaquiline as compared to isoniazid and pyrazinamide. The nanosystem prepared has a good polydispersity index and zeta potential. SEM images confirmed the dynamic light scattering particle size and PDI. It indicated that a nanosized and uniformly shaped multi-layered spherical nanosystem was formed. Furthermore, physiochemical property (FTIR, XRD, and TGA) data demonstrated good encapsulation of the drug and a more heat-stable copolymeric nanosystem as compared to the individual polymers. A high entrapment efficiency was obtained with very slow-release profiles. Overall, the nanosystem presents promising results for consideration in the treatment of TBP. However, further pharmacokinetic and pharmacodynamic studies are required to substantiate the effectiveness of the nanosystem against tuberculosis in TBP.

7.2. RESEARCH LIMITATIONS

In this study, the main limitations encountered were operational limitations in the procurement of the standard anti-TB drugs, which took months to arrive. Meanwhile, the research was initially to determine the permeability of all 4 standard anti-TB drugs across the pericardium and develop a nanosystem to improve their permeation. Due to limited time and difficulty in incorporating 4 drugs of different chemical properties into a nanosystem, we opted to compare the already reported permeable standard drugs to a single bactericidal anti-TB drug, bedaquiline.

7.3. RECOMMENDATIONS AND FUTURE PERSPECTIVES

The developed COS-MN-BDQ nanosystem displayed novelty and ultimately fulfilled the aims and objectives of this study. It showed a unique very slow *in vitro* drug release and outstanding *ex vivo* permeation results. For this reason, more future research is required to improve the data output.

- Bedaquiline, a lipophilic drug was compared to isoniazid and pyrazinamide (hydrophilic drugs), therefore further comparative studies with lipophilic drugs like rifampicin would provide a deepened understanding of the effect of lipophilicity in the permeation of drugs across the pericardium.
- The permeation of all anti-TB drugs in combination needs to be conducted to ascertain the effect of the drugs' permeation in the presence of other drugs.

- The nanosystem was prepared with polymers said to have host-directed properties. Therefore, immunomodulatory tests should be performed to determine the immunomodulatory properties of the nanosystem.
- Mannan is an active targeting ligand. Studies to determine the specificity and selectivity of cells with mannose receptors such as macrophages should be conducted. This may give light to a possible broadening of the scope of effectiveness of the nanosystem against other types of tuberculosis such as lymph node tuberculosis.
- *In vivo* studies are advised to understand the release mechanism of the nanosystem and based on the concurrence of results with the *ex vivo* studies, open a path for the marketing and commercialization of the product to pharmaceutical companies by Wits enterprise.

7.4. REFERENCES

Rolo, M., González-Blanco, B., Reyes, C. A., Rosillo, N., and López-Roa, P. (2023). Epidemiology and factors associated with Extra-pulmonary tuberculosis in a Low-prevalence area. Journal of Clinical Tuberculosis and Other Mycobacterial Diseases, 32, 100377.

APPENDIX A

ANIMAL RESEARCH ETHICS COMMITTEE
Registration number: AREC-101210-002

Date: 04/06/2021

Certificate reference: Waiver 04-06-2020-O
Category: O
Applicant: Simisola Ayodele
Department: Department of Pharmacy and Pharmacology (WITS)
Tel: 011 717 2552; **Email**: 1715904@students.wits.ac.za

Re: Waiver from the Animal Ethics Research Committee of the University of the Witwatersrand

This letter is to confirm that Simisola Ayodele, MSc student (1715904) under the supervision of Prof Yahya E Choonara, Prof Pradeep Kumar and Dr Armorel van Eyk (Department of Pharmacy and Pharmacology), does not require full Animal Ethics Research Committee clearance to undertake the work titled **'Targeted nanosystems for TB pericarditis intervention'**.

Reason for waiver
The project is using pericardium collected from adult male Sprague–Dawley rats euthanized by the WRAF (maximum 80 rats) and from domestic pigs euthanized by the WRAF or commercially available (maximum 12 pigs) for *in vitro* drug diffusion studies.

Details of the study
The *in vitro* drug diffusion studies will be performed at the Department of Pharmacy and Pharmacology, Division of Pharmacology.
The pericardium will be collected from the following sources, depending on availability:
1) Wits Central Animal Service Unit from domestic pigs euthanized for other purposes,
2) Wits Central Animal Service Unit old stock rats being terminated,
3) Local accredited and registered abattoirs in the Gauteng area. The abattoir that will be approached: McKenzie Butchery & Abattoir (Pty) Ltd, Tarlton (specializing in pigs)
All tissue waste will be disposed of using waste containers lined with disposable red color coded liners used for anatomical materials. Waste bins will be removed by registered hazard waste removal companies employed by the university.

The individual covered by the waiver are Simisola Ayodele, Prof Yahya E Choonara, Prof Pradeep Kumar and Dr Armorel van Eyk (Wits).

Please contact me should you require further information.

Yours sincerely

Prof Frederic Michel

Chair: Animal Research Ethics Committee
University of the Witwatersrand

APPENDIX B

UNIVERSITY OF THE WITWATERSRAND, JOHANNESBURG	HUMAN RESEARCH ETHICS COMMITTEE (MEDICAL)

2023/07/17

Drs A van Eyk and P van der Bijl
School of Therapeutic Sciences
Department of Pharmacy and Pharmacology
Medical School
University

Sent by e-mail to: 1715904@students.wits.ac.za

Dear Mr Ayodele

Re: **Protocol Ref No:** M200611
Protocol Title: *Permeability of human and porcine pericardium to anti- tuberculosis drugs*
Principal Investigators: Drs A van Eyk and P van der Bijl

Thank you for your letter of 2023/06/30.

I confirm that we have noted and approve of your progress report. Congratulations on your two publications to date.

Thank you for keeping us informed.

Yours Sincerely

.....
Mr I Burns
For the Human Research Ethics Committee (Medical)

.....
Dr CB Penny, Chairperson, Human Research Ethics Committee (Medical)

APPENDIX C

Biomedicine & Pharmacotherapy 162 (2023) 114588

Contents lists available at ScienceDirect

Biomedicine & Pharmacotherapy

journal homepage: www.elsevier.com/locate/biopha

Review

Advances in immunomodulatory strategies for host-directed therapies in combating tuberculosis

Simisola Ayodele [a], Pradeep Kumar [a], Armorel van Eyk [b], Yahya E. Choonara [a,*]

[a] Wits Advanced Drug Delivery Platform Research Unit, Department of Pharmacy and Pharmacology, School of Therapeutic Sciences, Faculty of Health Sciences, University of the Witwatersrand, Johannesburg, 7 York Road, Parktown, 2193, South Africa
[b] Department of Pharmacy and Pharmacology, University of the Witwatersrand, Johannesburg, 7 York Road, Parktown, 2193, South Africa

ARTICLE INFO

Keywords:
Tuberculosis
Drug Resistance
Pattern Recognition Receptors (PRRs)
Repurposed Drugs
Host-Directed Therapies (HDTs)
Immunomodulators

ABSTRACT

Tuberculosis (TB) maintains its infamous status regarding its detrimental effect on global health, causing the highest mortality by a single infectious agent. The presence of resistance and immune compromising disease favours the disease in maintaining its footing in the health care burden despite various anti-TB drugs used to fight it. Main factors contributing to resistance and difficulty in treating disease include prolonged treatment duration (at least 6 months) and severe toxicity, which further leads to patient non-compliance, and thus a ripple effect leading to therapeutic non-efficacy. The efficacy of new regimens demonstrates that targeting host factors concomitantly with the *Mycobacterium tuberculosis* (M.tb) strain is urgently required. Due to the huge expenses and time required of up to 20 years for new drug research and development, drug repurposing may be the most economical, circumspective, and conveniently faster journey to embark on. Host-directed therapy (HDT) will dampen the burden of the disease by acting as an immunomodulator, allowing it to defend the body against antibiotic-resistant pathogens whilst minimizing the possibility of developing new resistance to susceptible drugs. Repurposed drugs in TB act as host-directed therapies, acclimatizing the host immune cell to the presence of TB, improving its antimicrobial activity and time taken to get rid of the disease, whilst minimizing inflammation and tissue damage. In this review, we, therefore, explore possible immunomodulatory targets, HDT immunomodulatory agents, and their ability to improve clinical outcomes whilst minimizing the risk of drug resistance, through various pathway targeting and treatment duration reduction.

APPENDIX D

Surface-Modified Drug Delivery Systems for Tuberculosis Intervention

Simisola Ayodele, Pradeep Kumar, Armorel van Eyk, and Yahya E. Choonara

Abstract Tuberculosis (TB) presents as the second most lethal infectious disease after HIV/AIDS and has presented difficulty in treatment over the years, due to prolonged duration of therapy and side effects of the drugs resulting in patient non-compliance and the development of multidrug resistance (MDR) strains. Anti-TB drugs incorporated in nanosystems may reduce side effects by delivering the drug selectively into infection reservoirs such as macrophages, which may assist in clearing the TB bacilli faster and reducing the duration of therapy. The rapid development of nanosciences has improved the targeted delivery of therapeutics, offering great benefits in the treatment of chronic diseases. Nanosystems demonstrate great prospect by specific and selective targeting, supported by their ability to be surface functionalized with targeting ligands. This chapter will therefore demonstrate the state of the art in the development of surface-modified nanotechnology incorporated with anti-TB therapeutics.

Keywords Tuberculosis · Polymeric nanosystems · Surface modifications · MDR TB · Therapeutics

APPENDIX E

Synthesis of Novel Mannan-Chitosan Oligosaccharide Lactate Nanoparticles for the Enhanced *Ex Vivo* Permeation of Bedaquiline across the Pericardium in Tuberculosis Pericarditis

Simisola Ayodele [1], Pradeep Kumar [1], Armorel van Eyk [2], Pieter van der Bijl (jr)[3], Yahya E. Choonara [1]*

[1] Wits Advanced Drug Delivery Platform Research Unit, Department of Pharmacy and Pharmacology, School of Therapeutic Sciences, Faculty of Health Sciences, University of the Witwatersrand, Johannesburg, 7 York Road, Parktown, 2193, South Africa

[2] Department of Pharmacy and Pharmacology,
University of the Witwatersrand, Johannesburg, 7 York Road, Parktown, 2193, South Africa

[3] Netcare Kuilsriver Hospital, Kuilsriver, 33 van Riebeeck Road, Kuils River, 7580, South Africa

***Corresponding Author:**
Professor Yahya E. Choonara
Tel: +27-11-717-2052
Fax: +27-11-642-4355
Email: yahya.choonara@wits.ac.za

APPENDIX F

RP-HPLC Method Development and Validation for the Determination of Bedaquiline in Nanosystems at Physiological pH 7.4

Simisola Ayodele [1], Pradeep Kumar [1], Armorel van Eyk [2], Yahya E. Choonara [1]*

[1] Wits Advanced Drug Delivery Platform Research Unit, Department of Pharmacy and Pharmacology, School of Therapeutic Sciences, Faculty of Health Sciences, University of the Witwatersrand, Johannesburg, 7 York Road, Parktown, 2193, South Africa

[2] Department of Pharmacy and Pharmacology,
University of the Witwatersrand, Johannesburg, 7 York Road, Parktown, 2193, South Africa

***Corresponding Author:**
Professor Yahya E. Choonara
Tel: +27-11-717-2052
Fax: +27-11-642-4355
Email: yahya.choonara@wits.ac.za

APPENDIX G

2023 RSG SCIENCE COMMUNICATION AWARD

THIS ACKNOWLEDGES

Simisola Ayodele

FOR AN EXCELLENT PERFORMANCE AT THE 2023 WADDP RSG SCIENCE COMMUNICATION COMPETITION, OBTAINING

SECOND PLACE

Professor Yahya Choonara
Director (WADDP research unit)

06/09/2023
Date

APPENDIX H

1. Method: Synthesis of Superparamagnetic Iron Oxide Nanoparticles (SPIONs) Incorporated Nanosystem

1.1. Synthesis of Naked SPIONs

Using $FeCl_3 \cdot 6H2O$ and $FeCl_2 \cdot 4H2O$ in the presence of NaOH, the SPIONs were synthesized with and without nitrogen and compared. The prior synthesis employed the use of a closed nitrogen system to control oxidation and possibly reduce particles. SPIONs were synthesized in a 2-necked round bottom flask, by slowly adding NaOH (1 g pellets in 25 ml distilled water) dropwise at a rate of 0.5 $ml.min^{-1}$ to $FeCl_3 \cdot 6H2O$ (0.5 g) and $FeCl_2 \cdot 4H2O$ (1 g) in 10ml of distilled water mixture at 75 °C. The nanosystem was left to stir for another 1 hour under nitrogen and heat. After removal from the heat source, the nanosystem was stirred at room temperature under nitrogen. The formed SPIONs were sonicated using the ultrasonic cleaner and washed with 20 ml nitrogen-purged water in triplicate whilst being collected magnetically using a neodymium magnet, all done in triplicate. The same process was repeated once with 20 ml ethanol rinse done in triplicate to remove surfactants. The SPIONs were then vacuum oven-dried at 60 degrees for 24 h.

1.2. Synthesis of Mesoporous Silica-SPIONs

25 mg Nitrogen-synthesized SPIONs were dissolved in 7 ml of 32:8:1 ratio Ethanol: Milli-Q water: 25% Ammonia and ultrasound-sonicated for 30 min. 1.5 ml TEOS was added dropwise and after 15 min 0.5 ml APTES was also added dropwise and stirred for 3 h. Thereafter the nanoparticles were washed several times with ethanol and water, and vacuum oven dried overnight at 60 °C.

1.3. Synthesis of Mannan Conjugated Silica-SPIONs

100 mg silica-coated SPIONS was dissolved in 40 ml water, 75mg mannose, 25 mg FITC, 125 mg EDC, and 100 mg NHS were dissolved in 20 ml water. The SPIONs were slowly added to the mannose solution and stirred for 6 h. The nanoparticles were washed with distilled water 3 times, frozen for 24 h and lyophilized for 12 h.

1.4. Physicochemical Characterization of the SPIONs

1.4.1. Determination of Particle Size, Zeta Potential, and Morphology

A nano zetasizer instrument (NanoZS, Malvern Panalytical, Malvern, UK) was used to obtain the average hydrodynamic size of the nanoparticles and the surface zeta potential of the nanoparticles by dynamic light scattering and electrophoretic light scattering, respectively. The suspension (0.1 ml) was diluted into 10 ml of distilled water. The resultant samples (1 ml) were transferred into disposable cuvettes to determine the hydrodynamic size and polydispersity index while 0.8 ml was transferred into zeta potential disposable folded capillary cells (DTS 1070) for surface charge analysis at 25 °C.

1.4.2. X-ray Diffraction (XRD) Analysis

The degree of crystalline transition of SPIONs to SiO_2-SPIONs and mannan conjugated SiO_2-SPIONs was analysed employing X-ray diffractometry (XRD) (Rigaku MiniFlex, Rigaku Inc., Tokyo, Japan). The dry samples of SPIONs were mounted on aluminium sample holders and measured at a current of 40 kV and 15 mA CuKα radiation. The scanning measurement was in the 2θ range of 10°–90°, with a scan rate of $10°.min^{-1}$.

1.4.3. Fourier Transform Infrared (FTIR) Spectroscopy

Fourier transform infrared spectroscopy (Spectrum 100, PerkinElmer Inc., Waltham, MA, USA) was used for comparative analysis of SiO_2 SPIONs and mannan-conjugated SiO_2-SPIONs to identify the difference in the vibrational transition of the chemical bonds in the molecule. The bonds present will confirm the attachment of mannan to the nanosystem.

2. Results: Synthesized Superparamagnetic Iron Oxide Nanoparticles (SPIONs) Incorporated Nanosystem Physiochemical and Physiomechanical Properties

2.1. Assessment of Synthesized SPIONs, Silica SPIONs and Mannan Conjugated SPIONs regarding Particle Size and Morphology

The average size of the Silica-coated SPIONs after synthesis was found to be 140 nm as in Figure H1

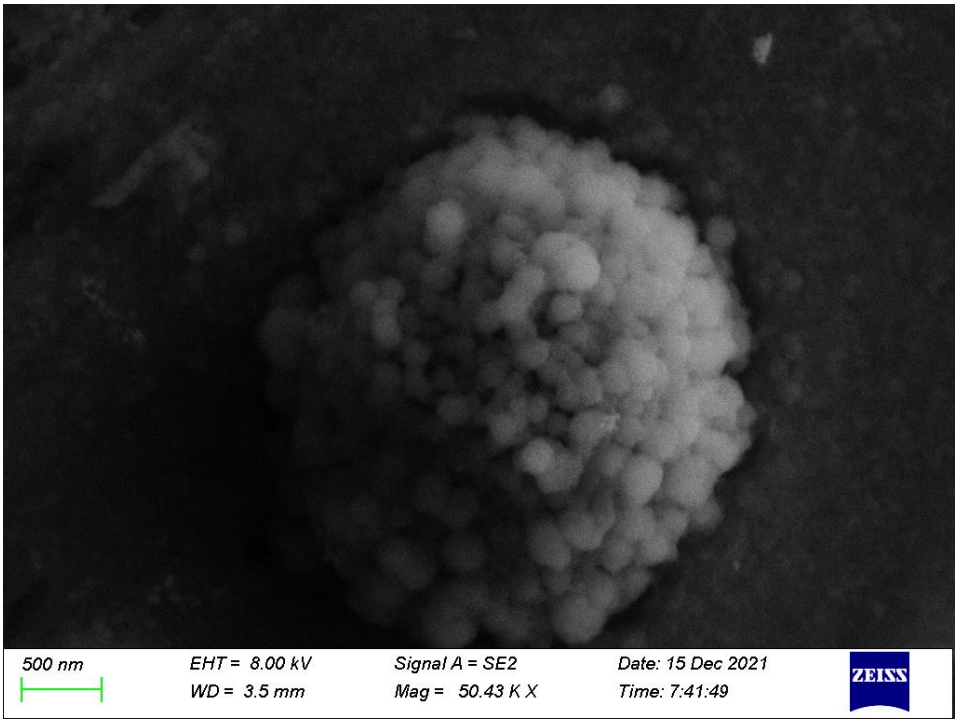

Figure H1: Smooth electron microscopy images showing 140 nm silica-coated superparamagnetic iron oxide nanoparticles.

2.2. Determination of Powder Diffraction of Mannan Conjugated Silica-Coated SPIONs in Comparison to SPIONs and Silica-Coated SPIONs

The diffraction patterns in Figure H2 show the crystalline nature of SPIONs and how coating with SiO_2 and mannan interacts with it. XRD peaks of naked SPIONs and silica-coated SPIONs show the same pattern as reported in the literature (Kulkarni et al., 2014). The naked SPIONs show sharp distinct peaks, with a lack of secondary peaks, indicating a good, homogenous, crystal, and pure magnetite nanoparticle. A broad peak at ~25 °C confirms the presence of amorphous silica in the silica-coated SPIONs sample (Kulkarni et al., 2014). No additional peaks were detected in the mannan-conjugated silica-coated SPIONs implying the failure in attachment of mannan to the surface of the nanosystem.

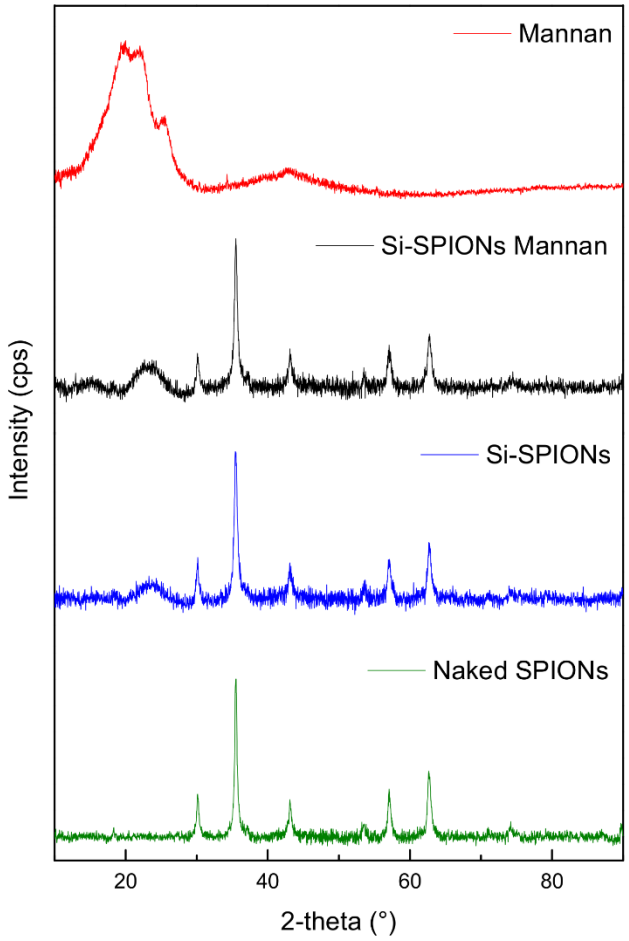

Figure H2: XRD images of the Naked SPIONs, Mesoporous Silica SPIONs, Mannan conjugated Mesoporous Silica and Mannan.

2.3. Assessment of Functional Transformation of Silica-Coated SPIONs and Mannan Conjugated SPIONs

The FTIR spectra of silica-coated SPIONs and mannan-conjugated SPIONs are overlayed in Figure H3. The characteristic peak at ~1100 cm^{-1} corresponds to the bending vibration of the Si−O bond (Kulkarni et al., 2014). Bands at 1630 cm^{-1} are also observed depicting the absorbed water on the surface of the samples. The absence of a peak at 2929 cm^{-1} represents the symmetric and asymmetric CH- stretching vibrations found in polysaccharides (Hong et al., 2021; Zhao et al., 2022), indicating that the conjugation step failed and mannan was not functionalized unto the SPIONs nanosystem.

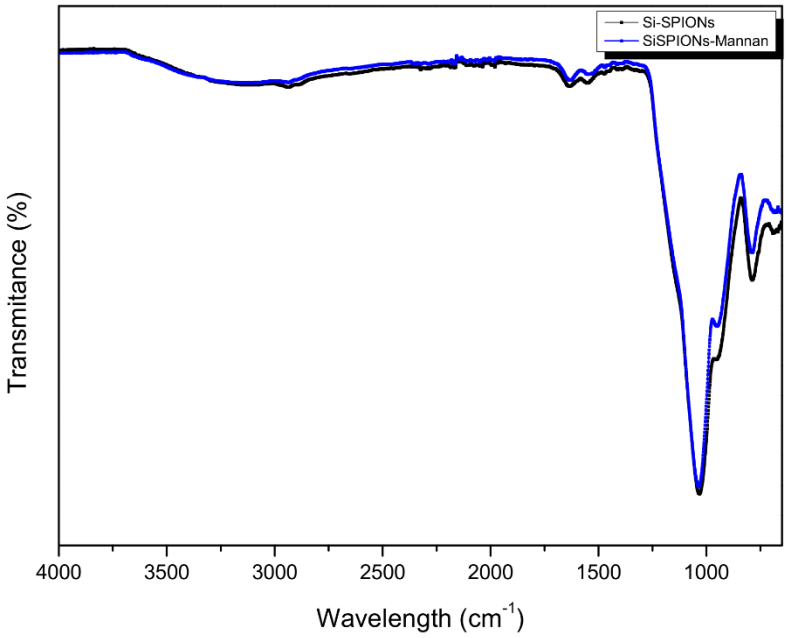

Figure H3: FTIR images of the Mesoporous Silica SPIONs, Mannan conjugated Mesoporous Silica Nanoparticles.

APPENDIX I

SA AYODELE FINAL MASTERS' CORRECTED THESIS TURN-IT-IN.docx

by Simisola Ayodele

Submission date: 08-Nov-2023 11:17PM (UTC+0200)
Submission ID: 2222073950
File name: SA_AYODELE_FINAL_MASTERS_27_CORRECTED_THESIS_TURN-IT-IN.docx (5.98M)
Word count: 18569
Character count: 104600

SA AYODELE FINAL MASTERS' CORRECTED THESIS TURN-IT-IN.docx

ORIGINALITY REPORT

15%	13%	11%	0%
SIMILARITY INDEX	INTERNET SOURCES	PUBLICATIONS	STUDENT PAPERS

PRIMARY SOURCES

1	www.mdpi.com Internet Source	1%
2	dspace.nwu.ac.za Internet Source	1%
3	hdl.handle.net Internet Source	1%
4	www.researchgate.net Internet Source	1%
5	repository.sustech.edu Internet Source	1%
6	Ravindra V. Badhe, Divya Bijukumar, Dharmesh R. Chejara, Mostafa Mabrouk et al. "A composite chitosan-gelatin bi-layered, biomimetic macroporous scaffold for blood vessel tissue engineering", Carbohydrate Polymers, 2017 Publication	<1%
7	academic.oup.com Internet Source	<1%